

NUCLEOTIDE EXCISION REPAIR

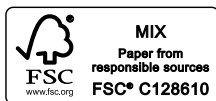
THROUGH THE LOOKING GLASS



**CRISTINA
RIBEIRO-SILVA**

Nucleotide excision repair through the looking glass

Cristina Ribeiro-Silva



Colophon

ISBN: ISBN: 978-94-028-2015-7

Cover design: Ovidiu Stanciu & Cristina Ribeiro-Silva
Layout: Cristina Ribeiro-Silva
Printed by: Ipskamp Printing

Copyright © Cristina Ribeiro-Silva 2020, Rotterdam, The Netherlands

All rights reserved. No part of this thesis may be reproduced, stored or transmitted in any form or by any means without the prior written permission of the author or from the publishers holding the copyright of published articles.

Nucleotide excision repair through the looking glass

Nucleotide excisiereparatie onder de loep

Thesis

to obtain the degree of Doctor from the
Erasmus University Rotterdam
by command of the
rector magnificus

Prof. dr. R.C.M.E. Engels

and in accordance with the decision of the Doctorate Board.
The public defense shall be held on

Tuesday, 9th June 2020 at 15:30 hrs

by

Ana Cristina Ribeiro da Silva
Born in Lisbon, Portugal

Doctoral Committee

Promoter: Prof. dr. W. Vermeulen

Other members: Prof. dr. H. van Attikum
Dr. ir. J.A.F. Marteyn
Dr. T. Mahmoudi

Copromoter: Dr. H. Lans

TABLE OF CONTENTS

7 Chapter 1

General introduction &
scope of the thesis

33 Chapter 2

DNA damage sensitivity
of SWI/SNF-deficient cells
depends on TFIIH subunit
p62/GTF2H1

79 Chapter 3

Ubiquitin and TFIIH-
stimulated DDB2 dissociation
drives DNA damage hand-
over in nucleotide excision
repair

119 Chapter 4

ATP-dependent chromatin
remodeler CHD1 promotes
nucleotide excision repair

149 Chapter 5

SWI/SNF: Complex complexes
in genome stability and cancer

177 Chapter 6

Concluding remarks &
future directions

193 Appendix (&)

Summary
Samenvatting
Curriculum vitae
List of publications
PhD portfolio
Acknowledgements

Introduction

DNA damage

DNA lesions are a fact of life. It is estimated that, daily, each of our cells is confronted with approximately 10^4 - 10^5 new DNA lesions^{1,2}. Left unrepaired, these lesions can interfere with essential genome processes, such as transcription and replication^{3,4}, having immediate and long term consequences. For instance, lesions in the transcribed strand of genes halt transcription and directly interfere with gene expression, which, on the long term, favors progeria following damage-induced senescence or apoptosis. Meanwhile, erroneous replication of a damaged DNA template can introduce mutations that alter genetic information and can lead to aberrant chromosome segregation, both contributing to genome instability⁴⁻⁷. Although very rarely mutations turn out to be beneficial to the organism, i.e., when they favor biodiversity and adaptive evolution, most often mutations are the hallmark for genetic disease and tumorigenesis. DNA integrity and the proper functioning of the genome are liable to insults arising from multiple sources that directly damage the DNA, among which are: 1) (by)products of our cellular metabolism, such as reactive oxidative and nitrogen species, alkylating and lipid peroxidation products; 2) spontaneous chemical instability of DNA under physiological conditions, such as base hydrolysis and deamination; and 3) external/environmental agents such as ultra-violet (UV) light, ionizing radiation and numerous harmful chemicals^{1,7,8}. Because DNA is the only biomolecule that is never completely renewed throughout a cell's lifetime, its integrity relies solely on the repair of existing molecules to safeguard its faithful expression and the transmission of genetic information to the next generations.

DNA repair: a multiplex response to numerous constant threats

Cells utilize a range of specialized DNA damage repair mechanisms, signaling pathways, tolerance processes and cell cycle checkpoints, collectively called the DNA damage response (DDR), to cope with DNA injuries⁹. Depending on the type of damage, the location of the damage in the genome, the type of cell and the cell cycle stage, a specific pathway of the DDR is activated. By transiently halting cell cycle progression, these genome caretaking tools can provide cells with a time window for repair to prevent lesion-induced mutagenesis and chromosome missegregation

during replication and mitosis, respectively. Alternatively, rather than halting the cell cycle, replication-blocking lesions can be temporarily ignored to allow cell cycle progression if that is more convenient to cell survival. Under these circumstances, the activation of DNA damage tolerance pathways allows alternative DNA polymerases, in a process called translesion synthesis (TLS), to bypass the lesion at the expense of fidelity. In addition, to prevent tumorigenesis, cells with too extreme damage load can be directed into apoptosis. Genetic diseases, neurological degeneration, premature aging and increased cancer susceptibility are severe fallouts of inherited DDR defects that illustrate the human's health reliance on an operational DDR^{3,4,9,10}.

The crux of the cell's defense against DNA damage is embodied by a range of complementary DNA repair mechanisms able to recognize and remove most types of DNA damage (Fig. 1)^{4,9}. DNA mismatch repair (MMR), base excision repair (BER) and nucleotide excision repair (NER) have similar strategies to remove DNA lesions that affect only a single DNA strand, relying on the excision of one or more bases by nucleases including the damaged base(s). The ensuing gap is filled and closed by DNA polymerases and ligases, respectively, with newly synthesized DNA using the complementary and undamaged strand as template. MMR is mainly active during replication and prevents mutagenesis by removing misincorporated bases or small insertion or deletion loops caused by replicative slippage^{11,12}. BER protects organisms from accumulating endogenous DNA damage induced by free radicals and other reactive chemicals derived from the cell's metabolism and environment sources. Particularly, BER can repair oxidized, deaminated or alkylated nucleotides that do not significantly disturb Watson-Crick base pairing^{1,13}. In BER, lesion-specific DNA glycosylases recognize and excise the damaged base by cleaving the N-glycosidic bond between the base and the deoxyribose, leaving an apurinic/apyrimidinic (AP) site. Subsequent incision of the deoxyribose by APE1 generates a single-strand break that is repaired by DNA synthesis of a single nucleotide (short-patch BER) or a longer stretch of nucleotides (long-patch BER)^{14,15}. Single-strand breaks are repaired in a similar manner involving BER proteins. Helix-distorting lesions, such as UV-induced photoproducts and intrastrand crosslinks are repaired by NER, described below in more detail as this process is the main focus of

this thesis.

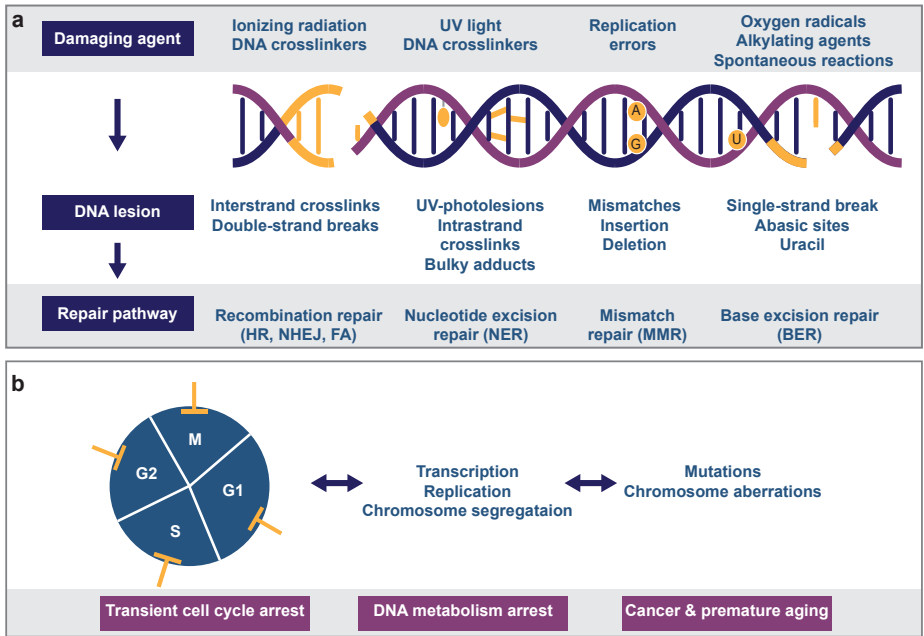


Figure 1. DNA damage, repair pathways and DNA damage consequences. (a) Overview of common endogenous and environmental DNA damaging agents, examples of DNA lesions induced by these and the most relevant repair pathways cells used to remove each type of lesion. Abbreviations: HR, homologous recombination; NHEJ, non-homologous end-joining; FA, fanconi anaemia; NER, nucleotide excision repair; MMR, mismatch repair; BER, base excision repair. (b) DNA damage-induced transient arrest of cell-cycle phases, G1, S, G2 or M, interruption of DNA metabolism processes, e.g., transcription, replication and chromosome segregation, and long-term consequences of DNA damage, including mutations and chromosome aberrations and their biological effects.

Two major pathways facilitate the repair of more destructive lesions, such as double-strand breaks (DSBs). These lesions affect both strands of the DNA helix and can arise, for instance, from replication fork stalling or collapse (e.g., after chemotherapeutic drug treatment), enzymatic incisions (e.g., by Cas9 or during class switch recombination in developing lymphocytes), or exposure to ionizing radiation (IR, e.g., X-rays). DSBs are resolved mainly by homologous recombination (HR) or non-homologous end-joining (NHEJ), depending on the cell cycle stage and the genomic location of the break. While NHEJ re-ligates broken ends throughout all phases of the cell cycle^{16,17}, this process is considered to be error-prone since the two strands are processed before ligation, which may result in the removal

or addition of several nucleotides. HR is only active during the S and G2 phases of the cell cycle as it employs the intact sister chromatid as a repair template to repair the break in an error-free manner. During HR, trimming the two DNA ends creates 3' overhangs that invade the sister chromatid which is then used as a template to synthesize any missing DNA. Specific endonucleases help resolve the Holliday junction structure and the nicks are finally ligated back together^{16–18}.

Other destructive and more complex lesions are interstrand crosslinks (ICLs), which form covalent bonds between the two DNA strands. ICLs can be induced by chemicals such as the chemotherapeutic drug cisplatin, and are extremely toxic as they block transcription and replication¹⁹. Moreover, because repair of these lesions requires the repair of both strands, they are particularly challenging for cells to deal with and collaborative efforts of multiple DDR repair mechanisms are therefore required¹⁶. The cell cycle stage dictates the choice of a particular repair response, but the exact mechanisms in place are still poorly understood. In S phase, stalled replication forks due to ICLs are recognized by the Fanconi anemia (FA) pathway proteins that orchestrate, via incision, the unhooking of the ICL from one of the DNA strands. The repair reaction is finalized by the activities of other DDR mechanisms, including TLS²⁰, HR²¹ and NER²². TLS fills the gap in the complementary DNA strand opposite of the unhooked crosslink, which is then used by HR as template to repair the DSB in the incised DNA²³. NER is thought to repair the unhooked crosslink, and has also been implicated, together with TLS, in the removal of ICLs in non-replicating cells^{24,25}.

Nucleotide excision repair

NER is unique in its ability to repair a wide range of lesions that arise from diverse and different genotoxic insults because, in contrast to most other DNA repair pathways, NER detects the structural consequences of DNA damage, i.e., helix-destabilization, instead of the DNA lesion itself²⁶. These helix-distorting lesions include the UV-induced cyclobutane pyrimidine dimers (CPDs) and pyrimidine-pyrimidone (6–4) photoproducts (6-4PPs), ROS-induced cyclopurines, chemically-induced bulky adducts and chemotherapy drug-induced (e.g., cisplatin) intrastrand crosslinks^{27,28}. More than 30 proteins are involved in the intricate network of NER,

and cooperate to perform four essential steps: 1) damage detection; 2) damage verification; 3) excision of a single-stranded DNA segment; and 4) DNA synthesis and ligation to restore the gap. Depending on where in the genome lesions occur, two different damage detection sub-pathways can initiate NER. Transcription-coupled repair (TC-NER) detects lesions in the transcribed strand of active genes^{10,28}, whereas global genome repair (GG-NER) detects lesions anywhere in the genome. The biological significance of the NER pathway is clinically evident from a range of different cancer-prone, developmental and/or progeroid disorders that arise from specific hereditary NER deficiencies^{10,28}.

DNA damage detection by TC-NER

Transcription blocking lesions compromise cellular viability and function and promote premature (DNA-damage induced) aging, as a consequence of lower gene expression and increased apoptosis^{10,28,29}. To counteract the cytotoxic effects of these lesions that stall RNA Polymerase II (Pol II) molecules, TC-NER is activated with the recruitment of CSB, CSA and UVSSA proteins^{28,30} (Fig. 2a). The transient interaction between CSB and Pol II during transcription is stabilized when Pol II cannot be pushed forward by the helicase/translocase activity of CSB due to a transcription-blocking lesion^{31,32}. CSA, which is part of the larger E3 ubiquitin ligase CRL4^{CSA} complex, is recruited to the lesion by CSB and directs the poly-ubiquitylation and proteasomal degradation of CSB following UV irradiation^{33,34}. Subsequent binding of UVSSA, assisted by the histone chaperone FACT and stabilized by CSA, counteracts CSB degradation and stabilizes its binding to the lesion site by recruiting the de-ubiquitylation enzyme USP7^{30,35–37}. UVSSA also recruits transcription factor IIH (TFIIH) via direct interaction with TFIIH's subunit GTF2H1 (also known as p62)^{35,38}.

DNA damage detection by GG-NER

The great majority of helix-destabilizing DNA lesions are detected by GG-NER, which examines the entire genome, coding and non-coding, for severe DNA damage-induced helix distortions^{27,28}. XPC, as part of the heterotrimeric XPC-CETN2-RAD23B complex^{39–41}, is capable of detecting a broad range of structurally unrelated lesions. XPC employs an indirect, stepwise damage recognition and binding mode, in which transient interactions with DNA precede the formation of a stable and immobile

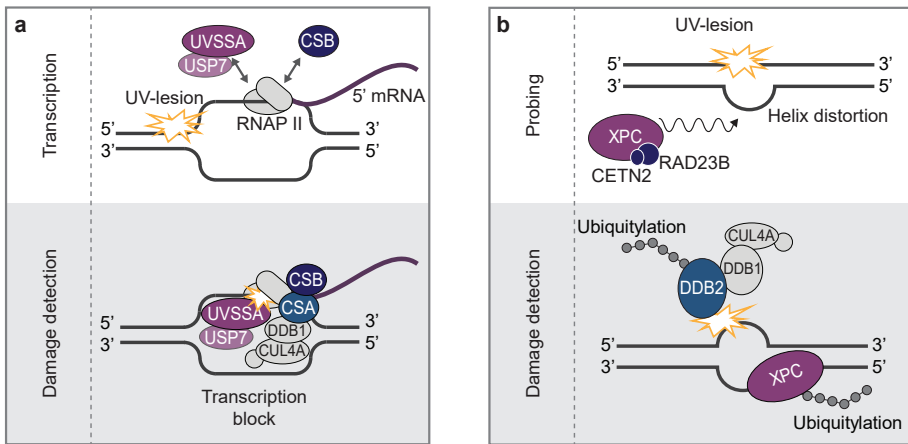


Figure 2. DNA damage detection in NER. (a) TC-NER is initiated when an elongating RNA Pol II molecule is stalled by a lesion in the transcribed strand of an active gene, leading to the increased binding and recruitment of TC-NER factors CSB, CSA (as part of the CRL4^{CSA} complex), UVSSA and USP7. (b) In GG-NER, damage detection is carried out by XPC which probes the DNA for helix-distorting lesions, in complex with RAD23B and CETN2 proteins. DDB2, in complex with DDB1 as part of the CRL4^{DDB2} complex, binds specifically to UV-induced lesions and facilitates recognition of DNA damage by XPC, in particular CPDs, which only mildly destabilize the DNA helix. The E3 ubiquitin ligase CRL4^{DDB2} ubiquitylates DDB2 and XPC to regulate their affinity and binding to damaged DNA.

DNA-bound complex^{42–45}. While XPC diffuses through the nucleus, it probes the DNA for lesions that thermodynamically destabilize the DNA double helix and disrupt Watson-crick pairing. Without contacting the lesion directly, XPC becomes fully and stably bound to the extruding nucleotides in the undamaged strand^{44,46,47}. TFIIH is recruited by interactions between its helicase XPB and core GTF2H1 subunits with XPC^{38,48,49}. Because XPC also detects mismatches and aberrant DNA structures that are not processed by NER, examination by TFIIH of whether genuine DNA damage is present plays a crucial role in ensuring the fidelity of the NER reaction (described in more detail below).

Despite being the main damage sensor in GG-NER, XPC requires the auxiliary function of the UV-DDB complex, comprising DDB1 and DDB2, to efficiently recognize UV-induced photolesions^{47,50,51}. In particular, UV-induced CPDs are poor substrates for XPC since they only mildly destabilize the DNA helix^{40,52,53}. To enable their repair, DDB2 stimulates XPC recruitment by directly binding and flipping out the damaged bases, which

then become a suitable substrate for XPC⁵⁴ (Fig. 2b). The UV-DDB complex is part of a larger E3 ubiquitin-ligase complex (CRL4^{DDB2}), containing CUL4A, RBX1, and the COP9 signalosome⁵⁵. The binding of DDB2 to UV-lesions triggers the COP9 signalosome dissociation, which stimulates the E3 ubiquitin-ligase activity of the complex^{33,55,56}. The main targets of the E3 ubiquitin-ligase activity of the complex are core histones H2A, H3 and H4, XPC and DDB2 itself^{55,57–59}. While ubiquitylation of DDB2 decreases its affinity to UV-DNA lesions and targets DDB2 for proteasomal degradation, ubiquitylation of XPC increases XPC's affinity to DNA lesions *in vitro*^{58,60}. DNA damage binding of both DDB2 and XPC is tightly regulated by post-translational modifications (PTMs), such as SUMOylation⁶¹, ubiquitylation⁶² and PARylation^{63–65}. DNA damage handover from DDB2 to XPC and TFIIH is further described and studied in more detail in Chapter 3.

Core NER reaction: damage verification, dual incision and gap filling

Once damage has been detected by either TC- or GG-NER, both pathways converge into the same repair mechanism by recruiting TFIIH. TFIIH is loaded on the damaged strand 5' to the lesion, through a direct interaction with either XPC (via GG-NER) or UVSSA (via TC-NER)^{35,38,48,49}. TFIIH is a multifunctional complex that opens the DNA helix in both NER⁶⁶ and transcription initiation⁶⁷. The helicase XPB facilitates recruitment of TFIIH to DNA damage^{68,69}, whereas the XPD helicase verifies the presence of genuine NER substrates by unwinding the DNA in 5'–3' direction while scanning for helicase blocking lesions^{66,70}. In the absence of damage-stalled XPD, repair is aborted^{66,71}. The TFIIH complex is composed of ten subunits, all of which are necessary for its stability^{72–75}. In Chapter 2⁷⁶, we describe how SWI/SNF ATPases BRM and BRG1 promote transcription of TFIIH subunit GTF2H1, thus enabling TFIIH function in transcription and NER.

Damage verification is stimulated by the DNA damage binding protein XPA, which binds to nucleotides with altered chemical structures in ssDNA⁷⁷. XPA stimulates the release of the transcription-associated CAK subcomplex from TFIIH, consequently stimulating the helicase activity of XPD^{70,78,79}. Besides stimulating lesion verification by TFIIH, XPA also interacts with many core NER proteins^{27,80}, likely for optimal positioning of the NER endonucleases for incision⁸¹. For this reason, XPA is considered

to be a central coordinator of the NER reaction. The RPA protein complex, after damage verification, binds to single-stranded DNA to protect the non-damaged DNA strand from endonucleases. Together, XPA and RPA orient the two structure-specific endonucleases ERCC1-XPF and XPG to the damaged strand⁸²⁻⁸⁴. XPG recruitment (independently or simultaneously with TFIIH^{83,85}) enables the first incision, 5' to the lesion, by ERCC1-XPF, and the dual incision is then finalized by XPG itself, 3' to the lesion⁸⁴. The generated 22-30 nucleotide ssDNA is released, most likely together with TFIIH, and degraded⁸⁶. The final DNA gap filling step involves the recruitment of RFC, PCNA, either DNA polymerase δ (non-replicating cells), ϵ (mainly in replicating cells) or κ (non-replicating cells)⁸⁷⁻⁹⁰ for de novo DNA synthesis using the undamaged strand as template, and the recruitment of either DNA ligase I or III to seal the gap⁸⁸ (Fig. 3).

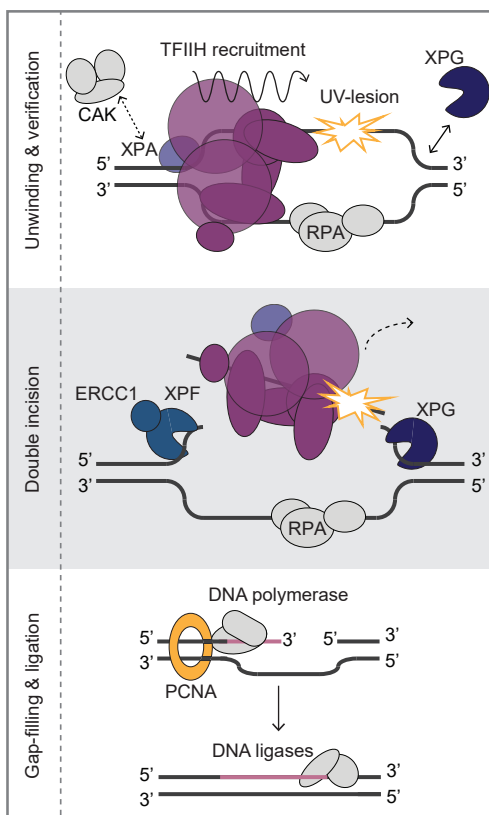


Figure 3. Core NER mechanism. After detection of DNA damage by either GG- or TC-NER, both pathways converge to a common core mechanism. The recruitment of TFIIH, via an interaction with XPC (in GG-NER) or with UVSSA (in TC-NER), results in the release of its transcription-associated CAK subcomplex, stimulated by XPA. The active helicase activity of TFIIH opens the double helix and verifies the presence of a lesion. XPA and RPA binding to the altered nucleotides in the single-stranded DNA and to the undamaged strand, respectively, facilitate the loading of the structure specific endonucleases ERCC1-XPF and XPG (recruited independently or simultaneously with TFIIH) to the damaged strand. ERCC1-XPF incision 5' of the lesion is followed by XPG 3' incision, resulting in the excision of a 22-30 oligonucleotide containing the DNA lesion. The first incision, by ERCC1-XPF, enables the PCNA-assisted gap-filling by DNA polymerases δ , ϵ or κ . DNA ligases I or III seal the nick and complete the DNA repair reaction.

Chromatin as an integral player in the DDR

Mammalian cells are capable of storing our genome in the constricted volume of their nucleus by condensing DNA and wrapping it around nuclear proteins in a DNA-protein complex defined as chromatin. Every 146/147 bp of DNA wrapped by a histone octamer with two copies of histones H2A, H2B, H3 and H4⁹¹ forms the basic unit of chromatin, the nucleosome. The electrostatic interactions between the phosphate backbone of the DNA and positively charged histones stabilize nucleosomes, while the linker DNA segments connect nucleosomes together. Additional short- and long-range interactions and histone H1 play an important role in stabilizing coiled higher-order chromatin structures⁹¹. In addition to its role in condensing and storing the DNA in the nucleus, chromatin serves as a way to control how DNA is used. For instance, processes such as transcription and replication require the access of specialized proteins to specific parts of the DNA. It is thus important that chromatin is modified to regulate the access of proteins to DNA during these processes, while it simultaneously serves as a transaction platform that regulates signaling events and protein docking during DNA transacting events.

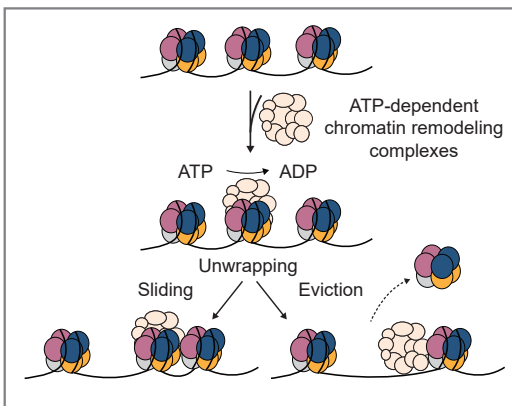


Figure 4. Schematic representation of ATP-dependent chromatin remodelling mechanisms. ATP-dependent chromatin remodelling complexes use distinct ways to rearrange chromatin at the expense of ATP. To alter the contacts between DNA and nucleosomes, these remodelers can unwrap, reposition (sliding) or evict nucleosomes, or alter their histone composition by replacing or ejecting histones.

Generally speaking, two major mechanisms control wrapping of DNA into nucleosomal units. The first involves histone modifiers that catalyze the covalent attachment or removal of functional groups or small proteins to protruding histone tails. These PTMs change the chemical properties of histones and/or change how histones interact with the DNA⁹² or other proteins. The many flavors and forms of PTMs combined serve as docking

and signaling sites for many chromatin related proteins. Examples of these chemical PTMs on histones include methylation, acetylation, phosphorylation, ubiquitylation, SUMOylation and PARylation, which also play important roles in the DDR⁹³. The second major mechanism in DNA wrapping involves ATP-dependent chromatin remodeling proteins/complexes that catalyze the disruption of DNA-histone contacts using the energy from ATP hydrolysis to slide, evict, unwrap nucleosomes or alter their composition⁹⁴⁻⁹⁶ (Fig. 4). In mammals, many structurally related chromatin remodeling proteins and complexes have been identified, including the SWI/SNF, CHD, ISWI and INO80 families. The SWI2/SNF2 superfamily of ATP-dependent chromatin remodelers is characterized by an ATPase domain consisting of two subdomains, DExx and HELICc⁹⁴. In addition to the split SWI2/SNF2 ATPase domain, each member of these

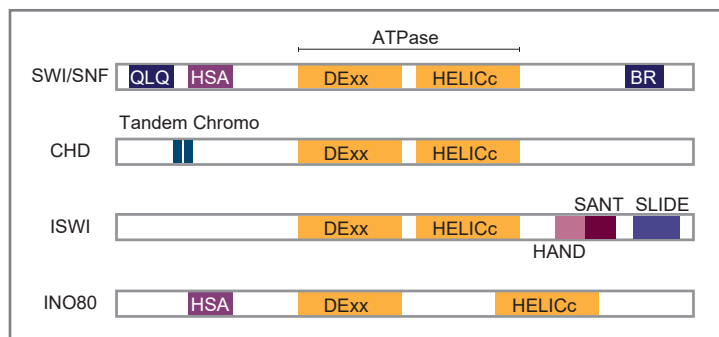


Figure 5. Schematic representation of the mammalian SWI2/SNF2 superfamily of ATP-dependent chromatin remodelers. The SWI2/SNF2 superfamily is characterized by an ATPase domain split in two parts: DExx and HELICc. The unique additional domains each subfamily member harbors within or adjacent to its ATPase domain, determines its specificity and classification into SWI/SNF, CHD, ISWI or INO80. The HSA and BR domains allow the SWI/SNF family to bind nuclear actin-related proteins as well as acetylated lysines, respectively. CHD chromatin remodelers contain a tandem chromodomain positioned at the N-terminus, which enables the binding to methylated lysines. The ISWI family has three domains (HAND, SANT and SLIDE) which mediate interactions with proteins and DNA. The INO80 family has a longer insertion between the split ATPase domains.

families contains specific but different additional functional domains within or adjacent to the ATPase domains^{94,96,97} (Fig. 5). The composition of these protein complexes is highly dynamic and may vary according to cell type, cell cycle stage or the event in place.

Many studies have shown that both chromatin modifying and ATP-dependent chromatin remodeling enzymes are involved in the mammalian DDR. In the past years, the number of chromatin remodelers that are implicated in the DDR has substantially increased, indicating that (re)-organization of chromatin structure is an intricate and essential component of the DDR *in vivo*^{93,98–101}. In Chapter 2⁷⁶, we study the specific involvement of SWI/SNF proteins in NER, while in Chapter 5¹⁰² we review their known functions in the DDR. In addition, a novel role for CHD1 in NER is described in Chapter 4. Deficiencies in both ATP-dependent chromatin remodelers¹⁰³ and DDR⁴ are linked to tumorigenesis, but the interplay between these two deficiencies and how they contribute to cancer development is still an active field of research.

The access, repair and restore model revised

A central question in the field of DNA repair is how, within the dynamic structure of chromatin where the lesion occurs, multi-subunit complexes can recognize and repair DNA lesions at any given moment and genomic location^{104–106}. Conversely, chromatin itself is subject to regulation during DNA repair. Approximately four decades ago, the observations by Smerdon and colleagues laid the foundations for a model of DNA repair within the context of chromatin, referred to as “access, repair and restore” (ARR)^{107,108}. The model suggested that chromatin changes are required for repair to take place, first by becoming more accessible to facilitate DNA damage recognition and second, after DNA repair is completed, to restore its original conformation^{107–110}. Pioneer observations of increased DNA accessibility following UV-C irradiation of human fibroblasts compelled a thorough examination of the phenomenon. Regions undergoing repair by NER were found to be transiently more sensitive to MNase digestion^{108,111} and to only recover their nuclease resistance over time¹⁰⁸. Similar results were observed with restriction enzymes¹¹² and DNase I digestion of UV-damaged chromatin^{113,114}. Although the initial major observations of nucleosome rearrangements were done in the context of repair by NER following UV-C irradiation, similar chromatin changes were soon observed following exposure to different kinds of DNA damaging agents^{115,116}. Follow-up efforts showing that nucleosomes were refractory to NER^{117–119} but also to DSB repair¹²⁰ and that both local and global relaxation of chromatin takes place upon DSB induction^{121–124} solidified the premise of

the ARR model, that is of active chromatin remodeling before DNA repair. Since then, the principles of repair within chromatin have broadened to include other DNA repair mechanisms.

However, the view of chromatin as a mere obstacle to DNA repair is evolving¹²⁵. Many chromatin proteins whose function is associated with chromatin condensation, including polycomb proteins and heterochromatin proteins 1 (HP1), are transiently recruited to DSB and stimulate repair^{109,126–128}, partly by repressing transcription at DSBs^{129–131}. HP1 proteins are also recruited to UV-induced DNA damage and their loss results in increased sensitivity to UV irradiation¹³². Although this challenged the original idea of the ARR model, it is consistent with studies showing that heterochromatin is not refractory to the diffusion of large proteins¹³³ and presented grounds for considering chromatin – and chromatin-associated factors/enzymes – as an integral part of the DDR. A recent

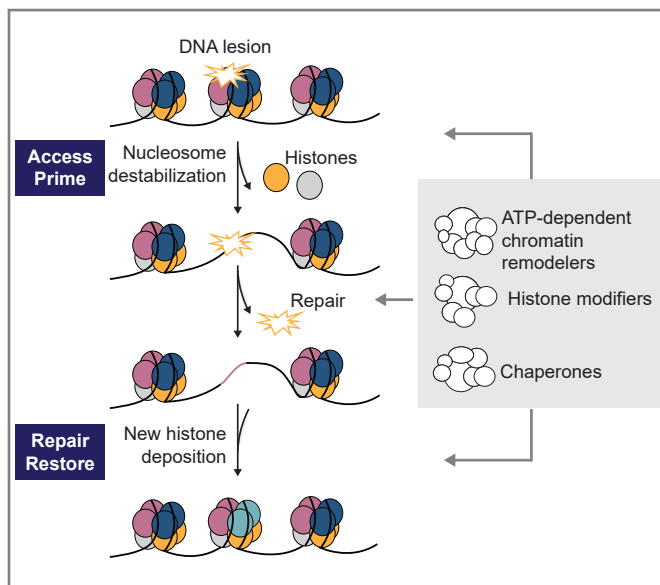


Figure 6. The revised access/prime-repair/restore model. In this simplified model representation, histone modifiers, chaperones and ATP-dependent chromatin remodelers reshape damaged chromatin by unfolding, refolding and repositioning of nucleosomes during repair.

proposed model revises the “access” step as an “access & priming” step instead, where chromatin also acts as a platform promoting the assembly of signaling and repair machineries in competent DDR regions^{109,125} (Fig. 6). This priming step may contribute to the regulation of DNA repair pathway choice or coordination between the DDR and nuclear events to suppress

mutagenic events and limit their oncogenic potential^{93,109,125}.

Many histone modifiers, chaperones and chromatin remodeling complexes have been suggested to promote or, at least to some degree, modulate repair of UV-damaged DNA. Although SWI/SNF proteins confer UV-resistance to the model organism *C. elegans*¹³⁴ and mammalian cells, literature presents discrepant evidence regarding which step in NER SWI/SNF proteins regulate^{135–139}. BRG1 and SNF5 are the most researched subunits; therefore, in Chapter 2⁷⁶, we investigated the putative role of BRM in NER. The mammalian INO80 complex was reported to facilitate the repair of 6-4PPs and CPDs¹⁴⁰ and, like the ALC1 chromatin remodeler⁶⁴, may function to facilitate damage detection by GG-NER, while the ISWI subunit SMARCA5 is required for TC-NER¹⁴¹. Surprisingly, not much is known regarding CHD proteins and the UV-DDR¹⁴². Consequently, in Chapter 4 we explored a putative function for CHD1 in NER. The histone chaperones FACT¹⁴³, HIRA¹⁴⁴ and CAF-1^{145–147} were also shown to be recruited to UV-C damaged chromatin. Interestingly, the direct interaction between CAF-1 and PCNA couples histone deposition (i.e., chromatin re-assembly) with repair-associated DNA synthesis¹⁴⁶, as part of a concerted process.

How the individual - and likely cooperative - action of these chromatin-modifying proteins contributes to the UV-DDR is still, unfortunately, unclear. The lack of clear follow-up studies leaves many questions open. Although studies in yeast have clearly shown that chromatin remodeling facilitates NER^{142,148,149}, it remains to be investigated whether the function of ATP-dependent chromatin remodeling enzymes during mammalian NER is actual chromatin remodeling activity or an uncharacterized activity. ATP-dependent chromatin remodelers have many cellular functions, making it a challenge to disentangle those functions from their activities in the DDR. Furthermore, they appear to act differently in different repair pathways⁹⁹. A current and future challenge, therefore, lies in decoding the precise activities, at the molecular level, of the many different chromatin modifying and remodeling proteins proposed to act in DDR and to understand how these act together at the same lesion to facilitate DNA repair.

Scope of this thesis

Likely most essential NER enzymes have been identified and the basic NER steps are accurately defined. Nevertheless, NER is thought to be tightly regulated by multiple PTMs and chromatin-modifying enzymes *in vivo*, of which the precise mechanisms are still largely not understood. The research presented in this thesis combined cell biology, biochemistry and microscopy methods to obtain a more comprehensive understanding of NER in intact and living cells, by studying the interplay between NER factors themselves and with ATP-dependent chromatin remodeling proteins.

Inactivating mutations in SWI/SNF proteins are amongst the most common mutations across chromatin remodeling enzymes in all human cancers. SWI/SNF proteins have been implicated in different DDR pathways, but conflicting observations have made it difficult to define a unified mechanism by which SWI/SNF acts in NER. In **Chapter 2**, we describe why the two SWI/SNF ATPases, BRM and BRG1, are necessary for efficient NER. Both BRM and BRG1 promote the expression of the essential TFIIH subunit GTF2H1 and, consequently, the stability and functionality of the TFIIH complex itself, both in transcription and in NER. In this chapter, we furthermore contemplate the potential of this finding, suggesting that SWI/SNF-deficiency-induced DDR-vulnerability could be exploited for precision cancer therapy.

The dynamic arrangement of NER factors entails temporal and spatial coordination for each NER protein and step, in order for efficient restoration of damaged DNA to take place. Despite the fact that multiple PTMs have been found to regulate the activity of GG-NER damage sensor proteins DDB2 and XPC, it remained unclear how their activity in detecting and handing over DNA damage to TFIIH is coordinated. In **Chapter 3**, we studied the interplay between the recruitment and dissociation of DDB2, XPC and TFIIH to UV-induced DNA damage. We show that timely DDB2 dissociation, after damage recognition by XPC, is as important as its recruitment to DNA lesions. Dissociation of DDB2 is required for DNA damage handover to XPC, and coincides with the arrival of the TFIIH complex and the formation of a stable XPC-TFIIH complex, which further stimulates DDB2 dissociation. CRL4^{DDB2}-mediated ubiquitylation of DDB2 following UV irradiation plays a major role in this damage handover, as

it promotes DDB2 dissociation and extraction from chromatin, DDB2 proteolytic degradation and, ultimately, prevents excessive DDB2 binding to lesions. Overall, our results demonstrate how the elegant interplay between GG- and core NER factors - which cooperate but also compete with one another - contributes to the correct spatiotemporal control of NER.

Several ATP-dependent chromatin remodeling proteins from the CHD family have been implicated in DSB repair, but their role in NER has hardly been investigated. Loss of CHD1 sensitizes cells to a range of DNA damage agents that induce helix-distorting DNA crosslinks mainly processed by NER. Due to the high mutation frequency of CHD1 in prostate cancer, a better understanding of CHD1 function in tumorigenesis and DDR may provide a rationale for new therapeutic avenues exploiting CHD1 vulnerabilities caused by CHD1 loss. Therefore, in **Chapter 4**, we sought to explore the putative role of CHD1 in NER. We found that CHD1 is likely a novel regulator of NER as its activity is required for optimal survival following UV irradiation. Furthermore, CHD1 is required for the DNA damage loading of late NER factors, such as XPF, but not earlier proteins such as DDB2, XPC, TFIIH and XPA. Instead of favoring damage handover in the early steps of the reaction, CHD1 appears to promote the progression from lesion verification to excision. Our findings endorse further research to clarify CHD1's specific contributions in NER and their overall impact on DDR and health.

Defects in both ATP-dependent chromatin remodelers and DDR are linked to tumorigenesis, but how the interplay between these defects promotes cancer development is only partially understood. In **Chapter 5**, we review the emerging functions of SWI/SNF ATP-dependent chromatin remodelers in DSB repair and NER, in light of our findings in Chapter 2, the DDR-related vulnerabilities that arise from SWI/SNF dysfunction and their potential application in precision cancer therapy.

In **Chapter 6**, we summarize and discuss the main findings of the experimental work described in Chapter 3 and Chapter 4 and provide future directions to study in-depth the implications of fine-tuning GG-NER, as well as to dissect CHD1's molecular function in NER.

References

1. Lindahl, T. Instability and decay of the primary structure of DNA. *Nature* vol. 362 709–715 (1993).
2. Hoeijmakers, J. H. J. DNA repair mechanisms. *Maturitas* **38**, 17–22 (2001).
3. Jackson, S. P. & Bartek, J. The DNA-damage response in human biology and disease. *Nature* vol. 461 1071–1078 (2009).
4. Hoeijmakers, J. H. J. DNA damage, aging, and cancer. *N. Engl. J. Med.* **361**, 1475–85 (2009).
5. Lans, H. & Hoeijmakers, J. H. J. Cell biology: Ageing nucleus gets out of shape. *Nature* **440**, 32–34 (2006).
6. Akbari, M. & Krokan, H. E. Cytotoxicity and mutagenicity of endogenous DNA base lesions as potential cause of human aging. *Mech. Ageing Dev.* **129**, 353–365 (2008).
7. Giglia-Mari, G., Zotter, A. & Vermeulen, W. DNA damage response. *Cold Spring Harb. Perspect. Biol.* **3**, 1–19 (2011).
8. Friedberg, E., Graham, C. W., Wolfram, S., Richard, D. W. & A. Schultz, Roger, Ellenberger, T. *DNA Repair and Mutagenesis, Second Edition. DNA Repair and Mutagenesis, Second Edition* (American Society of Microbiology, 2006).
9. Hoeijmakers, J. H. J. Genome maintenance mechanisms for preventing cancer. *Nature* **411**, 366–374 (2001).
10. Lans, H., Hoeijmakers, J. H. J., Vermeulen, W. & Marteijn, J. A. The DNA damage response to transcription stress. *Nat. Rev. Mol. Cell Biol.* (2019).
11. Gupta, D. & Heinen, C. D. The mismatch repair-dependent DNA damage response: Mechanisms and implications. *DNA Repair* vol. 78 60–69 (2019).
12. Liu, D., Keijzers, G. & Rasmussen, L. J. DNA mismatch repair and its many roles in eukaryotic cells. *Mutation Research - Reviews in Mutation Research* vol. 773 174–187 (2017).
13. Cadet, J., Sage, E. & Douki, T. Ultraviolet radiation-mediated damage to cellular DNA. *Mutation Research - Fundamental and Molecular Mechanisms of Mutagenesis* vol. 571 3–17 (2005).
14. Dianov, G. L. & Hübscher, U. Mammalian base excision repair: The forgotten archangel. *Nucleic Acids Research* vol. 41 3483–3490 (2013).
15. Krokan, H. E. & Bjørås, M. Base excision repair. *Cold Spring Harb. Perspect. Biol.* **5**, 1–22 (2013).
16. Ceccaldi, R., Rondinelli, B. & D'Andrea, A. D. Repair Pathway Choices and Consequences at the Double-Strand Break. *Trends in Cell Biology* vol. 26 52–64 (2016).
17. Scully, R., Panday, A., Elango, R. & Willis, N. A. DNA double-strand break repair-pathway choice in somatic mammalian cells. *Nat. Rev. Mol. Cell Biol.* **20**, 698–714 (2019).
18. Li, X. & Heyer, W. D. Homologous recombination in DNA repair and DNA damage tolerance. *Cell Research* vol. 18 99–113 (2008).
19. Lopez-Martinez, D., Liang, C. C. & Cohn, M. A. Cellular response to DNA interstrand crosslinks: the Fanconi anemia pathway. *Cellular and Molecular Life Sciences* vol. 73 3097–3114 (2016).
20. Budzowska, M., Graham, T. G., Soback, A., Waga, S. & Walter, J. C. Regulation of the Rev1–pol ζ complex during bypass of a DNA interstrand cross-link. *EMBO J.* **34**, 1971–1985 (2015).
21. Long, D. T., Räschle, M., Joukov, V. & Walter, J. C. Mechanism of RAD51-dependent DNA interstrand cross-link repair. *Science (80-.)*. **333**, 84–87 (2011).
22. Mouw, K. W. & D'Andrea, A. D. Crosstalk between the nucleotide excision repair and Fanconi anemia/BRCA pathways. *DNA Repair (Amst)*. **19**, 130–134 (2014).
23. Clauson, C., Schärer, O. D. & Niedernhofer, L. Advances in understanding the complex

- mechanisms of DNA inter strand cross-link repair. *Cold Spring Harb. Perspect. Med.* **3**, (2013).
24. Enoiu, M., Jiricny, J. & Schärer, O. D. Repair of cisplatin-induced DNA interstrand crosslinks by a replication-independent pathway involving transcription-coupled repair and translesion synthesis. *Nucleic Acids Res.* **40**, 8953–8964 (2012).
 25. Muniandy, P. A., Thapa, D., Thazhathveetil, A. K., Liu, S. ting & Seidman, M. M. Repair of laser-localized DNA interstrand cross-links in G1 phase mammalian cells. *J. Biol. Chem.* **284**, 27908–27917 (2009).
 26. Nouspikel, T. Nucleotide excision repair: Variations on versatility. *Cellular and Molecular Life Sciences* vol. 66 994–1009 (2009).
 27. Schärer, O. D. Nucleotide excision repair in Eukaryotes. *Cold Spring Harb. Perspect. Biol.* **5**, (2013).
 28. Marteiijn, J. a, Lans, H., Vermeulen, W. & Hoeijmakers, J. H. J. Understanding nucleotide excision repair and its roles in cancer and ageing. *Nat. Rev. Mol. Cell Biol.* **15**, 465–81 (2014).
 29. Ljungman, M. & Zhang, F. Blockage of RNA polymerase as a possible trigger for u.v. light-induced apoptosis. *Oncogene* **13**, 823–831 (1996).
 30. Schwertman, P. *et al.* UV-sensitive syndrome protein UVSSA recruits USP7 to regulate transcription-coupled repair. *Nat. Genet.* **44**, 598–602 (2012).
 31. Geijer, M. E. & Marteiijn, J. A. What happens at the lesion does not stay at the lesion: Transcription-coupled nucleotide excision repair and the effects of DNA damage on transcription in cis and trans. *DNA Repair (Amst)*. **71**, 56–68 (2018).
 32. Xu, J. *et al.* Structural basis for the initiation of eukaryotic transcription-coupled DNA repair. *Nature* **551**, 653–657 (2017).
 33. Fischer, E. S. *et al.* The molecular basis of CRL4 DDB2/CSA ubiquitin ligase architecture, targeting, and activation. *Cell* **147**, 1024–1039 (2011).
 34. Groisman, R. *et al.* CSA-dependent degradation of CSB by the ubiquitin-proteasome pathway establishes a link between complementation factors of the Cockayne syndrome. *Genes Dev.* **20**, 1429–1434 (2006).
 35. Nakazawa, Y. *et al.* Mutations in UVSSA cause UV-sensitive syndrome and impair RNA polymerase Ilo processing in transcription-coupled nucleotide-excision repair. *Nat. Genet.* **44**, 586–592 (2012).
 36. Zhang, X. *et al.* Mutations in UVSSA cause UV-sensitive syndrome and destabilize ERCC6 in transcription-coupled DNA repair. *Nat. Genet.* **44**, 593–597 (2012).
 37. Wienholz, F. *et al.* FACT subunit Spt16 controls UVSSA recruitment to lesion-stalled RNA Pol II and stimulates TC-NER. *Nucleic Acids Res.* (2019).
 38. Okuda, M., Nakazawa, Y., Guo, C., Ogi, T. & Nishimura, Y. Common TFIIH recruitment mechanism in global genome and transcription-coupled repair subpathways. *Nucleic Acids Res.* **45**, 13043–13055 (2017).
 39. Sugasawa, K. *et al.* Xeroderma pigmentosum group C protein complex is the initiator of global genome nucleotide excision repair. *Mol. Cell* **2**, 223–32 (1998).
 40. Sugasawa, K. *et al.* A multistep damage recognition mechanism for global genomic nucleotide excision repair. *Genes Dev.* **15**, 507–521 (2001).
 41. Nishi, R. *et al.* Centrin 2 Stimulates Nucleotide Excision Repair by Interacting with Xeroderma Pigmentosum Group C Protein. *Mol. Cell Biol.* **25**, 5664–5674 (2005).
 42. Hoogstraten, D. *et al.* Versatile DNA damage detection by the global genome nucleotide excision repair protein XPC. *J. Cell Sci.* **121**, 2850–9 (2008).
 43. Camenisch, U. *et al.* Two-stage dynamic DNA quality check by xeroderma pigmentosum

- group C protein. *EMBO J.* **28**, 2387–2399 (2009).
44. Min, J. H. & Pavletich, N. P. Recognition of DNA damage by the Rad4 nucleotide excision repair protein. *Nature* **449**, 570–575 (2007).
 45. Velmurugu, Y., Chen, X., Slogoff Sevilla, P., Min, J.-H. & Ansari, A. Twist-open mechanism of DNA damage recognition by the Rad4/XPC nucleotide excision repair complex. *Proc. Natl. Acad. Sci.* **113**, E2296–E2305 (2016).
 46. Mu, H., Geacintov, N. E., Broyde, S., Yeo, J. E. & Schärer, O. D. Molecular basis for damage recognition and verification by XPC-RAD23B and TFIIH in nucleotide excision repair. *DNA Repair* vol. 71 33–42 (2018).
 47. Sugasawa, K. Molecular Mechanism of DNA Damage Recognition for Global Genomic Nucleotide Excision Repair: A Defense System Against UV-Induced Skin Cancer. in *DNA Repair Disorders* 1–23 (Springer Singapore, 2018).
 48. Yokoi, M. *et al.* The xeroderma pigmentosum group C protein complex XPC-HR23B plays an important role in the recruitment of transcription factor IIH to damaged DNA. *J. Biol. Chem.* **275**, 9870–9875 (2000).
 49. Bernardes de Jesus, B. M., Bjørås, M., Coin, F. & Egly, J. M. Dissection of the molecular defects caused by pathogenic mutations in the DNA repair factor XPC. *Mol. Cell. Biol.* **28**, 7225–7235 (2008).
 50. Tang, J. Y., Hwang, B. J., Ford, J. M., Hanawalt, P. C. & Chu, G. Xeroderma pigmentosum p48 gene enhances global genomic repair and suppresses UV-induced mutagenesis. *Mol. Cell* **5**, 737–44 (2000).
 51. Moser, J. *et al.* The UV-damaged DNA binding protein mediates efficient targeting of the nucleotide excision repair complex to UV-induced photo lesions. *DNA Repair (Amst.)* **4**, 571–582 (2005).
 52. Reardon, J. T. & Sancar, A. Recognition and repair of the cyclobutane thymine dimer, a major cause of skin cancers, by the human excision nuclease. *Genes Dev.* **17**, 2539–2551 (2003).
 53. Wakasugi, M. *et al.* DDB accumulates at DNA damage sites immediately after UV irradiation and directly stimulates nucleotide excision repair. *J. Biol. Chem.* **277**, 1637–1640 (2002).
 54. Scrima, A. *et al.* Structural Basis of UV DNA-Damage Recognition by the DDB1-DDB2 Complex. *Cell* **135**, 1213–1223 (2008).
 55. Groisman, R. *et al.* The ubiquitin ligase activity in the DDB2 and CSA complexes is differentially regulated by the COP9 signalosome in response to DNA damage. *Cell* **113**, 357–367 (2003).
 56. Scrima, A. *et al.* Detecting UV-lesions in the genome: The modular CRL4 ubiquitin ligase does it best! *FEBS Letters* vol. 585 2818–2825 (2011).
 57. El-Mahd, M. A. *et al.* Cullin 4A-mediated proteolysis of DDB2 protein at DNA damage sites regulates in vivo lesion recognition by XPC. *J. Biol. Chem.* **281**, 13404–13411 (2006).
 58. Sugasawa, K. *et al.* UV-induced ubiquitylation of XPC protein mediated by UV-DDB-ubiquitin ligase complex. *Cell* **121**, 387–400 (2005).
 59. Kapetanaki, M. G. *et al.* The DDB1-CUL4ADDB2 ubiquitin ligase is deficient in xeroderma pigmentosum group E and targets histone H2A at UV-damaged DNA sites. *Proc. Natl. Acad. Sci. U. S. A.* **103**, 2588–2593 (2006).
 60. Rapić-Otrin, V., McLenigan, M. P., Bisi, D. C., Gonzalez, M. & Levine, A. S. Sequential binding of UV DNA damage binding factor and degradation of the p48 subunit as early events after UV irradiation. *Nucleic Acids Res.* **30**, 2588–2598 (2002).
 61. Akita, M. *et al.* SUMOylation of xeroderma pigmentosum group C protein regulates DNA damage recognition during nucleotide excision repair. *Sci. Rep.* **5**, 10984 (2015).

62. van Cuijk, L. *et al.* SUMO and ubiquitin-dependent XPC exchange drives nucleotide excision repair. *Nat. Commun.* **6**, 7499 (2015).
63. Robu, M. *et al.* Poly(ADP-ribose) polymerase 1 escorts XPC to UV-induced DNA lesions during nucleotide excision repair. *Proc. Natl. Acad. Sci.* **114**, E6847–E6856 (2017).
64. Pines, A. *et al.* PARP1 promotes nucleotide excision repair through DDB2 stabilization and recruitment of ALC1. *J. Cell Biol.* **199**, 235–249 (2012).
65. Robu, M. *et al.* Role of poly (ADP-ribose) polymerase-1 in the removal of UV-induced DNA lesions by nucleotide excision repair. *Proc. Natl. Acad. Sci. U. S. A.* **110**, 1–6 (2013).
66. Sugasawa, K., Akagi, J. ichi, Nishi, R., Iwai, S. & Hanaoka, F. Two-Step Recognition of DNA Damage for Mammalian Nucleotide Excision Repair: Directional Binding of the XPC Complex and DNA Strand Scanning. *Mol. Cell* **36**, 642–653 (2009).
67. Compe, E. & Egly, J. M. TFIIH: When transcription met DNA repair. *Nature Reviews Molecular Cell Biology* vol. 13 343–354 (2012).
68. Coin, F., Oksenysh, V. & Egly, J. M. Distinct Roles for the XPB/p52 and XPD/p44 Subcomplexes of TFIIH in Damaged DNA Opening during Nucleotide Excision Repair. *Mol. Cell* **26**, 245–256 (2007).
69. Oksenysh, V., de Jesus, B. B., Zhovmer, A., Egly, J.-M. & Coin, F. Molecular insights into the recruitment of TFIIH to sites of DNA damage. *EMBO J.* **28**, 2971–2980 (2009).
70. Li, C. L. *et al.* Tripartite DNA Lesion Recognition and Verification by XPC, TFIIH, and XPA in Nucleotide Excision Repair. *Mol. Cell* **59**, 1025–1034 (2015).
71. Mathieu, N., Kaczmarek, N., R uthemann, P., Luch, A. & Naegeli, H. DNA quality control by a lesion sensor pocket of the xeroderma pigmentosum group D helicase subunit of TFIIH. *Curr. Biol.* **23**, 204–212 (2013).
72. Giglia-Mari, G. *et al.* A new, tenth subunit of TFIIH is responsible for the DNA repair syndrome trichothiodystrophy group A. *Nat. Genet.* **36**, 714–719 (2004).
73. Vermeulen, W. *et al.* Sublimiting concentration of TFIIH transcription/DNA repair factor causes TTD-A trichothiodystrophy disorder. *Nat. Genet.* **26**, 307–13 (2000).
74. Botta, E. *et al.* Reduced level of the repair/transcription factor TFIIH in trichothiodystrophy. *Hum. Mol. Genet.* **11**, 2919–2928 (2002).
75. Luo, J. *et al.* Architecture of the Human and Yeast General Transcription and DNA Repair Factor TFIIH. *Mol. Cell* **59**, 794–806 (2015).
76. Ribeiro-Silva, C. *et al.* DNA damage sensitivity of SWI/SNF-deficient cells depends on TFIIH subunit p62/GTF2H1. *Nat. Commun.* **9**, 4067 (2018).
77. Camenisch, U., Dip, R., Schumacher, S. B., Schuler, B. & Naegeli, H. Recognition of helical kinks by xeroderma pigmentosum group a protein triggers DNA excision repair. *Nat. Struct. Mol. Biol.* **13**, 278–284 (2006).
78. Kovic, G. *et al.* Structural basis of TFIIH activation for nucleotide excision repair. *Nat. Commun.* **10**, (2019).
79. Coin, F. *et al.* Nucleotide Excision Repair Driven by the Dissociation of CAK from TFIIH. *Mol. Cell* **31**, 9–20 (2008).
80. Rademakers, S. *et al.* Xeroderma Pigmentosum Group A Protein Loads as a Separate Factor onto DNA Lesions. *Mol. Cell. Biol.* **23**, 5755–5767 (2003).
81. Volker, M. *et al.* Sequential assembly of the nucleotide excision repair factors in vivo. *Mol. Cell* **8**, 213–224 (2001).
82. De Laat, W. L. *et al.* DNA-binding polarity of human replication protein A positions nucleases in nucleotide excision repair. *Genes Dev.* **12**, 2598–2609 (1998).

83. Zotter, A. *et al.* Recruitment of the Nucleotide Excision Repair Endonuclease XPG to Sites of UV-Induced DNA Damage Depends on Functional TFIIH. *Mol. Cell. Biol.* **26**, 8868–8879 (2006).
84. Staresincic, L. *et al.* Coordination of dual incision and repair synthesis in human nucleotide excision repair. *EMBO J.* **28**, 1111–1120 (2009).
85. Dunand-Sauthier, I. *et al.* The spacer region of XPG mediates recruitment to nucleotide excision repair complexes and determines substrate specificity. *J. Biol. Chem.* **280**, 7030–7037 (2005).
86. Kemp, M. G., Reardon, J. T., Lindsey-Boltz, L. A. & Sancar, A. Mechanism of release and fate of excised oligonucleotides during nucleotide excision repair. *J. Biol. Chem.* **287**, 22889–22899 (2012).
87. Ogi, T. *et al.* Three DNA Polymerases, Recruited by Different Mechanisms, Carry Out NER Repair Synthesis in Human Cells. *Mol. Cell* **37**, 714–727 (2010).
88. Moser, J. *et al.* Sealing of Chromosomal DNA Nicks during Nucleotide Excision Repair Requires XRCC1 and DNA Ligase III α in a Cell-Cycle-Specific Manner. *Mol. Cell* **27**, 311–323 (2007).
89. Lehmann, A. R. DNA polymerases and repair synthesis in NER in human cells. *DNA Repair* vol. 10 730–733 (2011).
90. Shivji, M. K. K., Wood, R. D., Podust, V. N. & Hübscher, U. Nucleotide Excision Repair DNA Synthesis by DNA Polymerase ϵ in the Presence of PCNA, RFC, and RPA. *Biochemistry* **34**, 5011–5017 (1995).
91. Luger, K., Dechassa, M. L. & Tremethick, D. J. New insights into nucleosome and chromatin structure: an ordered state or a disordered affair? *Nat. Rev. Mol. Cell Biol.* **13**, 436–47 (2012).
92. Kouzarides, T. Chromatin Modifications and Their Function. *Cell* vol. 128 693–705 (2007).
93. Luijsterburg, M. S. & Van Attikum, H. Chromatin and the DNA damage response: The cancer connection. *Mol. Oncol.* **5**, 349–367 (2011).
94. Clapier, C. R. & Cairns, B. R. The biology of chromatin remodeling complexes. *Ann Rev Biochem* **78**, 273–304 (2009).
95. Narlikar, G. J., Sundaramoorthy, R. & Owen-Hughes, T. Mechanisms and functions of ATP-dependent chromatin-remodeling enzymes. *Cell* **154**, 490–503 (2013).
96. Zhou, C. Y., Johnson, S. L., Gamarra, N. I. & Narlikar, G. J. Mechanisms of ATP-Dependent Chromatin Remodeling Motors. *Annu. Rev. Biophys.* **45**, 153–181 (2016).
97. Petty, E. & Pillus, L. Balancing chromatin remodeling and histone modifications in transcription. *Trends Genet.* **29**, 621–629 (2013).
98. Aydin, Ö. Z., Vermeulen, W. & Lans, H. ISWI chromatin remodeling complexes in the DNA damage response. *Cell Cycle* vol. 13 3016–3025 (2014).
99. Lans, H., Marteiijn, J. A. & Vermeulen, W. ATP-dependent chromatin remodeling in the DNA-damage response. *Epigenetics and Chromatin* **5**, 4 (2012).
100. Hauer, M. H. & Gasser, S. M. Chromatin and nucleosome dynamics in DNA damage and repair. *Genes and Development* vol. 31 2204–2221 (2017).
101. Agarwal, P. & Miller, K. M. The nucleosome: orchestrating DNA damage signaling and repair within chromatin. *Biochem. Cell Biol.* **94**, 381–395 (2016).
102. Ribeiro-Silva, C., Vermeulen, W. & Lans, H. SWI/SNF: Complex complexes in genome stability and cancer. *DNA Repair (Amst)*. **77**, 87–95 (2019).
103. Pierre, R. S. & Kadoch, C. Mammalian SWI/SNF complexes in cancer: emerging therapeutic opportunities. *Current Opinion in Genetics and Development* vol. 42 56–67 (2017).

104. Essers, J., Vermeulen, W. & Houtsmuller, A. B. DNA damage repair: anytime, anywhere? *Curr. Opin. Cell Biol.* **18**, 240–246 (2006).
105. Dinant, C., Houtsmuller, A. B. & Vermeulen, W. Chromatin structure and DNA damage repair. *Epigenetics Chromatin* **1**, 9 (2008).
106. Misteli, T. & Soutoglou, E. The emerging role of nuclear architecture in DNA repair and genome maintenance. *Nat. Rev. Mol. Cell Biol.* **10**, 243–54 (2009).
107. Smerdon, M. J. DNA repair and the role of chromatin structure. *Curr. Opin. Cell Biol.* **3**, 422–428 (1991).
108. Smerdon, M. J. & Lieberman, M. W. Nucleosome rearrangement in human chromatin during UV-induced DNA- repair synthesis. *Proc. Natl. Acad. Sci. U. S. A.* **75**, 4238–41 (1978).
109. Soria, G., Polo, S. E. & Almouzni, G. Prime, Repair, Restore: The Active Role of Chromatin in the DNA Damage Response. *Molecular Cell* vol. 46 722–734 (2012).
110. Green, C. M. & Almouzni, G. When repair meets chromatin. First in series on chromatin dynamics. *EMBO Reports* vol. 3 28–33 (2002).
111. Cleaver, J. E. Nucleosome structure controls rates of excision repair in DNA of human cells. *Nature* **270**, 451–453 (1977).
112. Baxter, B. K. & Smerdon, M. J. Nucleosome unfolding during DNA repair in normal and xeroderma pigmentosum (group C) human cells. *J. Biol. Chem.* **273**, 17517–17524 (1998).
113. Bodell, W. J. & Banerjee, M. R. The influence of chromatin structure on the distribution of DNA repair synthesis studied by nuclease digestion. *Nucleic Acids Res.* **6**, 359–370 (1979).
114. Smerdon, M. J. & Lieberman, M. W. Distribution Within Chromatin of Deoxyribonucleic Acid Repair Synthesis Occurring at Different Times After Ultraviolet Radiation. *Biochemistry* **19**, 2992–3000 (1980).
115. Sidik, K. & Smerdon, M. J. Nucleosome Rearrangement in Human Cells following Short Patch Repair of DNA Damaged by Bleomycin. *Biochemistry* **29**, 7501–7511 (1990).
116. Sidik, K. & Michael, J. S. Nuclease sensitivity of repair-incorporated nucleotides in chromatin and nucleosome rearrangement in human cells damaged by methyl methanesulfonate and methylnitrosourea. *Carcinogenesis* **5**, 245–253 (1984).
117. Gong, F., Kwon, Y. & Smerdon, M. J. Nucleotide excision repair in chromatin and the right of entry. *DNA Repair* vol. 4 884–896 (2005).
118. Wang, Z. G., Wu, X. H. & Friedberg, E. C. Nucleotide excision repair of DNA by human cell extracts is suppressed in reconstituted nucleosomes. *J. Biol. Chem.* **266**, 22472–8 (1991).
119. Araki, M. *et al.* Reconstitution of damage DNA excision reaction from SV40 minichromosomes with purified nucleotide excision repair proteins. *Mutat. Res. - DNA Repair* **459**, 147–160 (2000).
120. Lemaître, C. & Soutoglou, E. Double strand break (DSB) repair in heterochromatin and heterochromatin proteins in DSB repair. *DNA Repair (Amst)*. **19**, 163–168 (2014).
121. Kruhlak, M. J. *et al.* Changes in chromatin structure and mobility in living cells at sites of DNA double-strand breaks. *J. Cell Biol.* **172**, 823–834 (2006).
122. Dellaire, G., Kepkay, R. & Bazett-Jones, D. P. High resolution imaging of changes in the structure and spatial organization of chromatin, γ -H2A.X and the MRN complex within etoposide-induced DNA repair foci. *Cell Cycle* **8**, 3750–3769 (2009).
123. Ziv, Y. *et al.* Chromatin relaxation in response to DNA double-strand breaks is modulated by a novel ATM- and KAP-1 dependent pathway. *Nat. Cell Biol.* **8**, 870–876 (2006).
124. Smeenk, G. & van Attikum, H. The chromatin response to DNA breaks: leaving a mark on genome integrity. *Annu. Rev. Biochem.* **82**, 55–80 (2013).

125. Polo, S. E. & Almouzni, G. Chromatin dynamics after DNA damage: The legacy of the access-repair-restore model. *DNA Repair (Amst)*. **36**, 114–121 (2015).
126. Visser, J. H. A., Van Lohuizen, M. & Citterio, E. The emerging role of Polycomb repressors in the response to DNA damage. *Journal of Cell Science* vol. 125 3939–3948 (2012).
127. Lee, Y. H., Kuo, C. Y., Stark, J. M., Shih, H. M. & Ann, D. K. HP1 promotes tumor suppressor BRCA1 functions during the DNA damage response. *Nucleic Acids Res.* **41**, 5784–5798 (2013).
128. Alagoz, M. *et al.* SETDB1, HP1 and SUV39 promote repositioning of 53BP1 to extend resection during homologous recombination in G2 cells. *Nucleic Acids Res.* **43**, 7931–7944 (2015).
129. Gong, F. *et al.* Screen identifies bromodomain protein ZMYND8 in chromatin recognition of transcription-associated DNA damage that promotes homologous recombination. *Genes Dev.* **29**, 197–211 (2015).
130. Ui, A., Nagaura, Y. & Yasui, A. Transcriptional elongation factor ENL phosphorylated by ATM recruits polycomb and switches off transcription for DSB repair. *Mol. Cell* **58**, 468–482 (2015).
131. Kakarougkas, A., Downs, J. A. & Jeggo, P. A. The PBAF chromatin remodeling complex represses transcription and promotes rapid repair at DNA double-strand breaks. *Mol. Cell. Oncol.* **2**, 1–4 (2015).
132. Luijsterburg, M. S. *et al.* Heterochromatin protein 1 is recruited to various types of DNA damage. *J. Cell Biol.* **185**, 577–86 (2009).
133. Bancaud, A. *et al.* Molecular crowding affects diffusion and binding of nuclear proteins in heterochromatin and reveals the fractal organization of chromatin. *EMBO J.* **28**, 3785–3798 (2009).
134. Lans, H. *et al.* Involvement of global genome repair, transcription coupled repair, and chromatin remodeling in UV DNA damage response changes during development. *PLoS Genet.* **6**, 41 (2010).
135. Zhang, L., Zhang, Q., Jones, K., Patel, M. & Gong, F. The chromatin remodeling factor BRG1 stimulates nucleotide excision repair by facilitating recruitment of XPC to sites of DNA damage. *Cell Cycle* **8**, 3953–3959 (2009).
136. Ray, A. *et al.* Human SNF5/INI1, a component of the human SWI/SNF chromatin remodeling complex, promotes nucleotide excision repair by influencing ATM recruitment and downstream H2AX phosphorylation. *Mol. Cell. Biol.* **29**, 6206–6219 (2009).
137. Zhao, Q. *et al.* Modulation of nucleotide excision repair by mammalian SWI/SNF chromatin-remodeling complex. *J. Biol. Chem.* **284**, 30424–30432 (2009).
138. Watanabe, R., Kanno, S., Mohammadi Roushandeh, A., Ui, A. & Yasui, A. Nucleosome remodelling, DNA repair and transcriptional regulation build negative feedback loops in cancer and cellular ageing. *Philos. Trans. R. Soc. B Biol. Sci.* **372**, 20160473 (2017).
139. Kothandapani, A., Gopalakrishnan, K., Kahali, B., Reisman, D. & Patrick, S. M. Downregulation of SWI/SNF chromatin remodeling factor subunits modulates cisplatin cytotoxicity. *Exp. Cell Res.* **318**, 1973–1986 (2012).
140. Jiang, Y. *et al.* INO80 chromatin remodeling complex promotes the removal of UV lesions by the nucleotide excision repair pathway. *Proc. Natl. Acad. Sci.* **107**, 17274–17279 (2010).
141. Aydin, Ö. Z. *et al.* Human ISWI complexes are targeted by SMARCA5 ATPase and SLIDE domains to help resolve lesion-stalled transcription. *Nucleic Acids Res.* **42**, 8473–8485 (2014).
142. Waters, R., van Eijk, P. & Reed, S. Histone modification and chromatin remodeling during NER. *DNA Repair (Amst)*. **36**, 105–113 (2015).
143. Dinant, C. *et al.* Enhanced chromatin dynamics by FACT promotes transcriptional restart after UV-induced DNA damage. *Mol. Cell* **51**, 469–479 (2013).

144. Adam, S., Polo, S. & Almouzni, G. Transcription recovery after DNA damage requires chromatin priming by the H3.3 histone chaperone HIRA. *Cell* **155**, 94–106 (2013).
145. Green, C. M. & Almouzni, G. Local action of the chromatin assembly factor CAF-1 at sites of nucleotide excision repair in vivo. *EMBO J.* **22**, 5163–5174 (2003).
146. Moggs, J. G. *et al.* A CAF-1-PCNA-Mediated Chromatin Assembly Pathway Triggered by Sensing DNA Damage. *Mol. Cell. Biol.* **20**, 1206–1218 (2000).
147. Gaillard, P. H. L. *et al.* Chromatin assembly coupled to DNA repair: A new role for chromatin assembly factor I. *Cell* **86**, 887–896 (1996).
148. Yu, S., Teng, Y., Waters, R. & Reed, S. H. How chromatin is remodelled during DNA repair of UV-Induced DNA damage in *Saccharomyces cerevisiae*. *PLoS Genet.* **7**, (2011).
149. Van Eijk, P. *et al.* Nucleosome remodeling at origins of global genome–nucleotide excision repair occurs at the boundaries of higher-order chromatin structure. *Genome Res.* **29**, 74–84 (2019).

DNA damage sensitivity of SWI/SNF- -deficient cells depends on TFIID subunit p62/GTF2HI

2

Cristina Ribeiro-Silva¹, Özge Z. Aydin^{1,2}, Raquel Mesquita-Ribeiro³, Jana Slyskova¹, Angela Helfricht¹, Jurgen A. Martejn¹, Jan H.J. Hoeijmakers¹, Hannes Lans^{1,*}, Wim Vermeulen^{1,*}

1. Department of Molecular Genetics, Onco Institute, Erasmus MC, University Medical Center Rotterdam, Dr. Molewaterplein 40, 3015 GD, Rotterdam, The Netherlands

2. Current address: Molecular Biology and Genetics Department, Koç University, Istanbul, Turkey

3. School of Life Sciences, University of Nottingham, NG7 2UH, Nottingham, United Kingdom

Published in Nature Communications, October 2018; 9(1): 4067

Abstract

Mutations in SWI/SNF genes are amongst the most common across all human cancers, but efficient therapeutic approaches that exploit vulnerabilities caused by SWI/SNF mutations are currently lacking. Here, we show that the SWI/SNF ATPases BRM/SMARCA2 and BRG1/SMARCA4 promote the expression of *p62/GTF2H1*, a core subunit of the Transcription Factor IIH (TFIIH) complex. Inactivation of either ATPase subunit downregulates GTF2H1 and therefore compromises TFIIH stability and function in transcription and nucleotide excision repair (NER). We also demonstrate that cells with permanent BRM or BRG1 depletion have the ability to restore *GTF2H1* expression. As a consequence, the sensitivity of SWI/SNF-deficient cells to DNA damage induced by UV irradiation and cisplatin treatment depends on GTF2H1 levels. Together, our results expose GTF2H1 as a potential novel predictive marker of platinum drug sensitivity in SWI/SNF deficient cancer cells.

Introduction

Compiled sequencing efforts have revealed the high prevalence of mutations in chromatin remodeling genes across many different types of cancer^{1,2}. Inactivating mutations in subunits of the SWI/SNF ATP-dependent chromatin remodeling complexes are amongst the most frequently mutated genes in human cancers^{3,4}, which argues for a major role in cancer pathogenesis. SWI/SNF complexes contain one of two mutually exclusive catalytic ATPase subunits, BRM/SMARCA2 or BRG1/SMARCA4, and multiple core and accessory subunits that together form a variety of functionally distinct complexes⁵. BRM and BRG1 use the energy of ATP to remodel chromatin, through which they regulate transcription, DNA damage repair (DDR) and replication and impact a variety of cellular processes including cell differentiation and growth^{1,5,6}.

Mutations in SWI/SNF subunits result in aberrant chromatin structures, increased genomic instability and perturbation of transcriptional programs, which are all hallmarks of cancer that can contribute to cell transformation and tumorigenesis^{1,5-7}. Because the products of these typically loss-of-function mutations do not constitute obvious drug targets, efficient therapeutic strategies to target tumor cells with mutant SWI/SNF genes are still lacking. Detailed insight into the molecular mechanisms of the many anti-tumorigenic cellular functions of SWI/SNF is required in order to develop such strategies.

SWI/SNF proteins have been implicated in multiple DDR mechanisms, including double strand break (DSB) repair and nucleotide excision repair (NER), and are thought to coordinate signaling and efficient recruitment of repair proteins to chromatin^{6,8,9}. NER removes a wide range of structurally unrelated helix-distorting DNA lesions, including cyclobutane pyrimidine dimers (CPDs) and 6-4 photoproducts (6-4PPs) induced by UV-light, ROS-induced cyclopurines and intrastrand crosslinks generated by chemotherapeutic platinum drugs^{10,11}. If not repaired, these lesions interfere with transcription and replication, which can result in cell death or lead to mutations and genome instability that contribute to oncogenesis. Depending on the location of DNA lesions, two distinct DNA damage detection mechanisms can trigger NER. Transcription-

coupled NER (TC-NER) is initiated when RNA Polymerase II is stalled by lesions in the transcribed strand and requires the CSB/ERCC6, CSA/ERCC8, and UVSSA proteins^{11,12}. Global-genome NER (GG-NER) detects lesions anywhere in the genome by the concerted action of the damage sensor protein complexes UV-DDB, comprised of DDB1 and DDB2, and XPC-RAD23B-CETN2¹³. XPC and CSB are essential for the subsequent recruitment of the core NER factors to damaged DNA, starting with the transcription factor IIH (TFIIH)^{12,14}, a 10-subunit complex involved in both transcription initiation and NER¹⁵. In NER, the XPB/ERCC3 ATPase and the structural component p62/GTF2H1 of the TFIIH complex are thought to anchor the complex to chromatin, via an interaction with XPC^{14,16,17}, while the XPD/ERCC2 helicase is believed to unwind DNA and verify the presence of proper NER substrates¹⁸. Subsequent recruitment of XPA and RPA stimulates damage verification and facilitates the recruitment and correct positioning of the endonucleases XPF/ERCC4-ERCC1 and XPG/ERCC5, which excise the damaged strand¹⁹. After excision, the resulting single-stranded 22-30 nucleotide DNA gap is restored by DNA synthesis and ligation¹¹.

In vitro, NER is more efficient on naked DNA templates than on chromatinized DNA²⁰, on which it was found to be stimulated by yeast SWI/SNF²¹, suggesting that chromatin remodeling is necessary to facilitate access to damaged DNA and efficient repair of lesions^{8,9,20}. Using SWI/SNF mutant *C. elegans*, we found that SWI/SNF proteins protect organisms against UV irradiation, implying a role for SWI/SNF in promoting NER *in vivo* as well²². Several additional studies in yeast and mammals further indicate that SWI/SNF proteins are important for the UV-induced DDR²³⁻²⁷. However, conflicting observations on whether SWI/SNF regulates damage detection or facilitates later repair steps have made it difficult to deduce the exact mechanism underlying SWI/SNF activity in NER. Furthermore, the majority of studies have focused on the role of the BRG1 ATPase or the SNF5 subunit, but a putative role for BRM has never been investigated in detail.

In this study, we show that both BRM and BRG1 are necessary for efficient NER by promoting the expression of TFIIH subunit GTF2H1. Furthermore, we find that cells with permanent BRM or BRG1 loss have the ability to

restore GTF2H1 levels. As a consequence, DNA damage sensitivity of BRM- or BRG1-deficient cells correlates with GTF2H1 protein levels, which could, potentially, be used to select SWI/SNF-deficient cancers that are more sensitive to platinum drug chemotherapy.

Results

SWI/SNF is required for efficient NER

To test for SWI/SNF involvement in GG-NER, we measured UV-induced unscheduled DNA synthesis (UDS) in C5RO primary fibroblasts depleted of BRM or BRG1 by siRNA. BRM and BRG1 knockdown cells showed a clear decrease in UDS, comparable to cells in which the core NER factor XPA was depleted (Fig. 1a,b; Supplementary Fig. 1a). In addition, we measured Recovery of RNA Synthesis (RRS) after UV-C irradiation in U2OS cells depleted of SWI/SNF, to test involvement in TC-NER. After irradiation, transcription levels in cells with BRM or BRG1 knockdown failed to recover to the same degree as in control cells (Fig. 1c,d; Supplementary Fig. 1b). These results indicate that both BRM and BRG1 are essential for a robust GG- and TC-NER activity after UV irradiation.

To date, most efforts to study SWI/SNF function in NER have focused on BRG1, which prompted us to direct our efforts to BRM and to determine in which NER step this SWI/SNF ATPase plays a role. We used immunofluorescence (IF) to monitor the recruitment of endogenous key NER proteins to local UV-C damage (LUD) - induced by irradiation through a microporous membrane-, 30 min after damage induction in siBRM treated U2OS cells. Recruitment of the early DNA damage sensors DDB2 and XPC to LUD, marked by CPD staining, was unaffected by BRM depletion (Fig. 1e,f, Supplementary Fig. 1c). We validated these results by real-time confocal imaging of XPC-GFP recruitment to LUD induced by a 266 nm microbeam laser, which confirmed that XPC assembly kinetics were unchanged after BRM depletion (Supplementary Fig. 1d). Also, recruitment of CSB, which is difficult to assess using IF, to microbeam LUD was unaffected by BRM depletion (Supplementary Fig. 1e). Strikingly, however, BRM depletion significantly reduced the recruitment to LUD of the TFIIH proteins XPB, XPD and GTF2H1 and downstream proteins XPA

and XPF, as measured by IF (Fig. 1e,f). These results show that BRM does not facilitate lesion detection in GG- and TC-NER but is required for the recruitment of the downstream NER damage verification and excision machinery, thus explaining why NER is compromised in its absence.

BRM is required for the recruitment of TFIIH to chromatin

To dissect how BRM depletion impairs NER, we focused on the TFIIH complex and measured real-time XPB-GFP accumulation at 266 nm laser induced LUD, which was significantly lower (more than 2 fold) after BRM knockdown (Fig. 2a,b, Supplementary Fig. 1f). We confirmed this result with an additional independent siRNA (siBRM#2) to exclude siRNA off-target effects (Supplementary Fig. 1g). Using Fluorescence Recovery After Photobleaching (FRAP), we also measured UV-induced XPB-GFP immobilization. As previously observed²⁸, a fraction of XPB immobilized in response to UV-C irradiation in control conditions, as a result of TFIIH binding to UV-damaged DNA (Supplementary Fig.1h). However, this UV-induced XPB immobilization was substantially reduced when BRM was depleted by siRNA (Supplementary Fig. 1h and quantified in Fig. 2c). These results further corroborate our IF experiments (Fig. 1e,f) and suggest that BRM is needed for efficient damage loading of TFIIH.

We also assessed damage-induced chromatin loading of TFIIH in U2OS cells with cellular fractionation, which confirmed that UV-induced loading of TFIIH subunits XPB and XPD, but not of XPC, was strongly reduced after BRM depletion (Fig. 2d,e). Strikingly, even in the absence of DNA damage, TFIIH association with chromatin was reduced, whereas its non-chromatin bound pool did not change significantly after BRM knockdown (Supplementary Fig. 2a). This implies that TFIIH is unable to efficiently interact with DNA irrespective of whether there is DNA damage or not. In addition, we noticed that association of BRM itself with chromatin did not change after DNA damage (Fig. 2d). We also could not detect recruitment of BRM to LUD inflicted by irradiation through a microporous membrane on IF (Supplementary Fig. 2b) and did not observe recruitment of GFP-tagged BRM to LUD inflicted by 266 nm microbeam laser, as analyzed by real-time confocal imaging (Supplementary Fig. 2c). These results suggest that BRM is not actively recruited to sites of UV damage. Moreover, immunoprecipitation of XPB-GFP did not reveal an interaction of TFIIH

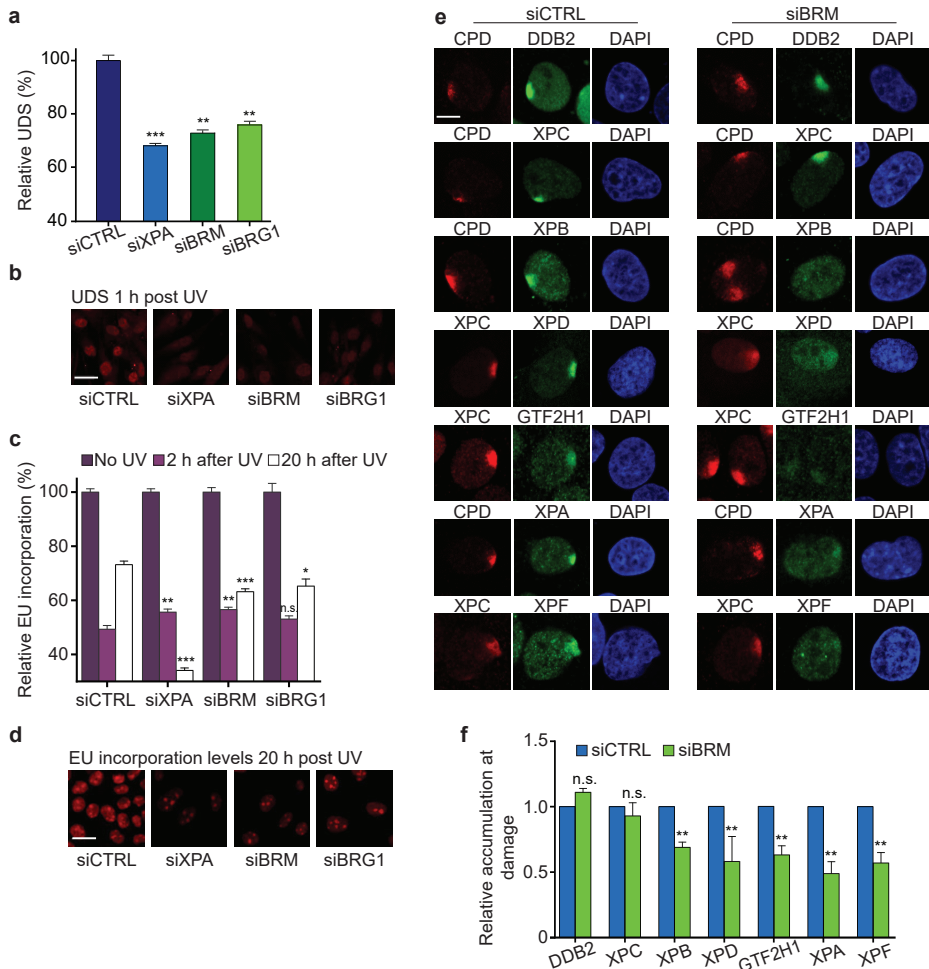


Figure 1. SWI/SNF is required for efficient NER. (a) Quantification of Unscheduled DNA Synthesis (UDS) in C5RO primary fibroblasts treated with non-targeting control (CTRL), XPA, BRM and BRG1 siRNAs (Supplementary Fig. 1a). UDS was determined by EdU incorporation for 1 h after UV-C (16 J/m²) irradiation followed by fluorescent staining of the incorporated EdU. Fluorescence was quantified and normalized to control, set to 100%. Mean & S.E.M. of >200 cells per sample from two independent experiments. **P < 0.01, ***P < 0.001, relative to siCTRL. (b) UDS representative pictures, 1 h after UV-C. Scale bar: 25 μ m. (c) Quantification of Recovery of RNA Synthesis (RRS) in U2OS cells treated with non-targeting control (CTRL), XPA, BRM and BRG1 siRNAs (Supplementary Fig. 1b). Transcription levels in non-irradiated cells and in cells 2 and 20 h after UV-C irradiation (6 J/m²) were determined by a 2 h pulse-labeling with the uridine analogue EU and subsequent fluorescent staining and measurement of incorporated EU. RRS levels were normalized to non-irradiated cells, set to 100%. Mean and S.E.M. of >200 cells per condition from at least two independent experiments. * P < 0.05, *** P < 0.001, relative to each siCTRL in each time point. (d) RRS representative pictures, 20 h after UV-C irradiation. Scale bar: 25 μ m. (e) Immunofluorescence (IF) showing recruitment of the indicated NER proteins (green channel) to local UV-C damage (LUD) in U2OS cells treated with control or BRM siRNAs (Supplementary Fig. 1c). Cells were fixed 30 min after inducing LUD with UV-C irradiation

(60 J/m²) through a microporous membrane (8 μm). UV lesions were marked with staining against CPD or XPC, red channel. DNA was stained with DAPI. Scale bar: 5 μm. (f) Quantification of NER proteins recruitment to LUD. Relative accumulation at LUD (over nuclear background) after siBRM was normalized to control, in which nuclear background was set at 0 and maximal signal at LUD set to 1.0 for each protein. Mean and S.E.M. of >100 cells per sample, of at least two independent experiments, except for GTF2H1 which was only performed once. ** P < 0.01, relative to siCTRL. n.s., non-significant.

with BRM, neither in the presence nor absence of UV-DNA damage (Supplementary Fig. 2d), while GTF2H1 was successfully co-purified with XPB-GFP, as expected. These observations indicate that BRM is not associated with TFIIH nor directly involved in its recruitment to chromatin, but suggest that BRM affects TFIIH chromatin binding in another way, possibly by regulating its general activity, stability or expression of its subunits.

BRM stabilizes TFIIH by promoting *GTF2H1* expression

The TFIIH complex consists of 10 subunits and becomes unstable if one of these is impaired^{15,29–31}. Given the fact that SWI/SNF acts in transcription regulation, we considered the possibility that BRM transcriptionally regulates one or more TFIIH genes. Therefore, we analyzed the individual expression of all TFIIH genes by real-time-qPCR (RT-qPCR) in U2OS cells after BRM knockdown. While expression of most TFIIH genes was unaffected by BRM knockdown, *GTF2H1* expression was strongly reduced (Fig. 3a). Immunoblot analysis revealed that this also resulted in lowered GTF2H1 protein levels (Fig. 3b), which we further corroborated by IF staining of GTF2H1 after BRM depletion using an independent siRNA (siBRM#2), to exclude siRNA off-target effects (Supplementary Fig. 3a,b). Besides GTF2H1, we also found mildly reduced expression of *XPB*, both at the mRNA and protein level. In contrast, protein levels of XPD and CCNH - whose mRNA levels were mildly increased -, and of TFIIIEβ, XPC and DDB2 were unaltered after BRM depletion (Fig. 3a,b). To verify that BRM can regulate *GTF2H1* transcriptionally, we re-analyzed published whole-genome BRM ChIP-seq data for HepG2³² and RWPE1³³ cells. In both cell types we observed an enrichment of BRM ChIP-seq signal at the *GTF2H1* promoter region, suggesting the association of BRM with active regulatory regions of the *GTF2H1* gene (Fig. 3c, Supplementary Fig. 3c). These results therefore suggest that BRM promotes *GTF2H1* expression and may explain why BRM depletion leads to defects in TFIIH chromatin loading, as GTF2H1 was shown to be essential for the structural integrity

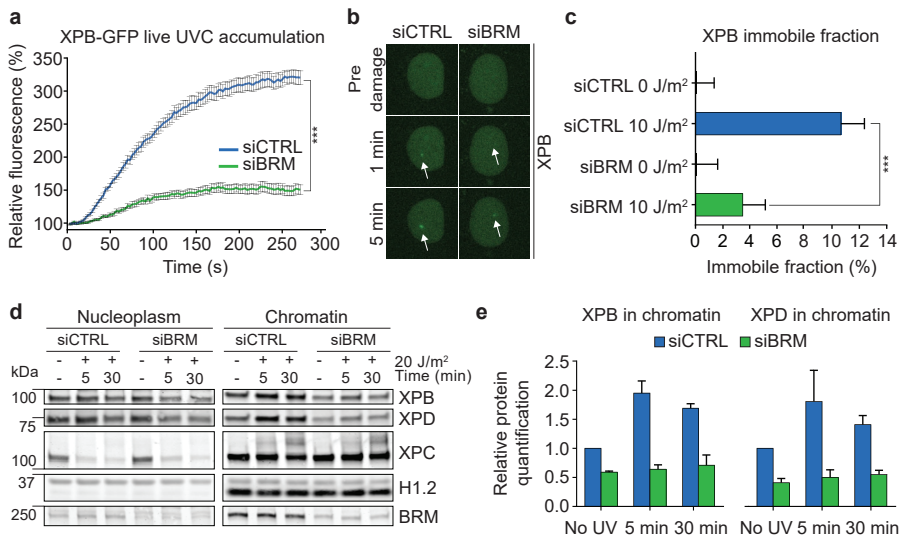


Figure 2. BRM is required for the recruitment of TFIIH to chromatin. (a) Real-time imaging of XPB-GFP accumulation at 266 nm UV-C laser-induced LUD in XPCS2BA cells treated with control and BRM siRNA (siCTRL and siBRM, respectively; Supplementary Fig. 1f). Pre-damage fluorescence intensity (nuclear background) was set to 100% (t=0). Mean & S.E.M. of three independent experiments each with more than 10 cells per condition. $P < 0.0001$, compared to siCTRL. (b) Representative images of real-time recruitment of XPB-GFP, which resides exclusively in the nucleus, to laser generated LUD. Arrows indicate LUD regions. (c) Quantification of XPB-GFP immobile fraction in XPCS2BA fibroblasts. The mobility of XPB-GFP was determined by Fluorescence Recovery After Photobleaching (FRAP) in mock and UV-C irradiated (10 J/m²) cells treated with non-targeting control (CTRL) or BRM siRNAs, as depicted in Supplementary Fig. 1h. The UV-induced immobile fraction (mean & S.E.M. from three independent experiments, with at least 10 cells measured per condition each time) was determined as described in Supplementary Fig. 1h. *** $P < 0.001$ relative to UV-irradiated siCTRL. (d) Immunostaining of soluble (nucleoplasm) and chromatin-bound XPB, XPD, XPC, BRM and H1.2 (as loading control) in U2OS cells treated with non-targeting control (CTRL) or BRM siRNAs. Cells were collected for protein fractionation at different time points after UV-C irradiation (20 J/m²). (e) Relative quantification of chromatin-bound XPB and XPD, normalized to non-irradiated siCTRL, set to 1.0. Mean & S.E.M. of two independent experiments. Full-size immunoblot scans are provided in Supplementary Fig. 6a.

of the TFIIH complex³¹.

To assess whether TFIIH indeed becomes unstable in the absence of BRM, we determined the half-life of XPB in BRM-depleted U2OS cells after blocking protein synthesis with cycloheximide (CHX) treatment. Quantification of XPB protein levels, normalized to DDB2, revealed a strongly accelerated proteasome-dependent degradation of XPB in the absence of BRM (Fig. 3d,e; Supplementary Fig. 3d). Importantly, XPB was similarly less stable in cells depleted of GTF2H1 by siRNA (Fig. 3d,e). To confirm that BRM

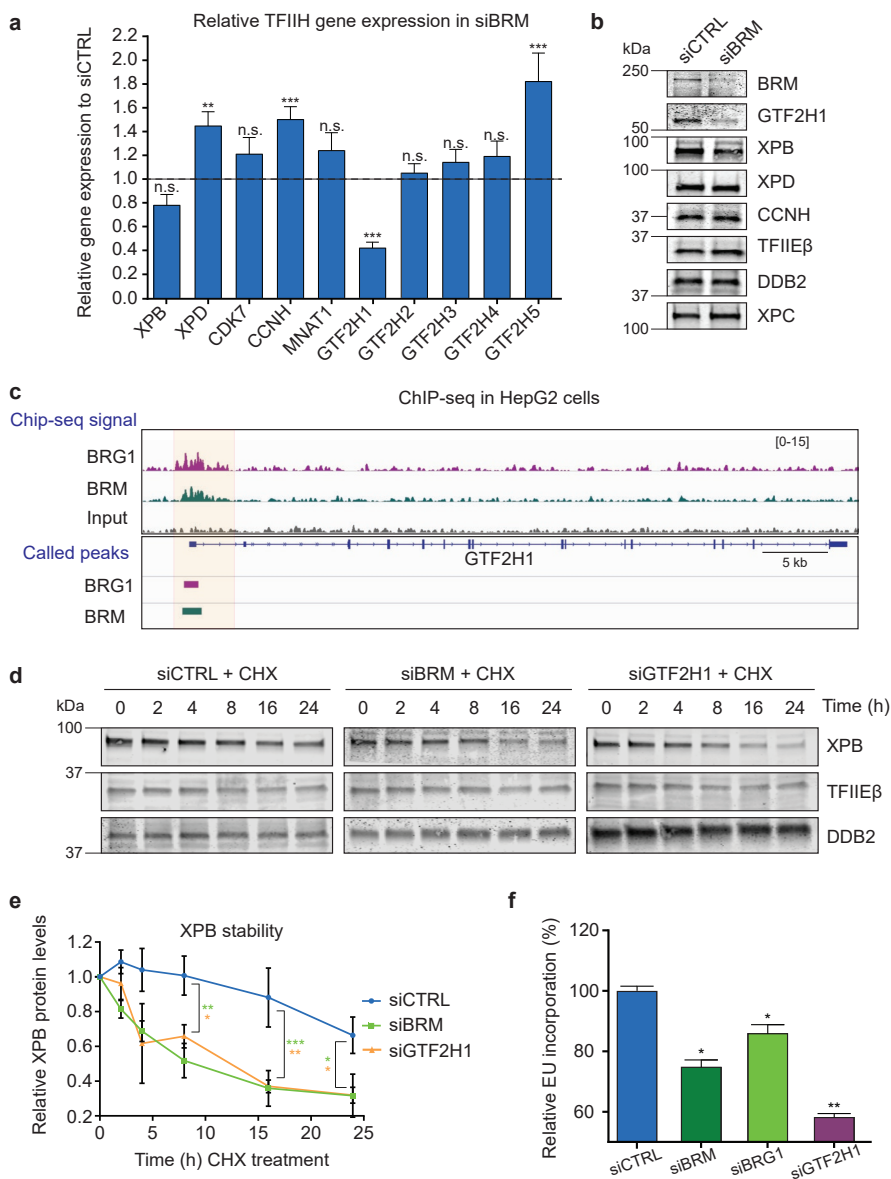


Figure 3. BRM stabilizes TFIIH by promoting GTF2H1 expression. (a) Relative quantification of individual TFIIH genes expression in U2OS cells treated with control (CTRL) or BRM siRNAs, as determined with RT-qPCR. Individual basal gene expression in BRM knockdown was normalized to siCTRL levels, which were set to 1.0 (dotted line in graph). *GAPDH* expression was used for normalization. Mean & S.E.M. of at least three independent experiments. ** $P < 0.01$, *** $P < 0.001$ relative expression in each gene to siCTRL. n.s., non-significant. (b) Immunoblot analysis of TFIIH protein levels (GTF2H1, XPB, XPD, CCNH), TFIIIE β , DDB2 and XPC from whole cell extracts of U2OS treated with control (CTRL) or BRM siRNAs. Representative immunoblots of two independent experiments. (c) BRG1 and BRM co-occupancy of *GTF2H1* promoter. Re-analysis of

published ChIP-seq data in which ChIP-seq signal density (top) and respective peaks (bottom) illustrate BRG1 (purple) and BRM (green) enrichment at the promoter of *GTF2H1* in HepG2 cells (upon shNS transfection³²). Promoter region of interest highlighted in light orange, signal density in reads per million. **(d)** XPB protein stability was evaluated in U2OS cells treated with control (CTRL) or BRM siRNAs at different time points after addition of 100 μ M cycloheximide (CHX) to inhibit protein synthesis. Immunostainings of TFIIE β and DDB2 were used as negative and loading controls, respectively. **(e)** Quantification of XPB protein levels normalized to DDB2 in time after addition of CHX. The total amount of XPB in whole cell lysates was set to 1.0 at t=0. Mean & S.E.M. of at least three independent experiments. * P < 0.05, ** P < 0.01, *** P < 0.001 for each time point of siBRM (green) or siGTF2H1 (orange) relative to siCTRL. **(f)** Relative quantification of transcription levels in U2OS cells treated with non-targeting control (CTRL), BRM, BRG1 or GTF2H1 siRNAs. Transcription was determined by measuring EU incorporation in non-irradiated cells 48 h after siRNA treatment. EU relative fluorescence intensity was set to 100% in siCTRL treated cells. Mean & S.E.M. of >200 cells from two (siGTF2H1) and three (siBRM and siBRG1) independent experiments. Full-size immunoblot scans are provided in Supplementary Fig. 6b,c.

depletion specifically affected TFIH and not other transcription factors as well (whose DNA-binding might be regulated by BRM^{5,34}), we tested the stability of subunit beta of transcription initiation factor IIE (TFIIE β). TFIIE β is involved in recruiting TFIH to the transcription initiation complex³⁵, but its stability was not affected by BRM knockdown (Fig. 3d, Supplementary Fig. 3e). These results, therefore, suggest that the TFIH complex is less stable in the absence of BRM because of reduced amounts of GTF2H1 that limit the stable assembly of functional TFIH complexes. This likely impairs the stability of TFIH subunits and TFIH function in transcription and NER. Indeed, either BRM or GTF2H1 depletion also reduced transcription levels in U2OS cells, likely due to limiting amounts of TFIH (Fig. 3f).

GTF2H1 expression rescues TFIH function in BRM/BRG1 depleted cells

To demonstrate that impaired TFIH function in BRM knockdown cells is mainly a consequence of GTF2H1 downregulation, we tested if ectopic expression of GFP-GTF2H1 or XPB-GFP (as control) reversed impaired TFIH DNA damage recruitment. Overexpression of both TFIH subunits did not affect XPD recruitment to LUD in control U2OS cells (Fig. 4a,b). However, overexpression of GFP-GTF2H1, but not of XPB-GFP, rescued XPD accumulation to LUD in BRM and GTF2H1 depleted cells, confirming that reduced GTF2H1 expression, as a consequence of BRM depletion, impairs TFIH function.

Since BRG1 depletion also resulted in GG- and TC-NER defects (Fig. 1a-d), similar to BRM, we tested whether BRG1 knockdown also affected

TFIIH function via GTF2H1. Depletion of BRG1 led to lower overall transcription (Fig. 3f) and reduced GTF2H1 protein levels, as assessed by both immunoblot (Supplementary Fig. 3f) and IF using independent siRNAs to exclude off-target effects (Supplementary Fig. 3g,h). BRG1 was furthermore found to co-occupy the *GTF2H1* promoter together with BRM (Fig. 3c, Supplementary Fig. 3c). Also, BRG1 depletion led to reduced XPD recruitment to LUD (Supplementary Fig. 3i), which was rescued by ectopic expression of GTF2H1, but not of XPB (Fig. 4b,c). BRG1 did not localize to LUD induced by irradiation through a microporous membrane (Supplementary Fig. 2b) or by 266 nm microbeam laser (Supplementary Fig. 2c), implying that the protein itself does not directly participate in the NER reaction. Moreover, both siBRM and siBRG1 did not alter cell cycle distribution (Supplementary Fig. 3j) nor did they further decrease reduced XPD recruitment following GTF2H1 depletion (Supplementary Fig. 3k), indicating that BRM and BRG1 do not impair TFIIH recruitment due to indirect effects on the cell cycle or independently of GTF2H1. Overall, these results indicate that the activity of both BRM and BRG1 is necessary to ensure normal GTF2H1 levels and TFIIH function, and, therefore, NER performance.

Chronic BRG1-deficient cancer cells restore GTF2H1

Because BRM and BRG1 are frequently mutated in cancer³, we investigated if cancer cell lines with SWI/SNF mutations showed low GTF2H1 protein levels, as these cells would then likely be more susceptible to DNA damaging chemotherapeutic drugs. Unexpectedly, BRG1-deficient non-small cell lung cancer (NSCLC) lines A549 and H1299^{36–38} showed normal GTF2H1 levels in comparison to U2OS (Fig. 5a,b). Strikingly, however, BRM knockdown in these NSCLC cell lines resulted in lower GTF2H1 expression, demonstrating that SWI/SNF-mediated expression of GTF2H1 is not cell type-specific. BRG1 knockdown only resulted in lower GTF2H1 levels in U2OS cells, which are wild-type for BRG1, but not in the BRG1-deficient A549 and H1299 cell lines (Fig. 5a,b), confirming again that GTF2H1 downregulation in U2OS cells is not due to an siRNA-mediated off-target effect. We next tested GTF2H1 protein levels by IF in additional BRG1 and/or BRM deficient cancer cell lines. However, also BRG1-deficient Panc-1 and Hs 700T cells, BRM deficient A2780 cells and BRM/BRG1-deficient SW13 and C33A cells, all consistently showed normal or even increased GTF2H1

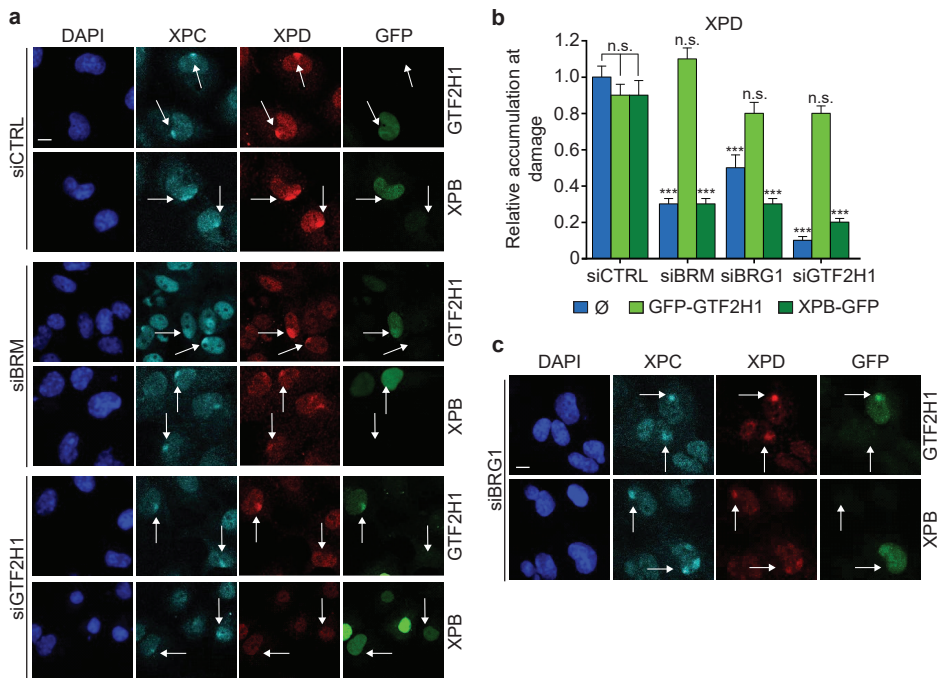


Figure 4. GTF2H1 expression rescues TFIIH in BRM/BRG1 depleted cells. Representative IF of XPD recruitment (red channel) to LUD marked by XPC (cyan channel). U2OS cells were fixed 30 min after local UV-C irradiation (60 J/m^2) through a microporous membrane ($8 \mu\text{m}$). (a) U2OS cells were treated with control (CTRL), BRM or GTF2H1 siRNAs and transiently transfected with TFIIH subunits XPB or GTF2H1 fused to GFP (green channel). Scale bar: $10 \mu\text{m}$. (b) Quantification of XPD recruitment to LUD. Relative accumulation at LUD (over nuclear background) in each condition was normalized to control (siCTRL without transient transfection of TFIIH subunits, indicated by “empty” symbol), in which nuclear background was set at 0 and maximal signal at LUD set to 1.0 (> 50 cells per sample, mean & S.E.M. from four independent experiments). *** $P < 0.001$, relative to siCTRL without transient transfection of TFIIH subunits. (c) U2OS cells were treated with siRNA against BRG1 and transiently transfected with TFIIH subunits XPB or GTF2H1 fused to GFP (green channel). Scale bar: $10 \mu\text{m}$. Arrows highlight LUD in a mixed population of non-transfected and transfected cells with GFP-GTF2H1 or XPB-GFP (green cells in the right panel). n.s., non-significant.

levels, as compared to MRC5, Hs 578T and U2OS cells (Supplementary Fig. 4a,b). The puzzling finding that chronic BRG1 and/or BRM deficiency in these cancer cell lines does not lead to permanent downregulation of GTF2H1, whereas transient depletion does, indicates that there might be an adaptive, compensatory mechanism in these cells that restores GTF2H1 expression to prevent chronic TFIIH dysfunction.

BRM and BRG1 have been shown to be able to compensate for some of each other’s functions^{36,39} and in many BRG1-deficient cancer cells including

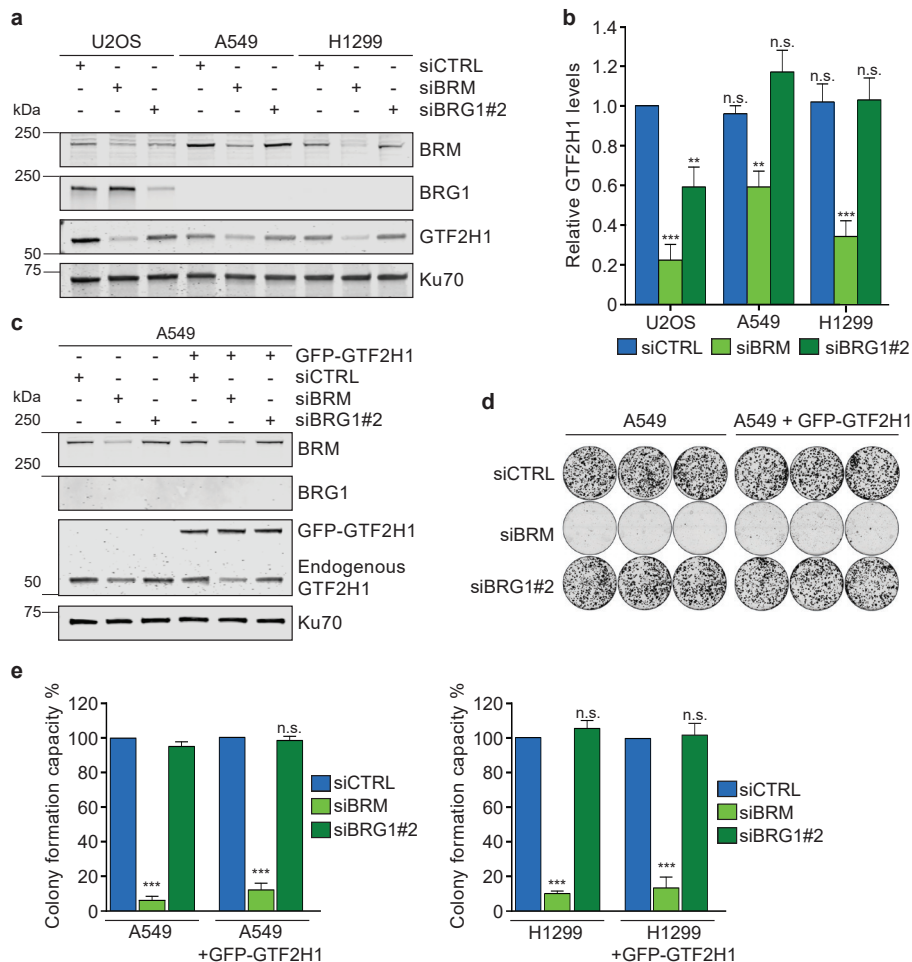


Figure 5. Cancer cells with chronic BRG1 deficiency restore GTF2H1 expression. (a) Immunoblot showing total protein levels of BRM, BRG1 and GTF2H1, in cell lysates of U2OS and BRG1-deficient non-small lung cancer cell (NSCLC) lines A549 and H1299 treated with control (CTRL), BRG1 or BRM siRNAs. Ku70 was used as loading control. (b) Relative quantification of GTF2H1 protein levels in U2OS, A549 and H1299 cells transfected with control (CTRL), BRG1 or BRM siRNA. GTF2H1 levels were normalized to Ku70 and the total relative amount of GTF2H1 in whole cell lysates was set to 1.0 in U2OS siCTRL. Mean & S.E.M. from at least three independent experiments ** $P < 0.01$, *** $P < 0.001$, n.s., non-significant. (c) A549 cells with and without stable expression of GFP-GTF2H1, driven by the ectopic PGK promoter, were treated with control (CTRL), BRM or BRG1 siRNAs. Cell lysates were analyzed by immunoblotting against BRM and GTF2H1. Ku70 was used as loading control. (d) A549 cells, with or without stable expression of GFP-GTF2H1 were seeded 48 h after transfection with control (CTRL), BRM or BRG1 siRNAs, in triplicate, at a density of 1000 cells per well and grown for 12 before fixation and staining. (e) Quantification of colony forming capacity of A549 (shown in d) and H1299 (shown in Supplementary Fig. 4e) cell lines with or without stable GFP-GTF2H1 expression and treated with control (CTRL), BRM or BRG1 siRNAs. Clonal capacity was normalized to 100% in control conditions (CTRL). Mean & S.E.M. of three independent experiments, each performed in triplicate. *** $P < 0.001$, n.s., non-significant, relative to siCTRL. Full-size immunoblot scans are provided in Supplementary Fig. 7a,b.

A549 and H1299, BRM has even become essential for cellular growth^{36,38,40}. To test if regulation of GTF2H1 levels are in part responsible for BRM having become essential in BRG1-deficient cells, we generated A549 and H1299 cell lines stably expressing GFP-GTF2H1 (Fig. 5c, Supplementary Fig. 4c). siRNA-mediated BRM knockdown in these cells only reduced the expression of endogenous GTF2H1 (Fig. 5c, Supplementary Fig. 4c,d), guaranteeing that expression of the *GFP-GTF2H1* transgene, driven by the ectopic PGK promoter, is preserved even in the absence of both SWI/SNF ATPases. We then performed colony forming assays and found that siRNA-mediated depletion of BRM led to profound growth inhibition of BRG1-deficient A549 and H1299 cells. This, however, was not rescued by stable GFP-GTF2H1 expression (Fig. 5c-e, Supplementary Fig. 4e). As expected, control and BRG1 siRNA did not affect the proliferation capacity of these BRG1 deficient cells. These results indicate that synthetic lethality induced by BRM depletion in BRG1-deficient cancer cells is not dependent on GTF2H1 expression and likely involves other functions of these ATPases.

DNA damage sensitivity of BRM cells correlates with GTF2H1 levels

To confirm that cells can restore GTF2H1 expression as adaptation to chronic SWI/SNF dysfunction and to investigate the functional consequences, we permanently knocked out BRM and BRG1 in immortalized MRC5 fibroblasts, by transfection with sgRNAs targeting either *BRM* (sgBRM) or *BRG1* (sgBRG1). After careful selection of transfected cells, we confirmed by immunoblotting that this heterogeneous pool of transfected cells showed an overall highly efficient depletion of BRM or BRG1 and a concomitant downregulation of GTF2H1 levels (Fig. 6a,b). However, after culturing cells for multiple passages, IF of the heterogeneous pool of BRM and BRG1 knockout cells revealed that individual cells had either retained the low GTF2H1 expression or restored it to wild-type level (Supplementary Fig. 5a). Establishment of multiple clonal cell lines from the MRC5 sgBRM pool of cells showed that many clones exhibited normal GTF2H1 levels, despite having no detectable BRM expression (Supplementary Fig. 5b). These striking findings show that cells are often able to adapt to the loss of one of the ATPase SWI/SNF subunits by restoring normal GTF2H1 expression levels.

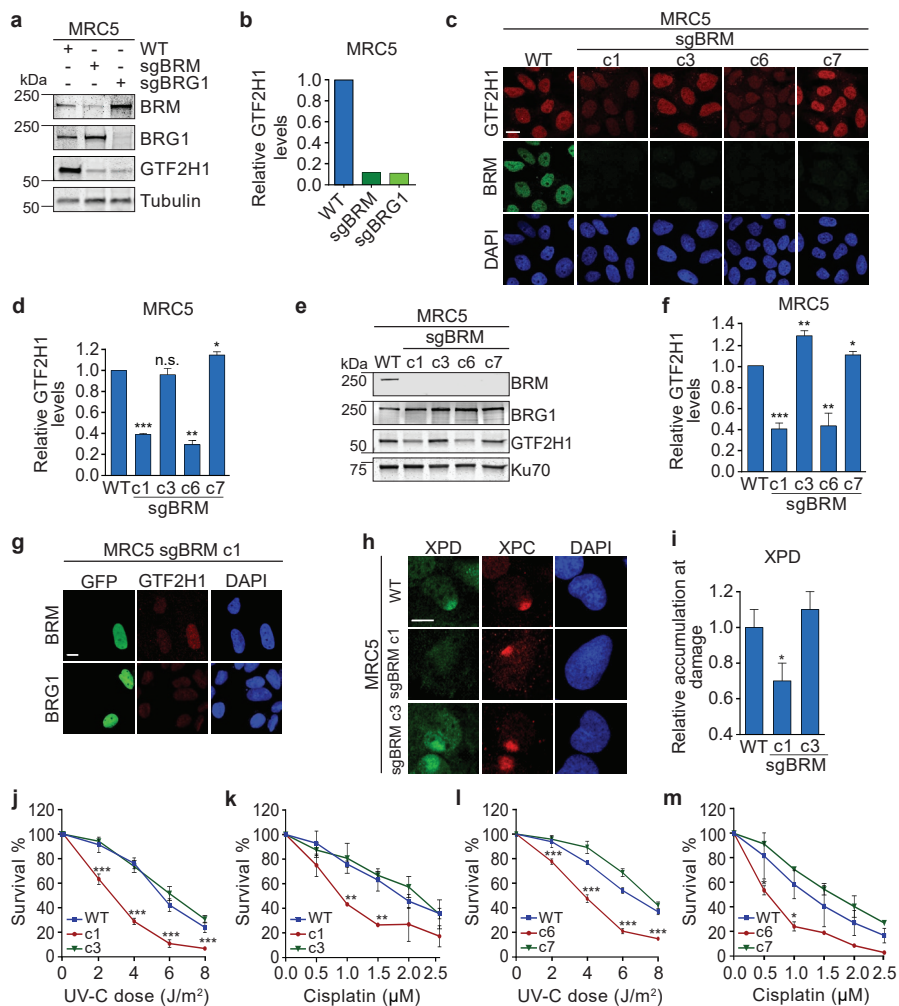


Figure 6. DNA damage sensitivity of BRM deficient cells correlates with GTF2H1 expression. (a) Immunoblot of BRM, BRG1 and GTF2H1 in MRC5 wild-type (WT) cells and cells transfected with sgRNA against BRM or BRG1. (b) Quantification of GTF2H1 levels in immunoblot shown in (a), corrected by Tubulin loading control, and set to 1.0 in MRC5 WT. (c) IF of total GTF2H1 and BRM levels in MRC5 WT and sgBRM knockout clones c1, c3, c6 and c7. Scale bar: 10 μ m. (d) Quantification of GTF2H1 IF signal (shown in c). Total GTF2H1 levels were normalized to MRC5 WT, set to 1.0. Mean & S.E.M. of >200 cells from two independent experiments (e) Immunoblot of BRM, BRG1 and GTF2H1 levels in MRC5 WT and sgBRM clones c1, c3, c6 and c7. (f) Quantification of GTF2H1 levels shown in (e), as described in (b), using Ku70 as loading control. Mean & S.E.M. from four independent experiments. (g) GTF2H1 levels in a mixed population of MRC5 sgBRM knockout clone c1 cells non-transfected or transfected with BRM-GFP or BRG1-GFP. Scale bar: 5 μ m. (h) XPD recruitment to LUD in MRC5 WT and sgBRM knockout clones c1 and c3, 30 min after damage. Scale bar: 5 μ m. (i) Relative quantification of XPD recruitment to LUD (shown in h) in MRC5 WT and sgBRM knockout clones c1 and c3, normalized to WT, as described in the methods. Mean & S.E.M. of >65 cells per sample. (j) UV-C colony survival of MRC5 WT cells and sgBRM knockout clones c1 and c3. (k) Cisplatin colony

survival of MRC5 WT and BRM knockout clones c1 and c3. **(l)** UV-C colony survival of MRC5 WT cells and BRM knockout clones c6 and c7. **(m)** Cisplatin colony survival of MRC5 WT cells and BRM knockout clones c6 and c7. Colony number was normalized to untreated conditions. Mean & S.E.M. of four (UV-survival) and two (cisplatin-survival) independent experiments, each performed in triplicate, are presented. * $P < 0.05$, ** $P < 0.01$, *** $P < 0.001$, relative to WT, n.s., non-significant. Full-size immunoblot scans are provided in Supplementary Fig. 7c,d.

We next selected two clones with low (c1 and c6) and two clones with normal (c3 and c7) GTF2H1 expression and confirmed the reduced and rescued GTF2H1 levels and BRM knockout by IF and immunoblot (Fig. 6c-f) and by sequencing the sgBRM target region (Supplementary Fig. 5c). Transient expression of BRM-GFP in c1 cells increased GTF2H1 expression (Fig. 6g), clearly demonstrating not only that the lower GTF2H1 levels are caused by BRM depletion but also that these are reversible. Transient BRG1-GFP expression, however, did not increase GTF2H1 protein levels in these cells (Fig. 6g). Likewise, stable ectopic expression of GFP-tagged BRG1 in U2OS cells did not prevent the reduction in GTF2H1 levels after siBRM treatment (Supplementary Fig. 5d). These results suggest that restoration of GTF2H1 levels, as observed in cells with chronic BRM/BRG1 deficiency, is likely not due to compensation by the other ATPase.

Due to the central function of TFIIH in NER, we considered whether GTF2H1 levels in BRM knockout cells correlate with NER capacity and thus with sensitivity to DNA damaging agents. XPD recruitment to LUD was severely impaired in c1 cells with low GTF2H1 levels, but not in c3 cells with normal GTF2H1 levels (Fig. 6h,i). Clonal UV-survival assays corroborated these observations, showing that only c1 cells were UV-hypersensitive (Fig. 6j). These intriguing results could imply that cancer cells that have lost the activity of SWI/SNF subunit(s) may be differentially sensitive to DNA damaging chemotherapeutics depending on their GTF2H1 levels. Platinum-based drugs such as cisplatin are widely administered to treat various types of solid tumors⁴¹ and kill cells by inducing DNA intra- and interstrand crosslinks that are mainly repaired by NER⁴² and interstrand crosslink repair. Therefore, we tested cisplatin sensitivity of c1 and c3 cells to evaluate if this also correlates with their GTF2H1 expression levels. Markedly, c1 cells, but not c3 cells, showed increased sensitivity to cisplatin (Fig. 6k). To verify these findings, we also tested DNA damage sensitivity of BRM knockout clones c6 and c7, exhibiting respectively low and restored GTF2H1 levels (Fig. 6c-f). UV and cisplatin survival of these

clones (Fig. 6l,m) confirmed that indeed GTF2H1 levels in BRM knockout cells determine NER capacity and sensitivity to DNA damage. These results indicate that loss of BRM sensitizes cells to cisplatin only if GTF2H1 protein levels are lowered, and imply that GTF2H1 levels could be used as a predictive marker for platinum drug sensitivity of SWI/SNF-deficient cancers.

Discussion

Inactivating mutations in SWI/SNF subunit genes are amongst the most recurrent mutations found in all human cancers^{3,4}. For instance, *BRG1* is mutated in 90% of small cell ovarian, 27% of skin and 5% of small cell lung cancers^{1,7,37}. The homologous SWI/SNF ATPase *BRM* is also recurrently lost in multiple primary tumors and cancer cell lines, such as in over 15% of lung, ovarian and breast cancers⁴³ and was found to protect mice against UV-induced skin cancer⁴⁴. It is thus advantageous to identify general vulnerabilities caused by SWI/SNF deficiency in pathways with anti-tumorigenic function, to create opportunities for the development of effective therapeutic approaches.

In this study, we show that both BRM and BRG1 promote normal TFIIH function in transcription and NER by regulating the expression of the *GTF2H1* gene (Fig. 7). Both RT-qPCR and immunoblot analysis revealed significantly lower expression of GTF2H1 and mildly lower expression of XPB after BRM knockdown. Both these TFIIH subunits are required for recruitment of the TFIIH complex to damaged DNA^{14,16}, but only the ectopic expression of GTF2H1 - not of XPB - rescued the binding of TFIIH to DNA damage in BRM and BRG1 depleted cells. This shows that lowered levels of GTF2H1, caused by BRM or BRG1 knockdown, act as a limiting factor for the assembly of functional TFIIH complexes, in agreement with recent literature describing GTF2H1 as essential for TFIIH complex integrity and stability^{31,45}. Limiting amounts of functional TFIIH complexes likely impair overall TFIIH functions, in accordance with the observed decreased transcription levels and lower NER performance (Fig. 7).

ATP-dependent chromatin remodelers like SWI/SNF are thought to make

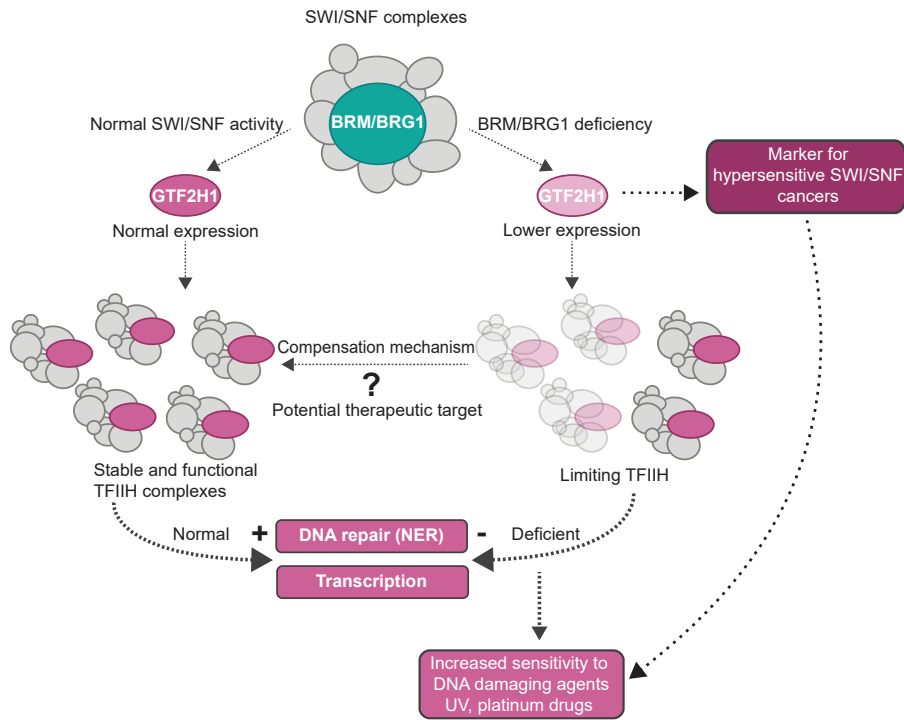


Figure 7. Low GTF2H1 expression as a predictive marker for DNA damage hypersensitive SWI/SNF cancers. BRM- and BRG1-containing SWI/SNF complexes promote the expression of the *GTF2H1* gene, a subunit of the TFIIH complex. In BRM- and BRG1-wild-type cells, normal expression of GTF2H1 allows the assembly of stable and functional TFIIH complexes, proficient in transcription and NER. When BRM or BRG1 are deficient, expression of GTF2H1 is lower, limiting the assembly of functional TFIIH complexes. As a consequence, transcription levels and NER capacity are lower, and cells become more sensitive to DNA damaging agents like UV and chemotherapeutic platinum drugs. Therefore, low GTF2H1 levels can likely be used as a marker to identify SWI/SNF cancers with increased sensitivity to chemotherapeutic drugs. However, cells with permanent loss of either BRM or BRG1 subunit can also adapt and restore the expression of GTF2H1, thus presenting normal transcription and NER activity. The mechanism underlying this adaption response is currently unknown, but if elucidated could be therapeutically exploited to specifically target SWI/SNF cancers with restored GTF2H1 expression, leaving surrounding non-tumor tissues intact.

chromatin more accessible to DNA repair proteins^{8,9,20}. In line with this idea, the yeast Snf5 and Snf6 SWI/SNF subunits were shown to bind XPC and mediate UV-induced nucleosome remodeling²³, while in humans BRG1 was reported to facilitate XPC recruitment to damaged DNA²⁵. However, in another study, a different role for human BRG1 in NER was proposed, in facilitating XPG and PCNA - but not DDB2 and XPC - recruitment to sites of damaged DNA²⁴. Our data, indeed, shows that both BRG1 and BRM are essential for efficient recruitment of late NER factors (TFIIH

and downstream NER proteins) rather than for binding of the early DNA damage sensing factors (XPC, DDB2, and CSB) to DNA lesions. Impaired recruitment of the late NER factors in the absence of SWI/SNF is, however, not caused by reduced chromatin accessibility, but an indirect result of limiting amounts of functional TFIIH. Furthermore, we did not observe BRM and BRG1 recruitment to UV-damaged DNA, further corroborating that SWI/SNF's main involvement in the UV-DDR is not in the control of chromatin accessibility at sites of UV damage.

SWI/SNF complexes are thought to be recruited to chromatin to remodel nucleosomes in enhancer and promoter regions to regulate transcription^{7,46}. In line with this, we observed in two different cell types that BRM and BRG1 ChIP-seq signals are enriched at the *GTF2H1* promoter. SWI/SNF's influence on gene expression is, however, contextual, in that it represses some promoters while it stimulates others⁵, which may also be evident from the differential effect of BRM knockdown on transcription of TFIIH genes that we observed. One major way through which SWI/SNF promotes transcription is by antagonizing the repressive activity of Polycomb complexes, as loss of SWI/SNF was shown to lead to repression of Polycomb target genes^{47,48}. Nevertheless, we were unable to alleviate downregulation of *GTF2H1* upon knockdown of BRM or BRG1 with specific inhibitors targeting EZH2, a functional enzymatic component of the Polycomb repressive Complex 2. This suggests that other mechanisms, possibly involving repressive chromatin structures or epigenetic marks, account for the diminished *GTF2H1* expression.

Besides NER, SWI/SNF chromatin remodeling complexes are also involved in other DDR pathways^{8,9,49}, including regulation of DSB repair by non-homologous end-joining and/or homologous recombination^{50,51}. It is, thus, likely that SWI/SNF mutations found in cancer contribute to increased genomic instability by disrupting multiple DDR pathways. As the majority of BRG1-deficient tumors are negative for mutations in other genes that can be targeted by existing therapies⁴⁰, it would be advantageous to exploit DDR deficiencies in SWI/SNF cancers therapeutically. Based on our analysis, one such DDR deficiency could be impaired NER due to downregulation of *GTF2H1* expression, rendering SWI/SNF cancers more sensitive to DNA damaging chemotherapeutic drugs such as cisplatin

(Fig. 7). However, we observed that in multiple established BRG1 and/or BRM-deficient cancer cell lines, GTF2H1 levels were not lowered, which is probably due to an, yet unknown, adaptation mechanism to compensate for the loss of BRM/BRG1 activity (Fig. 7). Previous studies showed partial mutual compensation between both ATPases^{36,38,40}. Nevertheless, the fact that normal GTF2H1 levels were observed in cells lacking both BRG1 and BRM and that overexpression of BRG1 did not increase GTF2H1 levels in BRM deficient cells suggests that BRM and BRG1 do not compensate for each other in regulating GTF2H1 expression. Our experiments with MRC5 BRM knockout cell lines confirm that cells can adapt to the loss of one of the SWI/SNF ATPases. Although knockout of BRM led to an initial overall reduction in GTF2H1 levels, after prolonged culturing and clonal selection we observed that many clones displayed normal GTF2H1 expression. Importantly, cells exhibited hypersensitivity to DNA damage induction by UV irradiation and cisplatin treatment only when GTF2H1 levels were low.

Recently, it was suggested that BRG1 expression could be used as a predictive biomarker for platinum-based chemotherapy response in NSCLC lines^{52,53}. However, as we here demonstrate, sensitivity of SWI/SNF-deficient cells to DNA damaging agents such as cisplatin mainly depends on GTF2H1 expression levels. Therefore, reduced GTF2H1 expression may be a better predictive marker for platinum-drug sensitivity of SWI/SNF-deficient cancers (Fig. 7). Moreover, given the importance of TFIIH for transcription and repair, elucidating the mechanisms underlying SWI/SNF regulation of GTF2H1 expression and those that allow cells to adapt and restore GTF2H1 levels will be key to develop new strategies targeting SWI/SNF cancers. Such knowledge could potentially reveal how to revert the adaptation response to lower GTF2H1 levels, rendering SWI/SNF-deficient cells more susceptible to platinum drug chemotherapy.

Methods

Cell lines, culture conditions and treatments. U2OS (ATCC), SV40-immortalized human fibroblasts MRC5 (ATCC) and XP4PA⁵⁴ (XPC-deficient, with stable expression of XPC-GFP), XPCS2BA (XPB-deficient, with stable expression of XPB-GFP²⁸) and CS1AN (CSB-deficient, with stable expression

of GFP-CSB⁵⁵) were cultured under standard conditions in a 1:1 mixture of DMEM (Lonza) and Ham's F10 (Lonza) supplemented with 10% fetal calf serum (FCS). C5RO primary fibroblasts (established in our laboratory) were cultured in Ham's F10 supplemented with 12% FCS; H1299 NSCLC (provided by Dr. Bert van der Horst), A549 NSCLC (provided by Dr. Suzan Pas), Hs 578T⁵⁶ breast cancer, A2780³⁸ ovarian cancer (provided by Corine Beaufort and Dr. John Martens), Hs 700T³⁶ and Panc-1⁵⁷ pancreatic cancer (provided by Dr. Bernadette van den Hoogen), SW13³⁶ adrenal cortex carcinoma and C33A³⁶ cervical carcinoma (provided by Dr. Jan van der Knaap) cells were cultured in a 1:1 mixture of DMEM (Lonza) and RPMI (Sigma) medium supplemented with 10% FCS. Stable XPC-GFP expressing XP4PA cells were generated using lentiviral transduction and selected with 0.3 µg/mL Puromycin and FACS. Stable GFP-GTF2H1 expressing cells (A549, H1299) were generated using lentiviral transduction and selection with 5-10 µg/mL Blasticidin. Stable BRM-GFP and BRG1-GFP expressing U2OS cells were generated using transfection and selection with 10 µg/mL Blasticidin. All cells were cultured in medium containing 1% penicillin-streptomycin at 37°C and 5% CO₂. siRNA transfections were performed using RNAiMax (Invitrogen) 2 days before each experiment, according to the manufacturer's instructions. Plasmids transfections were performed using FuGENE 6 (Promega), according to the manufacturer's instructions. All cell lines were regularly tested for mycoplasma contamination.

Plasmids, sgRNA, and siRNA. Full-length human cDNAs of GTF2H1, BRG1 and BRM (a kind gift from Dr. Kyle Miller⁵⁸), were fused to GFP and inserted into pLenti-PGK-Blast-DEST⁵⁹ to generate plasmids GFP-GTF2H1, BRG1-GFP and BRM-GFP. Full-length human XPC cDNA was fused to GFP and inserted into pLenti-CMV-Puro-DEST⁵⁹ to generate plasmid XPC-GFP. For the generation of knockout cell lines, sgRNA sequences targeting *BRM* (GTCTCCAGCCCTATGTCTGG) and *BRG1* (CAGCTGGTTCTGGTTAAATG) coding regions were cloned into pLenti-CRISPR-V1⁶⁰. Cloning and plasmid details are available upon request. siRNA oligomers were purchased from GE Healthcare: CTRL (D-001210-05), BRM#1 (J-017253-06), BRM#2 (J-017253-07), BRG1 (L-010431-00), BRG1#2 (J-010431-06), BRG1#3 (J-010431-07), GTF2H1 (L-010924-00) and XPA (MJAWM-000011).

UV-C irradiation. UV-C irradiation was inflicted using a germicidal lamp

(254 nm; TUV lamp, Phillips) with the indicated doses after washing cells with PBS. Local damage was generated using 60 J/m² of UV irradiation through an 8 µm polycarbonate filter (Millipore), as described in van Cuijk *et al*⁶¹.

Unscheduled DNA Synthesis and Recovery of RNA Synthesis.

Fluorescent UDS and RRS were performed as described before⁶². In short, for UDS C5RO primary fibroblasts were grown on coverslips and treated with siRNAs 48 h before UV-C irradiation (16 J/m²). After irradiation, cells were incubated for 1 h in medium containing 5-ethynyl-2'-deoxyuridine (EdU, Invitrogen). For RRS, U2OS cells were seeded on coverslips and 48 h after siRNA transfection irradiated with 6 J/m² UV-C and allowed to recover for 2 or 20 h. Irradiated and non-irradiated cells were incubated for 2 h in medium containing 5-ethynyl-uridine (EU, Jena Biosciences). Cells were fixed in 4% paraformaldehyde and permeabilized with 0.1% Triton X-100 in PBS. EdU or EU incorporation was visualized by incubating cells for 1 h at room temperature with Click-it reaction cocktail containing Atto 594 Azide (60 µM, Atto Tec.), Tris-HCl (50 mM, pH 7.6), CuSO₄*5H₂O (4mM, Sigma) and ascorbic acid (10 mM, Sigma). After washes in 0.1% Triton-X100 in PBS, DNA was stained with DAPI (Sigma), and slides were mounted using Aqua-Poly/Mount (Polysciences, Inc.). Images were acquired using an LSM700 microscope equipped with a 40x Plan-apochromat 1.3 NA oil immersion lens (Carl Zeiss Micro Imaging Inc.). UDS and RRS levels were quantified by measuring the total nuclear fluorescence intensities (in at least 100 cells per experiment) with FIJI image analysis software. Intensity levels were averaged and normalized to the fluorescence levels in control conditions, which were set at 100%.

Immunofluorescence. Cells were grown on coverslips, fixed in 4% paraformaldehyde and permeabilized in PBS containing 0.5% Triton X-100. DNA was denatured for 5 min with 70 mM NaOH to allow CPD binding by the antibody. Next, cells were incubated for 1 h with blocking solution 3% BSA in PBS-T (0.1% Tween 20) and subsequently incubated with antibodies diluted in 1% BSA with PBS-T (0.1% Tween 20) for 1-2 h at room temperature or overnight at 4°C. To visualize primary antibodies, cells were incubated for 1 h at room temperature with secondary antibodies conjugated to Alexa fluorochromes 488, 555 or 633 (Invitrogen). DNA

was stained with DAPI (Sigma), and slides were mounted using Aqua-Poly/Mount (Polysciences, Inc.). Antibodies used are summarized in Supplementary tables 1 and 2. Images were acquired using an LSM700 microscope equipped with a 40x Plan-apochromat 1.3 NA oil immersion lens (Carl Zeiss Micro Imaging Inc.). Using FIJI image analysis software, we determined protein accumulation at lesion sites by dividing the overall fluorescence signal intensity at LUDs by the protein overall nuclear intensity. In Fig. 1f and Fig. 6g zero accumulation (nuclear background) was set at 0 and maximum accumulation (above nuclear background) in control conditions at 1.0.

Fluorescence Recovery After Photobleaching (FRAP). FRAP experiments were performed as previously described^{61,63}, using a Leica TCS SP5 microscope (with LAS AF software, Leica) equipped with a 40x/1.25 NA HCX PL APO CS oil immersion lens (Leica Microsystems), at 37°C and 5% CO₂. Briefly, a strip spanning the nucleus width (512x16 pixels) at 1400 Hz of a 488 nm laser, with a zoom of 12x was used to measure the fluorescence signal every 100 ms until a steady-state was reached (pre-bleach). Fluorescence signals were then photobleached using 100% power of the 488 nm laser and recovery of fluorescence in the strip was monitored every 22 ms until a steady-state was reached. Fluorescence signals were normalized to the average pre-bleach fluorescence after background signal subtraction. Three independent experiments were performed, with the acquisition of 10 cells for each condition in each experiment. The immobile fraction (F_{imm}), shown in Fig. 2c, was determined using the fluorescence intensity recorded immediately after bleaching (I_0) and the average fluorescence signal after reaching steady-state from the unchallenged cells ($I_{final,unc}$) and UV-irradiated cells ($I_{final,UV}$)⁶¹:

$$F_{imm} = 1 - \frac{I_{final,UV} - I_0,UV}{I_{final,unc} - I_0,UV} .$$

Real-time protein recruitment to UV-C laser induced damage.

To induce local UV-C DNA damage in living cells, a 2 mW pulsed (7.8 kHz) diode pumped solid state laser emitting at 266 nm (Rapp Opto Electronic, Hamburg GmbH) coupled to a Leica TCS SP5 confocal microscope was used, as described previously⁶². Cells seeded on quartz coverslips were imaged and irradiated via a Ultrafluar quartz 100x/1.35 NA glycerol

immersion lens (Carl Zeiss Micro Imaging Inc.) at 37°C and 5% CO₂. Resulting accumulation curves were corrected for background values and normalized to the relative fluorescence signal before local irradiation.

Chromatin fractionation. U2OS cells were grown to confluency on 10 cm dishes, UV-C irradiated with the indicated dose and lysed in lysis buffer (30 mM HEPES pH 7.6, 1 mM MgCl₂, 130 mM NaCl, 0.5% Triton X-100, 0.5 mM DTT and EDTA-free protease inhibitor cocktail (Roche)), at 4°C for 30 min. Non-chromatin bound proteins were recovered by centrifugation (10 min, 4°C, 16100 *g*). Chromatin-containing pellet was resuspended in lysis buffer supplemented with 250 U/μL of Benzonase (Merck Millipore) and incubated for 1 h at 4°C. Equal amounts of sample were used for SDS-PAGE gels and immunoblotting analysis.

Cycloheximide (CHX) protein stability assay. Protein synthesis was inhibited by adding 100 μM CHX (Enzo) to cells in culture. Concomitantly, for the experiment shown in Supplementary Fig. 3a, protein degradation was inhibited by adding 10 μM MG132 (Sigma) before the addition of CHX. Cells were lysed at the indicated time points after CHX addition, for 30 min at 4°C in RIPA buffer (25 mM Tris-HCl pH 7.5, 150 mM NaCl, 6mM EDTA, 0.1% SDS, 1% Triton X-100, 1% NP-40, supplemented with EDTA-free protease inhibitor cocktail (Roche)). Whole cell extracts were recovered by centrifugation (20 min at 4°C and 1400 *g*) and quantified using the BCA Protein Assay Kit (Pierce, ThermoFisher Scientific). Equal amounts of protein from total cell lysates were used for immunoblot analysis.

Immunoblotting. Protein samples (whole cell extracts or cell fractionations) were 2 x diluted in sample buffer (125 mM Tris-HCl pH 6.8, 20% Glycerol, 10% 2-β-Mercaptoethanol, 4% SDS, 0.01% Bromophenol Blue) and boiled for 5 min at 98°C. Equal amounts of protein from whole cell lysates were separated in SDS-PAGE gels and transferred onto PVDF membranes (0.45 μm, Merck Millipore). After 1 h of blocking in 5% BSA in PBS-T (0.05% Tween 20), membranes were incubated with primary antibodies in PBS-T for 1-2 h at room temperature, or at 4°C overnight. Secondary antibodies were incubated for 1 h at room temperature. Membranes were washed 3 x 10 mins in PBS-T after antibody incubation. Probed membranes were visualized with the Odyssey CLx Infrared Imaging

System (LI-COR Biosciences). Antibodies are listed in Supplementary Table 1 and 2. Immunoblots were quantified using ImageStudio Lite (ver. 5.2, LI-COR Biosciences). Full-size immunoblot scans are provided in Supplementary Fig. 6,7.

Colony forming assays. For colony survival assays after DNA damage, cells were seeded in triplicate in 6-well plates (400 cells/well) and treated with increasing doses or concentrations of UV-C or cisplatin, respectively, 1 day after seeding. After 5-7 days, colonies were fixed and stained. For the colony forming assay shown in Fig. 5d,e and Supplementary Fig. 4e, cells were seeded in triplicate in 6-well plates (750-1000 cells/well) 48 h after siRNA transfection. After 12 days, cells were fixed and stained. Fixing and staining solution: 0.1 % w/v Coomassie Blue (Bio-Rad) was dispersed in a 50% Methanol, 10% Acetic Acid solution. Colonies were counted with the integrated colony counter GelCount (Oxford Optronix).

Real-Time Reverse Transcriptase PCR (RT-qPCR). Total RNA was isolated from siRNA-transfected U2OS cells using the RNeasy mini kit (Qiagen). cDNA was synthesized using iScript cDNA Synthesis Kit (Bio-Rad), accordingly to manufacturer's instructions. TFIIH genes and GAPDH expression levels were analyzed using RT-qPCR with the PowerUP SYBR Green Master Mix (ThermoFischer Scientific) in a Bio-Rad CFX96 device. Primers used are listed in Supplementary Table 3. The relative gene expression of TFIIH genes was calculated according to the comparative quantification cycle (Cq) method and normalized to *GAPDH* expression. The expression level of each TFIIH gene in BRM knockdown cells was normalized to expression in control siRNA treated cells. Expression levels were measured in triplicate in two independent experiments.

Re-analysis of public ChIP-seq data. To dissect BRG1/BRM enrichment in GTF2H1, we re-analyzed published BRG1/BRM ChIP-seq datasets from liver cancer HepG2 cells upon transfection with non-targeting shRNA (Fig. 3c; GEO accession GSE102559³²) and BRG1/BRM ChIP-seq datasets from RWPE1-SCHLAP1 cells (Supplementary Fig. 3c; GEO accession GSE114392³³). ChIP-seq raw data was obtained from the Sequence Read Archive repository (SRA, NCBI; SRP115303 and SRP145601) and uploaded to the Galaxy platform⁶⁴. Reads were aligned to the human genome (hg19

build) with BWA (Galaxy Version 0.7.17.4), poor quality alignments and duplicates were subsequently filtered with SAMtools (Galaxy Version 1.1.2) $-q$ 20. To visualize ChIP-seq signal density, replicate datasets were merged with SAMtools and further processed using bamcoverage tool (Galaxy Version 2.5.0.0), DeepTools suite⁶⁵ with binsize 30, reads extended to 150 bp and normalized to reads per kilobase per million (RPKM); resulting bigwig files were visualized using IGV genome browser⁶⁶. Peaks were determined with MACS2 peak caller (Galaxy Version 2.1.1.20160309.0⁶⁷) using the *predictd* function to estimate fragment size for all datasets and the following analysis parameters $-qval=0.01$ $-nomodel$ $-extsize=d$ $-broad$ $-broadcutoff$ 0.05 $-keepdup$ -all. Resulting peaks were filtered against the ENCODE blacklist regions and finally visualized in IGV browser. Promoter region annotation for *GTF2H1* gene was obtained from the Ensembl database (GRCh37 assembly, Chr11: 18,340,602-18,346,999).

Immunoprecipitation. The procedure for *in vivo* crosslink and immunoprecipitation was described previously¹² and applied with minor alterations. Briefly, after UV-C irradiation (20 J/m²), cells were cultured for 30 min before crosslinking in 1% paraformaldehyde in PBS for 5 min at room temperature. Crosslinking reaction was stopped with 0.125 M of glycine and cells were collected in ice cold PBS supplemented with 1 mM PMSF and 10% glycerol. All subsequent steps were performed at 4°C. Following centrifugation, cell pellet was resuspended in lysis buffer (50 mM HEPES pH 7.8, 0.15 M NaCl, 0.5% NP-40, 0.25% Triton X-100, and 10% glycerol). After 30 min incubation, the suspension was spun down, and supernatant (soluble fraction) was removed. The pellet was washed with Wash buffer (0.01 M Tris-HCl pH 8.0, 0.2 M NaCl), spun down and resuspended in 1 × RIPA buffer (0.01 M Tris-HCl pH 7.5, 0.15 M NaCl, 1% Triton X-100, 1% NP-40, 0.1% SDS). Chromatin was sheared using a Bioruptor Sonicator (Diagenode) using cycles of 30 s ON, 30 s OFF during 10 min, after which samples were centrifuged. The supernatant containing crosslinked chromatin was used for immunoprecipitation. All buffers were supplemented with 0.1 mM EDTA, 0.5 mM EGTA, 1 mM PMSF and a mixture of proteinase and phosphatase inhibitors. For immunoprecipitation, extracts were incubated with GFP-trap beads (Chromotek), overnight at 4°C. Subsequently, beads were washed 5 times in RIPA buffer and elution of the precipitated proteins was performed by extended boiling in 2x

Laemmli sample buffer for immunoblotting analysis.

Cell cycle profiling. For cell cycle analysis, cells were fixed in 70% ethanol, followed by DNA staining with 50 µg/ml propidium iodide (Invitrogen) in the presence of RNase A (0.1 mg/mL). Cell sorting was performed on a BD LSRFortessa™ flow cytometer (BD Bioscience) using FACSDiva software. Obtained data was quantified with Flowing software 2.5.1 (by Perttu Terho in collaboration with Turku Bioimaging).

Statistical Analysis. Mean values and S.E.M. error bars are shown for each experiment. Unpaired, two-tailed *t* tests were used to determine statistical significance between groups. In all experiments, between-group variances were similar and data were symmetrically distributed. For analysis of graphs in Fig. 2a and Supplementary Fig. 1g, a ROC curve analysis was performed with significance levels set to 0.05. All analysis were performed using Graph Pad Prism version 7.03 for Windows (GraphPad Software, La Jolla California USA). P values expressed as * $P < 0.05$; ** $P < 0.01$, *** $P < 0.001$ were considered to be significant. n.s., non-significant.

Data availability

The raw ChIP-seq data sets analyzed during the current study were obtained via the Sequence Read Archive repository (SRA, NCBI), [<https://www.ncbi.nlm.nih.gov/sra>], with the data set identifiers SRP115303 and SRP145601. Other relevant data generated during the current study are available from the corresponding author on reasonable request. Individual data points are provided in Supplementary data file 1.

Competing interests

The authors declare no competing interests

Author contributions

CRS, HL, JS and AH performed all experiments. OZA initiated this study

and contributed reagents. RMR, JAM and JHJH analyzed data and advised. CRS, HL, and WV designed experiments, analyzed data and wrote the manuscript. All authors reviewed the manuscript.

Acknowledgments

The authors would like to thank Dr. Serena Bruens and Dr. Akos Gyenis for advice, reagents and technical assistance with RT-qPCR experiments; Dr. David Cano and Mireille Van de Veer for technical assistance and the Erasmus MC Optical Imaging Center for microscopy support. The CCNH antibody clone 2D4 was kindly provided by Dr. Jean-Marc Egly, pcDNA6.2-BRM-emGFP plasmid by Dr. Kyle Miller. We thank Dr. Suzan Pas, Dr. Bernadette van den Hoogen, Corine Beaufort, Dr. John Martens, Dr. Bert van der Horst and Dr. Jan van der Knaap for BRG1 and BRM deficient cells. This work was supported by a Marie Curie Initial Training Network funded by the European Commission 7th Framework Programme (grant 316390), a European Research Council Advanced Grant (grant 340988-ERC-ID), a Worldwide Cancer Research Award (grant 15-1274), Dutch Scientific Organization (ALW grants 854.11.002 and 864.13.004). This work is part of the OncoCode Institute which is partly financed by the Dutch Cancer Society and was funded by a grant from the Dutch Cancer Society (KWF grant 10506).

References

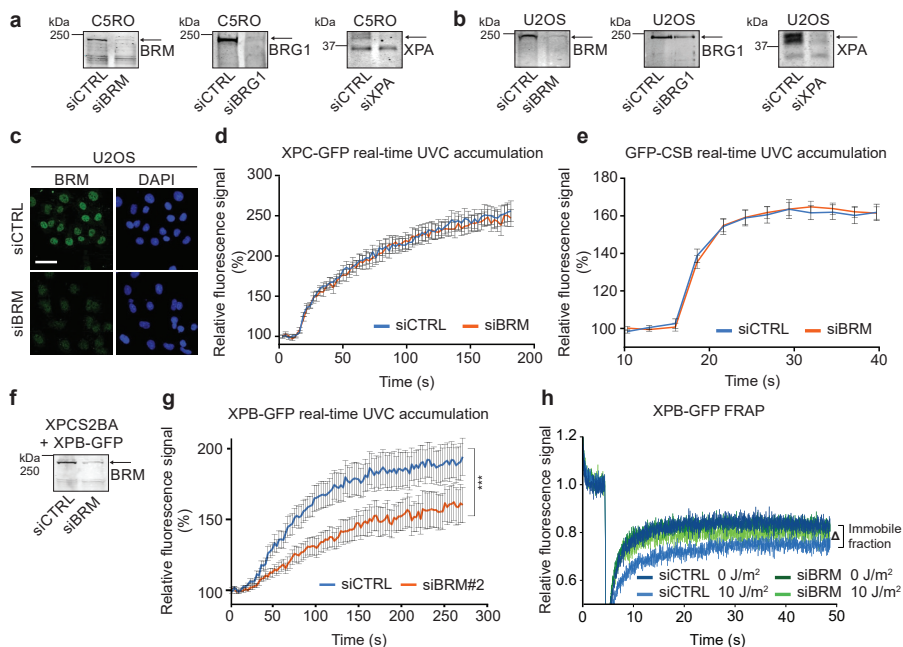
1. Kadoch, C. & Crabtree, G. R. Mammalian SWI/SNF chromatin remodeling complexes and cancer: Mechanistic insights gained from human genomics. *Sci. Adv.* **1**, e1500447–e1500447 (2015).
2. Morgan, M. A. & Shilatifard, A. Chromatin signatures of cancer. *Genes Dev.* **29**, 238–249 (2015).
3. Kadoch, C. *et al.* Proteomic and bioinformatic analysis of mammalian SWI/SNF complexes identifies extensive roles in human malignancy. *Nat. Genet.* **45**, 592–601 (2013).
4. Shain, A. H. & Pollack, J. R. The Spectrum of SWI/SNF Mutations, Ubiquitous in Human Cancers. *PLoS One* **8**, (2013).
5. Wilson, B. G. & Roberts, C. W. M. SWI/SNF nucleosome remodellers and cancer. *Nat. Rev. Cancer* **11**, 481–492 (2011).
6. Brownlee, P. M., Meisenberg, C. & Downs, J. A. The SWI/SNF chromatin remodelling complex: Its role in maintaining genome stability and preventing tumourigenesis. *DNA Repair (Amst)*. **32**, 127–133 (2015).
7. Hodges, C., Kirkland, J. G. & Crabtree, G. R. The many roles of BAF (mSWI/SNF) and PBAF complexes in cancer. *Cold Spring Harb. Perspect. Med.* **6**, (2016).
8. Luijsterburg, M. S. & Van Attikum, H. Chromatin and the DNA damage response: The cancer connection. *Molecular Oncology* **5**, 349–367 (2011).
9. Lans, H., Marteijn, J. A. & Vermeulen, W. ATP-dependent chromatin remodeling in the DNA-damage response. *Epigenetics Chromatin* **5**, 4 (2012).
10. Schärer, O. D. Nucleotide excision repair in Eukaryotes. *Cold Spring Harb. Perspect. Biol.* **5**, (2013).
11. Marteijn, J. a, Lans, H., Vermeulen, W. & Hoeijmakers, J. H. J. Understanding nucleotide excision repair and its roles in cancer and ageing. *Nat. Rev. Mol. Cell Biol.* **15**, 465–81 (2014).
12. Fousteri, M., Vermeulen, W., van Zeeland, A. A. & Mullenders, L. H. F. Cockayne Syndrome A and B Proteins Differentially Regulate Recruitment of Chromatin Remodeling and Repair Factors to Stalled RNA Polymerase II In Vivo. *Mol. Cell* **23**, 471–482 (2006).
13. Sugasawa, K. Molecular mechanisms of DNA damage recognition for mammalian nucleotide excision repair. *DNA Repair (Amst)*. **44**, 110–117 (2016).
14. Yokoi, M. *et al.* The xeroderma pigmentosum group C protein complex XPC-HR23B plays an important role in the recruitment of transcription factor IIH to damaged DNA. *J. Biol. Chem.* **275**, 9870–9875 (2000).
15. Giglia-Mari, G. *et al.* A new, tenth subunit of TFIIH is responsible for the DNA repair syndrome trichothiodystrophy group A. *Nat. Genet.* **36**, 714–719 (2004).
16. Bernardes de Jesus, B. M., Bjørås, M., Coin, F. & Egly, J. M. Dissection of the molecular defects caused by pathogenic mutations in the DNA repair factor XPC. *Mol. Cell. Biol.* **28**, 7225–7235 (2008).
17. Oksenyich, V., de Jesus, B. B., Zhovmer, A., Egly, J.-M. & Coin, F. Molecular insights into the recruitment of TFIIH to sites of DNA damage. *EMBO J.* **28**, 2971–2980 (2009).
18. Sugasawa, K., Akagi, J. ichi, Nishi, R., Iwai, S. & Hanaoka, F. Two-Step Recognition of DNA Damage for Mammalian Nucleotide Excision Repair: Directional Binding of the XPC Complex and DNA Strand Scanning. *Mol. Cell* **36**, 642–653 (2009).
19. Staresinic, L. *et al.* Coordination of dual incision and repair synthesis in human nucleotide

- excision repair. *EMBO J.* **28**, 1111–1120 (2009).
20. Gong, F., Kwon, Y. & Smerdon, M. J. Nucleotide excision repair in chromatin and the right of entry. *DNA Repair* **4**, 884–896 (2005).
 21. Hara, R. & Sancar, A. The SWI / SNF Chromatin-Remodeling Factor Stimulates Repair by Human Excision Nuclease in the Mononucleosome Core Particle. *Mol. Cell. Biol.* **22**, 6779–6787 (2002).
 22. Lans, H. *et al.* Involvement of global genome repair, transcription coupled repair, and chromatin remodeling in UV DNA damage response changes during developm. *PLoS Genet.* **6**, 41 (2010).
 23. Gong, F., Fahy, D. & Smerdon, M. J. Rad4-Rad23 interaction with SWI/SNF links ATP-dependent chromatin remodeling with nucleotide excision repair. *Nat. Struct. Mol. Biol.* **13**, 902–907 (2006).
 24. Zhao, Q. *et al.* Modulation of nucleotide excision repair by mammalian SWI/SNF chromatin-remodeling complex. *J. Biol. Chem.* **284**, 30424–30432 (2009).
 25. Zhang, L., Zhang, Q., Jones, K., Patel, M. & Gong, F. The chromatin remodeling factor BRG1 stimulates nucleotide excision repair by facilitating recruitment of XPC to sites of DNA damage. *Cell Cycle* **8**, 3953–3959 (2009).
 26. Klochendler-Yeivin, A., Picarsky, E. & Yaniv, M. Increased DNA damage sensitivity and apoptosis in cells lacking the Snf5/Ini1 subunit of the SWI/SNF chromatin remodeling complex. *Mol. Cell. Biol.* **26**, 2661–74 (2006).
 27. Ray, A. *et al.* Human SNF5/INI1, a component of the human SWI/SNF chromatin remodeling complex, promotes nucleotide excision repair by influencing ATM recruitment and downstream H2AX phosphorylation. *Mol. Cell. Biol.* **29**, 6206–6219 (2009).
 28. Hoogstraten, D. *et al.* Rapid Switching of TFIIH between RNA Polymerase I and II Transcription and DNA Repair In Vivo. *Mol. Cell* **10**, 1163–1174 (2002).
 29. Vermeulen, W. *et al.* Sublimiting concentration of TFIIH transcription/DNA repair factor causes TTD-A trichothiodystrophy disorder. *Nat. Genet.* **26**, 307–13 (2000).
 30. Botta, E. *et al.* Reduced level of the repair/transcription factor TFIIH in trichothiodystrophy. *Hum. Mol. Genet.* **11**, 2919–2928 (2002).
 31. Luo, J. *et al.* Architecture of the Human and Yeast General Transcription and DNA Repair Factor TFIIH. *Mol. Cell* **59**, 794–806 (2015).
 32. Raab, J. R., Runge, J. S., Spear, C. C. & Magnuson, T. Co-regulation of transcription by BRG1 and BRM, two mutually exclusive SWI/SNF ATPase subunits. *Epigenetics Chromatin* **10**, 62 (2017).
 33. Raab, J. R. *et al.* SWI/SNF remains localized to chromatin in the presence of SCHLAP1. *bioRxiv* 322065 (2018). doi:10.1101/322065
 34. Kadam, S. & Emerson, B. M. Transcriptional specificity of human SWI/SNF BRG1 and BRM chromatin remodeling complexes. *Mol. Cell* **11**, 377–389 (2003).
 35. Ohkuma, Y., Hashimoto, S., Wang, C. K., Horikoshi, M. & Roeder, R. G. Analysis of the role of TFIIIE in basal transcription and TFIIH-mediated carboxy-terminal domain phosphorylation through structure-function studies of TFIIIE- α . *Mol. Cell. Biol.* **15**, 4856–4866 (1995).
 36. Strobeck, M. W. *et al.* Compensation of BRG-1 function by Brm. *J. Biol. Chem.* **277**, 4782–4789 (2002).
 37. Medina, P. P. *et al.* Frequent BRG1/SMARCA4-Inactivating mutations in human lung cancer cell lines. *Hum. Mutat.* **29**, 617–622 (2008).
 38. Hoffman, G. R. *et al.* Functional epigenetics approach identifies BRM/SMARCA2 as a critical

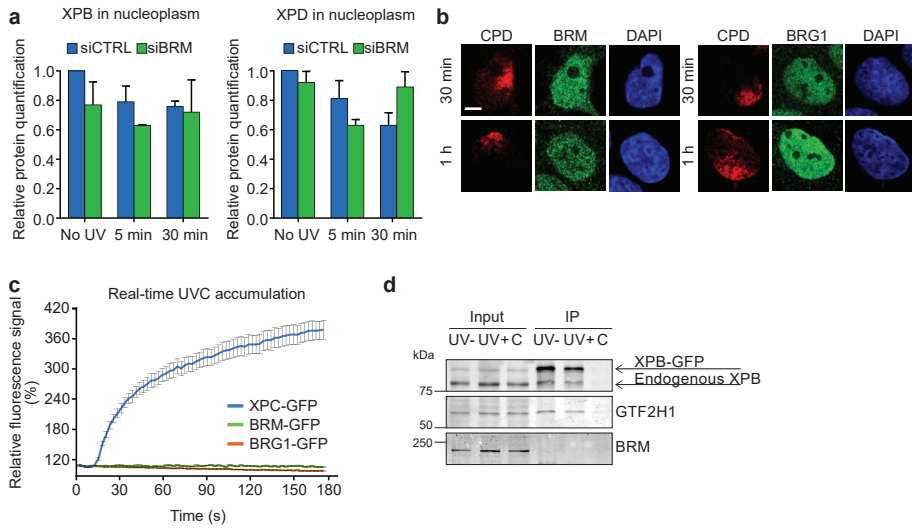
- synthetic lethal target in BRG1-deficient cancers. *Proc. Natl. Acad. Sci.* **111**, 3128–3133 (2014).
39. Reisman, D. N. *et al.* Concomitant down-regulation of BRM and BRG1 in human tumor cell lines : differential effects on RB-mediated growth arrest vs CD44 expression. *Oncogene* **21**, 1196–1207 (2002).
40. Oike, T. *et al.* A synthetic lethality-based strategy to treat cancers harboring a genetic deficiency in the chromatin remodeling factor BRG1. *Cancer Res.* **73**, 5508–5518 (2013).
41. Cohen, S. M. & Lippard, S. J. Cisplatin: From DNA damage to cancer chemotherapy. *Progress in Nucleic Acid Research and Molecular Biology* **67**, 93–130 (2001).
42. Diadducts, I. D. N. A., Reardon, J. T., Vaisman, A., Chaney, S. G. & Sancar, A. Efficient Nucleotide Excision Repair of Cisplatin , Oxaliplatin , and Bis-aceto- ammine-dichloro-cyclohexylamine-platinum (IV) (JM216) Platinum. *Cancer Res.* **59**, 3968–3971 (1999).
43. Glaros, S. *et al.* The reversible epigenetic silencing of BRM: implications for clinical targeted therapy. *Oncogene* **26**, 7058–7066 (2007).
44. Halliday, G. M. *et al.* The absence of Brm exacerbates photocarcinogenesis. *Exp. Dermatol.* **21**, 599–604 (2012).
45. Greber, B. J. *et al.* The cryo-electron microscopy structure of human transcription factor IIH. *Nature* **549**, 414–417 (2017).
46. Helming, K. C., Wang, X. & Roberts, C. W. M. Vulnerabilities of mutant SWI/SNF complexes in cancer. *Cancer Cell* **26**, 309–317 (2014).
47. Wilson, B. G. *et al.* Epigenetic antagonism between Polycomb and SWI/SNF complexes during oncogenic transformation. *Cancer Cell* **18**, 316–328 (2010).
48. Kadoch, C. *et al.* Dynamics of BAF–Polycomb complex opposition on heterochromatin in normal and oncogenic states. *Nat. Genet.* **49**, 213–222 (2016).
49. Brownlee, P. M., Meisenberg, C. & Downs, J. A. The SWI/SNF chromatin remodeling complex: Its role in maintaining genome stability and preventing tumourigenesis. *DNA Repair (Amst)*. **32**, 127–133 (2015).
50. Ogiwara, H. *et al.* Histone acetylation by CBP and p300 at double-strand break sites facilitates SWI/SNF chromatin remodeling and the recruitment of non-homologous end joining factors. *Oncogene* **30**, 2135–2146 (2011).
51. Park, J.-H. *et al.* Mammalian SWI/SNF complexes facilitate DNA double-strand break repair by promoting γ -H2AX induction. *EMBO J.* **25**, 3986–3997 (2006).
52. Bell, E. H. *et al.* SMARCA4/BRG1 Is a Novel Prognostic Biomarker Predictive of Cisplatin-Based Chemotherapy Outcomes in Resected Non-Small Cell Lung Cancer. *Clin. Cancer Res.* **22**, 2396–2404 (2016).
53. Kothandapani, A., Gopalakrishnan, K., Kahali, B., Reisman, D. & Patrick, S. M. Downregulation of SWI/SNF chromatin remodeling factor subunits modulates cisplatin cytotoxicity. *Exp. Cell Res.* **318**, 1973–1986 (2012).
54. Daya-Grosjean, L., James, M. R., Drougard, C. & Sarasin, A. An immortalized xeroderma pigmentosum, group C, cell line which replicates SV40 shuttle vectors. *Mutat. Res.* **183**, 185–96 (1987).
55. Van Den Boom, V. *et al.* DNA damage stabilizes interaction of CSB with the transcription elongation machinery. *J. Cell Biol.* **166**, 27–36 (2004).
56. Bartlett, C., Orvis, T. J., Rosson, G. S. & Weissman, B. E. BRG1 mutations found in human cancer cell lines inactivate Rb-mediated cell-cycle arrest. *J. Cell. Physiol.* **226**, 1989–97 (2011).
57. Shain, A. H. *et al.* Convergent structural alterations define SWItch/Sucrose NonFermentable (SWI/SNF) chromatin remodeler as a central tumor suppressive complex in pancreatic cancer.

- Proc. Natl. Acad. Sci. U. S. A.* **109**, E252-9 (2012).
58. Gong, F. *et al.* Screen identifies bromodomain protein ZMYND8 in chromatin recognition of transcription-associated DNA damage that promotes homologous recombination. *Genes Dev.* **29**, 197–211 (2015).
 59. Campeau, E. *et al.* A versatile viral system for expression and depletion of proteins in mammalian cells. *PLoS One* **4**, (2009).
 60. Shalem, O. *et al.* Genome-Scale CRISPR-Cas9 Knockout Screening in Human Cells. *Science (80-.)*. **343**, 84–87 (2014).
 61. van Cuijk, L. *et al.* SUMO and ubiquitin-dependent XPC exchange drives nucleotide excision repair. *Nat. Commun.* **6**, 7499 (2015).
 62. Aydin, Ö. Z. *et al.* Human ISWI complexes are targeted by SMARCA5 ATPase and SLIDE domains to help resolve lesion-stalled transcription. *Nucleic Acids Res.* **42**, 8473–8485 (2014).
 63. Houtsmuller, A. B. & Vermeulen, W. Macromolecular dynamics in living cell nuclei revealed by fluorescence redistribution after photobleaching. *Histochem. Cell Biol.* **115**, 13–21 (2001).
 64. Afgan, E. *et al.* The Galaxy platform for accessible, reproducible and collaborative biomedical analyses: 2018 update. *Nucleic Acids Res.* (2018). doi:10.1093/nar/gky379
 65. Ramírez, F. *et al.* deepTools2: a next generation web server for deep-sequencing data analysis. *Nucleic Acids Res.* **44**, W160-5 (2016).
 66. Robinson, J. T. *et al.* Integrative genomics viewer. *Nat. Biotechnol.* **29**, 24–6 (2011).
 67. Feng, J., Liu, T., Qin, B., Zhang, Y. & Liu, X. S. Identifying ChIP-seq enrichment using MACS. *Nat. Protoc.* **7**, 1728–1740 (2012).

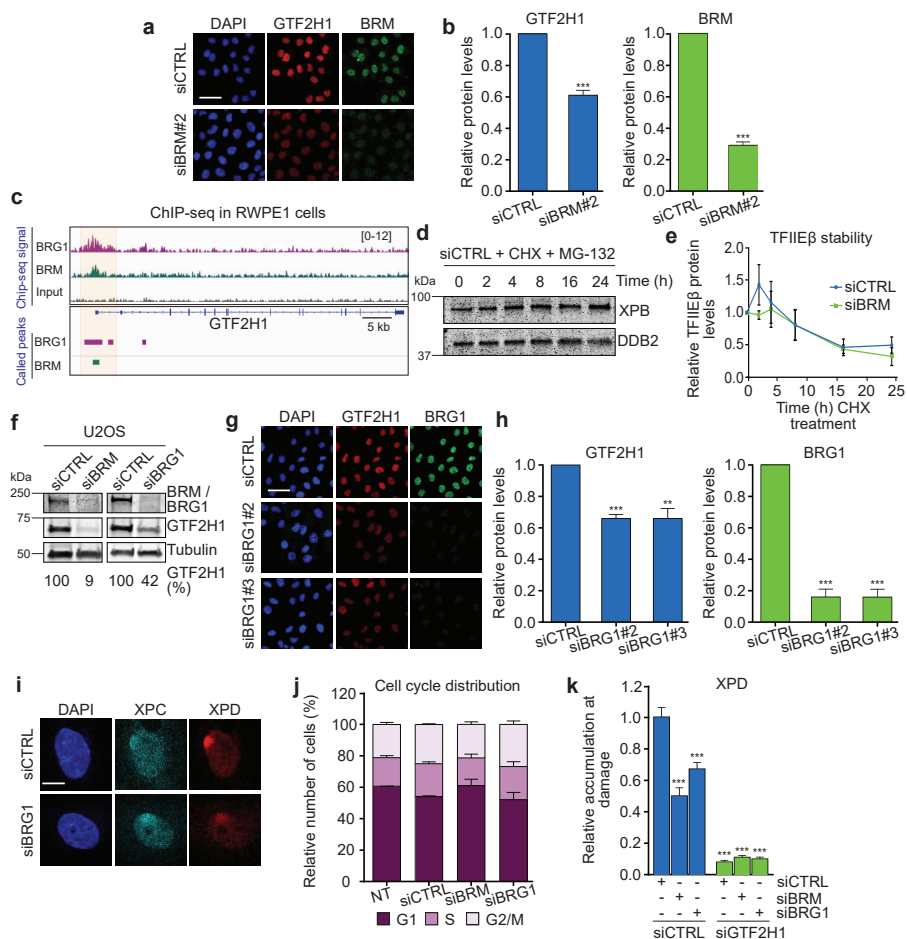
Supplementary data



Supplementary Fig. 1. BRM is required for recruitment of XPB but not of GG- and TC-NER damage sensor proteins XPC and CSB. (a,b) Immunoblot analysis of total cell lysates demonstrating siRNA-mediated downregulation of BRM, BRG1 and XPA in (a) C5RO (related to Fig. 1a,b) and (b) U2OS cells (related to Fig. 1c,d). The same total amount of protein from each cell lysate was loaded in each lane. (c) Immunofluorescence images demonstrating BRM siRNA-mediated depletion in U2OS cells (related to Fig. 1e,f). Scale bar: 50 μ m. (d) XPC-GFP and (e) GFP-CSB accumulation at LUD, induced with a 266 nm UV-C laser, measured in real time by confocal imaging. Pre-damage relative fluorescence intensity was set to 100% (t=0). (d) XP4PA with stable XPC-GFP expression were treated with control (CTRL) or BRM siRNAs. Representative results of three independent experiments with similar results (mean & S.E.M., at least 10 cells per condition in each experiment). (e) CS1AN cells with stable GFP-CSB expression were treated with control (CTRL) or BRM siRNAs (mean & S.E.M. of at least 10 cells per condition). (f) Immunoblot analysis of total cell lysates demonstrating siRNA-mediated downregulation of BRM in XPCS2BA patient cell lines complemented with XPB-GFP, referring to Fig. 2a,b. The same total amount of protein from each cell lysate was loaded in each lane. (g) XPB-GFP accumulation at LUD, induced with a 266 nm UV-C laser, measured in real time by confocal imaging. Pre-damage relative fluorescence intensity was set to 100% (t=0). XPCS2BA cells with stable expression of XPB-GFP were treated with control (CTRL) and BRM siRNAs. Mean & S.E.M. of at least 10 cells per condition, $P < 0.0001$, relative to siCTRL. (h) FRAP analysis of XPB-GFP in mock treated or UV-irradiated (10 J/m²) XPCS2BA cells transfected with control (CTRL) or BRM siRNAs. XPB-GFP was bleached in a strip across the nucleus and fluorescence recovery was measured over 50 s and normalized to pre-bleach. The immobile XPB-GFP fraction depicted in Fig. 2c was calculated after subtracting the bleach-depth intensities, by dividing the average recovered fluorescence intensity of UV-irradiated cells by the average recovered fluorescence intensity of mock treated cells, over the last 10 s of the measurements as explained in the methods. FRAP graph is the average of 3 independent experiments, with at least 10 cells measured per condition each time.



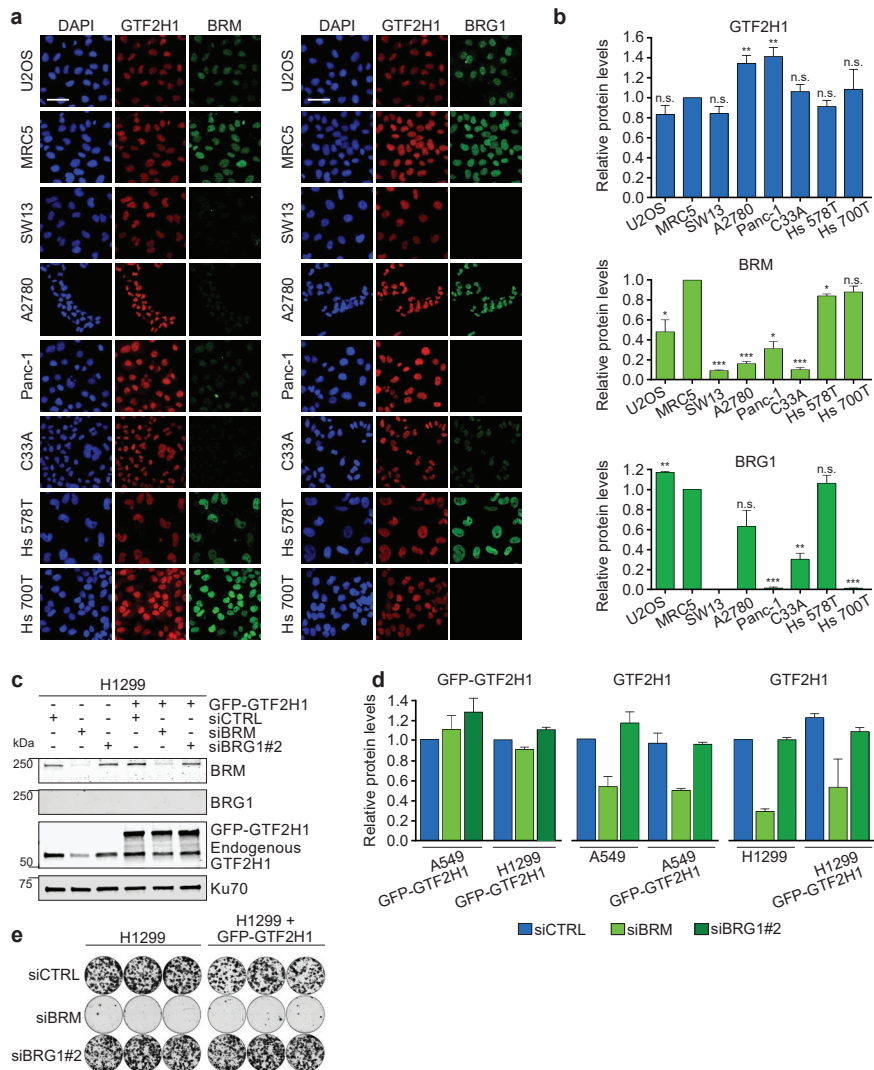
Supplementary Fig. 2. BRM and BRG1 are not localized to sites of UV damage. (a) Relative quantification of the immunostaining of soluble (nucleoplasm) XPB and XPD (shown in Fig. 2d) from U2OS cells treated with control (CTRL) or BRM siRNAs before and after (5 and 30 min) UV-C irradiation (20 J/m²). Mean & S.E.M. of two independent experiments. (b) Immunofluorescence showing absence of recruitment of BRM and BRG1 to LUD in U2OS cells. Cells were fixed 30 min and 1 h after inducing LUD with UV-C irradiation (60 J/m²) through a microporous membrane (8 μm). UV lesions were marked with staining against CPD (red channel). Scale bar: 5 μm. (c) XPC-GFP (in XP4PA), BRM-GFP and BRG1-GFP (in U2OS) accumulation at LUD, induced with a 266 nm UV-C laser, measured in real time by confocal imaging. Pre-damage relative fluorescence intensity was set to 100% (t=0). Mean & S.E.M. of at least 15 cells per condition. (d) Immunoblot analysis of input and GFP immunoprecipitation (IP) from XPB-GFP expressing XPCS2BA cells, 30 min after mock (UV-) or global UV-C (20 J/m²; UV+) treatment and from non-treated XPCS2BA control cells, without XPB-GFP (C). Samples were analyzed with antibodies against XPB, GTF2H1 and BRM.



Supplementary Fig. 3 | Lower GTF2H1 expression after BRM or BRG1 knockdown affects TFIIH

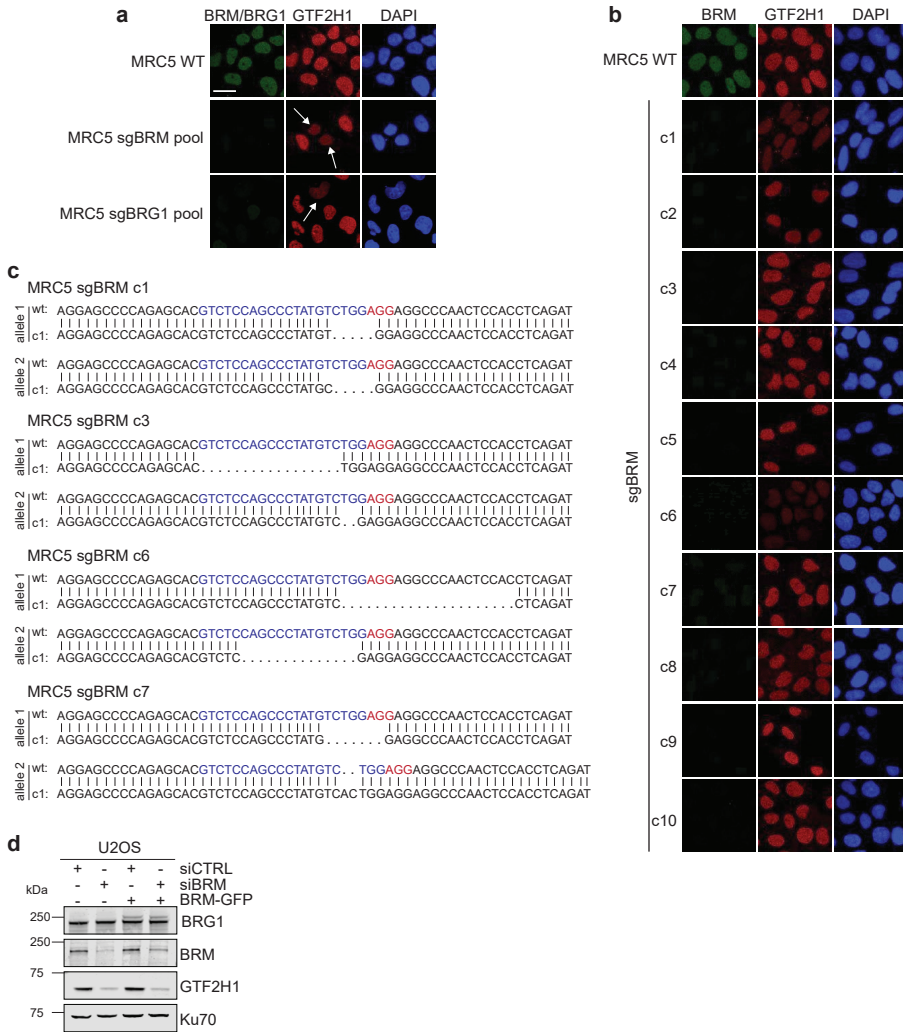
stability and function. (a) Immunofluorescence of GTF2H1 and BRM protein levels in U2OS cells treated with control (CTRL) or BRM siRNA RNA. For BRM, an independent siRNA (BRM#2) was used to exclude off-target effects. Scale bar: 50 μ m. (b) Quantification of GTF2H1 and BRM fluorescence intensity, shown in (a). Total levels of GTF2H1 and BRM were normalized to control (CTRL) siRNA, set to 1.0 (mean & S.E.M. of three independent experiments, with > 110 cells per sample per experiment). ***P < 0.001, relative to siCTRL. (c) BRG1 and BRM co-occupancy of GTF2H1 promoter in RWPE1 cells. Re-analysis of published BRG1 and BRM ChIP-seq data from RWPE1 cells (overexpressing lncRNA SCHLAP1) in which ChIP-seq signal density (top) and respective peaks (bottom) illustrate BRG1 (purple) and BRM (green) enrichment at the promoter of GTF2H1 (GEO accession GSE114392). Promoter region is highlighted in light orange, signal density in reads per million. (d) XPB stability was analyzed in U2OS cells treated with control (CTRL) siRNA and with 100 μ M cycloheximide (CHX) to inhibit protein synthesis. Cells were pretreated with 50 μ M of proteasome inhibitor MG-132, 45 min prior to CHX addition. DDB2 immunostaining was used as loading control. Representative immunoblots of two independent experiments with similar results. (e) Quantification of TFIIH β protein levels normalized to DDB2 in time after addition of cyclohexamide (CHX) in U2OS cells treated with control (CTRL) or BRM siRNAs (as shown in Fig. 3d). The total amount of TFIIH β in whole cell lysates was set to 1.0 at t=0 in

each condition. Mean & S.E.M. of two independent experiments. **(f)** Immunoblots of BRM, BRG1 and GTF2H1 protein levels from whole cell lysates of U2OS cells treated with non-targeting (CTRL), BRM or BRG1 siRNAs. Tubulin was used as a loading control to normalize quantified GTF2H1 protein levels, indicated below the blot (normalized to siCTRL, set to 100%). **(g)** Immunofluorescence of GTF2H1 and BRG1 protein levels after BRG1 siRNA-mediated depletion with two additional independent siRNAs (BRG1#2, BRG1#3) in U2OS cells, to exclude off-target effects. Scale bar: 50 μm . **(h)** Quantification of GTF2H1 and BRG1 fluorescence intensity, shown in (g). Total levels of GTF2H1 and BRG1 were normalized to control (CTRL). Mean & S.E.M. of three independent experiments with > 110 cells per sample per experiment. ** $P < 0.01$, *** $P < 0.001$, relative to siCTRL. **(i)** Immunofluorescence of XPD recruitment (red channel) to LUD marked by XPC (cyan channel) in U2OS cells treated with control (CTRL) or BRG1 siRNAs. U2OS cells were fixed 30 min after local UV-C irradiation (60 J/m^2) through a microporous membrane (8 μm) Scale bar: 5 μm . **(j)** Knockdown of BRM or BRG1 does not affect cell cycle distribution. U2OS cells were transfected with the indicated siRNAs or mock treated (NT). The average percentage of cells in G1 (dark purple), S (lighter purple) and G2/M (light pink) phase is presented. Mean & S.E.M. of at least two independent experiments. **(k)** Quantification of XPD recruitment to UV-lesions within 30 mins after UV-C irradiation (60 J/m^2) in U2OS cells treated with control (CTRL), BRM, BRG1 and GTF2H1 siRNAs. Relative accumulation of XPD at LUD (over nuclear background) in each condition was normalized to cells treated only with siCTRL, in which nuclear background was set as 0 and maximal signal at LUD set to 1.0 (>47 cells per sample, mean & S.E.M.). *** $P < 0.001$, relative to cells treated only with siCTRL.

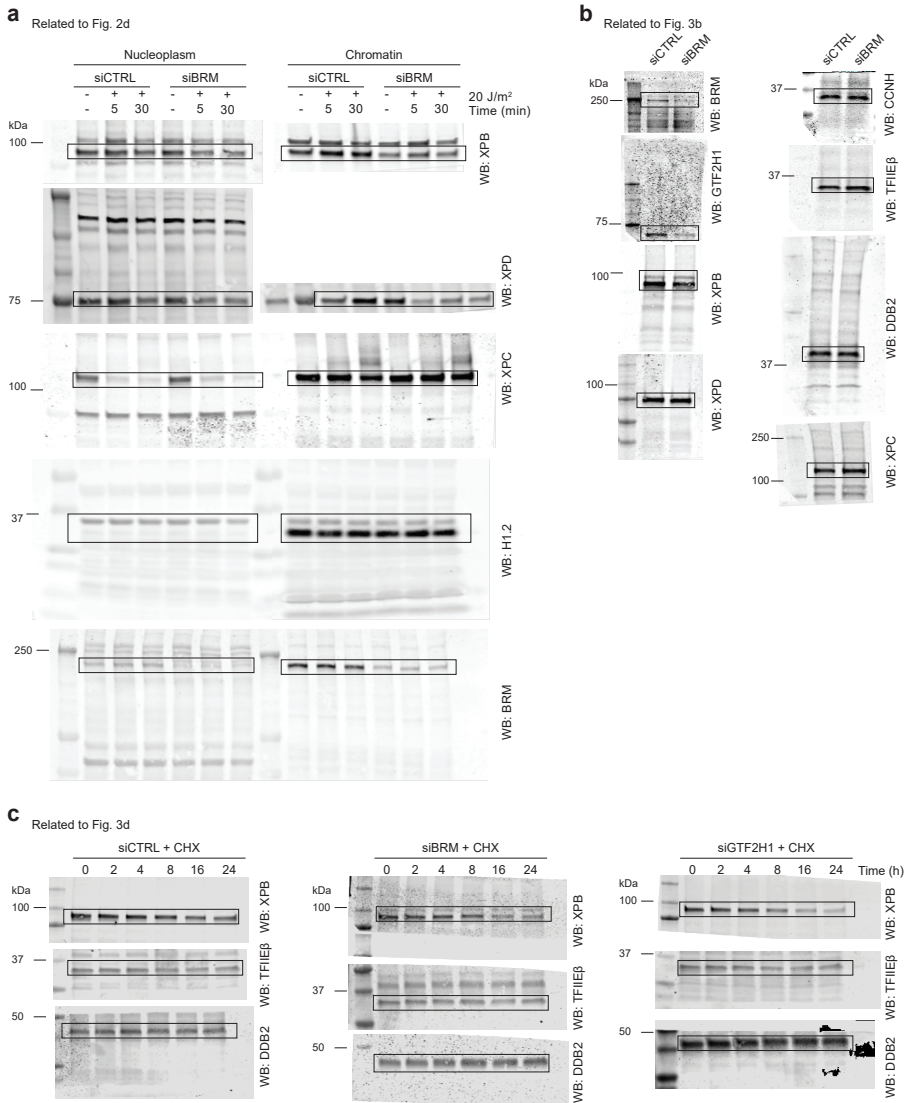


Supplementary Fig. 4. GTF2H1 expression in SWI/SNF-deficient cancer cell lines. (a) Immunofluorescence analysis of GTF2H1, BRM and BRG1 levels in SWI/SNF-deficient cancer cell lines SW13 (adrenal cortex), A2780 (ovarian), Panc-1 (pancreatic), C33A (cervix), Hs 578T (breast) and Hs 700T (pancreatic). As reference, U2OS (osteosarcoma) and MRC5 (human fibroblasts) were used. Scale bar: 50 μ m. (b) Quantification of GTF2H1, BRM and BRG1 fluorescence intensity, shown in (a). Total protein levels were normalized to MRC5, set to 1.0. Mean & S.E.M. of four (GTF2H1) and two (BRM, BRG1) independent experiments with > 100 cells per sample per experiment. * P < 0.05, ** P < 0.01, *** P < 0.001, relative to MRC5. n.s., non-significant. (c) Whole cell lysate of H1299 cells with and without stable expression of GFP-GTF2H1, treated with control (CTRL), BRM or BRG1 (BRG1#2) siRNAs, were analyzed by immunoblotting against BRG1, BRM and GTF2H1. Ku70 was used as loading control. (d) Relative quantification of ectopic GFP-GTF2H1 and endogenous GTF2H1 levels in H1299 (depicted in c) and A549 (depicted in Fig. 5c) cells, with and without stable expression of GFP-GTF2H1, treated with control (CTRL), BRM or BRG1 (BRG1#2) siRNAs. GFP-GTF2H1 and GTF2H1 levels

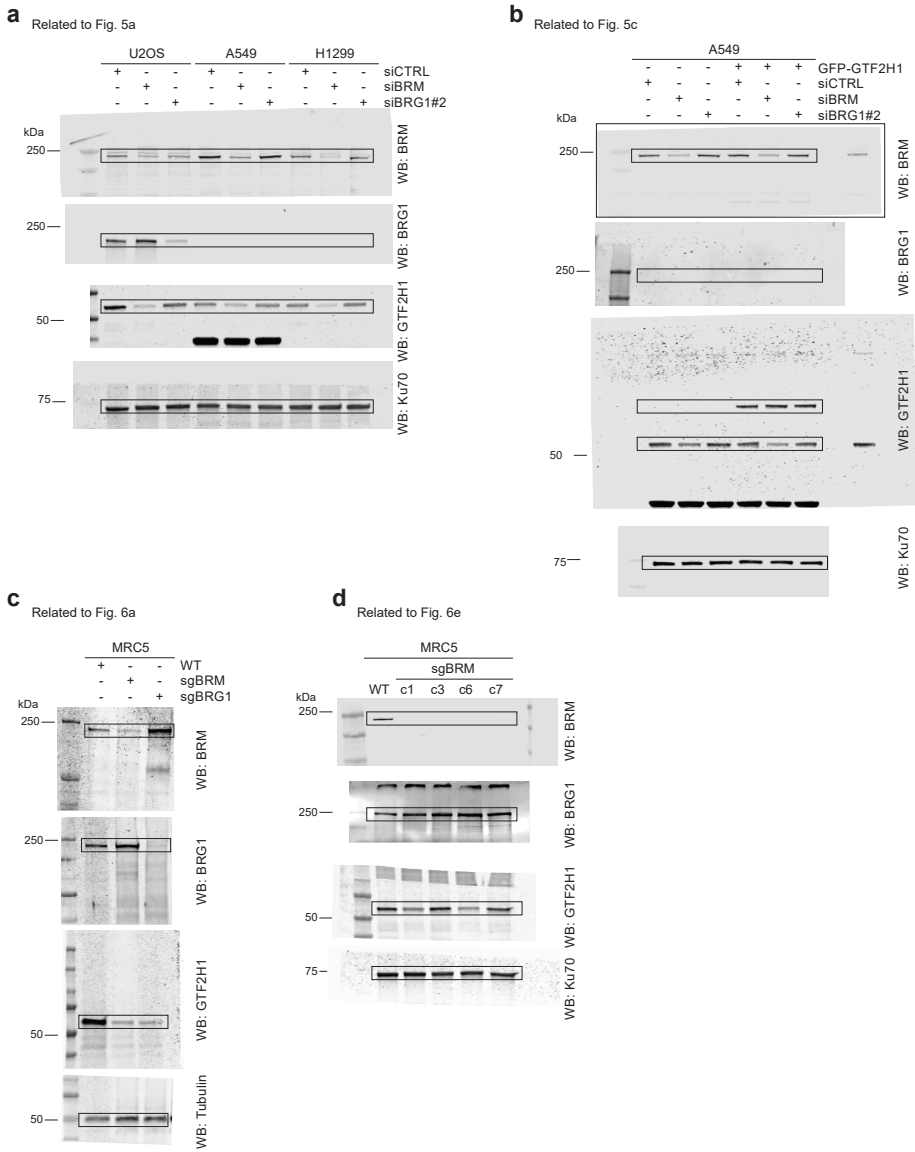
were normalized to Ku70 and to siCTRL, set to 1.0 (mean & S.E.M. from two independent experiments).
(e) H1299 cells, with or without stable expression of GFP-GTF2H1 were seeded 48 h after transfection with control (CTRL), BRM or BRG1 (BRG1#2) siRNAs, in triplicate, at a density of 750 cells per well and grown for 12 before fixation and staining.



Supplementary Fig. 5. Cells with permanent loss of BRM or BRG1 can restore GTF2H1 expression levels. (a) Immunofluorescence analysis of GTF2H1 levels in MRC5 WT cells and heterogeneous pool of sgBRM or sgBRG1 transfected cells. Arrows depict cells that have retained low GTF2H1 levels. To verify the knockouts, specific antibodies against BRM or BRG1 were used (green channel). Scale bar: 25 μ m. (b) Immunofluorescence analysis of BRM and GTF2H1 levels in MRC5 WT and single BRM knockout (sgBRM) clones. (c) Sequence of the sgBRM target region in MRC5 BRM knockout clones c1, c3, c6 and c7. Blue indicates the sgBRM target sequence. Red indicates the PAM sequence. All deletions (in alleles of c1, c3, c6 and c7) and the insertion (in one of the alleles of c7) are predicted to severely truncate BRM. (d) Immunoblot analysis of GTF2H1 levels in U2OS cells without and with stable ectopic expression of BRG1-GFP, treated with control (CTRL) or BRM siRNAs. Immunoblots were stained against GTF2H1, BRM, BRG1 and Ku70 as loading control.



Supplementary Fig. 6. Full-size immunoblot scans shown in Fig. 2d (a), Fig. 3d (b) and Fig. 3d (c).



Supplementary Fig. 7. Full-size immunoblot scans shown in Fig. 5a (a), Fig. 5c (b), Fig. 6a (c) and Fig. 6e (d).

Supplementary Table 1. Primary Antibody list and working dilutions.

Source, Reference	Antibody	Dilutions	
		Immunoblotting	Immunofluorescence
Abcam, ab181136	DDB2	1/1000	1/1000
Bethyl, A301-121A	XPC	1/2000	1/2000
Santa Cruz, sc-293	XPB	1/1000	1/1000
Abcam, ab54676	XPD	1/1000	1/150
Abcam, ab55199	GTF2H1	1/500	1/500
Sigma, WH0002965M1	GTF2H1	1/500	1/500
Novus Biologicals, NBP2-38556	GTF2H1	1/500	1/200
Santa Cruz, sc-853	XPA	1/250	1/50
Santa Cruz, sc-136153	XPF	N.A.	1/100
MBL international, TDM-2	CPD	N.A.	1/1000
Abcam, ab15597	BRM	1/800	1/250
Santa Cruz, sc-6450	BRM	N.A.	1/200
Sigma Aldrich, B8184	BRG1	1/3000	1/1000
Abcam, ab110641	BRG1	1/10000	1/500
2D4 clone	CCNH	1/1000	N.A.
Abcam, ab17677	Histone H1.2	1/1000	N.A.
Abcam, ab187143	TFIIIE β	1/1000	N.A.
Santa Cruz, sc-1487	Ku70	1/1000	N.A.
Santa Cruz, sc-17789	Ku70	1/1000	N.A.
Sigma Aldrich, B512	Tubulin	1/10000	N.A.

Supplementary Table 2. Secondary Antibody list and working dilutions.

Source, Reference	Antibody	Dilutions	
		Immunoblotting	Immunofluorescence
Sigma, sab4600215	Anti-rabbit, CF IRDye 770	1/10000	N.A.
Sigma, sab4600200	Anti-rabbit, CF IRDye 680	1/10000	N.A.
Sigma, sab4600214	Anti-mouse, CF IRDye 770	1/10000	N.A.
Sigma, sab4600199	Anti-mouse, CF IRDye 680	1/10000	N.A.
Sigma, sab4600375	Anti-goat, CF IRDye 770	1/10000	N.A.
Invitrogen, A11034	Anti-rabbit, Alexa Fluor 488	N.A.	1/1000
Invitrogen, A21429	Anti-rabbit, Alexa Fluor 555	N.A.	1/1000
Invitrogen, A21207	Anti-rabbit, Alexa Fluor 594	N.A.	1/1000
Invitrogen, A21072	Anti-rabbit, Alexa Fluor 633	N.A.	1/1000
Invitrogen, A11001	Anti-mouse, Alexa Fluor 488	N.A.	1/1000
Invitrogen, A21424	Anti-mouse, Alexa Fluor 555	N.A.	1/1000
Invitrogen, A21467	Anti-goat, Alexa Fluor 488	N.A.	1/1000

Supplementary Table 3. List of primers used for RT-qPCR.

Gene	Sense primer	Antisense Primer	Amplicon size (bp)
CCNH	5'- TCACCCAGGATAATAATGCTCA-3'	5'-CAGTATCTGTTCAAGTGCCTTCT-3'	136
CDK7	5'-GGAGCCCCAATAGAGCTTATACA-3'	5'-TCCACACCTACACCATACATCC-3'	97
GTF2H1	5'-GACCTTGTTGTGAGTCAAGTGA-3'	5'-CCTGCTTATGATTGGATGTGGAA-3'	100
GTF2H2	5'-CGTATGGGATTTCCCTCAGCAC-3'	5'-AGCCTCCTAATGTAAGCCCTG-3'	115
GTF2H3	5'-GAATGGCAGACTTGGAGACTTC-3'	5'-GCAAAGTTTCTGTATGTTGACCC-3'	176
GTF2H4	5'-ACCCCATTTTCCGCCAGAAC-3'	5'- CGGCGTACTTGTCAAGGGAG-3'	126
GTF2H5	5'-AAGACATTGATGACACTCACGTC-3'	5'-GGGAAAAAGCATTTTGGTCCATT-3'	96
MNAT1	5'-GGTTGCCCTCGGTGAAGAC-3'	5'-AGTTGCTCTTCTGAGTGGAGT-3'	160
ERCC3	5'-CTAACTGCCTACTCCTTGTATGC-3'	5'-TCCATAGCTGACAGTACACAAGT-3'	141
ERCC2	5'-AGAAGGTGATTGAAGAGCTTCG-3'	5'-ACCTCAGGGTGAATACACAAGT-3'	121
GAPDH	5'-AAGGTGAAGGTCGGAGTCAA-3'	5'-ACCATGTAGTTGAGGTCAATG-3'	125

Ubiquitin and TFIIH-stimulated DDB2 dissociation drives DNA damage handover in nucleotide excision repair

3

Cristina Ribeiro-Silva¹, Mariangela Sabatella^{1,2}, Angela Helfricht¹, Arjan F. Theil¹,
Wim Vermeulen^{1,*}, Hannes Lans^{1,*}

1. Department of Molecular Genetics, OncoCode Institute, Erasmus MC, University Medical Center Rotterdam, Dr. Molewaterplein 40, 3015 GD, Rotterdam, The Netherlands

2. Current address: Princess Máxima Center for pediatric oncology, Heidelberglaan 25, 3584 CT, Utrecht, The Netherlands

Submitted

Abstract

DNA damage sensors DDB2 and XPC initiate global genome nucleotide excision repair (NER) to protect DNA from mutagenesis caused by helix-distorting lesions. XPC recognizes helical distortions by binding to unpaired ssDNA opposite of DNA lesions. DDB2 binds to UV-induced lesions directly and facilitates efficient recognition by XPC. We show that not only lesion-binding but also timely DDB2 dissociation is required for DNA damage handover to XPC and swift progression of the multistep repair reaction. DNA-binding induced DDB2 ubiquitylation and ensuing degradation regulate its homeostasis to prevent excessive lesion (re) binding. Additionally, damage handover from DDB2 to XPC coincides with the arrival of the TFIIH complex, which further promotes DDB2 dissociation and formation of a stable XPC-TFIIH damage verification complex. Our results reveal a reciprocal coordination between DNA damage recognition and verification within NER and illustrate that timely repair factor dissociation is vital for correct spatiotemporal control of a multistep repair process.

Introduction

Global-genome nucleotide excision repair (GG-NER) is an essential DNA repair machinery that protects cells against a wide range of structurally unrelated DNA lesions, including the highly mutagenic UV-induced cyclobutane-pyrimidine dimers (CPDs) and 6-4 pyrimidine-pyrimidone photoproducts (6-4PPs)¹⁻³. If not repaired, these lesions interfere with transcription and replication, thereby compromising genomic stability and instigating mutagenesis associated with premature aging and skin cancer^{4,5}. In mammalian cells, GG-NER is initiated by the main damage sensor XPC, as part of the heterotrimeric XPC-CETN2-RAD23B complex, whose substrate versatility derives from its indirect damage recognition mode⁶. As XPC diffuses through the nucleus, it continuously probes DNA searching for thermodynamically helix-destabilized structures⁷ that allow the intercalation of its double β -hairpin domain into the DNA before dissociation⁸⁻¹⁰. In this way, XPC captures and binds extruding nucleotides in the undamaged strand without contacting the lesion itself¹¹.

XPC recruitment to UV-induced DNA damage is stimulated by the UV-DDB complex, comprising of DDB1 and DDB2^{6,12}. DDB2 binds directly to and flips out UV-induced damaged bases to create a more suitable substrate for XPC¹²⁻¹⁵. This activity is particularly relevant for GG-NER of CPDs, which generate only minor DNA helix distortions that are, otherwise, not efficiently recognized by XPC¹⁶. Additionally, DDB2 is thought to facilitate XPC recruitment within chromatinized DNA through its ability to promote chromatin reorganization^{17,18}. The UV-DDB complex is part of a larger E3 ubiquitin-ligase complex (CRL4^{DDB2}), also containing CUL4A, RBX1, and the COP9 signalosome¹⁹. When DDB2 binds to UV-lesions the COP9 signalosome dissociates, which stimulates the E3 ubiquitin-ligase activity of the complex^{19,20}. Several proteins were reported to be ubiquitinated by CRL4^{DDB2}, including core histones H2A, H3 and H4, XPC and DDB2 itself^{19,21-23}.

Because XPC also detects mismatches and other DNA helix distortions that are not processed by NER, subsequent damage verification plays a crucial role in ensuring the fidelity of NER. XPC binding to helix-destabilizing lesions recruits the transcription factor IIH (TFIIH) complex

through interactions with its helicase XPB and core GTF2H1 (also known as p62) subunits^{24–26}. TFIIH's other helicase, XPD, verifies the presence of genuine NER substrates by unwinding the DNA in 5'–3' direction while scanning for helicase blocking lesions^{27,28}. Damage verification is stimulated by the DNA damage binding protein XPA, which, together with the ssDNA binding RPA protein complex, also recruits and positions the endonucleases XPF-ERCC1 and XPG, completing the formation of the pre-incision complex. Incision of the DNA 5' and 3' of the lesion by XPF-ERCC1 and XPG, respectively, leads to the removal of a 22–30 nucleotide long ssDNA enclosing the lesion^{2,3,29}. The resulting gap is restored by *de novo* DNA synthesis and ligation³⁰.

Due to the complexity of the dynamic arrangement of NER factors, temporal and spatial coordination of each NER step is required for efficient repair and accurate restoration of damaged DNA. The sequential damage detection, verification, excision and gap-filling steps give NER the appearance of a linearly ordered, multistep cascade. However, how the progression from one step to the next is coordinated and how each of these consecutive steps feed back onto each other is not yet fully known. The early steps of GG-NER are under tight control by post-translational protein modifications (PTMs), likely to ensure proper damage handover to subsequent NER steps. For instance, the CRL4^{DDB2} complex catalyzes the polyubiquitylation of DDB2 after binding to UV lesions, stimulating its extraction from DNA by the ubiquitin-dependent segregase p97/VCP and targeting DDB2 for proteasomal degradation^{20,31–33}. Furthermore, CRL4^{DDB2} reversibly ubiquitylates XPC, which was suggested to stabilize its association with DNA²². Subsequent sumoylation^{34–36} and RNF111-mediated³⁷ ubiquitylation of XPC were suggested to promote its dissociation to favor XPG binding. Besides, Poly [ADP-ribose] polymerase 1 activity appears to fine-tune the E3 ubiquitin ligase activity of the CRL4^{DDB2} complex and the ubiquitylation and DNA damage binding of XPC³⁸ and DDB2^{39,40}. Despite extensive evidence of PTM-mediated regulation of both DDB2 and XPC, it is still unclear how, once damage is detected, the DNA association and dissociation of XPC and DDB2, respectively, are coordinated with the recruitment of TFIIH to execute damage verification.

In this study, we show that damage verification differently feeds back on

DDB2 and XPC, as TFIIH recruitment coincides with DDB2 dissociation but stabilizes XPC binding to damaged chromatin. Interestingly, although binding of DDB2 to DNA damage is required for optimal repair of UV-induced lesions, its timely dissociation after damage detection is needed to promote the formation of a stable XPC-TFIIH-DNA complex. Our results suggest that the ubiquitylation and proteolytic degradation of DDB2 regulate its DNA damage sensing activity by limiting its availability, thus facilitating proper damage handover and the swift progress of the NER reaction.

Results

Differential regulation of damage sensing proteins DDB2 and XPC by downstream NER factors

We studied how, in living cells, the association of DDB2 and XPC with DNA damage is affected by the recruitment of the downstream NER machinery that verifies and excises the damage. To this end, we measured the UV-C induced change in mobility of GFP-tagged DDB2 and XPC with Fluorescence Recovery After Photobleaching (FRAP). Incomplete fluorescence recovery reflects transient immobilization of GFP-tagged proteins, such as binding to damaged DNA^{7,41,42}. A change in the immobile fraction after UV, therefore, indicates that either less or more proteins are bound to damaged DNA or that each protein is bound for a shorter or longer time. SV40-immortalized human fibroblasts stably expressing GFP-DDB2 or XPC-GFP were treated with siRNA against either GTF2H1, to interfere with damage verification, or against XPG, to block excision, or with non-targeting siRNA as control (CTRL). Following UV-irradiation, a significant fraction of DDB2 molecules was transiently bound to UV-damaged DNA (Fig 1a, b). Interestingly, this UV-induced DDB2 immobilization increased after depletion of GTF2H1 and, to a lesser extent, also after XPG knockdown (Fig. 1a, b). Also, UV-induced XPC immobilization increased after XPG knockdown. In striking contrast however, XPC binding decreased when GTF2H1 was depleted (Fig. 1c, d). These observations show that downstream NER proteins differentially regulate DDB2 and XPC. While damage verification via TFIIH promotes stable XPC binding to damaged DNA, it appears that TFIIH recruitment coincides with or even stimulates DDB2 dissociation, possibly

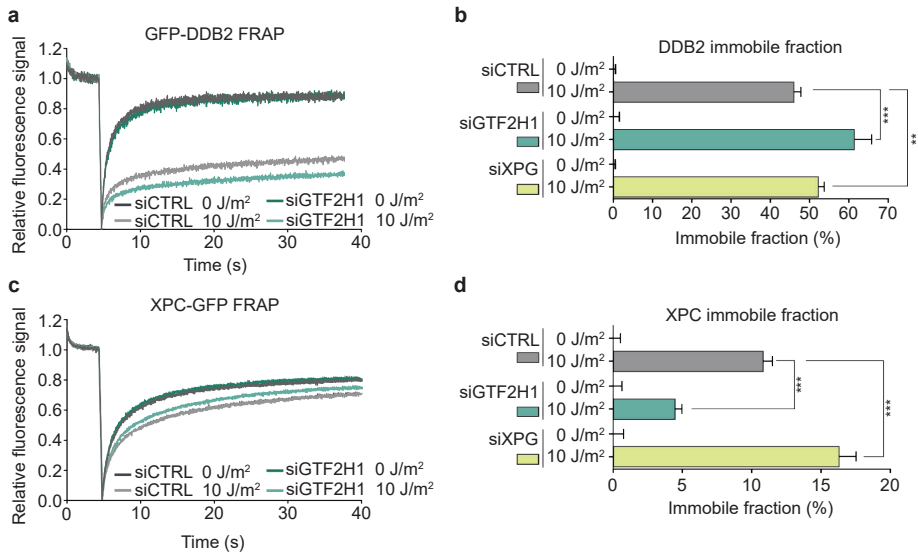


Figure 1. Differential regulation of damage sensing proteins DDB2 and XPC by downstream NER factors. (a) Fluorescence Recovery After Photobleaching (FRAP) analysis of DDB2 mobility in mock or UV-C irradiated (10 J/m²) VH10 cells stably expressing GFP-DDB2 and transfected with control (CTRL) or GTF2H1 siRNAs. GFP-DDB2 fluorescence recovery was measured in a strip across the nucleus after bleaching, normalized to bleach depth and to the average pre-bleach intensities (1.0). (b) Percentage of GFP-DDB2 immobile fraction in VH10 fibroblasts treated with control (CTRL), GTF2H1 or XPG siRNAs, determined from FRAP analyses as depicted in (a). Percentage immobile fraction represents the ratio between the average recovered fluorescence intensity of UV- and mock-treated cells, over the last 10 s of the measurements, as explained in the methods. (c) FRAP analysis of XPC mobility in mock or UV-C irradiated (10 J/m²) XP4PA cells stably expressing XPC-GFP and transfected with control (CTRL) or GTF2H1 siRNAs. XPC-GFP fluorescence recovery was measured and normalized as described in (a). (d) Percentage of XPC-GFP immobile fraction in XP4PA cells treated with control (CTRL), GTF2H1 or XPG siRNAs, determined by FRAP analysis as depicted in (c) and described in (b). Graphs and FRAP curves depict mean & SEM of > 30 cells from three independent experiments. ** P < 0.01, *** P < 0.001, relative to siCTRL control 10 J/m².

to allow proper damage verification. However, when the verification step is still intact but the excision of DNA damage is blocked (i.e., with siXPG), the binding of both DDB2 and XPC to damaged DNA increases. The slowly ascending slopes of the FRAP curves after UV (Fig. 1a, c) suggest that both DDB2 and XPC molecules are not statically bound but are also released within the time course of the FRAP experiments, reflecting dynamic binding and dissociation.

Persistent DNA damage detection in the absence of lesion excision

To verify the increased binding of endogenous DDB2 and XPC to DNA damage in the absence of repair, we used our recently established XPF

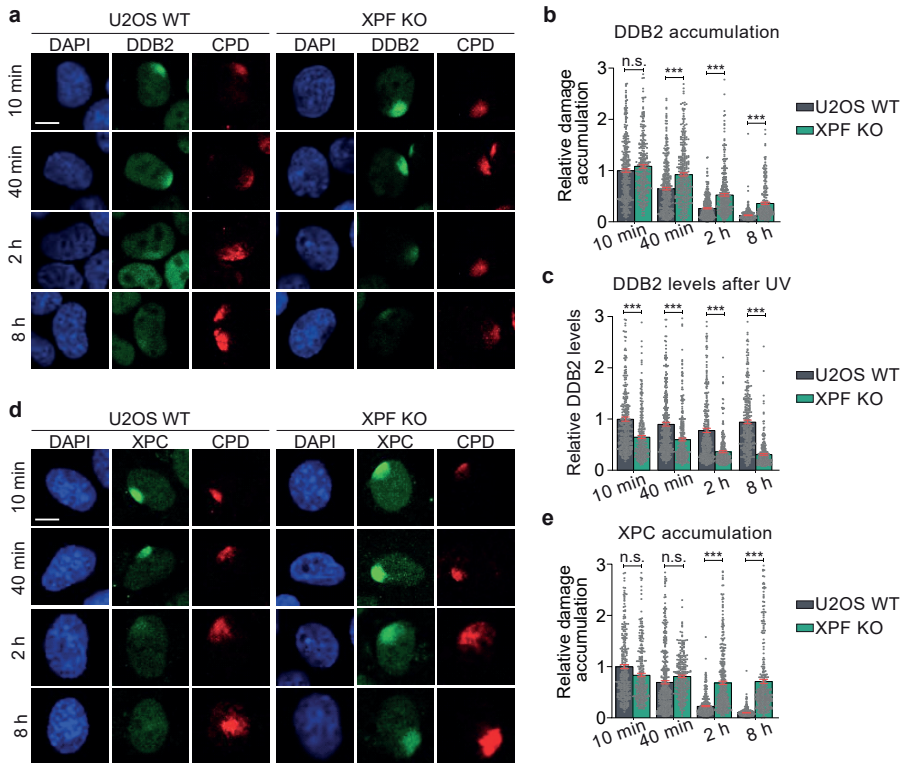


Figure 2. Persistent DNA damage detection in the absence of lesion excision. (a) Representative immunofluorescence (IF) images of endogenous DDB2 accumulation at local UV-C damage (LUD) in U2OS wild-type (WT) and U2OS XPF knockout (XPF KO) cells. Cells were fixed 10 min, 40 min, 2 h and 8 h after LUD (marked by CPD staining) induced with UV-C irradiation (60 J/m^2) through a microporous membrane ($8 \mu\text{m}$). (b) Quantification of DDB2 accumulation at LUD, as depicted in (a). DDB2 accumulation was normalized to the nuclear background and to U2OS WT 10 min after UV-C, which was set to 1.0. (c) Total DDB2 protein levels determined by measuring total nuclear fluorescent signal intensities in nuclei such as depicted in (a) and normalized to U2OS WT 10 min, which was set to 1.0. (d) Representative IF images of endogenous XPC accumulation at LUD in U2OS WT and XPF KO cells, as described in (a). (e) Quantification of XPC accumulation at LUD, as depicted in (d) and described in (b). Mean & SEM of > 250 cells for DDB2 and > 270 for XPC from five independent experiments. * $P < 0.05$, ** $P < 0.01$, *** $P < 0.001$. Scale bars in (a) and (d): $5 \mu\text{m}$.

knockout (XPF KO) U2OS cells⁴³ as an excision-deficient model cell line in which damage verification still takes place and U2OS wild-type (WT) as a NER-proficient cell line. Using immunofluorescence (IF), we monitored the accumulation of endogenous DDB2 and XPC in time at local UV damage (LUD), generated by UV-C irradiation (60 J/m^2) through a microporous membrane. LUD was visualized by counterstaining for CPDs, which are only slowly repaired in human cells and, therefore, still detectable within the time course of our experiment⁴⁴.

In WT cells, DDB2 accumulated rapidly (within 10 min) at LUD and its accumulation slowly declined in time, likely reflecting the removal of easily accessible and rapidly repairable lesions (such as 6-4PPs) (Fig. 2a, b). In excision-deficient XPF KO cells, early accumulation of DDB2 did not differ greatly from that in WT cells, but at later time points (40 min, 2 and 8 h) we observed an increased accumulation of DDB2 at LUD (Fig. 2a, b). This suggests that DDB2 keeps being recruited to persisting, unrepaired lesions when these are not excised. After binding to UV-damaged DNA, DDB2 is ubiquitylated and targeted for proteasome-mediated degradation^{22,31}. Thus, if DDB2 is continuously binding to and dissociating from damaged DNA, it is expected that in time, an increasing amount of DDB2 molecules would be degraded. Indeed, we noticed a significant decline in total DDB2 protein levels in time in the locally irradiated XPF KO cells (Fig. 2c). Such decline was not observed in U2OS WT cells, apparently because the amount of DDB2 molecules that binds to LUD and is degraded is too small to be detected on the total protein level. Besides, inhibition of DDB2 degradation with proteasome inhibitor MG132 led to even higher DDB2 accumulation, persisting in time in XPF KO cells (Supplementary Fig. 1a, b). This suggests that DDB2 degradation normally prevents rebinding to lesions by downregulating its availability. In NER proficient WT cells, however, DDB2 accumulation did not increase in the absence of proteasome activity, showing that DDB2 dissociation from damage occurs normally and is uncoupled from its subsequent degradation.

XPC also showed a rapid accumulation (within 10 min) at LUD in WT cells, which slowly diminished in time as the bulk of lesions were being removed. Interestingly, XPC accumulation at LUD did not decrease in time in the XPF KO cells (Fig. 2d, e). These results indicate that if lesions are not excised, the DNA damage sensing proteins DDB2 and XPC are continuously recruited to sites of DNA damage, implying that multiple rounds of damage detection keep on taking place. However, their fate after binding DNA damage is dramatically different. The accentuated DDB2 degradation could imply that the dissociation of DDB2 and its subsequent degradation are necessary for NER to proceed. XPC, on the other hand, is required for, and becomes more stably bound by, TFIIH recruitment.

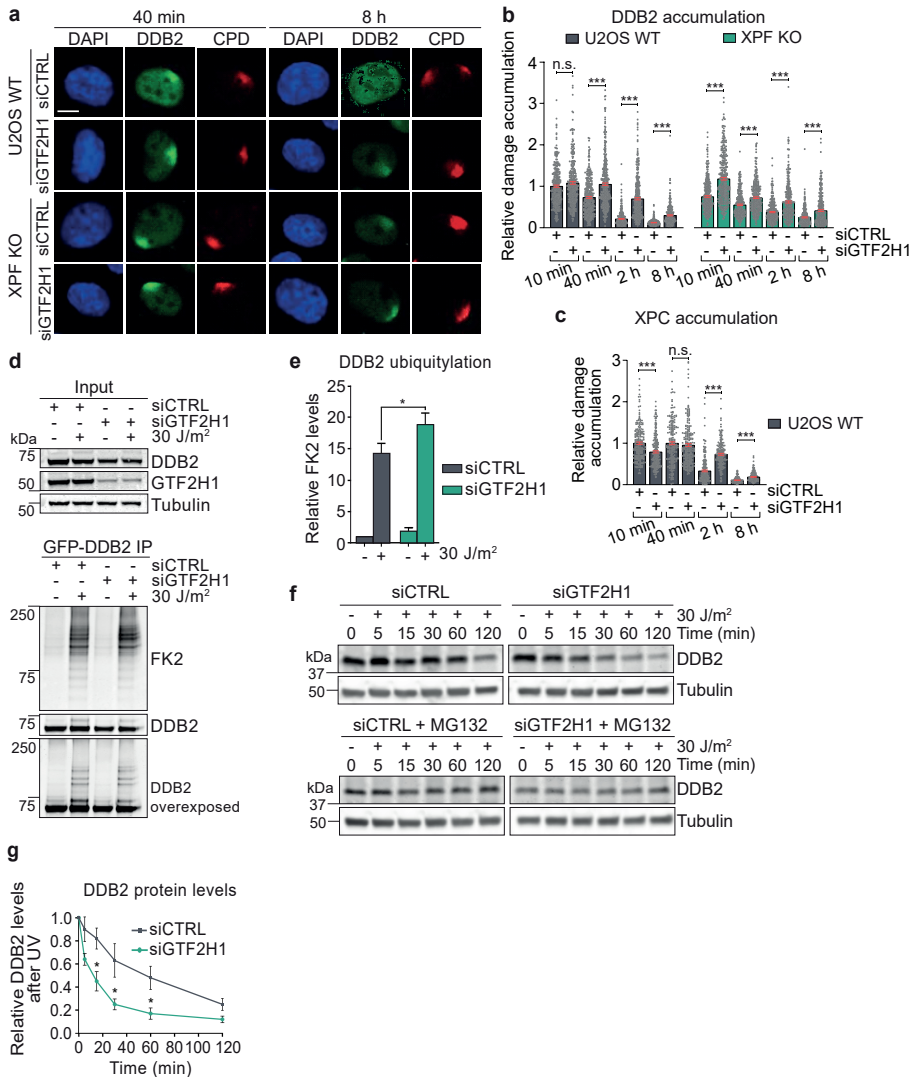


Figure 3. FTHI recruitment promotes DDB2 dissociation and stable XPC binding to DNA damage. (a) Representative IF images of endogenous DDB2 accumulation at LUD in U2OS WT and XPF KO cells treated with control (CTRL) or GTF2H1 siRNAs, 40 min and 8 h after UV-C irradiation (60 J/m²) through a microporous membrane (8 μm). Scale bar: 5 μm. (b, c) Quantification of endogenous (b) DDB2, or (c) XPC accumulation at LUD in U2OS WT and XPF KO cells treated with CTRL or GTF2H1 siRNAs, 10 min, 40 min, 2 h and 8 h after damage, as described in (a). DDB2 and XPC accumulation was normalized to the nuclear background and to U2OS siCTRL 10 mins, which was set to 1.0. Mean & SEM of > 280 cells in (b) or > 165 cells in (c) from two independent experiments. Representative IF images of endogenous XPC are shown in Supplementary Fig. 1c. (d) Immunoblot analysis of DDB2 ubiquitylation in VH10 cells stably expressing GFP-DDB2, before or 15 min after UV-C irradiation (30 J/m²) and treated with CTRL or GTF2H1 siRNAs. Immunoblots of total cell lysates (Input) were stained with antibodies against DDB2, GTF2H1 and Tubulin as loading control. GFP-DDB2 was immunoprecipitated (IP) using GFP beads and IP fractions (GFP-DDB2 IP) samples were analyzed

for ubiquitylation and DDB2, using anti-ubiquitin (FK2) and DDB2 antibodies, respectively. (e) Quantification of FK2 (ubiquitin) levels in the GFP-DDB2 IP fraction as shown in (d). FK2 levels were normalized to DDB2 levels and to 1.0 in non-irradiated siCTRL samples. Mean & SEM of three independent experiments. (f) Immunoblot analysis of UV-induced DDB2 proteolysis in U2OS cells treated with CTRL or GTF2H1 siRNAs in the absence and presence of the MG132 proteasome inhibitor. 50 μ M of MG132 proteasome inhibitor was added to cells 30 mins before irradiation. Total cell lysates were prepared at the indicated time points after UV irradiation (30 J/m²) and analyzed by immunoblotting with DDB2 antibody. Tubulin staining was used as loading control. (g) Quantification of DDB2 levels in time after UV irradiation in the absence of the MG132 proteasome inhibitor, determined by immunoblotting as depicted in (f). DDB2 signal was normalized to the loading control Tubulin and to 1.0 in non-irradiated samples. Mean & SEM of three independent experiments. * P < 0.05, ** P < 0.01, *** P < 0.001, n.s., non-significant.

TFIIH recruitment promotes DDB2 dissociation and stable XPC binding to DNA damage

Because our FRAP analysis suggested that TFIIH recruitment promotes the stable binding of XPC to DNA damage and the dissociation of DDB2 (Fig. 1), we next tested whether endogenous DDB2 and TFIIH might exchange at sites of damaged DNA to promote efficient XPC association with damaged DNA. Using IF, we found that depletion of GTF2H1 led to increased and prolonged accumulation of endogenous DDB2 at LUD in U2OS WT cells (Fig. 3a, b). Strikingly, even in XPF KO cells, in which DDB2 is already continuously recruited due to the complete absence of repair, depletion of GTF2H1 still led to a significantly increased and prolonged DDB2 accumulation at damage (Fig. 3a, b). This is in line with the FRAP data, showing a stronger UV-induced DDB2 immobilization after GTF2H1 than after XPG depletion (Fig. 1b) and, therefore, suggests that TFIIH recruitment coincides with, and might even promote, DDB2 dissociation. Also in support of our FRAP data, the depletion of GTF2H1 in WT cells led to a delay in XPC recruitment to LUD, i.e., XPC accumulation peaked at a later time point (Fig. 3c, Supplementary Fig. 1c).

As part of the CRL4^{DDB2} complex, DDB2 itself is a substrate of the complex's E3 ubiquitin ligase activity^{19,21,22,31}. Interestingly, in *in vitro* ubiquitylation assays, more DDB2 ubiquitylation was observed in the absence of XPC, which has led to the speculation that XPC recruitment protects DDB2 from excessive auto-ubiquitylation and degradation, thus enabling DDB2 to perform multiple rounds of damage detection³². As we observed increased DDB2 and delayed XPC DNA damage recruitment after GTF2H1 knockdown (Fig. 1, 3), we tested whether the absence of TFIIH at damage results in higher DDB2 ubiquitylation levels, promoting its degradation.

Immunoblot analysis of GFP-DDB2 immunoprecipitated from UV-irradiated cells clearly showed a significant increase in UV-induced DDB2 ubiquitylation after siGTF2H1, marked by increased FK2 antibody staining recognizing mono- and poly-ubiquitylated protein conjugates (Fig. 3d, e). In accordance, depletion of GTF2H1 in U2OS cells accelerated the UV-induced and proteasome-dependent DDB2 proteolysis (Fig. 3f, g). Our observations suggest that the recruitment of TFIIH promotes the stable binding of XPC to damaged DNA and the dissociation of DDB2, thereby preventing excessive DDB2 auto-ubiquitylation and degradation.

DDB2 retention impairs stable XPC and TFIIH association with DNA damage

To further investigate the interplay between TFIIH arrival and DDB2 dissociation, we devised an approach to increase the residence time of DDB2 to test whether this would affect the recruitment of XPC and TFIIH. Previously, the ubiquitin-dependent segregase p97/VCP was shown to facilitate the extraction of ubiquitylated DDB2 from UV-damaged chromatin³³. Therefore, we used a specific inhibitor of VCP (VCPi) to impair DDB2 chromatin extraction, and measured recruitment of DDB2 to LUD using IF (Fig. 4a, b). In the presence of VCPi, DDB2 initial accumulation at LUD was indeed higher and gradually disappeared in time, albeit with delayed kinetics (Fig. 4a, b). This was corroborated by FRAP analysis on GFP-DDB2, which showed an increased UV-induced immobilization upon VCPi treatment, suggesting that DDB2 molecules are longer bound to DNA damage (Fig. 4c). Contrary, XPC and XPB accumulation at LUD was delayed and suppressed by VCPi, in particular at early time points (Fig. 4d-g). Interestingly, at these early time points, recruitment of XPC and XPB mirrored that of DDB2, i.e., whenever DDB2 accumulation was higher due to VCPi, XPC and XPB recruitment was lower. It thus appears that prolonged binding of DDB2 to damaged chromatin impairs the early steps of NER, implying that dissociation of DDB2 is required to promote the stable association of XPC and TFIIH with damaged DNA.

Since the VCP segregase has many clients in addition to ubiquitylated DDB2, we tested whether the inhibition of XPC and TFIIH recruitment by VCPi is exclusively dependent on the excessive presence of DDB2 (as part of CRL4^{DDB2}) at UV-damaged sites. To this end, we generated U2OS DDB2

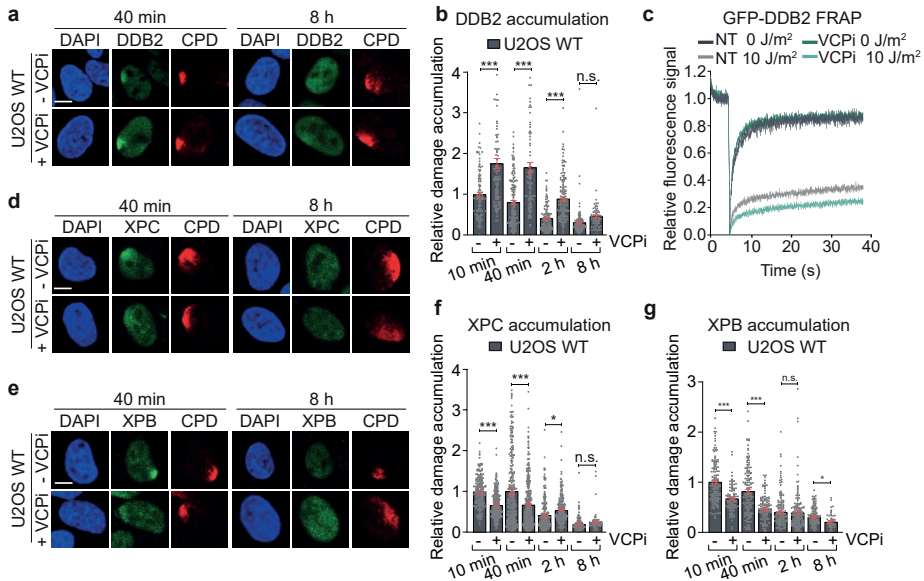


Figure 4. DDB2 retention impairs stable XPC and TFIIH association with DNA damage. (a) Representative IF images of endogenous DDB2 accumulation at LUD in U2OS WT cells in the absence or presence of VCP inhibitor (VCPi). 1 h before LUD induction, 10 μ M VCPi was added and 40 min and 8 h after local UV irradiation (60 J/m²) through a microporous membrane (8 μ m), cells were fixed and analyzed by IF. Scale bars: 5 μ m. (b) Quantification of endogenous DDB2 accumulation at LUD, normalized to the nuclear background and to mock-treated U2OS WT 10 min after UV-C, which was set to 1.0. U2OS cells mock- or VCPi-treated were fixed 10 min, 40 min, 2 h and 8 h after LUD induction. Mean & SEM of > 100 from two independent experiments. (c) FRAP analysis of GFP-DDB2 mobility in VH10 cells before and immediately after UV irradiation (10 J/m²), in the presence or absence of VCPi (10 μ M) added 1 h before irradiation. GFP-DDB2 fluorescence recovery was measured in a strip across the nucleus after bleaching and normalized to the average pre-bleach intensity (1.0). Curves represent the average of > 30 cells per condition from three independent experiments. (d, e) Recruitment of endogenous (d) XPC and (e) XPB to LUD in U2OS WT cells in the absence or presence of VCP inhibitor (VCPi), as described in (a). Scale bars: 5 μ m. (f, g) Quantification of endogenous accumulation of (f) XPC and (g) XPB at LUD as described in (b). Mean & SEM of > 165 cells for XPC and > 100 cells for XPB from three and two independent experiments, respectively. * P < 0.05, ** P < 0.01, *** P < 0.001, n.s., non-significant.

knockout cells by CRISPR/Cas9-mediated gene disruption and confirmed the absence of DDB2 expression and recruitment to DNA damage by immunoblot and IF (Supplementary Fig. 2a, Fig. 5a, b). Accumulation of both XPC and XPB was impaired in the absence of DDB2 (Fig. 5c-f), in agreement with the known role of DDB2 in facilitating lesion recognition by XPC^{6,12,45}. Importantly, we did not observe any additional effect of VCPi on XPC and XPB accumulation in the DDB2 KO cells (Fig. 5c-f).

To confirm this by FRAP analysis, we generated a GFP-XPB knock-in

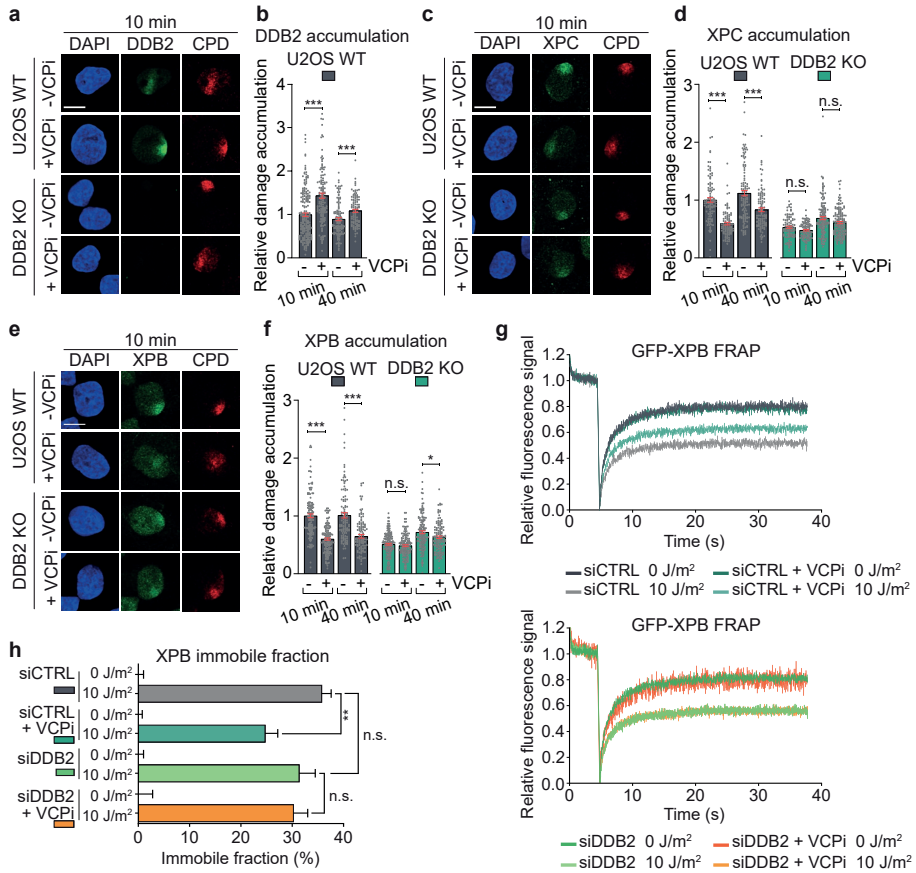


Figure 5. VCP-mediated extraction of DDB2 from damaged chromatin facilitates stable binding of XPC and TFIIH.

(a) Representative IF images of endogenous DDB2 accumulation at LUD in U2OS WT and DDB2 KO cells 10 min after UV irradiation (60 J/m²) through a microporous membrane (8 μm). (b) Quantification of endogenous DDB2 accumulation at LUD, normalized to the nuclear background and to U2OS WT 10 min, which was set to 1.0. U2OS cells were fixed 10 min and 40 min after LUD induction, as described in (a). Mean & SEM of > 120 cells from two independent experiments. (c) Representative IF of endogenous XPC accumulation at LUD in U2OS WT and DDB2 KO cells 10, as described in (a). (d) Quantification of endogenous XPC accumulation at LUD, as described in (b). Mean & SEM > 106 from two independent experiments. (e) Representative IF of endogenous XPB accumulation at LUD in U2OS WT and DDB2 KO cells, as described in (a). (f) Quantification of XPB accumulation at LUD, as described in (b). Mean & SEM of > 100 cells from two independent experiments. (g) FRAP analysis of endogenously GFP-tagged XPB mobility before and 1 h after UV irradiation (10 J/m²), in the presence and absence of DDB2 and/or VCP activity. MRC5 cells with GFP knock-in at the *ERCC3/XPB* locus were transfected with control (CTRL) or DDB2 siRNAs and incubated with mock or VCPi (10 μM) 1 h before UV irradiation. GFP-XPB fluorescence recovery was measured in a strip across the nucleus for 30 s after bleaching and normalized to the average pre-bleach intensity (1.0). (h) Percentage of endogenous XPB immobile fraction in MRC5 cells treated with CTRL or DDB2 siRNAs and/or VCPi, determined from FRAP analysis as depicted in (g). Mean & SEM of > 30 cells per condition from three independent experiments. * P < 0.05, ** P < 0.01, *** P < 0.001, n.s., non-significant. Scale bars: 5 μm.

(KI) MRC-5 human fibroblast cell line, by inserting GFP in front of the endogenous *XPB/ERCC3* gene using CRISPR/Cas9-mediated homology-directed repair (Supplementary Fig. 2b,c). After confirming that the KI cell line behaves as WT MRC-5 in response to UV irradiation (Supplementary Fig. 2d-f), validating the functionality of GFP-tagged XPB, we measured the mobility of this endogenous GFP-XPB in response to UV with and without VCPi using FRAP (Fig. 5g, h). UV irradiation led to a strong immobilization of XPB, which was partially inhibited by VCPi, corroborating our IF experiments. This inhibition by VCPi was not observed after treatment with siRNA against DDB2 (Fig. 5g, h), unequivocally showing that the reduced XPC and XPB accumulation after VCPi is dependent on DDB2. Previously, it was shown in *in vitro* cell-free NER excision and reconstituted NER assays that the CRL4^{DDB2} complex blocks repair in the absence of functional ubiquitylation, because of which it was suggested that ubiquitylation regulates the displacement of DDB2 by XPC at DNA lesions²². Together with our data, this supports a scenario in which the displacement of ubiquitylated DDB2 by VCP promotes damage handover to XPC and the formation of a stably bound damage verification complex together with TFIIH.

Reciprocal coordination of DNA damage handover in GG-NER

We expected DDB2 to become more susceptible to auto-ubiquitylation by the CRL4^{DDB2} complex due to its increased and continuous recruitment to LUD after treatment with VCPi. However, we found that both VCPi and MG132 treatments strongly suppressed DDB2 ubiquitylation after UV (Supplementary Fig. 3a ,b). This explains why in the VCPi- and MG132-treated XPF KO cells, in the absence of repair, DDB2 still accumulated at LUD 8 h after UV irradiation, because DDB2 cannot be proteolytically degraded after UV (Fig. 3a, b, f, Supplementary Fig. 1a, b). We also noticed that, likely due to depletion of the free ubiquitin pool in cells⁴⁶, VCPi prevented efficient UV-induced XPC ubiquitylation (Supplementary Fig. 3c, d), which was hypothesized to increase the affinity of XPC for DNA damage^{22,47,48}. Therefore, we devised an alternative strategy to retain DDB2 in damaged chromatin while preserving the functionality of the CRL4^{DDB2} E3 ubiquitin ligase activity in modifying its substrates, except for DDB2 itself. Previously it has been reported that the N-terminal tail of DDB2 contains several lysines that are targeted for ubiquitylation by

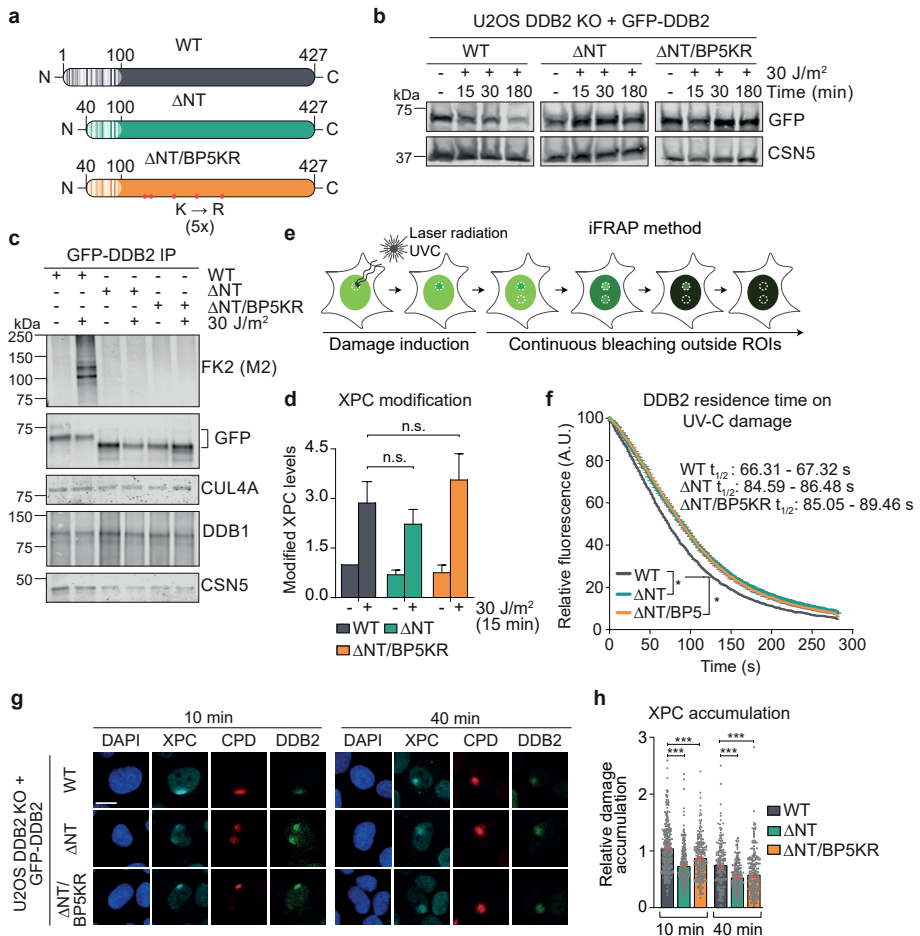


Figure 6. DDB2 ubiquitylation facilitates its extraction from DNA damage to promote damage handover to XPC. (a) Schematic overview of wild-type DDB2 (WT, 427 aminoacids) and deletion mutants lacking the first 40 amino acids in the N-terminal region (depicted in white stripes) of DDB2 (ΔNT) or carrying additionally five lysine (K) to arginine (R) substitutions (depicted as red dots; designated ΔNT/BP5KR). N and C indicate the amino- and carboxy termini, respectively, of DDB2 polypeptide. (b) Immunoblot of UV-induced DDB2 proteolysis in U2OS DDB2 KO cells, stably complemented with GFP-tagged DDB2 WT, ΔNT or ΔNT/BP5KR DDB2. Total cell lysates were prepared at the indicated time points after global UV-C irradiation (30 J/m²) and DDB2 proteins levels were analyzed with a DDB2 antibody. CSN5 staining was used as loading control. (c) Immunoblot of DDB2 binding partners and UV-induced ubiquitylation in U2OS DDB2 KO cells stably expressing WT, ΔNT or ΔNT/BP5KR DDB2, before and 15 min after UV-C irradiation (30 J/m²). Total cell lysates were subjected to GFP immunoprecipitation (IP) and IP samples were analyzed using anti-ubiquitin FK2, GFP, DDB1, CUL4A and CSN5 antibodies. (d) Quantification of ubiquitylated XPC in whole cell lysates of U2OS DDB2 KO cells stably expressing WT, ΔNT or ΔNT/BP5KR GFP-DDB2, as analyzed by immunoblot depicted in Supplementary Fig. 4b, c. Modified XPC levels were normalized to Tubulin and to the mock-treated WT DDB2 condition, which was set to 1.0. Mean and SEM of four independent experiments. (e) Schematic depiction of the inverse Fluorescence after Photobleaching (iFRAP) method. Accumulation of a fluorescent protein to local 266 nm UV-C-laser-induced damage was measured until it reaches a steady-state

level, after which the GFP-derived fluorescence outside the UV-damaged and control area was bleached. The loss of fluorescence in the control and UV-damaged areas was measured. **(f)** iFRAP analysis of WT (grey line), Δ NT (green line) and Δ NT/BP5KR (yellow line) GFP-DDB2 dissociation from local UV DNA damage in U2OS DDB2 KO cells. Fluorescence loss, which reflects DDB2 dissociation, was measured over time, normalized to background and to fluorescence levels before bleaching. Mean & SEM of > 30 cells per condition from three independent experiments. **(g)** Representative IF images of endogenous XPC (cyan channel) accumulation at LUD (marked by CPD, red channel) in U2OS DDB2 KO cells stably complemented with WT, Δ NT or Δ NT/BP5KR GFP-DDB2 (green channel). Cells were fixed 10 and 40 min after UV irradiation (60 J/m^2) through a microporous membrane ($8 \mu\text{m}$). **(h)** Quantification of endogenous XPC accumulation at LUD, normalized to the nuclear background and to WT 10 min after UV-C, which was set to 1.0. Mean & SEM of > 163 cells from three independent experiments. * $P < 0.05$, *** $P < 0.001$, n.s., non-significant. Scale bars: $5 \mu\text{m}$.

the CRL4^{DDB2} complex and are required for degradation of DDB2 after UV-induced damage^{20,32}. In addition, structural studies of the CRL4^{DDB2} complex have identified five potential ubiquitylation lysines outside the N-terminal domain (K146, 151, 187, 233 and 278)²⁰. Ablation of the first 40 N-terminal amino acids of DDB2 (Δ NT), which include seven lysines (K4, 5, 11, 22, 35, 36 and 40), together with lysine-to-arginine substitutions of the additional five putative ubiquitylated lysines (Δ NT/BP5KR), was shown to inhibit the vast majority of DDB2 UV-induced ubiquitylation *in vitro*³². Therefore, we stably complemented our U2OS DDB2 KO cell line with GFP-tagged full-length wild-type (WT), Δ NT and Δ NT/BP5KR DDB2 cDNA (Fig. 6a). In contrast to WT GFP-DDB2, both the Δ NT and the Δ NT/BP5KR GFP-DDB2 mutants resisted degradation and were not ubiquitylated after UV irradiation (Fig. 6b, c, Supplementary Fig. 4a). All GFP-DDB2 variants co-immunoprecipitated DDB1, CUL4A and CSN5 proteins, showing that the assembly of the CRL4^{DDB2} complex is not disturbed by the mutations generated in DDB2 (Fig. 6c). Importantly, the ubiquitylation of XPC after UV irradiation, which is abrogated in DDB2 KO cells, was similarly rescued by WT, Δ NT and Δ NT/BP5KR GFP-DDB2, indicating that the mutated CRL4^{DDB2} complexes are fully functional (Fig. 6d, Supplementary Fig. 4b, c).

To investigate whether indeed the dissociation of DDB2 from UV-damaged was impeded by the mutations that prevent its ubiquitylation, we measured the residence time of the GFP-DDB2 variants at damaged sites, using inverse fluorescence recovery after photobleaching (iFRAP)^{37,49}. To this end, cells were locally irradiated by 266 nm UV-C laser to induce accumulation of GFP-tagged proteins at the damaged areas. After reaching steady-state accumulation, the nuclear fluorescent signal was bleached with the exception of the damaged area and a non-damaged

control area. Next, the fluorescence decay over time in these two areas was measured (Fig. 6e), which reflects DDB2's residence time in damaged and undamaged chromatin³⁷. Accumulation at the laser-induced LUD was higher for the two DDB2 mutants (Supplementary Fig. 4d), and their residence time in damaged chromatin was on average 30% increased (Fig. 6f). This shows that Δ NT and Δ NT/BP5KR DDB2 proteins do not efficiently dissociate from DNA lesions, confirming that ubiquitylation facilitates DDB2 displacement. Therefore, using these cell lines, we tested by IF if prolonged DDB2 retention at UV damage inhibits stable XPC binding to DNA damage. In comparison with WT GFP-DDB2 complemented cells, endogenous XPC accumulation at LUD was reduced in the cell lines complemented with either the Δ NT or the Δ NT/BP5KR GFP-DDB2 mutants (Fig. 6g, h). These observations further support the concept that DDB2 dissociation is required to promote a stable association of XPC to damaged DNA.

Finally, we tested by iFRAP analysis if the recruitment of TFIIH affects the dissociation of DDB2. Interestingly, depletion of GTF2H1 resulted in prolonged binding of GFP-DDB2 to damaged chromatin (Supplementary Fig. 4e). These data indicate that the increased immobilization of DDB2 after GTF2H1 depletion observed in FRAP (Fig. 1a, b) is caused by prolonged DDB2 binding. Together, our results suggest that the initiation of GG-NER consists of reciprocally coordinated events during which, after facilitation of UV-damage detection by DDB2, XPC recruits TFIIH, which in turn facilitates the displacement of DDB2 and the stabilization of XPC association with DNA (Fig. 7).

Discussion

XPC (in complex with CETN2 and RAD23B) is the primary damage sensor of GG-NER and, as such, recruits the TFIIH complex to DNA damage^{24,25,50,51} to verify the presence of NER lesions^{27,28}. Earlier FRAP studies have suggested that mammalian XPC interrogates DNA integrity through continuous random probing and utilizes a stepwise mechanism to detect and bind DNA damage, in which it first transiently interacts with DNA before forming a stable and immobile damage-bound complex^{7,52}.

Crystal structures of the yeast XPC ortholog Rad4 bound to non-damaged DNA⁸, CPD or 6-4PP photolesions^{11,53}, recent *in vitro* temperature-jump spectroscopy⁹ and single-molecule imaging on yeast and human XPC⁵⁴⁻⁵⁶, together with computational modeling, point to a model in which damage recognition by XPC is characterized by consecutive stages: 1) a search complex with random motion; 2) a transiently stalled interrogation complex that untwists and bends the DNA, due to the insertion of XPC's BHD2 hairpin in the minor groove that opens the DNA around the lesion; and 3) a final recognition complex fully and stably bound to the DNA due to the insertion of XPC's BHD3 hairpin into the major groove at the lesion site without ever contacting the lesion directly^{6,10}. In this model, the capacity of XPC to recognize a lesion is dependent on its ability to open the damaged dsDNA and insert its BHD3 hairpin before diffusing away⁸. Strikingly, we found that in living cells, TFIIH is required for stable binding of XPC to damaged DNA (Fig. 1c, d, Fig. 3c). This suggests that TFIIH recruitment may either stabilize the transient interrogation complex, thus promoting the transition to a fully immobile recognition complex, or stabilize the recognition complex itself, by preventing reversion back to an interrogation complex. Accordingly, previous *in vitro* DNA binding studies have suggested that upon DNA binding, XPC can form a stable ternary complex with TFIIH and XPA that is even able to translocate along DNA²⁷. Also, recent modeling analysis based on the structural resolution of XPC and TFIIH indicates that damage verification by TFIIH can stabilize its interaction with XPC on DNA¹⁰. This model proposes that TFIIH is recruited to DNA through an interaction between its XPB subunit and the XPC C-terminus. Upon the release of the CAK subcomplex from TFIIH, stimulated by XPA, the TFIIH helicase XPD contacts the DNA and translocates on the damaged DNA strand in a 5' to 3' direction until it is blocked by a lesion, i.e., damage verification. In this conformation, the TFIIH subunit GTF2H1 is then able to interact with the N-terminus of XPC. Interestingly, XPA enhances lesion-scanning by TFIIH^{28,57} and we found by FRAP that, like TFIIH, XPA facilitates stable binding of XPC to UV-damaged DNA (Supplementary Fig. 5). Therefore, we propose that the formation of a stable XPC-TFIIH-DNA complex is stimulated by active damage verification activity and not solely by the recruitment of TFIIH.

The energetic barrier for XPC to open the dsDNA and form a stable

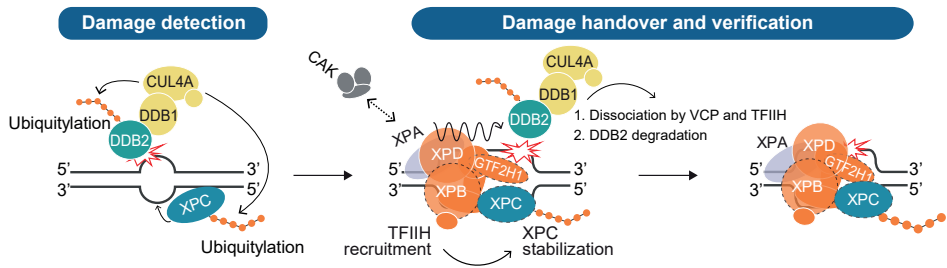


Figure 7. Reciprocal coordination of DNA damage detection and handover in GG-NER. DDB2 binds directly to UV-photoproducts, thereby stimulating XPC recruitment to CPDs and 6-4PPs. The CRL4 E3 ubiquitin ligase activity is activated upon DDB2 binding and ubiquitylates DDB2 and XPC. TFIIH is recruited via an interaction between its subunit XPB with XPC (interaction depicted with dotted lines). Upon TFIIH binding its trimeric CDK7-activating kinase (CAK) sub-complex is released and allows XPA binding, which further stimulates TFIIH's XPD helicase that unwinds the DNA in the 5'-3' direction while scanning for helicase blocking lesions. This configuration facilitates further interaction between TFIIH and XPC by allowing GTF2H1 to interact with XPC. Recruitment of TFIIH and ensuing damage verification promote the stable association of XPC with the undamaged strand and simultaneously facilitate the displacement of DDB2, which is also promoted by ubiquitylation-mediated extraction by VCP (1). The subsequent degradation of DDB2 (2) regulates its availability to rebind to lesions, possibly to avoid competition with the emerging NER pre-incision complex. The formation of a stable ternary XPC-TFIIH-XPA damage verification complex on the lesion and the unpaired DNA surrounding the lesion (created by this complex) provide substrate for the structure-specific endonucleases XPF-ERCC1 and XPG (the latter coinciding with XPC dissociation), which completes the formation of the pre-incision complex.

XPC-DNA recognition complex is higher for lesions that do not strongly distort the DNA duplex⁵⁸. This explains the much lower affinity of XPC for CPDs, which only minimally distort the DNA, as compared to the more helix-destabilizing 6-4PPs¹⁶. DDB2 assists XPC in recognizing UV-induced lesions by directly binding the lesions and kinking the DNA duplex¹⁵ and is thus more relevant for CPDs, albeit it stimulates the repair of 6-4PPs *in vivo* as well^{32,59}. Contrary to XPC, in the absence of TFIIH, we observed increased binding and recruitment of DDB2 to local UV-induced damage (Fig. 3a, b). Moreover, using iFRAP, we measured prolonged DDB2 retention at lesion sites (Supplementary Fig. 4e), suggesting that DDB2 dissociation coincides with TFIIH recruitment and the stabilization of the XPC-TFIIH-DNA complex. Previously, it was shown that tethering DDB2 to chromatin recruits XPC but never TFIIH, whereas tethering XPC recruits TFIIH but never DDB2, implying that DDB2 and TFIIH associate with XPC on DNA damage in a mutually exclusive manner⁶⁰. Furthermore, the superimposition of the crystal structures of DDB2 and yeast XPC/Rad4 bound to DNA indicates that the two proteins cannot stably bind the

same lesion simultaneously, as both interact with the DNA minor groove around the lesion^{10,11,15,53}. However, lesion-bound CRL4^{DDB2} is required for XPC ubiquitylation²², arguing that DDB2 and XPC should – temporarily – coexist, prior to the handover of the damage to the XPC-TFIIH verification complex. Furthermore, XPC uses separate domains to bind to DNA adjacent and opposite of the lesion in a stepwise manner^{11,52,53}. We thus envision that when XPC is recruited to DNA damage, DDB2 and TFIIH exchange to promote its stable binding. In this scenario, TFIIH recruitment to XPC and binding to DNA stimulates DDB2 release and, hence, the transition of XPC from an interrogation to a stably bound recognition complex.

In compliance with this hypothesis, it was found that *in vitro* reconstituted NER is inhibited by the addition of DDB2 in the absence of ubiquitylation factors that mediate its release²². Moreover, here we observed that also in living cells when DDB2 is retained at DNA lesions, recruitment of XPC and XPB is inhibited (Fig. 5, 6). Altogether, these results imply that excessive DDB2, e.g., its prolonged binding, can impede the stable binding of subsequent NER factors.

We found that unrepaired lesions, i.e., after loss of XPG or XPF, lead to persistent DNA damage sensing by DDB2 and XPC (Fig. 1, 2), similar to the persistent targeting of the core NER machinery to DNA damage after the loss of functional XPF that we described before⁴³. XPC is believed to dissociate from DNA lesions concomitantly with XPG recruitment^{37,61}. Therefore, its increased and persistent accumulation in XPF KO cells (Fig. 2d, e) likely reflects continuous binding to and dissociation from lesions that remain accessible. In the case of DDB2, this continuous binding to and dissociation from DNA lesions causes an accelerated UV-induced degradation, rescued by proteasome inhibition (Fig. 2a, b, Supplementary Fig. 1a, b). It was previously estimated, based on photobleaching experiments, that DDB2 can rebind DNA damage multiple times before being degraded⁴¹. Combined with the fact that most other NER proteins, like XPC, are not degraded after UV, this indicates that the effective DDB2 concentration must be tightly regulated in order to promote proper handover of damage to XPC and TFIIH.

Ubiquitylation plays a key role in controlling DDB2 association with lesions,

both by lowering its affinity towards DNA^{22,32} as well as by lowering its protein concentration through degradation^{19,21}. Besides, ubiquitylated DDB2 is actively extracted from chromatin by the VCP segregase, which was shown to facilitate repair and to prevent chromosomal aberrations^{32,33}. Here, we show that impairing DDB2 dissociation, by inhibiting VCP activity or mutating the DDB2 ubiquitylated lysine residues, compromises recruitment of the downstream NER machinery to lesions. Nonetheless, we still observed DDB2 dissociation from damage in VCP-inhibited cells, albeit delayed (Fig. 4a, b). A similar delayed release from damaged chromatin was previously observed with DDB2 lysine mutants, implying that ubiquitylation promotes but is not essential for DDB2 dissociation³². Additionally, we found that inhibition of UV-induced DDB2 degradation by MG132 treatment did not prevent its release from damage in NER proficient cells and allowed DDB2 to rebind persistent lesions over time in NER deficient cells (Supplementary Fig. 1a, b). Hence, the degradation of DDB2 regulates its availability to recognize and bind to damaged DNA and is separate from its extraction and dissociation from DNA. As DDB2 has a stronger affinity for UV photolesions than XPC^{13,62}, its degradation likely prevents that too many DDB2 molecules are available to rebind the same lesions. These results suggest that similar to the recruitment of TFIIH, DDB2 ubiquitylation promotes proper DNA damage handover and the formation of a stable XPC-TFIIH-DNA lesion verification complex.

In summary, here we present evidence of a dynamic interplay between NER DNA damage sensors DDB2 and XPC and the TFIIH verification complex. Based on our findings and relevant literature, we propose that the following key events take place in the transition from damage detection to verification (see also Fig 7). First, DDB2 binds directly to UV-photolesions and stimulates the recruitment of XPC. Ubiquitylation (by CRL4^{DDB2}) of DDB2 reduces its affinity towards UV-lesions and accelerates its dissociation via extraction by VCP. Dissociated ubiquitylated DDB2 is targeted for proteasomal degradation, which decreases its effective concentration. Upon XPC recruitment, also TFIIH is recruited via an interaction with XPB, which coincides with or even stimulates the dissociation of DDB2. Possibly, DDB2 displacement is facilitated by physical competition for the binding space in the vicinity of the lesion or by TFIIH's translocation activity. Ubiquitylation of XPC (by CRL4^{DDB2}) increases its affinity for DNA damage

while TFIIH recruitment, likely due to the XPA-stimulated activation of its helicase activity, stabilizes XPC DNA binding through the formation of an XPC-TFIIH-DNA complex via an additional interaction between XPC and GTF2H1 (Fig. 7). Besides ubiquitylation, many more PTMs have been reported to control DDB2 and XPC activity, including PARylation, sumoylation and phosphorylation^{34,36–40,63,64}. Therefore, it would be interesting to investigate in the future how these PTMs may be controlling the dynamic damage handover between NER initiation and verification factors.

Methods

Cell lines, culture conditions and treatments. U2OS wild-type (WT), DDB2 KO and XPF KO⁴³, SV40-immortalized human fibroblasts XP4PA (XPC-deficient, with stable expression of XPC-GFP), hTERT-immortalized human fibroblasts VH10 (with stable expression of GFP-DDB2³⁹) and MRC-5 (with GFP-XPB knock-in (KI)) were cultured at 37°C in a humidified atmosphere with 5% CO₂ in a 1:1 mixture of DMEM (Lonza) and Ham's F10 (Lonza) supplemented with 10% fetal calf serum (FCS) and 1% penicillin-streptomycin. XP4PA cells with stable expression of XPC-GFP were generated using lentiviral transduction and selection with 0.3 µg/mL Puromycin and FACS⁶⁵. To generate GFP-XPB KI cells, MRC-5 cells were transiently transfected with pLentiCRISPR-v2⁶⁶ carrying an sgRNA targeting near the START codon of the *XPB/ERCC3* locus, and pCRBluntIIPOPO carrying GFP cDNA flanked by XPB homology sequences. After selection with 2 µg/mL Puromycin and FACS, a clonal cell line was isolated and verified by sequencing and functional analysis (Supplementary Fig. 2b-f). To generate U2OS DDB2 KO cells, U2OS cells were transiently transfected with pLentiCRISPR-v2⁶⁶ containing an sgRNA targeting near the START codon of the *DDB2* locus. Transfected cells were selected with puromycin and correct DDB2 KO clone was isolated and verified by sequencing and functional analysis (Fig. 5a, Supplementary Fig. 2a). U2OS DDB2 KO cells with stable expression of WT, ΔNT or ΔNT/BP5KR GFP-DDB2 cDNA were generated using lentiviral transduction and selection with 10 µg/mL Blasticidin and FACS. siRNA transfections were carried out 48 h before each experiment using RNAiMax (Invitrogen) according to the

manufacturer's instructions. Plasmid transfections were performed using JetPei (Promega), according to the manufacturer's instructions. To inhibit proteasome or VCP activity, cells were treated with 50 μM MG132 (BML-PI102, Enzo) or 10 μM of VCPi (NMS-873, Selleckchem), respectively, 1 h before UV irradiation.

Plasmids, sgRNA, and siRNA. To generate an XPC-GFP plasmid, full-length human XPC cDNA was fused to GFP and inserted into pLenti-CMV-Puro-DEST⁶⁵. The pLenti6.3 WT GFP-DDB2 plasmid was kindly provided by Dr. A. Pines³⁹. ΔNT and $\Delta\text{NT}/\text{BP5KR}$ GFP-DDB2 plasmids were generated by deleting the first N-terminal 120 base pairs of DDB2 (ΔNT) and inserting a DDB2 fragment containing five lysine to arginine substitutions (BP5KR) from plasmid pIRESHyg-HA-DDB2-Ndel/BP5KR³², which was a kind gift from Dr. K. Sugawawa. The sgRNAs targeting the *XPB/ERCC3* (TCTGCTGCTGTAGCTGCCAT) and *DDB2* (CACCGCCTTCACACGGAGGACGCGA) loci were cloned into pLenti-CRISPR-V2⁶⁶. The homologous repair template, with GFP DNA flanked by XPB sequences, was generated by PCR and cloned into the pCRBluntII TOPO vector (Zero BluntTM TOPOTM PCR Cloning Kit, ThermoFischer Scientific). Additional cloning and plasmid details are available upon request. siRNA oligomers were purchased from GE Healthcare: CTRL (D-001210-05), DDB2 (J-011022-05), XPG (M-006626-01) and GTF2H1 (L-010924-00). siRNA knockdown efficiency was tested by western blot or IF for each experiment, as shown in Supplementary Fig. 6.

UV-C irradiation. Using a germicidal lamp (254 nm; TUV lamp, Phillips), cells were UV-C irradiated with the indicated doses after being washed with PBS. Local UV-damage (LUD) was generated using 60 J/m^2 of UV irradiation through an 8 μm polycarbonate filter (Millipore), as described previously⁶⁵.

Immunofluorescence. Cells were grown on 18 mm coverslips, fixed in 4% paraformaldehyde and permeabilized in PBS containing 0.5% Triton X-100. For visualization of local UV-induced DNA damage (LUD), DNA was denatured for 5 min with 70 mM NaOH. Next, cells were incubated in blocking buffer (3% BSA and 2.25% glycine in PBS-T (0.1% Tween 20)) for 1 h at room temperature. Primary antibodies were incubated for 1-2

h at room temperature or overnight at 4°C and secondary antibodies conjugated to Alexa fluorochromes 488 or 555 (Invitrogen) were incubated for 1 h at room temperature. Antibody incubation solution was 1% BSA in PBS-T. DNA was stained with DAPI (Sigma), and slides were mounted using Aqua-Poly/Mount (Polysciences, Inc.). Antibodies used are summarized in Supplementary tables 1 and 2. Image acquisition was performed using an LSM700 microscope equipped with a 40x Plan-apochromat 1.3 NA oil immersion lens (Carl Zeiss Micro Imaging Inc.). To quantify protein recruitment to lesion sites, the fluorescence signal intensity at LUD was divided by the nuclear intensity, as measured using FIJI image analysis software. Zero accumulation (nuclear background) was set to 0 and maximum accumulation (above nuclear background) in control or mock-treated conditions was set at 1.0.

Immunoprecipitation (IP). IP experiments were performed under denaturing conditions to detect DDB2 modifications. VH10 GFP-DDB2 cells were grown to confluency on 10 cm dishes and lysed 15 min after UV-C irradiation (30 J/m²) in lysis buffer (20 mM Tris-HCl pH 7.5, 50 mM NaCl, 0.5% NP-40, 1% SDS, 5 mM MgCl₂ and EDTA-free protease inhibitor cocktail (Roche)). Cell lysates were incubated with benzonase buffer (20 mM Tris-HCl pH 7.5, 50 mM NaCl, 0.5 % NP-40, 0.5% Sodium Deoxycholate, 0.5% SDS, EDTA-free protease inhibitor cocktail (Roche) and 0.25 U/μL Benzonase (Millipore)) for 45 min at room temperature in a tube rotator for digestion of chromatin. The suspension was spun down (15.000 g for 10 min) and the supernatant (Input) was used for GFP-DDB2 immunoprecipitation (GFP-DDB2 IP), by incubation of GFP-trap beads (Chromotek) for 2 h at room temperature. Beads were washed 5 x (20 mM Tris-HCl pH 7.5, 50 mM NaCl, 0.5 % NP-40, 0.5% Sodium Deoxycholate, 0.5% SDS and EDTA-free protease inhibitor cocktail (Roche)) and elution of immunoprecipitated proteins was performed by boiling the GFP-trap beads in 2x sample buffer for 5 min at 98°C. Input and GFP-DDB2 IP fractions were analyzed by immunoblotting.

Fluorescence Recovery After Photobleaching (FRAP). FRAP was performed as previously described^{65,67}. In short, the GFP fluorescence signal of our GFP-tagged proteins was measured in a strip across the nucleus (width 512 x 16 pixels, zoom 12 x), at 1400 Hz of a 488 nm laser

every 22 ms until a steady-state was reached (pre-bleach). Using 100% power of the 488 nm laser, the fluorescent signal in the strip was bleached and fluorescence recovery was monitored every 22 ms until recovery was complete. All FRAP experiments were acquired on a Leica TCS SP5 microscope (with LAS AF software, Leica) equipped with a 40x/1.25 NA HCX PL APO CS oil immersion lens (Leica Microsystems), at 37°C and 5% CO₂. Fluorescence signals were normalized to the average pre-bleach fluorescence after background signal subtraction. For the quantification of the immobile fractions (F_{imm}), shown in Figs. 1b, d; 5h; Supplementary Fig. 5, the average recovered fluorescence intensity of UV-irradiated cells ($I_{\text{final,UV}}$) was divided by the average recovered fluorescence intensity of unchallenged cells ($I_{\text{final,unc}}$) over the last 10 s of the measurements, after correction with the fluorescence intensity recorded immediately after bleaching (I_0)⁶⁵:

$$F_{\text{imm}} = 1 - \frac{I_{\text{final,UV}} - I_0, \text{UV}}{I_{\text{final,unc}} - I_0, \text{UV}} .$$

Inverse fluorescence recovery after photobleaching (iFRAP).

Accumulation of proteins to UV-C laser induced DNA damage was measured as described previously, on a Leica SP5 confocal microscope coupled to a 2 mW pulsed (7.8 kHz) diode pumped solid-state laser emitting at 266 nm (Rapp Opto Electronic, Hamburg GmbH)⁶⁵. Cells, grown on quartz coverslips, were imaged and irradiated through an Ultrafluor quartz 100 × /1.35 NA glycerol immersion lens (Carl Zeiss Micro Imaging Inc.) at 37 °C and 5% CO₂. Resulting accumulation curves were corrected for background values and normalized to the relative fluorescence signal before local irradiation. iFRAP was performed as previously described^{37,49}. Briefly, after accumulation reaches a steady state level accumulation, the entire cell is photobleached³⁷ with the exception of three areas in which the fluorescence decay was measured over time: the area of laser-induced UV-C damage, a non-damaged nuclear area and a cytoplasmic area (background). After background correction, signals in the damaged and non-damaged areas of the nucleus were normalized to the average fluorescence levels of pre-damage conditions. The half-time of protein residence in the damaged area was determined by applying a non-linear regression fitted to one phase exponential decay analysis to the iFRAP curves (Fig. 6f), using Graph Pad Prism version 8.21 for Windows (GraphPad

Software, La Jolla California USA).

Preparation of total cell extracts. Cells were washed twice in ice-cold PBS and lysed on ice for 15 min in RIPA buffer (25 mM Tris-HCl pH 8.0, 150 mM NaCl, 0.1% SDS, 1% NP-40, 0.5% Sodium Deoxycholate, 5 mM EDTA, 1 mM PMSF and EDTA-free protease inhibitor cocktail (Roche)). Soluble extracts were obtained by centrifugation at 14000 g for 30 min at 4°C and equal protein amounts were diluted in 2 x sample buffer for immunoblot analysis. 20 mM of N-ethylmaleimide (E3876, Sigma) (DUB inhibitor) was added to the RIPA buffer to improve visualization of XPC-ubiquitination bands (after UV)⁶⁸.

Immunoblotting. Protein samples (total cell extracts or immunoprecipitation fractions) were 2 x diluted in sample buffer (125 mM Tris-HCl pH 6.8, 20% Glycerol, 10% 2-β-Mercaptoethanol, 4% SDS, 0.01% Bromophenol Blue) and boiled for 5 min at 98°C. Proteins were separated in SDS-PAGE gels and transferred onto PVDF membranes (0.45 μm, Merck Millipore). 1 h after blocking the membranes in 5% BSA in PBS-T (0.05% Tween 20), primary antibodies (in PBS-T) were added for 1-2 h at room temperature, or at 4°C overnight. Secondary antibodies were incubated for 1 h at room temperature. After each step of antibody incubation, membranes were washed 3 x 10 min in PBS-T. Probed membranes were visualized and densitometrically analyzed with the Odyssey CLx Infrared Imaging System (LI-COR Biosciences). Antibodies are listed in Supplementary Table 1 and 2.

Statistical analysis. Mean values and SEM error bars are shown for each experiment. Multiple t-tests (unpaired, two-tailed) were used to determine statistical significance between groups followed by multiple comparison correction with the Holm-Sidak method when variances between groups were similar and data were symmetrically distributed. For the statistical significance analysis of IF data, we applied a One-Way ANOVA using the Brown-Forsythe and Welch ANOVA tests, followed by post-hoc analysis with the Games-Howel method. For analysis of graphs in Fig. 6f and Supplementary Fig. 4e, a ROC curve analysis was performed with significance levels set to 0.05. All analyses were performed using Graph Pad Prism version 8.21 for Windows (GraphPad Software, La Jolla

California USA). P values expressed as *P < 0.05; **P < 0.01, ***P < 0.001 were considered to be significant. n.s, non- significant.

Competing financial interests

The authors declare no competing financial interests.

Author contributions

CRS, and HL, and AFT performed all experiments. MS and AH contributed reagents and techniques. CRS, HL, and WV designed experiments, analyzed data and wrote the manuscript. All authors reviewed the manuscript.

Acknowledgments

The authors would like to thank Dr. A. Pines for kindly providing the pLenti6.3 GFP-DDB2 plasmid and Dr. K. Sugawara for the pIRESHyg-HA-DDB2-NdeI/ BP5KR plasmid and the Erasmus MC Optical Imaging Center for microscopy support. This work was financially supported by a Marie Curie Initial Training Network funded by the European Commission 7th Framework Programme (grant 316390), a European Research Council Advanced Grant (grant 340988-ERC-ID), a Worldwide Cancer Research Award (grant 15-1274), Dutch Scientific Organization (ALW grant 854.11.002) and the Dutch Cancer Society (KWF grant 10506) and by the gravitation program CancerGenomiCs.nl from the Netherlands Organization for Scientific Research. Oncode Institute is partly financed by the Dutch Cancer Society.

References

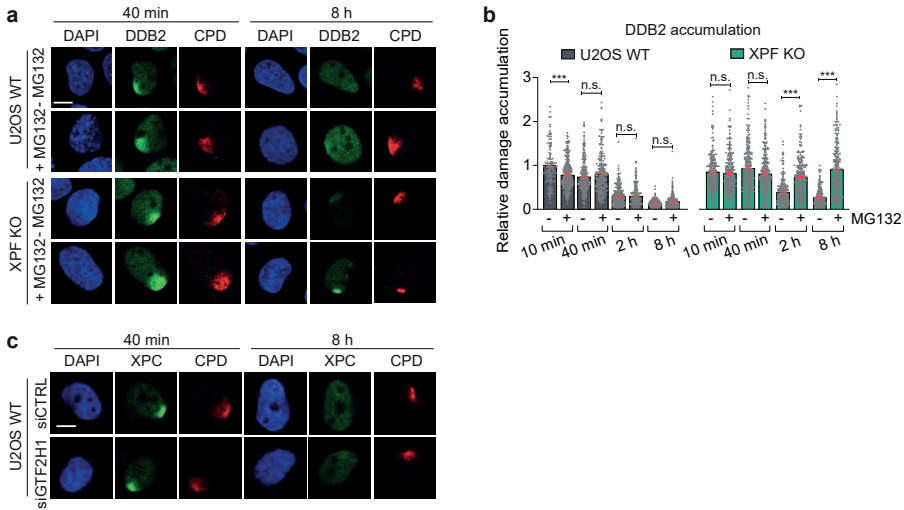
1. Cadet, J., Sage, E. & Douki, T. Ultraviolet radiation-mediated damage to cellular DNA. *Mutation Research - Fundamental and Molecular Mechanisms of Mutagenesis* 571, 3–17 (2005).
2. Marteijn, J. a, Lans, H., Vermeulen, W. & Hoeijmakers, J. H. J. Understanding nucleotide excision repair and its roles in cancer and ageing. *Nat. Rev. Mol. Cell Biol.* 15, 465–81 (2014).
3. Schärer, O. D. Nucleotide excision repair in Eukaryotes. *Cold Spring Harb. Perspect. Biol.* 5, (2013).
4. Hoeijmakers, J. H. J. DNA damage, aging, and cancer. *N. Engl. J. Med.* 361, 1475–85 (2009).
5. Cleaver, J. E. Cancer in xeroderma pigmentosum and related disorders of DNA repair. *Nature Reviews Cancer* 5, 564–573 (2005).
6. Sugasawa, K. Molecular Mechanism of DNA Damage Recognition for Global Genomic Nucleotide Excision Repair: A Defense System Against UV-Induced Skin Cancer. in *DNA Repair Disorders* 1–23 (Springer Singapore, 2018).
7. Hoogstraten, D. et al. Versatile DNA damage detection by the global genome nucleotide excision repair protein XPC. *J. Cell Sci.* 121, 2850–9 (2008).
8. Chen, X. et al. Kinetic gating mechanism of DNA damage recognition by Rad4/XPC. *Nat. Commun.* 6, 5849 (2015).
9. Velmurugu, Y., Chen, X., Slogoff Sevilla, P., Min, J.-H. & Ansari, A. Twist-open mechanism of DNA damage recognition by the Rad4/XPC nucleotide excision repair complex. *Proc. Natl. Acad. Sci.* 113, E2296–E2305 (2016).
10. Mu, H., Geacintov, N. E., Broyde, S., Yeo, J. E. & Schärer, O. D. Molecular basis for damage recognition and verification by XPC-RAD23B and TFIIH in nucleotide excision repair. *DNA Repair* 71, 33–42 (2018).
11. Min, J. H. & Pavletich, N. P. Recognition of DNA damage by the Rad4 nucleotide excision repair protein. *Nature* 449, 570–575 (2007).
12. Tang, J. Y., Hwang, B. J., Ford, J. M., Hanawalt, P. C. & Chu, G. Xeroderma pigmentosum p48 gene enhances global genomic repair and suppresses UV-induced mutagenesis. *Mol. Cell* 5, 737–44 (2000).
13. Wittschieben, B., Iwai, S. & Wood, R. D. DDB1-DDB2 (xeroderma pigmentosum group E) protein complex recognizes a cyclobutane pyrimidine dimer, mismatches, apurinic/apyrimidinic sites, and compound in DNA. *J. Biol. Chem.* 280, 39982–39989 (2005).
14. Wakasugi, M. et al. DDB accumulates at DNA damage sites immediately after UV irradiation and directly stimulates nucleotide excision repair. *J. Biol. Chem.* 277, 1637–1640 (2002).
15. Scrima, A. et al. Structural Basis of UV DNA-Damage Recognition by the DDB1-DDB2 Complex. *Cell* 135, 1213–1223 (2008).
16. Sugasawa, K. et al. A multistep damage recognition mechanism for global genomic nucleotide excision repair. *Genes Dev.* 15, 507–521 (2001).
17. Matsumoto, S. et al. DNA damage detection in nucleosomes involves DNA register shifting. *Nature* 571, (2019).
18. Luijsterburg, M. S. et al. DDB2 promotes chromatin decondensation at UV-induced DNA damage. *J. Cell Biol.* 197, 267–281 (2012).
19. Groisman, R. et al. The ubiquitin ligase activity in the DDB2 and CSA complexes is differentially regulated by the COP9 signalosome in response to DNA damage. *Cell* 113, 357–367 (2003).

20. Fischer, E. S. et al. The molecular basis of CRL4 DDB2/CSA ubiquitin ligase architecture, targeting, and activation. *Cell* 147, 1024–1039 (2011).
21. El-Mahd, M. A. et al. Cullin 4A-mediated proteolysis of DDB2 protein at DNA damage sites regulates in vivo lesion recognition by XPC. *J. Biol. Chem.* 281, 13404–13411 (2006).
22. Sugawara, K. et al. UV-induced ubiquitylation of XPC protein mediated by UV-DDB-ubiquitin ligase complex. *Cell* 121, 387–400 (2005).
23. Kapetanaki, M. G. et al. The DDB1-CUL4ADDB2 ubiquitin ligase is deficient in xeroderma pigmentosum group E and targets histone H2A at UV-damaged DNA sites. *Proc. Natl. Acad. Sci. U. S. A.* 103, 2588–2593 (2006).
24. Okuda, M., Nakazawa, Y., Guo, C., Ogi, T. & Nishimura, Y. Common TFIH recruitment mechanism in global genome and transcription-coupled repair subpathways. *Nucleic Acids Res.* 45, 13043–13055 (2017).
25. Yokoi, M. et al. The xeroderma pigmentosum group C protein complex XPC-HR23B plays an important role in the recruitment of transcription factor IIF to damaged DNA. *J. Biol. Chem.* 275, 9870–9875 (2000).
26. Bernardes de Jesus, B. M., Bjørås, M., Coin, F. & Egly, J. M. Dissection of the molecular defects caused by pathogenic mutations in the DNA repair factor XPC. *Mol. Cell. Biol.* 28, 7225–7235 (2008).
27. Sugawara, K., Akagi, J. ichi, Nishi, R., Iwai, S. & Hanaoka, F. Two-Step Recognition of DNA Damage for Mammalian Nucleotide Excision Repair: Directional Binding of the XPC Complex and DNA Strand Scanning. *Mol. Cell* 36, 642–653 (2009).
28. Li, C. L. et al. Tripartite DNA Lesion Recognition and Verification by XPC, TFIH, and XPA in Nucleotide Excision Repair. *Mol. Cell* 59, 1025–1034 (2015).
29. Staresinic, L. et al. Coordination of dual incision and repair synthesis in human nucleotide excision repair. *EMBO J.* 28, 1111–1120 (2009).
30. Ogi, T. et al. Three DNA Polymerases, Recruited by Different Mechanisms, Carry Out NER Repair Synthesis in Human Cells. *Mol. Cell* 37, 714–727 (2010).
31. Rapić-Otrin, V., McLenigan, M. P., Bisi, D. C., Gonzalez, M. & Levine, A. S. Sequential binding of UV DNA damage binding factor and degradation of the p48 subunit as early events after UV irradiation. *Nucleic Acids Res.* 30, 2588–2598 (2002).
32. Matsumoto, S. et al. Functional regulation of the DNA damage-recognition factor DDB2 by ubiquitination and interaction with xeroderma pigmentosum group C protein. *Nucleic Acids Res.* 43, 1700–1713 (2015).
33. Puumalainen, M. R. et al. Chromatin retention of DNA damage sensors DDB2 and XPC through loss of p97 segregase causes genotoxicity. *Nat. Commun.* 5, (2014).
34. Akita, M. et al. SUMOylation of xeroderma pigmentosum group C protein regulates DNA damage recognition during nucleotide excision repair. *Sci. Rep.* 5, 10984 (2015).
35. Wang, Q. E. et al. DNA repair factor XPC is modified by SUMO-1 and ubiquitin following UV irradiation. *Nucleic Acids Res.* 33, 4023–4034 (2005).
36. Poulsen, S. L. et al. RNF111/Arkadia is a SUMO-targeted ubiquitin ligase that facilitates the DNA damage response. *J. Cell Biol.* 201, 787–807 (2013).
37. van Cuijk, L. et al. SUMO and ubiquitin-dependent XPC exchange drives nucleotide excision repair. *Nat. Commun.* 6, 7499 (2015).
38. Robu, M. et al. Poly(ADP-ribose) polymerase 1 escorts XPC to UV-induced DNA lesions during nucleotide excision repair. *Proc. Natl. Acad. Sci.* 114, E6847–E6856 (2017).
39. Pines, A. et al. PARP1 promotes nucleotide excision repair through DDB2 stabilization and

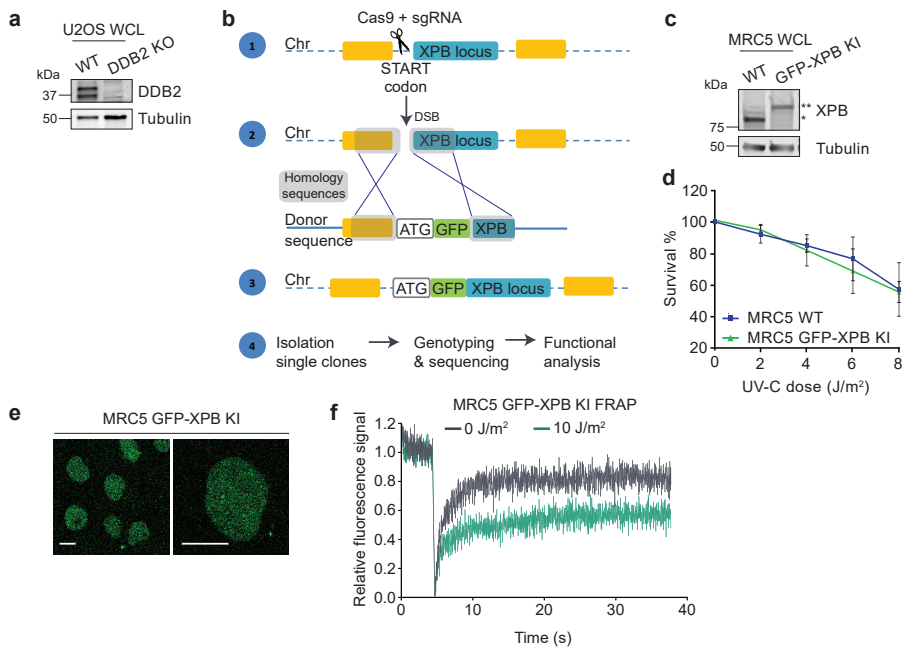
- recruitment of ALC1. *J. Cell Biol.* 199, 235–249 (2012).
40. Robu, M. et al. Role of poly (ADP-ribose) polymerase-1 in the removal of UV-induced DNA lesions by nucleotide excision repair. *Proc. Natl. Acad. Sci. U. S. A.* 110, 1–6 (2013).
 41. Luijsterburg, M. S. et al. Dynamic in vivo interaction of DDB2 E3 ubiquitin ligase with UV-damaged DNA is independent of damage-recognition protein XPC. *J. Cell Sci.* 120, 2706–2716 (2007).
 42. Vermeulen, W. Dynamics of mammalian NER proteins. *DNA Repair* 10, 760–771 (2011).
 43. Sabatella, M. et al. Repair protein persistence at DNA lesions characterizes XPF defect with Cockayne syndrome features. *Nucleic Acids Res.* 46, 9563–9577 (2018).
 44. Mitchell, D. L., Haipek, C. A. & Clarkson, J. M. (6-4)Photoproducts are removed from the DNA of UV-irradiated mammalian cells more efficiently than cyclobutane pyrimidine dimers. *Mutat. Res. - Mutat. Res. Lett.* 143, 109–112 (1985).
 45. Nishi, R. et al. UV-DDB-dependent regulation of nucleotide excision repair kinetics in living cells. *DNA Repair (Amst.)* 8, 767–776 (2009).
 46. Dantuma, N. P., Groothuis, T. A. M., Salomons, F. A. & Neeffjes, J. A dynamic ubiquitin equilibrium couples proteasomal activity to chromatin remodeling. *J. Cell Biol.* 173, 19–26 (2006).
 47. Fei, J. et al. Regulation of nucleotide excision repair by UV-DDB: Prioritization of damage recognition to internucleosomal dna. *PLoS Biol.* 9, (2011).
 48. Wang, Q. E. et al. Cellular ubiquitination and proteasomal functions positively modulate mammalian nucleotide excision repair. *Mol. Carcinog.* 42, 53–64 (2005).
 49. Dundr, M. et al. Like attracts like: Getting RNA processing together in the nucleus. *Science* 288, 1385–1389 (2000).
 50. Sugawara, K. et al. Xeroderma pigmentosum group C protein complex is the initiator of global genome nucleotide excision repair. *Mol. Cell* 2, 223–32 (1998).
 51. Volker, M. et al. Sequential assembly of the nucleotide excision repair factors in vivo. *Mol. Cell* 8, 213–224 (2001).
 52. Camenisch, U. et al. Two-stage dynamic DNA quality check by xeroderma pigmentosum group C protein. *EMBO J.* 28, 2387–2399 (2009).
 53. Paul, D. et al. Structure and mechanism of pyrimidine–pyrimidone (6-4) photoproduct recognition by the Rad4/XPC nucleotide excision repair complex. *Nucleic Acids Res.* 47, 6015–6028 (2019).
 54. Kong, M. et al. Single-Molecule Imaging Reveals that Rad4 Employs a Dynamic DNA Damage Recognition Process. *Mol. Cell* 64, 376–387 (2016).
 55. Cheon, N. Y., Kim, H.-S., Yeo, J.-E., Schärer, O. D. & Lee, J. Y. Single-molecule visualization reveals the damage search mechanism for the human NER protein XPC-RAD23B. *Nucleic Acids Res.* 47, 8337–8347 (2019).
 56. Janičijević, A. et al. DNA bending by the human damage recognition complex XPC-HR23B. *DNA Repair (Amst.)* 2, 325–336 (2003).
 57. Kocic, G. et al. Structural basis of TFIIH activation for nucleotide excision repair. *Nat. Commun.* 10, (2019).
 58. Jing, Y., Kao, J. F. & Taylor, J. S. Thermodynamic and base-pairing studies of matched and mismatched DNA dodecamer duplexes containing cis-syn, (6-4) and Dewar photoproducts of TT. *Nucleic Acids Res.* 26, 3845–3853 (1998).
 59. Moser, J. et al. The UV-damaged DNA binding protein mediates efficient targeting of the nucleotide excision repair complex to UV-induced photo lesions. *DNA Repair (Amst.)* 4, 571–

- 582 (2005).
60. Ziani, S. et al. Sequential and ordered assembly of a large DNA repair complex on undamaged chromatin. *J. Cell Biol.* 206, 589–598 (2014).
 61. Riedl, T., Hanaoka, F. & Egly, J.-M. The comings and goings of nucleotide excision repair factors on damaged DNA. *EMBO J.* 22, 5293–303 (2003).
 62. Batty, D., Ropic'-Otrin, V., Levine, A. S. & Wood, R. D. Stable binding of human XPC complex to irradiated DNA confers strong discrimination for damaged sites. *J. Mol. Biol.* 300, 275–290 (2000).
 63. Shah, P., Zhao, B., Qiang, L. & He, Y. Y. Phosphorylation of xeroderma pigmentosum group C regulates ultraviolet-induced DNA damage repair. *Nucleic Acids Res.* 46, 5050–5060 (2018).
 64. Maltseva, E. A., Rechkunova, N. I., Sukhanova, M. V. & Lavrik, O. I. Poly(ADP-ribose) polymerase 1 modulates interaction of the nucleotide excision repair factor XPC-RAD23B with DNA via Poly(ADP-ribosylation). *J. Biol. Chem.* 290, 21811–21820 (2015).
 65. Ribeiro-Silva, C. et al. DNA damage sensitivity of SWI/SNF-deficient cells depends on TFIID subunit p62/GTF2H1. *Nat. Commun.* 9, 4067 (2018).
 66. Sanjana, N. E., Shalem, O. & Zhang, F. Improved vectors and genome-wide libraries for CRISPR screening. *Nat. Methods* 11, 783–784 (2014).
 67. Houtsmuller, A. B. & Vermeulen, W. Macromolecular dynamics in living cell nuclei revealed by fluorescence redistribution after photobleaching. *Histochemistry and Cell Biology* 115, 13–21 (2001).
 68. Emmerich, C. H. & Cohen, P. Optimising methods for the preservation, capture and identification of ubiquitin chains and ubiquitylated proteins by immunoblotting. *Biochemical and Biophysical Research Communications* 466, 1–14 (2015).

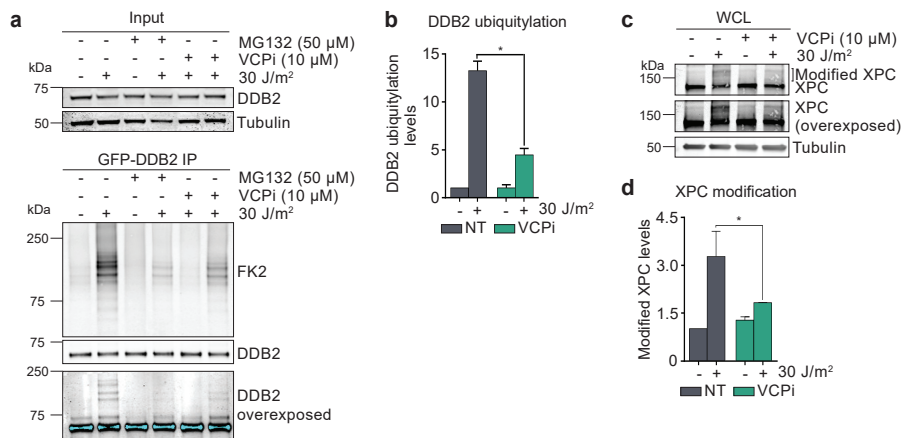
Supplementary data



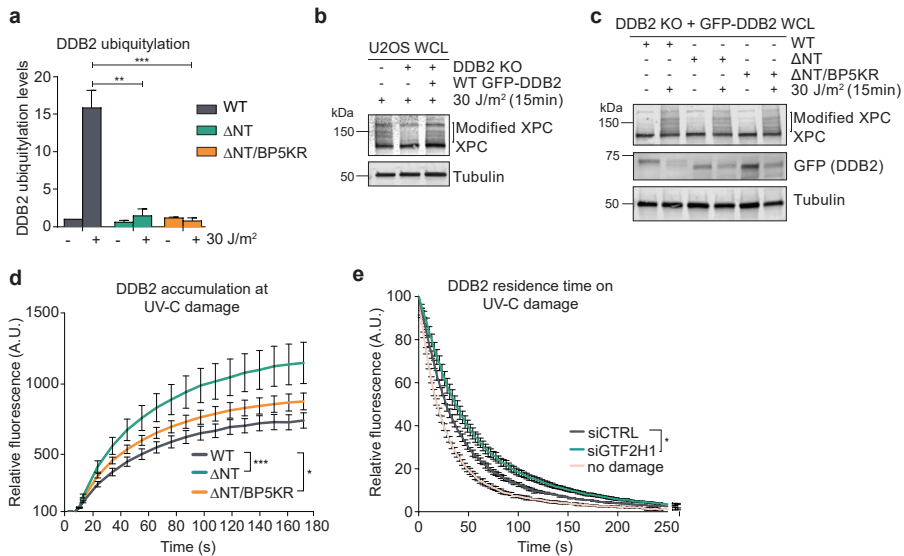
Supplementary Fig. 1. XPC and DDB2 recruitment to LUD. (a) Representative IF images of endogenous DDB2 accumulation at LUD in U2OS WT and XPF KO cells in the absence or presence of proteasome inhibitor MG132. 1 h before LUD induction, 50 μ M MG132 was added to cells, which were fixed 40 min and 8 h after local UV irradiation (60 J/m^2) through a microporous membrane (8 μ m). Scale bar: 5 μ m. (b) Quantification of endogenous DDB2 accumulation at LUD in U2OS WT and XPF KO cells, as described in (a). DDB2 accumulation was normalized to the nuclear background and to U2OS WT (- MG132) 10 min, which was set to 1.0. Mean & SEM of > 127 cells from three independent experiments. *** $P < 0.001$, n.s., non-significant. (c) Representative IF images of endogenous XPC recruitment to LUD (marked by CPD staining) 40 min and 8 h after UV-C (60 J/m^2) through a microporous membrane (8 μ m) in U2OS WT cells treated with control (CTRL) or GTF2H1 siRNAs. Quantified in Fig. 3c. Scale bar: 5 μ m.



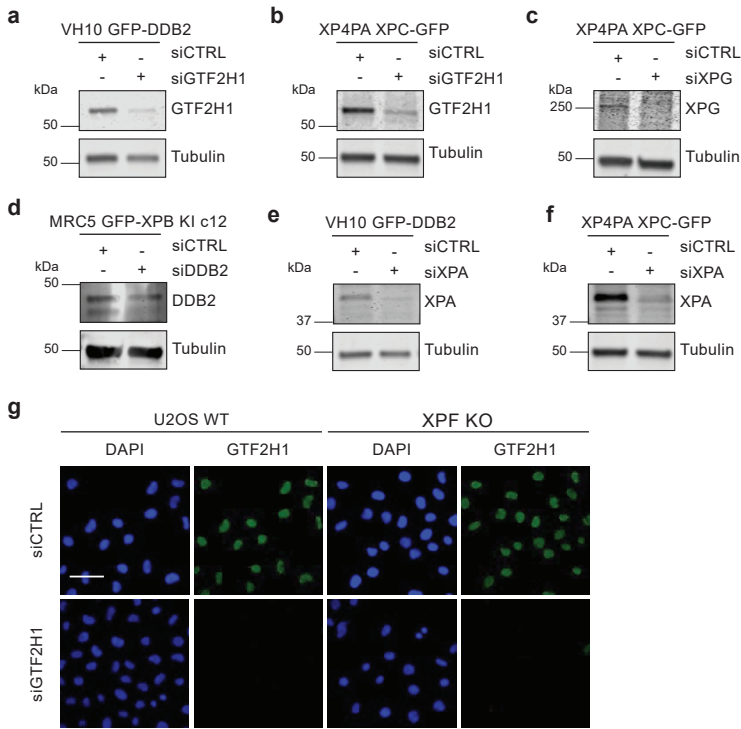
Supplementary Fig. 2. Generation of DDB2 KO and GFP-XPB knock-in cell lines. (a) Whole cell lysate (WCL) immunoblot analysis of U2OS WT and DDB2 KO cells with DDB2 antibody. Tubulin was used as loading control. (b) Schematic representation of the GFP knock-in (GFP-KI) strategy in the *XPB* locus using CRISPR-Cas9 homology-directed repair, generating cells with stable and endogenous expression of GFP-tagged XPB. (c) Whole cell lysate (WCL) immunoblot analysis of WT MRC5 cells and GFP-XPB KI clone with XPB antibody. Wild-type XPB is marked with * and GFP-XPB with **. Tubulin was used as loading control. (d) Colony survival after UV-C irradiation of WT MRC5 cells and GFP-XPB KI. Survival was plotted as the percentage of colonies obtained after treatment compared to the mean number of colonies from the mock-treated cells, set as 100%. Mean & SEM of three independent experiments, each performed in triplicate. (e) MRC5 GFP-XPB KI live cell confocal images showing nuclear GFP-XPB expression. Scale bars: 15 μm (left and right). (f) Characterization of endogenous XPB mobility in MRC5 GFP-XPB KI cells before and immediately after UV irradiation (10 J/m²) using FRAP analysis. GFP-XPB fluorescence recovery was measured in a strip across the nucleus after bleaching and normalized to the average pre-bleach intensity (1.0).



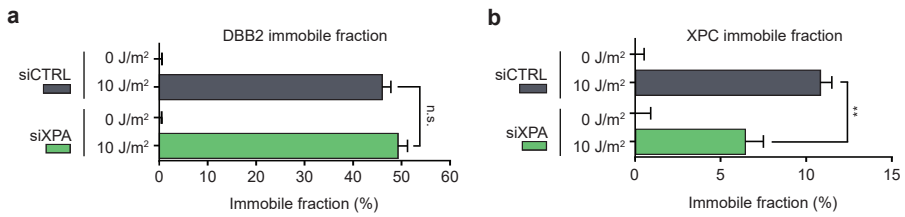
Supplementary Fig. 3. MG132 and VCPI inhibit UV-induced ubiquitylation of DDB2 and XPC. (a) Immunoblot analysis of DDB2-ubiquitylation levels in VH10 cells stably expressing GFP-DDB2, mock-treated or treated with 50 μ M of proteasome inhibitor MG132 or 10 μ M of VCPI, 30 min and 1 h before UV (30 J/m²), respectively. GFP-DDB2 IP fractions and total cell lysates (Input) were immunoblotted and probed with antibodies against ubiquitin (FK2) and DDB2. Tubulin was used as loading control. (b) Quantification of ubiquitin (FK2) levels in the GFP-DDB2 IP fraction depicted in (a). Ubiquitin levels were normalized to DDB2 and to the mock-treated condition, which was set to 1.0. * P < 0.05, relative to non-irradiated condition. Mean & SEM of two independent experiments. (c) Immunoblot analysis of XPC ubiquitylation in U2OS cells mock-treated or treated with VCPI (10 μ M), 1 h before UV (30 J/m²). Whole cell lysates (WCL) were analyzed by immunoblotting using an antibody against XPC. Tubulin staining was used as loading control. (d) Quantification of ubiquitin-modified XPC in WCL of U2OS, depicted in (c). Modified XPC levels were normalized to Tubulin and to the mock-treated condition, which was set to 1.0. Mean & SEM of three independent experiments. * P < 0.05, relative to UV-irradiated mock-treated cells.



Supplementary Fig. 4. Analysis of WT and mutant GFP-DDB2 cell lines. (a) Quantification of ubiquitin (FK2) levels in the GFP-DDB2 IP fraction revealed by immunoblotting and shown in Fig. 6c. Ubiquitin levels were normalized to DDB2 and to the mock-treated condition, which was set to 1.0. Mean & SEM of two independent experiments. (b) Immunoblot analysis of XPC ubiquitylation in whole cell lysate (WCL) of U2OS WT and DDB2 KO cells with or without stable expression of WT GFP-DDB2, prepared 15 min after UV (30 J/m²) and analyzed with an antibody against XPC. Tubulin staining was used as loading control. (c) Immunoblot analysis of XPC ubiquitylation in WCL of U2OS DDB2 KO cells with stable expression of WT, Δ NT, or Δ NT/BP5KR GFP-DDB2, stained with XPC, DDB2 and Tubulin antibodies. (d) Accumulation of WT, Δ NT and Δ NT/BP5KR GFP-DDB2 variants at LUD, induced with a 266 nm UV-C laser, measured in real-time by confocal imaging. Pre-damage relative fluorescence intensity was set to 100% (t=0). Mean & SEM of from > 30 cells per condition from three independent experiments. * P < 0.05, *** P < 0.001 regarding the last accumulation time point. (e) iFRAP analysis of WT GFP-DDB2 dissociation from non-damaged DNA (pink line) and from local UV DNA damage after control (CTRL, grey line) or GTF2H1 (green line) siRNA treatment in VH10 cells stably expressing wild type GFP-DDB2. Fluorescence was measured over time, normalized to background and to fluorescence levels before bleaching. Mean & SEM of > 30 cells per condition from three independent experiments.* P < 0.05.



Supplementary Fig. 5. Differential regulation of damage sensing proteins DDB2 and XPC by XPA. (a) Percentage of GFP-DDB2 immobile fraction in VH10 fibroblasts treated with control (CTRL) or XPA siRNAs, determined from FRAP analyses as described in Fig. 1. Percentage immobile fraction represents the ratio between the average recovered fluorescence intensity of UV- and mock-treated cells, over the last 10 s of the measurements, as explained in the methods. (b) Percentage of XPC-GFP immobile fraction in XP4PA cells treated with control (CTRL) or XPA siRNAs, determined by FRAP analysis as described in Fig. 1. Graphs in (a) and (b) depict mean & SEM of > 30 cells for each condition from three independent experiments. ** $P < 0.01$, n.s., non-significant.



Supplementary Fig. 6. Knockdown efficiency analysis. (a-f) Immunoblot analyses of total cell lysates demonstrating the efficiency of siRNA-mediated protein depletion with siRNAs against GTF2H1, XPG, XPA and DBB2 in the indicated cell lines and probed with antibodies against the respective proteins. Tubulin was used as loading control. (g) Immunofluorescence (IF) images stained with antibodies against GTF2H1, demonstrating the efficiency of GTF2H1 siRNA-mediated depletion in U2OS WT and XPF KO cells. Scale bar: 50 μ m.

Supplementary Table 1. Primary Antibody list and working dilutions.

Source, Reference	Antibody	Dilutions	
		Immunoblotting	Immunofluorescence
Abcam, ab181136	DDB2	1/1000	1/1000
Bethyl, A301-121A	XPC	1/2000	1/2000
Santa Cruz, sc-293	XPB	1/1000	1/1000
MBL international, TDM-2	CPD	N.A.	1/1000
Novus Biologicals, NBP2-38556	GTF2H1	1/500	N.A.
Santa Cruz, sc-853	XPA	1/250	N.A.
Bethyl, A301-484A	XPG	1/1000	N.A.
Enzo, BML-PW8810	FK2	1/1000	N.A.
Novus Biologicals, NB120-495	CSN5	1/2000	N.A.
Abcam, ab72548	CUL4A	1/1000	N.A.
Abcam, ab9194	DDB1	1/1000	N.A.
Abcam, Ab290	GFP	1/1000	N.A.
Sigma Aldrich, B512	Tubulin	1/10000	N.A.

Supplementary Table 2. Secondary Antibody list and working dilutions.

Source, Reference	Antibody	Dilutions	
		Immunoblotting	Immunofluorescence
Sigma, sab4600215	Anti-rabbit, CF IRDye 770	1/10000	N.A.
Sigma, sab4600200	Anti-rabbit, CF IRDye 680	1/10000	N.A.
Sigma, sab4600214	Anti-mouse, CF IRDye 770	1/10000	N.A.
Sigma, sab4600199	Anti-mouse, CF IRDye 680	1/10000	N.A.
Invitrogen, A11034	Anti-rabbit, Alexa Fluor 488	N.A.	1/1000
Invitrogen, A21429	Anti-rabbit, Alexa Fluor 555	N.A.	1/1000
Invitrogen, A11001	Anti-mouse, Alexa Fluor 488	N.A.	1/1000
Invitrogen, A21424	Anti-mouse, Alexa Fluor 555	N.A.	1/1000

ATP-dependent chromatin remodeler CHDI promotes nucleotide excision repair

4

Cristina Ribeiro-Silva, Wim Vermeulen, Hannes Lans

Department of Molecular Genetics, Oncode Institute, Erasmus MC, University Medical Center Rotterdam, Dr. Molewaterplein 40, 3015 GD, Rotterdam, The Netherlands

Abstract

A central question in the field of DNA repair is how multi-subunit complexes can recognize and repair DNA lesions within the highly dynamic chromatin structure. The popular “access, repair, restore” model suggests that access of repair proteins to DNA lesions and their subsequent repair depend on early chromatin rearrangement events. Nucleotide excision repair (NER) is a major DNA repair pathway that protects against UV-induced DNA damage, in which several proteins from the SWI/SNF, INO80 and ISWI ATP-dependent chromatin remodeling families have been implicated. Curiously, not much is known about the involvement of proteins from the structurally related CHD family in the UV-induced DNA damage response (UV-DDR), even though several CHD proteins have established roles in other DNA repair pathways. Here, we show that the ATP-dependent chromatin remodeler CHD1 is important for an optimal UV-DDR and appears to promote the lesion excision step during NER.

Introduction

Nucleotide excision repair (NER) is a major DNA repair pathway that promotes genome stability and integrity together with other DNA repair and signaling processes, as part of the DNA damage response (DDR). NER is unique in its ability to repair a wide range of different lesions that distort the DNA helical structure. The lesions repaired by NER can arise from various genotoxic insults^{1,2}, many of which are encountered in our daily lives such as UV-light, which induces the formation of cyclobutane pyrimidine dimers (CPDs) and pyrimidine (6-4) pyrimidone photoproducts (6-4PPs). The NER core pathway is well characterized and can be summarized in four essential and sequential steps: 1) lesion detection, 2) DNA unwinding and damage verification, 3) excision of a single-stranded DNA stretch containing the lesion and 4) DNA synthesis and ligation to restore the gap. Depending on the location of lesions, two damage recognition subpathways initiate NER. Global genome NER (GG-NER) targets lesions located anywhere in the genome and is initiated by the XPC protein as part of the XPC-RAD23B-CETN2 complex³. Strikingly, although in mammals NER is the sole repair pathway able to remove CPDs, the GG-NER initiating protein XPC has only poor affinity for this mildly helix-distorting lesion. These lesions are only efficiently recognized after priming by DDB2, as part of the Cullin-RBX1-based ubiquitin ligase CRL4^{DDB2} complex⁴⁻⁸. Transcription-coupled NER (TC-NER), on the other hand, exclusively repairs lesions located in the transcribed strand of active genes and is initiated by recruitment of the CSB, CSA and UVSSA proteins to lesion-stalled RNA Polymerase II (Pol II) complexes^{2,9}. Once the damage is detected, both subpathways converge to the same cascade reaction. First, transcription factor IIH (TFIIH) is recruited via an interaction between its subunits, GTF2H1 and the XPB helicase, with either XPC (in GG-NER) or UVSSA (in TC-NER)^{10,11}. TFIIH, mainly through its other helicase subunit XPD, unwinds the damaged DNA to create a substrate for the downstream endonucleases, while simultaneously examining if the lesion is a proper substrate for repair by NER^{12,13}. The XPA protein assists this verification step and facilitates, together with the RPA protein, the correct positioning of the endonucleases ERCC1/XPF and XPG that excise the lesion from the damaged strand¹⁴. The resulting single-stranded 22-30 nucleotide DNA gap is restored by *de novo* DNA synthesis and ligation^{2,15}.

Unlike scheduled DNA-transaction events such as transcription and replication that initiate from defined genomic loci, DNA damage is stochastic and thus DNA repair has to act anywhere in the genome at any time¹⁶. It is therefore expected that DNA repair efficiency is conditioned by the chromatin environment where the lesion occurs. Consequently, it is also likely that chromatin itself is subject to regulation as part of the DDR. In 1991, Smerdon¹⁷ coined the model of "Access, Repair, and Restore", proposing that chromatin changes are required to provide efficient access for damage-sensor proteins to initiate DNA repair. Once repair is completed, chromatin organization must be restored¹⁸⁻²⁰. Reports showing that chromatin changes after UV irradiation, that nucleosomes are refractory to NER activity and that NER efficiency is higher in naked than in chromatinized DNA have incited the search for chromatin modifiers that satisfy this premise²¹⁻²³. Since then, several ATP-dependent chromatin remodeling proteins have been implicated in NER. Among the four structurally related major ATP-dependent chromatin remodeling families, proteins from SWI/SNF²⁴⁻³³ (this thesis, Chapter 2 and Chapter 5), INO80³⁴⁻³⁶ and ISWI³⁷⁻³⁹ families have been the predominant targets of interest. Curiously, not much is known about the involvement of proteins from the CHD family in the UV-DDR⁴⁰.

The CHD (chromodomain helicase DNA-binding) chromatin remodeling family is composed of nine members divided into three classes: class I (CHD1 and CHD2), class II (CHD3, CHD4 and CHD5) and class III (CHD6, CHD7, CHD8, CHD9). Common traits shared between all nine proteins of the CHD family are the N-terminal tandem chromodomains and a central helicase-like ATPase domain⁴¹⁻⁴³. Yet, of the three CHD protein classes, only proteins from class I (CHD1 and CHD2) do not need to associate with other proteins (i.e., in complexes) to be targeted to DNA and can bind DNA directly in a specific manner⁴²⁻⁴⁴. Proteins of the CHD family are well-known regulators of transcription^{41,45}, but several CHD proteins also have established or emerging roles in the maintenance of genome stability, such as in double-strand break (DSB) repair (particularly CHD2, CHD3 and CHD4) and in the oxidative stress response (CHD6), and have been implicated in tumorigenesis^{43,44,46}.

Genomic profiling of human cancers identified CHD1 as the second most

frequently deleted or mutated gene (15–27%)^{47–49} in prostate cancer, which encouraged research beyond CHD1's canonical transcription functions. These research efforts have recently revealed a novel function of CHD1 early during DSB repair in facilitating the recruitment of homologous recombination (HR) proteins^{50–52}. Depletion of this chromatin remodeling protein furthermore sensitizes cells to a range of DNA damage-inducing agents, including ionizing radiation and chemotherapeutic drugs such as neocarzinostatin, mitomycin C, PARP-inhibitors and carboplatin^{50–52}. Interestingly, carboplatin, an analog of cisplatin, induces helix-distorting DNA crosslinks that are primarily recognized and resolved by NER⁵³. Therefore, we investigated a putative role of CHD1 in NER. We show that CHD1 is required for optimal UV-survival and NER activity and is rapidly recruited to local UV-C induced damage, suggesting a direct role in NER. However, we were unable to identify the molecular mechanism via which CHD1 is recruited to UV-lesions, which seems independent of NER. Furthermore, our results suggest that CHD1 may facilitate the assembly of the NER-specific endonucleases to promote lesion excision, although further research is required to clarify its specific activity.

Results

CHD1 promotes UV-survival and NER activity

To assess CHD1's involvement in NER, we performed a clonogenic UV-survival assay in U2OS cells transiently transfected with two different siRNAs targeting CHD1 (CHD1#1 and CHD1#2). Efficient depletion of CHD1 with either siRNA was confirmed by immunoblot (Supplementary Fig. 1a). Strikingly, we observed that CHD1 depletion decreased UV survival to an extent similar as depletion of the core GG-NER factor XPC (siXPC, Fig.1a, Supplementary Fig. 1a), suggesting that CHD1 is required for an optimal UV-induced DNA damage response (UV-DDR) and may function to promote NER.

To more directly test the involvement of CHD1 in NER, we measured the unscheduled DNA synthesis (UDS), i.e., the gap-filling DNA synthesis step in NER, after global UV-C irradiation (16 J/m²), which is a measure for GG-NER efficiency. UDS was determined by labeling the cells, directly

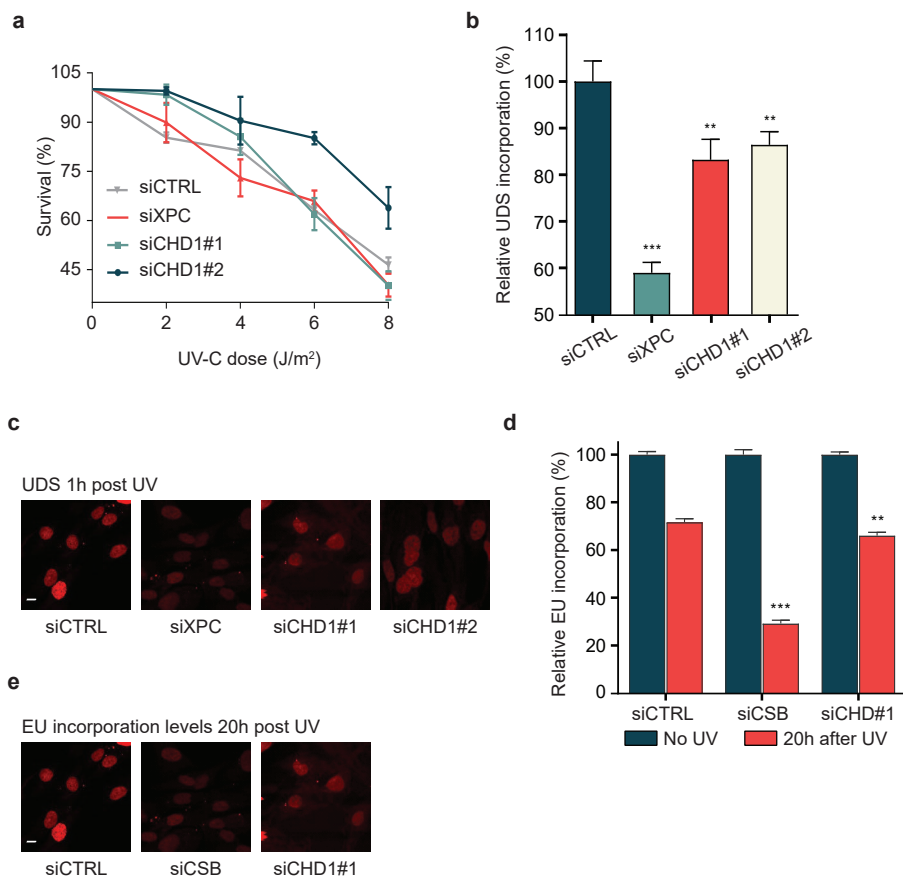


Figure 1. CHD1 promotes UV-survival and NER activity. (a) UV-C colony survival of U2OS cells transfected with non-targeting (CTRL), XPA and CHD1 (CHD1#1, CHD1#2) siRNAs. The number of colonies after UV was normalized to the amount at 0 J/m². Mean & S.E.M. error bars of three independent experiments. (b) Quantification of Unscheduled DNA Synthesis (UDS) in hTERT-immortalized VH10 human fibroblasts after transfection with non-targeting control (CTRL), XPC and CHD1 (CHD1#1, CHD1#2) siRNAs. Cells were labeled for 1 h with EdU after global UV-C irradiation (16 J/m²) and EdU incorporation levels were quantified by immunofluorescence and normalized to siCTRL treated cells, set to 100 % (n > 96 cells per sample; mean & S.E.M. error bars of two independent experiments). (c) UDS representative pictures, 1 h after UV-C, as detailed in (b). Scale bar: 25 μ m. (d) Quantification of Recovery of RNA Synthesis (RRS). U2OS cells, treated with non-targeting control (CTRL), CSB or CHD1 (CHD1#1) siRNAs were incubated with EU for 2 h. EU incorporation was quantified using immunofluorescence in non-irradiated cells and in cells 20 h after UV irradiation (6 J/m²), and RRS levels were normalized to non-irradiated cells, set to 100 % (n > 150 cells per condition; mean & S.E.M. error bars of at least two independent experiments). (e) RRS representative pictures 20 h after UV-C irradiation, as detailed in (d). Scale bar: 25 μ m. ** P < 0.01; *** P < 0.001.

after UV-irradiation, with the thymidine analog EdU^{54–56}. Non-dividing C5RO primary fibroblasts depleted of CHD1 using two different siRNAs (Supplementary Fig. 1b) showed significantly decreased UDS (Fig. 1b and

c). However, UDS levels were only diminished 13-17%, which was not as strong as after XPC depletion, suggesting that CHD1 does not have a core function in NER but instead has a facilitating or regulatory role.

GG-NER accounts for approximately 90% of the total repair executed by NER after UV-irradiation in cultured cells⁵⁶, which is why the UDS assay is not well suited to quantify the remaining 10% TC-NER activity. As the removal of transcription-blocking lesions by TC-NER allows for stalled transcription to restart^{55,57}, we measured the recovery of RNA synthesis (RRS) after UV irradiation by measuring the incorporation of 5-ethynyluridine (EU) into nascent RNA. As expected, U2OS cells depleted of the essential TC-NER factor CSB failed to recover the UV-induced transcription inhibition 20 h after global UV-C irradiation (6 J/m²) (Fig. 1d and e). Also, CHD1 depletion (siCHD1#1, from now on referred to as siCHD1) decreased the RRS levels, as evaluated in multiple independent RRS experiments. However, this decrease was only marginally different from the non-targeting siRNA control, although statistically significant (Fig. 1d, Supplementary Fig. 1b). A complicating factor in this assay is the fact that after CHD1 depletion transcription itself was lowered even in the absence of UV damage (Supplementary Fig. 1c). These lower transcription levels are likely because CHD1 also regulates transcription by maintaining proper chromatin structure at promoters and gene bodies⁵⁸⁻⁶³ to allow efficient transcription. Therefore, at this stage, it is difficult to conclude whether CHD1 has a role in TC-NER or not. Nonetheless, our results do show that CHD1 promotes optimal UV-survival and overall NER fitness.

CHD1 accumulates at UV-C induced DNA damage

To better understand why CHD1 is important for the UV-DDR, we tested whether it has a function directly at the site of damaged DNA by determining whether it localizes to UV-induced DNA damage. We generated a U2OS cell line with stable expression of CHD1-GFP (Supplementary Fig. 2a) to study its accumulation kinetics at sites of laser-induced local UV-C DNA damage (LUD) during real-time confocal imaging (Fig. 2a, b)⁶⁴. Because the applied 266 nm laser irradiation induces predominantly UV-specific DNA photolesions repaired by NER⁶⁴, it has been successfully used in the past to study accumulation kinetics of known and candidate-NER proteins^{38,65-68}. We found that CHD1-GFP was clearly and steadily recruited to UV-

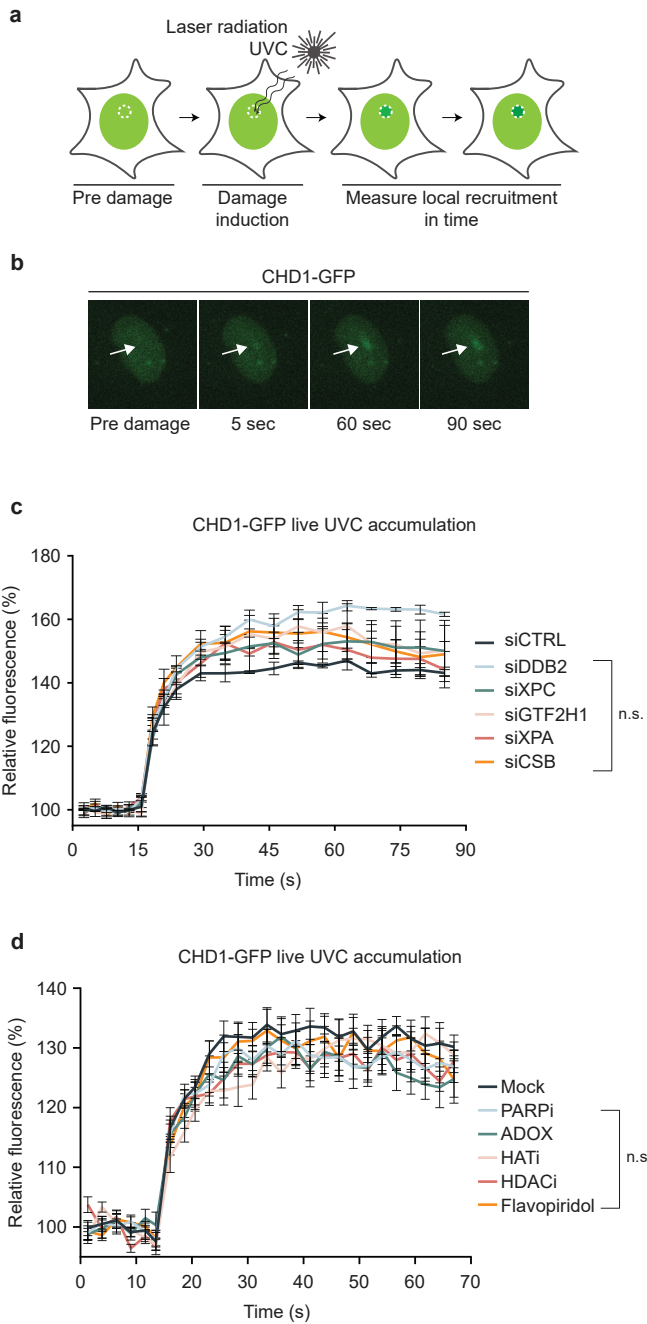


Figure 2. CHD1 is recruited to laser-induced local UV-C damage (LUD). (a) Graphic representation of the procedure for real-time imaging of the recruitment of GFP-tagged proteins to 266 nm laser induced local UV-C damage (LUD). (b) Representative time-stamp images of U2OS cells with stable ectopic expression

of CHD1-GFP, which resides exclusively in the nucleus, and the real-time recruitment of CHD1-GFP to laser-generated LUD. Arrows indicate the LUD region. **(c)** Real-time imaging of CHD1-GFP accumulation at 266 nm UV-C laser-induced LUD in U2OS cells treated with control (CTRL), DDB2, XPC, GTF2H1, XPA or CSB siRNAs (knockdown efficiency shown in Supplementary Fig. 2a). Pre-damage fluorescence intensity was set to 100 % ($t = 0$). Mean & S.E.M. of two independent experiments each with at least 7 cells per condition. siXPA, siGTF2H1 and siCSB were performed once, with at least 10 cells analyzed per condition. **(d)** Real-time imaging of CHD1-GFP accumulation at 266 nm UV-C laser-induced LUD in mock- or inhibitor-treated cells. Cells were incubated before imaging with inhibitors against: PARP-1 (PARPi, 10 μ M for 1 h), methyltransferases (ADOX, 20 μ M for 20 h), histone acetyltransferases (HATI; cocktail of 50 μ M of GNC5 and 50 nM of p300 inhibitor for 2 h), histone deacetylases (HDACi, 1 μ M TSA for 1 h) and transcription (Flavopiridol, 1 μ M for 1 h). The indicated incubation periods refer to pre-treatment before imaging and LUD. Inhibitors were kept at all time during the performance of the experiment. Mean & S.E.M. of at least 10 cells per condition.

induced DNA damage (Fig. 2b, c – dark blue line). As this suggests a function of CHD1 in NER, we investigated whether its accumulation at LUD was dependent on NER-initiating proteins DDB2, XPC and CSB, and the core NER factors GTF2H1, XPA by depleting these factors via siRNA-mediated knockdown (Supplementary Fig. 2b). Surprisingly, the LUD accumulation kinetics of CHD1 did not significantly change upon depletion of these NER-initiating factors (Fig. 2c). In addition, knockdown of either XPA or GTF2H1 showed that CHD1 is not recruited as part of the core NER machinery. These results, therefore, indicate that CHD1 recruitment either precedes damage detection by GG-NER or TC-NER or is independent of NER.

CHD1 is linked to active transcription of genes by Pol II. CHD1 is recruited to promoter-proximal nucleosomes via interactions with both the transcription pre-initiation complex and di- or trimethylated histone H3K4^{60,69}. CHD1 also interacts with many elongation factors, such as the PAF, FACT and DSIF complexes⁵⁹, and is specifically recruited to gene bodies in an elongation-dependent manner⁶¹. We, therefore, tested if recruitment of CHD1-GFP to laser-induced LUD is coupled to its function in transcription, first by inhibiting Pol II elongation with the CDK inhibitor Flavopiridol⁷⁰. However, we did not observe differences between the accumulation kinetics of CHD1-GFP in mock (Fig. 2d, black line) or Flavopiridol treated cells (Fig. 2d, orange line), suggesting that CHD1 recruitment to LUD is not dependent on productive Pol II elongation. Interaction of CHD1 with di- or trimethylated histone H3K4, via its two chromodomains⁶⁹, targets the remodeling function of CHD1 during transcription regulation. Therefore, we next examined whether this histone methylation governs CHD1

recruitment to sites of UV damage as well by pre-treating cells with the methyltransferase inhibitor Adenosine-2',3-dialdehyde (AdOX)^{38,71} (Fig. 2d, green line). However, also no difference in the accumulation of CHD1-GFP was observed in the presence of this inhibitor, leading us to conclude that CHD1 recruitment to LUD is independent of its role at gene promoters and bodies.

In yeast, CHD1 is a component of the acetyltransferase complexes SAGA (Spt-Ada-Gcn5-acetyltransferase) and SLIK (SAGA-like) and is required for their transcriptional activity⁷². Contrary, mouse CHD1 was also found associated with HDAC activity⁷³, which prompted us to test CHD1 recruitment to LUD in the presence of histone acetyltransferase (HATi, Fig. 2d, light pink) or histone deacetylase (HDACi, Fig. 2d, dark pink) inhibitors. However, we did not find any effect of acetylation or deacetylation inhibition on CHD1 recruitment to UV-C induced DNA damage. Finally, we tested if polyADP-ribosylation (PAR) is needed for the recruitment of CHD1 to LUD, as this modification regulates the recruitment and function of many DDR proteins, including some involved in NER and DSB repair, and is also especially implicated in the DNA damage recruitment of other CHD proteins, namely CHD2 and CHD4^{74–76}. However, we did not find differences between the recruitment of CHD1 to UV-lesions in mock or PARP inhibitor-treated cells (PARPi, Fig. 2d, light blue), suggesting that, unlike these CHD family members, CHD1 recruitment to DNA damage is not mediated by PAR moieties⁵⁰.

Despite extensive efforts, it is still unclear how CHD1 is recruited to local UV damage and whether this reflects a function at the site of damage that is related to a putative function in NER, as suggested by the UV-survival and UDS assays (Fig. 1a, b). Possibly, CHD1 is recruited independently or upstream of the NER machinery to facilitate its activity.

CHD1 and lesion recognition by GG-NER

In an attempt to make sense of the above described nondiscriminant analyses, we tested if CHD1 precedes NER and regulates the recruitment of NER proteins to LUD. Since GG-NER was reduced after CHD1 depletion (Fig. 1b), we first tested the effect of CHD1 depletion on the recruitment of endogenous DNA damage sensing proteins DDB2 and XPC to LUD

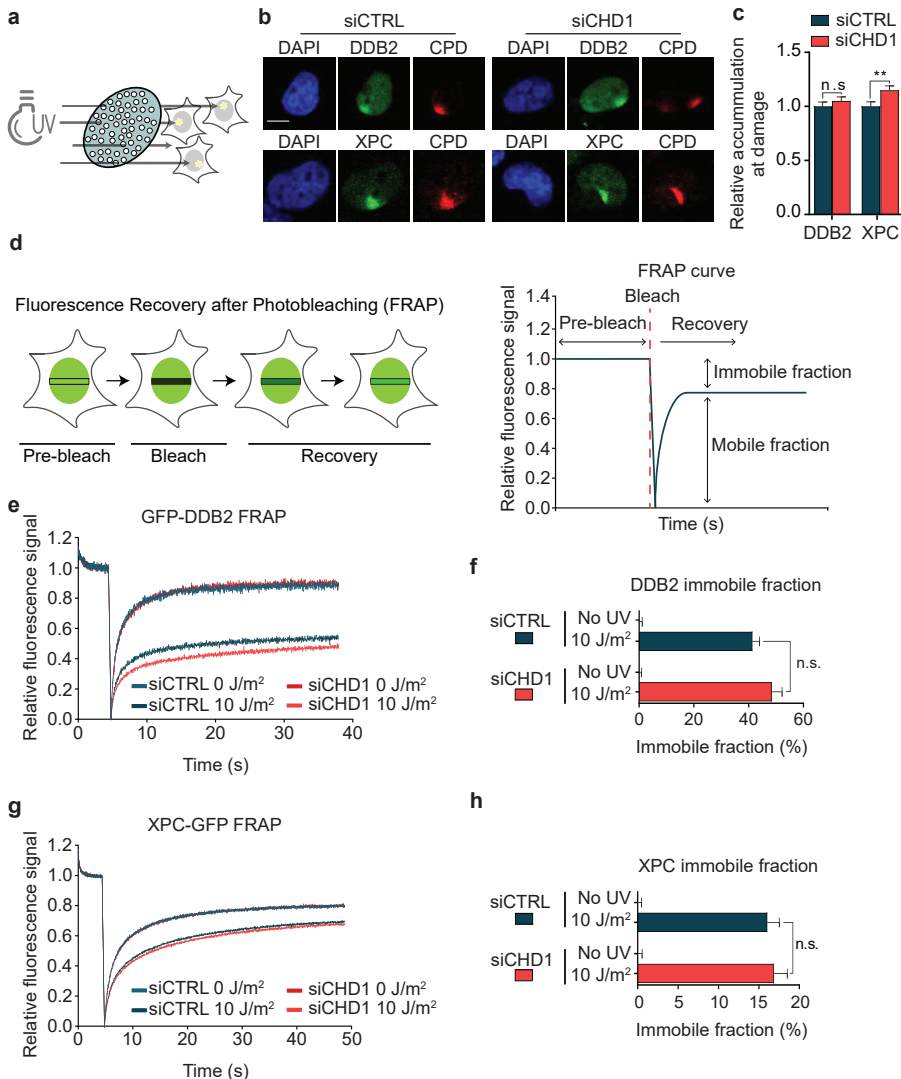


Figure 3. CHD1 and lesion recognition by GG-NER. (a) Graphic representation of local UV-C damage (LUD) induction by globally UV-C irradiating cells with a germicidal 254 nm TUV lamp through an 8 μ m polycarbonate filter. LUD will be generated only where the light passes through the filter pores. (b) Immunofluorescence (IF) representative pictures of DDB2 and XPC recruitment (green channel) to LUD in U2OS cells treated with control (CTRL) or CHD1 siRNAs. Cells were fixed 30 min after induction of LUD with UV-C irradiation (60 J/m²) through a microporous membrane (8 μ m), as depicted in (a). UV lesions were marked with staining against CPD (red channel). DNA was stained with DAPI. Scale bar: 5 μ m. (c) Quantification of DDB2 and XPC recruitment to LUD, normalized to siCTRL treated cells, in which nuclear background was set at 0 and maximal signal at LUD set to 1.0 for each protein (> 211 cells measured per condition, mean & S.E.M. of three (XPC) and four (DDB2) independent experiments. ** P < 0.01, relative to siCTRL control. n.s., non-significant. (d) Graphic representation of Fluorescence Recovery After Photobleaching (FRAP) analysis. In cells that express a protein of interest fused to GFP (depicted as green ovals), the fluorescence intensity in

a strip across the nucleus is recorded before, during and after photobleaching of the fluorescent signal (dark strip) and then corrected and normalized to the average pre-bleach intensity (1.0). FRAP allows to estimate the mobile and immobile fractions of GFP-tagged proteins before and after UV-irradiation. (e) FRAP analysis of GFP-DDB2 mobility in mock or UV-C irradiated (10 J/m^2) VH10 hTERT-immortalized cells transfected with control (CTRL) or CHD1 siRNAs. As described in (d), GFP-DDB2 was bleached in a strip across the nucleus and fluorescence recovery was measured over 30 s and normalized to pre-bleach. (f) Quantification of GFP-DDB2 immobile fraction. The immobile fraction was determined by dividing the average recovered fluorescence intensity of UV-irradiated cells by the average recovered fluorescence intensity of mock-treated cells, over the last 10 s of at least 10 measured cells per condition. n.s., non-significant. (g) FRAP analysis of XPC-GFP mobility in mock or UV-C irradiated (5 J/m^2) XP4PA cells transfected with control (CTRL) or CHD1 siRNAs, as described in (d, e). (h) Quantification of XPC-GFP immobile fraction, as explained in (f), over the last 10 s of at least 50 cells measured per condition. n.s., non-significant.

(marked by CPD staining), using immunofluorescence (IF) in U2OS cells 30 min after UV-C irradiation (60 J/m^2) through a microporous membrane^{26,77} (Fig. 3a). This showed that, although DDB2 localization to CPDs was unaffected, slightly more XPC localized to UV-lesions in the absence of CHD1 (siCHD1; Fig. 3b, c, Supplementary Fig. 2c). To verify these results, we used fluorescence recovery after photobleaching (FRAP) to measure protein mobility, which changes upon binding of a protein to UV-damaged chromatin and likely reflects participation in NER^{78,79}. Briefly, in a FRAP assay, the fluorescence signal of a fluorescently tagged protein is bleached in a strip across the nucleus and the recovery of the fluorescence signal is determined as a measure of the protein's mobility (Fig. 3d). With this technique, we measured the mobility of both GFP-DDB2 (stably expressed in VH10 hTERT-immortalized human fibroblasts) and XPC-GFP (stably expressed in XPC-deficient XP4PA SV40-immortalized human fibroblasts) before and after global UV-C irradiation (10 J/m^2) in the presence (siCTRL) or after depletion of CHD1 (siCHD1, Supplementary Fig. 2d). In non-damaged cells treated with siCTRL or siCHD1, the GFP-DDB2 fluorescent signal quickly recovered after bleaching (Fig. 3e), indicating that the protein freely diffuses through the nucleus, in line with previous observations^{78,80,81}. After global UV-C irradiation, the GFP-DDB2 fluorescent signal did not fully recover (Fig. 3e, f), indicating that a fraction of GFP-DDB2 is bound to damaged chromatin and, therefore, engaged in NER⁷⁹⁻⁸¹. However, this immobile fraction slightly, but not significantly, increased after depletion of CHD1.

Fluorescence of XPC-GFP recovered slower than GFP-DDB2 in unchallenged cells (Fig. 3g), which reflects its continuous probing of DNA to search for

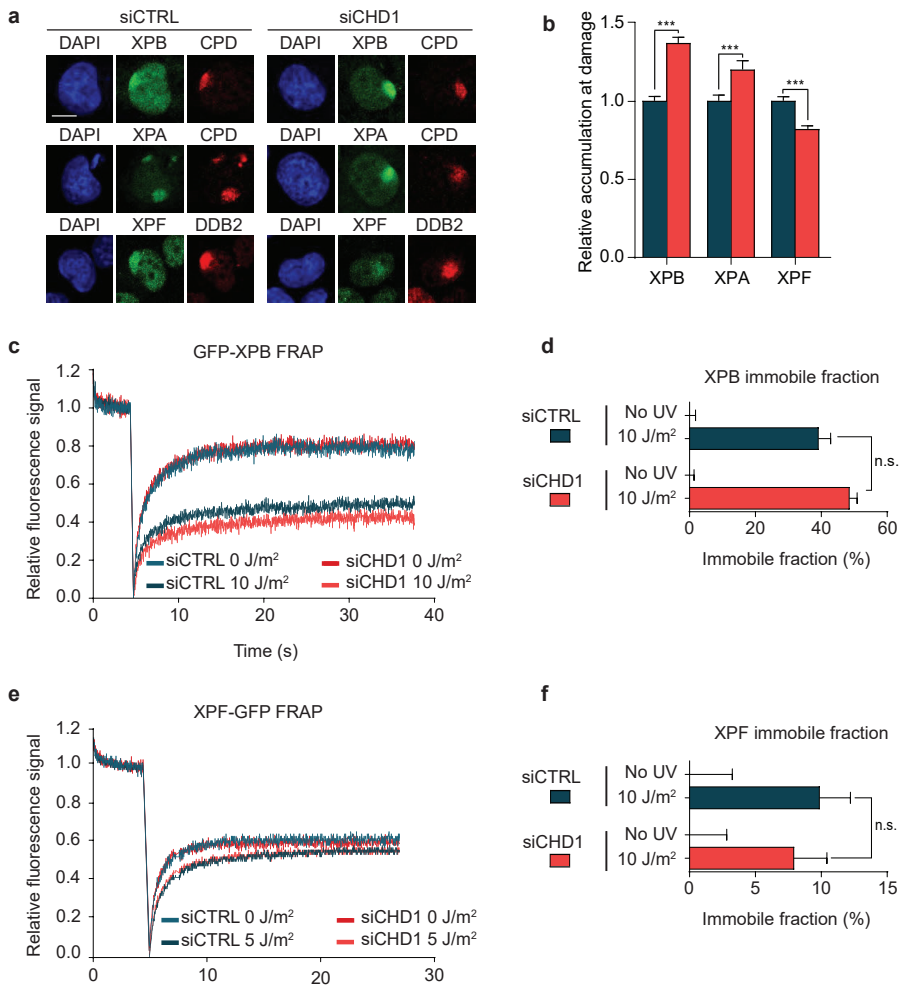


Figure 4. Role of CHD1 in lesion verification and excision. (a) IF representative pictures of XPB, XPA and XPF recruitment (green channel) to local UV-C damage (LUD) in U2OS cells treated with control (CTRL) or CHD1 siRNAs. Cells were fixed 30 min after induction of LUD with UV-C irradiation (60 J/m²) through a microporous membrane (8 μm), as depicted in Fig. 3a. UV lesions were marked with staining against CPD (red channel). DNA was stained with DAPI. Scale bar: 5 μm. (b) Quantification of XPB, XPA and XPF recruitment to LUD after CTRL and CHD1 siRNAs, as shown in (a). Fluorescence was normalized to CTRL siRNA treated cells, in which nuclear background was set at 0 and maximal signal at LUD set to 1.0 for each protein (> 202 cells per condition, mean & S.E.M. of four (XPA) and five (XPB, XPF) independent experiments. *** P < 0.001, relative to siCTRL control. n.s., non-significant. (c) FRAP analysis of endogenous XPB mobility in mock or UV-C irradiated (10 J/m²). MRC-5 cells with GFP knock-in at the XPB locus were transfected with control (CTRL) or CHD1 siRNAs and GFP-XPB fluorescence recovery was measured over 30 s and normalized to the average pre-bleach intensity (1.0). (d) Percentage of endogenous XPB immobile fraction in MRC-5 cells treated with CTRL or CHD1 siRNAs, determined from the FRAP analysis depicted in (c). Quantification of immobile fractions as described in Fig. 3f, over the last 10 s of at least 10 measured cells per condition.

n.s., non-significant. (e) FRAP analysis of XPF mobility in mock or UV-C irradiated (5 J/m²). U2OS XPF KO cells with stable expression of XPF-GFP were transfected with control (CTRL) or CHD1 siRNAs and XPF-GFP fluorescence recovery was measured over 30 s and normalized to the average pre-bleach intensity (1.0). (f) Percentage of XPF immobile fraction in MRC-5 cells treated with CTRL or CHD1 siRNAs, determined from the FRAP analysis depicted in (e). Quantification of immobile fractions as described in Fig. 3f, over the last 10 s of at least 10 measured cells per condition. n.s., non-significant.

DNA damage^{79,82,83}. The increased immobile fraction of XPC-GFP after UV irradiation, due to its binding to DNA damage, was not affected by CHD1 depletion (Fig. 3g, h). These FRAP data therefore suggest that CHD1 does not facilitate XPC binding to DNA. These results are not in line with the IF data (Fig. 3b, c), which appear to suggest that, in the absence of CHD1, either more XPC molecules are bound to damaged DNA or that each molecule stays longer bound. This apparent discrepancy could, however, be due to XPC-GFP overexpression in the cells used for the FRAP analysis, which might mask subtle differences in the mobility of a fraction of XPC.

CHD1 and lesion verification and excision

We next tested if, following damage detection, recruitment of core NER factors to UV-induced DNA damage, downstream of initiation factors, such as the TFIIH complex subunit XPB and the XPA and XPF proteins, is dependent on CHD1. Using IF (Fig. 3a), we found significantly increased localization of XPB and XPA to LUD after siRNA-mediated CHD1 depletion (Fig. 4a, b, Supplementary Fig. 2c). Surprisingly, the localization of XPF to LUD was strongly reduced (Fig. 4a, b). These results suggest that, in the absence of CHD1, NER is possibly impaired just before the excision step, leading to retention of upstream NER proteins XPC, XPB and XPA and reduced recruitment of XPF (Fig. 3b, 4a, b).

To verify these observations, we measured the UV-induced immobilization of XPB and XPF by FRAP. Endogenously GFP-tagged XPB (in MRC-5 SV40-immortalized human fibroblasts) showed slightly increased immobilization after UV-C irradiation (10 J/m²) in CHD1-depleted (siCHD1) cells in comparison to control siRNA-treated cells (siCTRL) (Fig. 4c, d, Supplementary Fig. 2d). Conversely, XPF-GFP (stably expressed in U2OS XPF knockout cells⁸⁴) showed slightly reduced immobilization after UV irradiation and CHD1 depletion (Fig. 4d, e, Supplementary Fig. 1a). Although the FRAP analysis of GFP-XPB and XPF-GFP UV-induced immobilization did not show statistically significant differences, likely because too few

cells were imaged to reach significance, these results corroborate the increased XPB and reduced XPF recruitment to UV-damaged chromatin in the absence of CHD1 observed by IF (Fig. 4a, b). Therefore, together, our IF and FRAP results suggest that CHD1 might promote NER progression from lesion verification to lesion excision.

Discussion

We show that CHD1 is quickly and steadily recruited to local UV-C laser-induced damage (Fig. 2) and promotes resistance to UV-induced DNA damage (Fig. 1). At the time this project was being undertaken, a paper was published reporting a novel function of CHD1 in NER by promoting the “handover” of UV lesions between XPC and TFIIH⁸⁵. In this study, it was shown that CHD1 recruitment to nucleosome cores after UV irradiation is dependent on XPC and that CHD1 depletion increased XPC recruitment but diminished recruitment of downstream NER factors TFIIH and XPA to LUD. Because of this, the authors concluded that CHD1 facilitates the displacement of XPC and thus promotes the recruitment of downstream GG-NER factors. Although we applied the same IF approach to study the recruitment of NER proteins to LUD after CHD1 knockdown, we obtained opposing results. Our results show that CHD1 depletion leads to decreased DNA damage recruitment of XPF but not of TFIIH and XPA (Fig. 4a, b). This suggests that CHD1 does not act to promote damage handover from XPC to TFIIH, but to promote NER progression from lesion verification (TFIIH/XPA) to lesion excision (e.g., XPF). Furthermore, using UV-C laser, we show that CHD1 recruitment to UV-induced DNA damage does not require XPC (Fig. 2b, green line). Nonetheless, in both studies, CHD1 is required for optimal NER, and although its precise function in NER appears still elusive, it is highly likely that CHD1 is a novel regulator of NER.

More research is needed to better elucidate and deepen our knowledge on the *modus operandi* of CHD1 in the UV-DDR. For instance, given CHD1’s transcriptional role, it would be of interest to study how CHD1 depletion affects specifically TC-NER, by using the recently developed amplified UDS assay⁸⁶ that allows a direct measurement of TC-NER-coupled DNA repair synthesis. CHD1’s transcriptional regulation is intrinsically linked

to its ATP-dependent chromatin remodeling activity and, as extensively reviewed, ATP-dependent remodeling proteins are thought to facilitate access of DNA repair proteins to DNA by making chromatin more accessible^{24,87,88}. In agreement with this hypothesis, CHD1 was found recently to facilitate the recruitment of HR proteins to DSBs⁵⁰⁻⁵². It would be interesting to investigate if CHD1 facilitates lesion removal by NER by remodeling chromatin after UV-induced DNA and whether CHD1 is responsible for nucleosome turnover in the course of repair by NER. It is, however, unlikely that such an activity would be to facilitate access for NER proteins, as our findings suggest that CHD1 facilitates a downstream step of NER, i.e., lesion excision, instead of damage detection, and its recruitment to UV lesions appears independent of NER. Recruitment and functional studies using specific domain mutants of CHD1 would enable us to determine whether CHD1 chromatin remodeling activity is required for its DNA damage localization and its facilitation of NER. Furthermore, we could specifically address whether CHD1 remodels chromatin at sites of UV lesions by measuring histone dynamics after UV, for instance using SNAP-tag technology, which would allow us to monitor parental histone dynamics after local UV-C irradiation⁸⁹, or quantitative fluorescence imaging techniques to measure histone exchange in chromatin after UV⁹⁰. The high mutation frequency of CHD1 in prostate cancer (15-27%) highlights the importance of CHD1 function in tumorigenesis and DDR. Loss of CHD1 may disrupt not only DSB repair but, as reported here, NER as well. Importantly, loss of CHD1 sensitizes cells to DNA damage, which is evident not only *in vitro* but is also observed *in vivo*, in mice, and *ex vivo*, in patient-derived organoids⁵¹. Thus, understanding the mechanistic function of CHD1 in NER (and other DDR pathways) may provide a rationale for the development of efficient therapeutic approaches that exploit specific DDR vulnerabilities caused by CHD1 deficiency.

Methods

Cell lines, culture conditions and treatments. U2OS (wild-type, WT, or with stable expression of CHD1-GFP), U2OS XPF knockout (KO, with stable expression of XPF-GFP)⁸⁴, SV-40-immortalized human fibroblasts XP4PA (with stable expression of XPC-GFP) and MRC-5 (with GFP knock-

in N-terminally positioned at XPB locus, this thesis, Chapter 3), and hTERT-immortalized human fibroblasts VH10 (with stable expression of GFP-DDB2⁸¹) were cultured under standard conditions in a 1:1 mixture of DMEM (Lonza) and Ham's F10 (Lonza) supplemented with 10% fetal calf serum (FCS). C5RO primary fibroblasts were cultured in Ham's F10 medium supplemented with 12% FCS. Stable CHD1-GFP expressing cells (U2OS) were generated using lentiviral transduction and selection in 10 µg/mL Blasticidin. siRNA was transfected two days before each experiment using RNAiMax (Invitrogen), according to the manufacturer's instructions. All cells were cultured in medium with 1% penicillin-streptomycin in a humidified atmosphere at 37°C and 5% CO₂. To inhibit methylation, cells were treated with 20 µM of Adenosine-2',3'-dialdehyde (AdOX, Sigma) for 20 h. For inhibition of histone acetyltransferase (HAT) activity cells were treated for 2 h with an inhibitor cocktail of 50 µM GCN5 (CPH2, Sigma) and 50 nM of p300 (CTK7A, Sigma). For inhibition of histone deacetylase (HDAC) activity, cells were incubated for 1 h with 1 µM of trichostatin A (TSA, Sigma). Transcription was inhibited by treating cells for 1 h with 1 µM of flavopiridol (Sigma). PARP-1 activity was inhibited by incubation for 1 h with 10 µM of PARP inhibitor (KU0058948 hydrochloride, Axon Medchem).

Plasmids and siRNA. To generate a CHD1-GFP plasmid, the full-length human CHD1 cDNA (PlasmID Repository Harvard Medical School) was fused to GFP and inserted into pLenti-PGK-Blast-DEST⁹¹. Further cloning and plasmid details are available upon request. siRNA oligomers were purchased from GE Healthcare Dharmacon: CTRL (D-001210-05), DDB2 (J-011022-05), XPC (MJAWM-000009), GTF2H1 (L-010924-00), XPA (MJAWM-000011), XPF (D-019946-04), CSB (J-004888-09), CHD1#1 (J-008529-08) and CHD1#2 (J-008529-06).

UV-C irradiation and laser-induced damage. Cells were globally irradiated with UV-C using a germicidal lamp (254 nm; TUV lamp, Phillips), with the indicated doses. Local UV-damage (LUD) was inflicted by using 60 J/m² of UV irradiation through an 8 µm polycarbonate filter (Millipore). To induce LUD in living cells during real-time confocal imaging, a 2 mW pulsed (7.8 kHz) diode-pumped solid-state laser emitting at 266 nm (Rapp Opto Electronic, Hamburg GmbH) was used, coupled to a an Untrafluor quartz 100x/1.35 NA glycerol immersion lens (Carl Zeiss Micro Imaging

Inc.) used with a Leica TCS SP5 confocal microscope^{26,38}.

UV colony formation assay. For UV survival, U2OS cells were seeded in triplicate in 6-well plates at a density of 400 cells/well and treated with increasing doses of UV-C, 18-24 h after seeding. After 5 days, colonies were fixed and stained with Coomassie Blue solution (50% methanol, 10% acetic acid, 1 g Brilliant Blue R (Sigma)). Colonies were counted with the integrated colony counter GelCount (Oxford Optronix).

Unscheduled DNA synthesis (UDS) and recovery of RNA synthesis (RRS). Fluorescent UDS and RRS were performed as described before²⁶ (this thesis, Chapter 2). Briefly, C5RO primary fibroblasts (for UDS) and U2OS (for RRS) were seeded on coverslips and treated with siRNAs 48 h before global UV-C irradiation (16 and 6 J/m², respectively). For UDS, cells were directly incubated for 1 h in medium containing ethynyl-2'-deoxyuridine (EdU, Invitrogen), while for RRS cells were allowed to recover for 20 h and then incubated for 1 h with medium containing 5-ethynyl-uridine (EU). Cells were fixed and permeabilized with 4% paraformaldehyde and 0.1% Triton X-100 in PBS, respectively. EdU (UDS) and EU (RRS) incorporation was visualized by incubation with a Click-it reaction cocktail containing Atto 594 Azide (60 μM, Atto Tec.), Tris-HCl (50 mM, pH 7.6), CuSO₄·5H₂O (4 mM, Sigma) and ascorbic acid (10 mM, Sigma), for 1 h at room temperature. After washes (0.1% Triton-X100 in PBS), DNA was stained with DAPI (Sigma) and slides were mounted with Aqua-Poly/Mount (Polysciences, Inc.). Images were acquired with an LSM700 confocal microscope with a 40x Plan-apochromat 1.3 NA oil immersion lens (Carl Zeiss Micro Imaging Inc.). EdU and EU incorporation levels were quantified by measuring the total nuclear fluorescence intensities (n > 90 cells per experiment) with FIJI image analysis software. Intensity levels were averaged and normalized to controls, which were set at 100%.

Real-time confocal imaging of protein recruitment to UV-C laser induced damage and fluorescence recovery after photobleaching (FRAP). All real-time imaging was performed on a Leica TCS SP5 confocal microscope (with LAS AF software, Leica) at 37°C and 5% CO₂. LUD was induced with a 2 mW pulsed (7.8 kHz) diode-pumped solid-state laser emitting at 266 nm (Rapp Opto Electronic, Hamburg

GmbH). Real-time protein recruitment in living cells seeded on quartz coverslips was measured via an Untrafluar quartz 100x/1.35 NA glycerol immersion lens (Carl Zeiss Micro Imaging Inc.) as described before^{26,38}. Accumulation curves were background corrected and normalized to the relative fluorescence signal before local irradiation. FRAP experiments were performed as described before^{26,92} (this thesis, Chapters 2 and 3). In summary, cells seeded on coverslips were imaged with a 40x/1.25 NA HCX PL APO CS oil immersion lens (Leica Microsystems) and the GFP signal was measured in a strip spanning the nucleus width (512 x 16 pixels) every 22 ms at 1400 Hz with a zoom of 12x before, during and after photobleaching. 100% power of the 488 nm laser was used for the photobleaching, after which fluorescence was monitored until recovery was complete. Fluorescence signals were normalized to the average pre-bleach fluorescence after background subtraction. Immobile fractions (F_{imm}), shown in Figs. 3f, h and 4d, f, were determined as a ratio between the recovered fluorescence in UV-irradiated ($I_{final,UV}$) and unchallenged cells ($I_{final,unc}$) over the last 10 s of measurements, after correction with bleaching intensity (I_0), simplified in the following equation:

$$F_{imm} = 1 - \frac{I_{final,UV} - I_0,UV}{I_{final,unc} - I_0,UV}$$

Immunofluorescence (IF). Cells were grown on 18 mm coverslips, fixed and permeabilized in 4% paraformaldehyde and 0.5% Triton X-100 in PBS, respectively. DNA was denatured for 5 min with 70 mM NaOH for the visualization of UV-lesions (LUD) with the CPD antibody. Blocking was performed for 1 h at room temperature with 3% BSA and 2.25% glycine in PBS-T (0.1% Tween 20). Antibody incubation was performed in 1% BSA in PBS-T. Primary antibodies were incubated for 1 h at room temperature or overnight at 4°C, while secondary antibodies were incubated for 1 h at room temperature, in the dark. DNA was stained with DAPI (Sigma) and slides were mounted using Aqua-Poly/Mount (Polysciences, Inc.). Images were acquired using an LSM700 microscope with a 40x Plan-apochromat 1.3 NA oil immersion lens (Carl Zeiss Micro Imaging Inc.). Protein recruitment to UV-lesions was determined using the fluorescence signal intensity at LUD and in the nucleus, with FIJI image analysis software. No accumulation (nuclear background) was set to 0 and maximum

accumulation in control conditions was set at 1.0. Antibodies used are summarized in Supplementary tables 1 and 2.

Total cell extract preparation and immunoblotting. Cells were washed with ice-cold PBS and lysed on ice for 15 min in RIPA buffer (25 mM Tris-HCl pH 8.0, 150 mM NaCl, 0.1% SDS, 1% NP-40, 0.5% Sodium Deoxycholate, 5 mM EDTA, 1 mM PMSF and EDTA-free protease inhibitor cocktail (Roche)). Soluble extracts were recovered by centrifugation at 14000 g for 20 min at 4°C and equal amounts of total protein were diluted in 2x sample buffer (125 mM Tris-HCl pH 6.8, 20% Glycerol, 10% 2-β-Mercaptoethanol, 4% SDS, 0.01% Bromophenol Blue) and boiled for 5 min at 98°C. Proteins were separated by SDS-PAGE electrophoresis and transferred onto PVDF membranes (0.45 μm, Merck Millipore) which were blocked in 5% BSA in PBS-T (0.05% Tween 20). Primary antibody incubation (in PBS-T) was performed for 1-2 h at room temperature, or overnight at 4°C and secondary antibodies were incubated for 1 h at room temperature in PBS-T. Membranes were washed 3 x 10 min in PBS-T after each antibody incubation, visualized and densitometrically analyzed with the Odyssey CLx Infrared Imaging System and Image Studio Lite software v5.2 (LI-COR Biosciences). Antibodies are listed in Supplementary Table 1 and 2.

Statistical Analysis. Mean values and SEM error bars are shown for each experiment. Unpaired t-tests were used to determine statistical significance between groups. For analysis of graphs in Fig. 2c, d, a ROC curve analysis was performed with significance levels set to 0.05. All analyses were performed in Graph Pad Prism version 8.1.1 for Windows (GraphPad Software, La Jolla California USA). Symbols used: ** P < 0.01; *** P < 0.001; ns, not significant.

Acknowledgments

The authors would like to thank Judith de Koning for technical assistance generating the U2OS CHD1-GFP stable cell line and Dr. Arjan Theil for advice, reagents and technical assistance. This work was supported by a

Marie Curie Initial Training Network funded by the European Commission 7th Framework Programme (316390), a European Research Council Advanced Grant (340988-ERC-ID), the Dutch Scientific Organization (ALW 854.11.002) and the Dutch Cancer Society (KWF 10506). This work is part of the Oncode Institute which is partly financed by the Dutch Cancer Society.

References

1. Schärer, O. D. Nucleotide excision repair in Eukaryotes. *Cold Spring Harb. Perspect. Biol.* **5**, (2013).
2. Marteijn, J. a, Lans, H., Vermeulen, W. & Hoeijmakers, J. H. J. Understanding nucleotide excision repair and its roles in cancer and ageing. *Nat. Rev. Mol. Cell Biol.* **15**, 465–81 (2014).
3. Sugasawa, K. Molecular mechanisms of DNA damage recognition for mammalian nucleotide excision repair. *DNA Repair (Amst)*. **44**, 110–117 (2016).
4. Tang, J. Y., Hwang, B. J., Ford, J. M., Hanawalt, P. C. & Chu, G. Xeroderma pigmentosum p48 gene enhances global genomic repair and suppresses UV-induced mutagenesis. *Mol. Cell* **5**, 737–44 (2000).
5. Moser, J. *et al.* The UV-damaged DNA binding protein mediates efficient targeting of the nucleotide excision repair complex to UV-induced photo lesions. *DNA Repair (Amst)*. **4**, 571–582 (2005).
6. Wakasugi, M. *et al.* DDB accumulates at DNA damage sites immediately after UV irradiation and directly stimulates nucleotide excision repair. *J. Biol. Chem.* **277**, 1637–1640 (2002).
7. Alekseev, S. *et al.* Cellular concentrations of DDB2 regulate dynamic binding of DDB1 at UV-induced DNA damage. *Mol. Cell. Biol.* **28**, 7402–13 (2008).
8. Groisman, R. *et al.* The ubiquitin ligase activity in the DDB2 and CSA complexes is differentially regulated by the COP9 signalosome in response to DNA damage. *Cell* **113**, 357–367 (2003).
9. Geijer, M. E. & Marteijn, J. A. What happens at the lesion does not stay at the lesion: Transcription-coupled nucleotide excision repair and the effects of DNA damage on transcription in cis and trans. *DNA Repair (Amst)*. **71**, 56–68 (2018).
10. Bernardes de Jesus, B. M., Bjørås, M., Coin, F. & Egly, J. M. Dissection of the molecular defects caused by pathogenic mutations in the DNA repair factor XPC. *Mol. Cell. Biol.* **28**, 7225–7235 (2008).
11. Okuda, M., Nakazawa, Y., Guo, C., Ogi, T. & Nishimura, Y. Common TFIIH recruitment mechanism in global genome and transcription-coupled repair subpathways. *Nucleic Acids Res.* **45**, 13043–13055 (2017).
12. Oksenyich, V., de Jesus, B. B., Zhovmer, A., Egly, J.-M. & Coin, F. Molecular insights into the recruitment of TFIIH to sites of DNA damage. *EMBO J.* **28**, 2971–2980 (2009).
13. Sugasawa, K., Akagi, J. ichi, Nishi, R., Iwai, S. & Hanaoka, F. Two-Step Recognition of DNA Damage for Mammalian Nucleotide Excision Repair: Directional Binding of the XPC Complex and DNA Strand Scanning. *Mol. Cell* **36**, 642–653 (2009).
14. Staresinic, L. *et al.* Coordination of dual incision and repair synthesis in human nucleotide excision repair. *EMBO J.* **28**, 1111–1120 (2009).
15. Ogi, T. *et al.* Three DNA Polymerases, Recruited by Different Mechanisms, Carry Out NER Repair Synthesis in Human Cells. *Mol. Cell* **37**, 714–727 (2010).
16. Essers, J., Vermeulen, W. & Houtsmuller, A. B. DNA damage repair: anytime, anywhere? *Curr. Opin. Cell Biol.* **18**, 240–246 (2006).
17. Smerdon, M. J. DNA repair and the role of chromatin structure. *Curr. Opin. Cell Biol.* **3**, 422–428 (1991).
18. Chodaparambil, J. V, Edayathumangalam, R. S., Bao, Y., Park, Y. J. & Luger, K. Nucleosome structure and function. *Ernst Schering Res. Found. Workshop* 29–46 (2006).
19. Happel, N. & Doenecke, D. Histone H1 and its isoforms: Contribution to chromatin structure

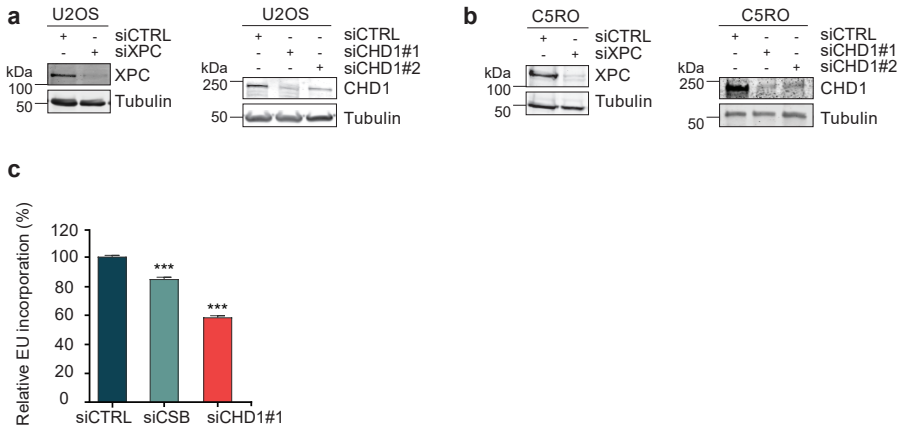
- and function. *Gene* **431**, 1–12 (2009).
20. Soria, G., Polo, S. E. & Almouzni, G. Prime, Repair, Restore: The Active Role of Chromatin in the DNA Damage Response. *Molecular Cell* **46**, 722–734 (2012).
 21. Gong, F., Kwon, Y. & Smerdon, M. J. Nucleotide excision repair in chromatin and the right of entry. *DNA Repair* **4**, 884–896 (2005).
 22. Wang, Z. G., Wu, X. H. & Friedberg, E. C. Nucleotide excision repair of DNA by human cell extracts is suppressed in reconstituted nucleosomes. *J. Biol. Chem.* **266**, 22472–8 (1991).
 23. Araki, M. *et al.* Reconstitution of damage DNA excision reaction from SV40 minichromosomes with purified nucleotide excision repair proteins. *Mutat. Res. - DNA Repair* **459**, 147–160 (2000).
 24. Lans, H., Marteiijn, J. A. & Vermeulen, W. ATP-dependent chromatin remodeling in the DNA-damage response. *Epigenetics and Chromatin* **5**, 4 (2012).
 25. Hara, R. & Sancar, A. The SWI / SNF Chromatin-Remodeling Factor Stimulates Repair by Human Excision Nuclease in the Mononucleosome Core Particle. *Mol. Cell. Biol.* **22**, 6779–6787 (2002).
 26. Ribeiro-Silva, C. *et al.* DNA damage sensitivity of SWI/SNF-deficient cells depends on TFIID subunit p62/GTF2H1. *Nat. Commun.* **9**, 4067 (2018).
 27. Gong, F., Fahy, D. & Smerdon, M. J. Rad4-Rad23 interaction with SWI/SNF links ATP-dependent chromatin remodeling with nucleotide excision repair. *Nat. Struct. Mol. Biol.* **13**, 902–907 (2006).
 28. Zhang, L., Zhang, Q., Jones, K., Patel, M. & Gong, F. The chromatin remodeling factor BRG1 stimulates nucleotide excision repair by facilitating recruitment of XPC to sites of DNA damage. *Cell Cycle* **8**, 3953–3959 (2009).
 29. Zhao, Q. *et al.* Modulation of nucleotide excision repair by mammalian SWI/SNF chromatin-remodeling complex. *J. Biol. Chem.* **284**, 30424–30432 (2009).
 30. Ray, A. *et al.* Human SNF5/INI1, a component of the human SWI/SNF chromatin remodeling complex, promotes nucleotide excision repair by influencing ATM recruitment and downstream H2AX phosphorylation. *Mol. Cell. Biol.* **29**, 6206–6219 (2009).
 31. Klochendler-Yeivin, A., Picarsky, E. & Yaniv, M. Increased DNA damage sensitivity and apoptosis in cells lacking the Snf5/Ini1 subunit of the SWI/SNF chromatin remodeling complex. *Mol. Cell. Biol.* **26**, 2661–74 (2006).
 32. McKenna, E. S. *et al.* Loss of the epigenetic tumor suppressor SNF5 leads to cancer without genomic instability. *Mol. Cell. Biol.* **28**, 6223–6233 (2008).
 33. Ribeiro-Silva, C., Vermeulen, W. & Lans, H. SWI/SNF: Complex complexes in genome stability and cancer. *DNA Repair (Amst)*. **77**, 87–95 (2019).
 34. Shen, X., Mizuguchi, G., Hamiche, A. & Carl, W. A chromatin remodelling complex involved in transcription and DNA processing. *Nature* **406**, 541–544 (2000).
 35. Sarkar, S., Kiely, R. & McHugh, P. J. The Ino80 chromatin-remodeling complex restores chromatin structure during UV DNA damage repair. *J. Cell Biol.* **191**, 1061–1068 (2010).
 36. Jiang, Y. *et al.* INO80 chromatin remodeling complex promotes the removal of UV lesions by the nucleotide excision repair pathway. *Proc. Natl. Acad. Sci.* **107**, 17274–17279 (2010).
 37. Lans, H. *et al.* Involvement of global genome repair, transcription coupled repair, and chromatin remodeling in UV DNA damage response changes during development. *PLoS Genet.* **6**, 41 (2010).
 38. Aydin, Ö. Z. *et al.* Human ISWI complexes are targeted by SMARCA5 ATPase and SLIDE domains to help resolve lesion-stalled transcription. *Nucleic Acids Res.* **42**, 8473–8485 (2014).

39. Aydin, Ö. Z., Vermeulen, W. & Lans, H. ISWI chromatin remodeling complexes in the DNA damage response. *Cell Cycle* **13**, 3016–3025 (2014).
40. Waters, R., van Eijk, P. & Reed, S. Histone modification and chromatin remodeling during NER. *DNA Repair (Amst)*. **36**, 105–113 (2015).
41. Marfella, C. G. A. & Imbalzano, A. N. The Chd family of chromatin remodelers. *Mutat. Res. - Fundam. Mol. Mech. Mutagen.* **618**, 30–40 (2007).
42. Hauk, G., McKnight, J. N., Nodelman, I. M. & Bowman, G. D. The Chromodomains of the Chd1 Chromatin Remodeler Regulate DNA Access to the ATPase Motor. *Mol. Cell* **39**, 711–723 (2010).
43. Stanley, F. K. T., Moore, S. & Goodarzi, A. A. CHD chromatin remodelling enzymes and the DNA damage response. *Mutation Research - Fundamental and Molecular Mechanisms of Mutagenesis* **750**, 31–44 (2013).
44. Rother, M. B. & van Attikum, H. DNA repair goes hip-hop: SMARCA and CHD chromatin remodellers join the break dance. *Philosophical Transactions of the Royal Society B: Biological Sciences* **372**, (2017).
45. Murawska, M. & Brehm, A. CHD chromatin remodelers and the transcription cycle. *Transcription* **2**, 244–253 (2011).
46. Mills, A. A. The chromodomain helicase DNA-binding chromatin remodelers: Family traits that protect from and promote cancer. *Cold Spring Harb. Perspect. Med.* **7**, (2017).
47. Grasso, C. S. *et al.* The mutational landscape of lethal castration-resistant prostate cancer. *Nature* **487**, 239–243 (2012).
48. Huang, S. *et al.* Recurrent deletion of CHD1 in prostate cancer with relevance to cell invasiveness. *Oncogene* **31**, 4164–4170 (2012).
49. Burkhardt, L. *et al.* CHD1 is a 5q21 tumor suppressor required for ERG rearrangement in prostate cancer. *Cancer Res.* **73**, 2795–2805 (2013).
50. Kari, V. *et al.* Loss of CHD1 causes DNA repair defects and enhances prostate cancer therapeutic responsiveness. *EMBO Rep.* **17**, 1609–1623 (2016).
51. Shenoy, T. R. *et al.* CHD1 loss sensitizes prostate cancer to DNA damaging therapy by promoting error-prone double-strand break repair. *Ann. Oncol. Off. J. Eur. Soc. Med. Oncol.* **28**, 1495–1507 (2017).
52. Zhou, J. *et al.* Human CHD1 is required for early DNA-damage signaling and is uniquely regulated by its N terminus. *Nucleic Acids Res.* **46**, 3891–3905 (2018).
53. Reardon, J. T., Vaisman, A., Chaney, S. G. & Sancar, A. Efficient nucleotide excision repair of cisplatin, oxaliplatin, and Bis-aceto-amine-dichloro-cyclohexylamine-platinum(IV) (JM216) platinum intrastrand DNA diadducts. *Cancer Res.* **59**, 3968–3971 (1999).
54. Friedberg, E. C. The discovery that xeroderma pigmentosum (XP) results from defective nucleotide excision repair. *DNA Repair (Amst)*. **3**, 183, 195 (2004).
55. Nakazawa, Y., Yamashita, S., Lehmann, A. R. & Ogi, T. A semi-automated non-radioactive system for measuring recovery of RNA synthesis and unscheduled DNA synthesis using ethynyluracil derivatives. *DNA Repair (Amst)*. **9**, 506–516 (2010).
56. Limsirichaikul, S. *et al.* A rapid non-radioactive technique for measurement of repair synthesis in primary human fibroblasts by incorporation of ethynyl deoxyuridine (EdU). *Nucleic Acids Res.* **37**, e31 (2009).
57. Mayne, L. V & Lehmann, A. R. Failure of RNA synthesis to recover after UV irradiation: an early defect in cells from individuals with Cockayne's syndrome and xeroderma pigmentosum. *Cancer Res.* **42**, 1473–8 (1982).

58. Smolle, M. *et al.* Chromatin remodelers Isw1 and Chd1 maintain chromatin structure during transcription by preventing histone exchange. *Nat. Struct. Mol. Biol.* **19**, 884–892 (2012).
59. Simic, R. *et al.* Chromatin remodeling protein Chd1 interacts with transcription elongation factors and localizes to transcribed genes. *EMBO J.* **22**, 1846–1856 (2003).
60. Lin, J. J. *et al.* Mediator coordinates PIC assembly with recruitment of CHD1. *Genes Dev.* **25**, 2198–2209 (2011).
61. Park, D., Shivram, H. & Iyer, V. R. Chd1 co-localizes with early transcription elongation factors independently of H3K36 methylation and releases stalled RNA polymerase II at introns. *Epigenetics and Chromatin* **7**, 32 (2014).
62. Albert, I. *et al.* Translational and rotational settings of H2A.Z nucleosomes across the *Saccharomyces cerevisiae* genome. *Nature* **446**, 572–576 (2007).
63. Pointner, J. *et al.* CHD1 remodelers regulate nucleosome spacing in vitro and align nucleosomal arrays over gene coding regions in *S. pombe*. *EMBO J.* **31**, 4388–403 (2012).
64. Dinant, C. *et al.* Activation of multiple DNA repair pathways by sub-nuclear damage induction methods. *J. Cell Sci.* **120**, 2731–2740 (2007).
65. Nishi, R. *et al.* UV-DDB-dependent regulation of nucleotide excision repair kinetics in living cells. *DNA Repair (Amst)*. **8**, 767–776 (2009).
66. Schwertman, P. *et al.* UV-sensitive syndrome protein UVSSA recruits USP7 to regulate transcription-coupled repair. *Nat. Genet.* **44**, 598–602 (2012).
67. van Cuijk, L. *et al.* SUMO and ubiquitin-dependent XPC exchange drives nucleotide excision repair. *Nat. Commun.* **6**, 7499 (2015).
68. Wienholz, F. *et al.* FACT subunit Spt16 controls UVSSA recruitment to lesion-stalled RNA Pol II and stimulates TC-NER. *Nucleic Acids Res.* (2019).
69. Sims, R. J. *et al.* Human but not yeast CHD1 binds directly and selectively to histone H3 methylated at lysine 4 via its tandem chromodomains. *J. Biol. Chem.* **280**, 41789–41792 (2005).
70. Steurer, B. *et al.* Live-cell analysis of endogenous GFP-RPB1 uncovers rapid turnover of initiating and promoter-paused RNA Polymerase II. *Proc. Natl. Acad. Sci.* **115**, 201717920 (2018).
71. Chen, D. H., Wu, K. T., Hung, C. J., Hsieh, M. & Li, C. Effects of adenosine dialdehyde treatment on in vitro and in vivo stable protein methylation in heLa cells. *J. Biochem.* **136**, 371–376 (2004).
72. Pray-Grant, M. G., Daniel, J. A., Schieltz, D., Yates, J. R. & Grant, P. A. Chd1 chromodomain links histone H3 methylation with SAGA- and SLIK-dependent acetylation. *Nature* **433**, 434–438 (2005).
73. Tai, H. H. *et al.* CHD1 associates with NCoR and histone deacetylase as well as with RNA splicing proteins. *Biochem. Biophys. Res. Commun.* **308**, 170–176 (2003).
74. Luijsterburg, M. S. *et al.* PARP1 Links CHD2-Mediated Chromatin Expansion and H3.3 Deposition to DNA Repair by Non-homologous End-Joining. *Mol. Cell* **61**, 547–562 (2016).
75. Polo, S. E., Kaidi, A., Baskcomb, L., Galanty, Y. & Jackson, S. P. Regulation of DNA-damage responses and cell-cycle progression by the chromatin remodelling factor CHD4. *EMBO J.* **29**, 3130–3139 (2010).
76. Pines, A., Mullenders, L. H., van Attikum, H. & Luijsterburg, M. S. Touching base with PARPs: Moonlighting in the repair of UV lesions and double-strand breaks. *Trends Biochem. Sci.* **38**, 321–330 (2013).
77. Volker, M. *et al.* Sequential assembly of the nucleotide excision repair factors in vivo. *Mol. Cell*

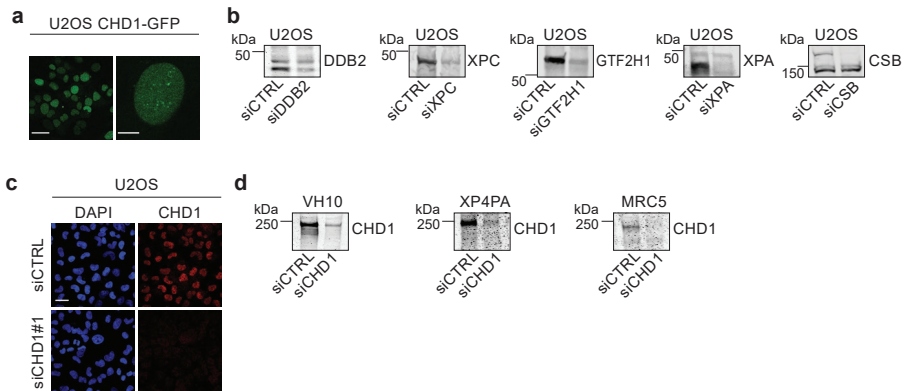
- 8**, 213–224 (2001).
78. Vermeulen, W. Dynamics of mammalian NER proteins. *DNA Repair (Amst)*. **10**, 760–771 (2011).
79. Hoogstraten, D. *et al.* Versatile DNA damage detection by the global genome nucleotide excision repair protein XPC. *J. Cell Sci.* **121**, 2850–9 (2008).
80. Luijsterburg, M. S. *et al.* Dynamic in vivo interaction of DDB2 E3 ubiquitin ligase with UV-damaged DNA is independent of damage-recognition protein XPC. *J. Cell Sci.* **120**, 2706–2716 (2007).
81. Pines, A. *et al.* PARP1 promotes nucleotide excision repair through DDB2 stabilization and recruitment of ALC1. *J. Cell Biol.* **199**, 235–249 (2012).
82. Clement, F. C. *et al.* Dynamic two-stage mechanism of versatile DNA damage recognition by xeroderma pigmentosum group C protein. *Mutat. Res. - Fundam. Mol. Mech. Mutagen.* **685**, 21–28 (2010).
83. Camenisch, U. *et al.* Two-stage dynamic DNA quality check by xeroderma pigmentosum group C protein. *EMBO J.* **28**, 2387–2399 (2009).
84. Sabatella, M. *et al.* Repair protein persistence at DNA lesions characterizes XPF defect with Cockayne syndrome features. *Nucleic Acids Res.* **46**, 9563–9577 (2018).
85. Rütthemann, P. *et al.* Chromatin remodeler CHD1 promotes XPC-to-TFIIH handover of nucleosomal UV lesions in nucleotide excision repair. *EMBO J.* **36**, 3372–3386 (2017).
86. Wienholz, F., Vermeulen, W. & Marteijn, J. A. Amplification of unscheduled DNA synthesis signal enables fluorescence-based single cell quantification of transcription-coupled nucleotide excision repair. *Nucleic Acids Res.* **45**, (2017).
87. Polo, S. E. & Almouzni, G. Chromatin dynamics after DNA damage: The legacy of the access-repair-restore model. *DNA Repair* **36**, 114–121 (2015).
88. Luijsterburg, M. S. & Van Attikum, H. Chromatin and the DNA damage response: The cancer connection. *Mol. Oncol.* **5**, 349–367 (2011).
89. Adam, S. *et al.* Real-Time Tracking of Parental Histones Reveals Their Contribution to Chromatin Integrity Following DNA Damage. *Mol. Cell* **64**, 65–78 (2016).
90. Dinant, C. *et al.* Enhanced chromatin dynamics by fact promotes transcriptional restart after UV-induced DNA damage. *Mol. Cell* **51**, 469–479 (2013).
91. Campeau, E. *et al.* A versatile viral system for expression and depletion of proteins in mammalian cells. *PLoS One* **4**, (2009).
92. Houtsmuller, A. B. & Vermeulen, W. Macromolecular dynamics in living cell nuclei revealed by fluorescence redistribution after photobleaching. *Histochemistry and Cell Biology* **115**, 13–21 (2001).

Supplementary data



Supplementary Fig. 1. (a) siRNA knockdown efficiencies and transcription levels after CHD1 depletion.

Immunoblot analysis of total cell lysates showing siRNA-mediated knockdown of XPC and CHD1 (CHD1#1 and CHD1#2) in (a) U2OS (related to Fig. 1a, d, e, and Fig. 4e, f) and (b) C5RO (related to Fig. 1b, c) cells. (c) Relative quantification of transcription levels in U2OS cells treated with non-targeting control (CTRL), CSB or CHD1 siRNAs. Transcription was determined by measuring incorporation of EU in non-irradiated cells 48 h after siRNA treatment. The relative EU fluorescence intensity was set to 100% in siCTRL treated cells. Mean & S.E.M. of > 150 cells from at least two independent experiments.



Supplementary Fig. 2. CHD1-GFP expressing cells and knockdown efficiency of used siRNAs.

(a) Live-cell confocal images of U2OS cells with stable CHD1-GFP showing nuclear localization. Scale bars: 25 and 5 μ m (left and right, respectively). (b) Immunoblot analysis of total cell lysates showing siRNA-mediated knockdown of DDB2, XPC, GTF2H1, XPA and CSB in U2OS CHD1-GFP cells (related to Fig. 2c). (c) Immunofluorescence (IF) representative pictures of CHD1 knockdown in U2OS cells with siRNA CHD1#1 in comparison with cells treated with a non-targeting (CTRL) siRNA (related to Fig. 3b, c, Fig. 4 and Supplementary Fig. 1d). Scale bar: 50 μ m. (d) Immunoblot analysis of total cell lysates showing CHD1 siRNA cells in VH10 (related to Fig. 3e, f), XP4PA (related to Fig. 3g, h) and MRC-5 (related to Fig. 4c, d).

Supplementary Table 1. Primary Antibody list and working dilutions.

Source, Reference	Antibody	Dilutions	
		Immunoblotting	Immunofluorescence
Abcam, ab181136	DDB2	1/1000	1/1000
Bethyl, A301-121A	XPC	1/2000	1/2000
Santa Cruz, sc-293	XPB	N.A.	1/1000
Abcam, ab54676	XPD	N.A.	1/150
Novus Biologicals, NBP2-38556	GTF2H1	1/500	N.A.
Santa Cruz, sc-853	XPA	1/250	1/50
Santa Cruz, sc-136153	XPF	N.A.	1/100
Bethyl, A301-218A	CHD1	1/2000	N.A.
Antibodies-online, ABIN2855858	CSB	1/1000	N.A.
MBL international, TDM-2	CPD	N.A.	1/1000
Sigma Aldrich, B512	Tubulin	1/10000	N.A.

Supplementary Table 2. Secondary Antibody list and working dilutions.

Source, Reference	Antibody	Dilutions	
		Immunoblotting	Immunofluorescence
Sigma, sab4600215	Anti-rabbit, CF IRDye 770	1/10000	N.A.
Sigma, sab4600199	Anti-mouse, CF IRDye 680	1/10000	N.A.
Invitrogen, A11034	Anti-rabbit, Alexa Fluor 488	N.A.	1/1000
Invitrogen, A21424	Anti-mouse, Alexa Fluor 555	N.A.	1/1000

SWI/SNF: Complex complexes in genome stability and cancer

5

Cristina Ribeiro-Silva, Wim Vermeulen, Hannes Lans

Department of Molecular Genetics, Oncode Institute, Erasmus MC, University Medical Center Rotterdam, Dr. Molewaterplein 40, 3015 GD, Rotterdam, The Netherlands

Published in DNA Repair, May 2019; 77: 87-95

1. Introduction

On a daily basis, each of our cells accumulates up to 10^4 - 10^5 DNA lesions that, if not adequately dealt with, can interfere with vital cellular processes such as transcription and replication, promoting genomic instability and eventually leading to tumorigenesis and premature aging^{1,2}. DNA lesions are a fact of life as they originate, to a large extent, from the spontaneous chemical instability of DNA in the cell's aqueous milieu, such as hydrolysis of bases, or from chemical attack by intracellular metabolites, such as reactive oxygen species derived from oxidative respiration. Genomic stress is further aggravated by exposure to a range of environmental chemicals and radiation. Some of the best studied environmental genotoxic agents are ultra-violet (UV) light, ionizing radiation (IR) and inter-strand crosslinking agents, due to their relevance for cancer development. Paradoxically, the latter two are also commonly used to treat cancer in radiotherapy and chemotherapy, respectively. Because DNA cannot be replaced, removal of damage is vital to protect cells against genetic erosion and transcription and replication stress. Evolution equipped cells with a sophisticated portfolio of specialized DNA repair and DNA damage signaling pathways, collectively called the DNA damage response (DDR), to cope with the different types of DNA lesions^{1,3}. A few of the different DNA repair pathways, relevant for this review, will be discussed in more detail below. The type of DNA lesion, its genomic location and chromatin environment, and the cell cycle phase determine which repair pathway is activated. Moreover, like all DNA-associated processes, DNA repair pathways have to overcome the physical barrier imposed by the condensed packaging of DNA into chromatin to efficiently access, detect, and repair lesions at any genomic location^{4,5}. In recent years, the number of chromatin modifying and remodeling enzymes found important for efficient DNA repair has increased tremendously, evidencing that (re-)organization of the highly dynamic chromatin structure is an intricate and essential component of the DDR *in vivo*⁶.

The nucleosome is the basic unit of chromatin, comprising approximately 146/147 bp of DNA wrapped around a histone octamer containing two copies of histones H2A, H2B, H3 and H4⁷. Each nucleosome is stabilized by electrostatic interactions between the phosphate backbone of DNA and

positively charged residues on histones, while short linker DNA segments link nucleosomes together. Folding and compaction of DNA into high-order structures is achieved by short and long-range interactions between nucleosomes, linker histone H1 and additional non-histone proteins. Dynamic rearrangement of the chromatin structure, via the concerted action of histone modifiers, histone chaperones, and ATP-dependent chromatin remodeling complexes, regulates the access and activity of DNA-transacting enzymes, including that of DDR proteins⁸. In eukaryotes, many structurally related ATP-dependent chromatin remodeling proteins and complexes have been identified, including the four major families, SWI/SNF, INO80, CHD, and ISWI, many of which have been implicated in DDR^{9–11}. Importantly, defects in both ATP-dependent chromatin remodelers¹² and DDR² are associated with tumorigenesis, but the interplay between these two with respect to cancer development is unfortunately only partially understood and currently an active field of research. In particular, the family of SWI/SNF chromatin remodeling complexes is frequently mutated in a wide variety of human cancers¹³. Therefore, we focus in this review on their emerging function in the DDR, specifically on their role in DNA double-strand break (DSB) repair and nucleotide excision repair (NER) and speculate on how this gained insight could be exploited for the development of new cancer prognostic markers, and therapeutic interventions.

2. SWI/SNF ATP-dependent chromatin remodelers

2.1 SWI/SNF complex composition and chromatin remodeling function

SWI/SNF (switching defective/sucrose non-fermenting) complexes were named after the two phenotypes in yeast that led to their discovery, through genetic screening for genes that regulate mating type switching and activate sucrose fermentation pathways^{14–16}. Evolutionary homologs of these multi-subunit protein complexes were later identified in *Drosophila* and mammals, and their role as major global regulators of transcription through ATP-dependent chromatin remodeling was firmly established^{17–19}.

SWI/SNF are heterogeneous complexes with the necessary skillset

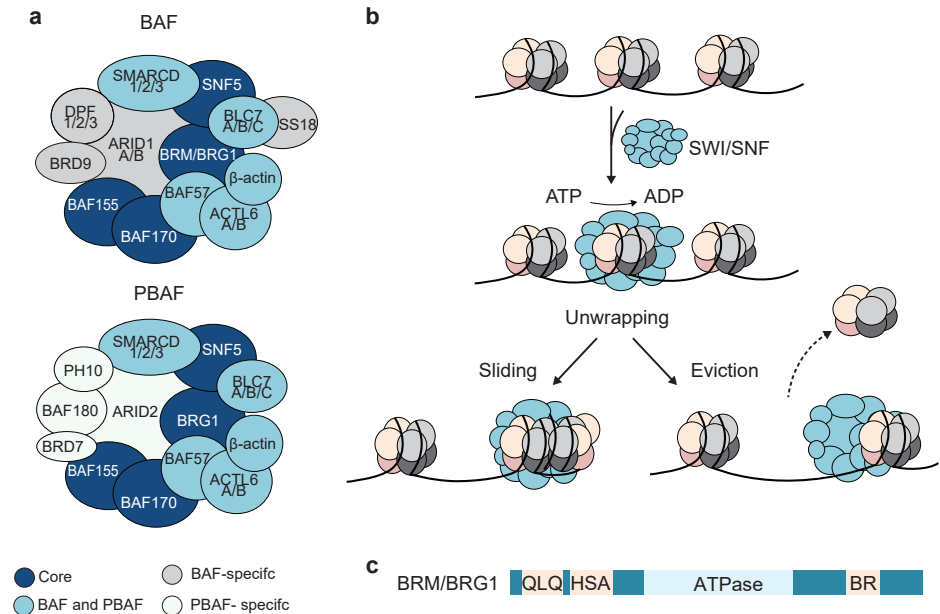


Figure 1. SWI/SNF ATP-dependent chromatin remodeling complexes. (a) BAF and PBAF complexes are the two major subtypes of SWI/SNF complexes and are determined by their subunit composition^{12,13,28,29,106,107}. (b) ATP-dependent chromatin remodeling activity of SWI/SNF complexes couples ATP-hydrolysis with directional movement of SWI/SNF that disrupts histone-DNA interactions at local nucleosomes^{8,22}. (c) BRM and BRG1 share the same functional domains that regulate sequence-specific DNA (BR, Bromo, and HAS, Helicase/SANT-associated) and protein (QLQ, Gln-Leu-Gln motif) interactions.

for diverse and specialized functions required in different cellular and developmental contexts^{20,21}. Mammalian SWI/SNF complexes always contain one of two mutually exclusive, though structurally highly related ATPases: BRM/SMARCA2 or BRG1/SMARCA4 (Fig. 1a, Table 1). These proteins couple ATP hydrolysis with directional translocation over DNA, thereby either repositioning nucleosomes, exchanging nucleosomes histone dimers or evicting entire histone octamers^{8,22} (Fig. 1b). In addition to the defining ATPase domain, BRM and BRG1 harbor domains for binding to actin and other proteins, such as the HSA and QLQ domains²³, and a bromodomain (BROMO) for binding to acetylated histones²⁴ (Table 1, Fig. 1c). Although BRG1 or BRM alone are sufficient for remodeling of nucleosomes *in vitro*²⁵, in the context of the cell the additional SWI/SNF core and accessory subunits play essential roles in targeting and regulating their remodeling activity^{26,27}. Depending on their subunit composition, SWI/SNF complexes are divided into two main categories, BAF and PBAF

(Fig. 1a). In humans, SNF5/SMARCB1, BAF155/SMARCC1, and BAF170/SMARCC2 are core SWI/SNF subunits found in every SWI/SNF complex (Fig. 1a, dark blue ovals)²⁵. BAF250A/ARID1A or BAF250B/ARID1B, BRD9 and SS18 are found exclusively in BAF complexes (Fig. 1a, grey ovals), while BAF200/ARID2, BAF180/PBRM1, PH10 and BRD7 are found solely in PBAF (polybromo BRG1-associated factor) complexes (Fig. 1a, white ovals)^{13,28}. Also, some accessory (family of) proteins are shared by BAF and PBAF, e.g., BAF57, β -actin, ACTL6 (A/B), BLC7(A/B/C) and DPF(1/2/3) (Fig. 1a, light blue ovals). Most subunits harbor one or more unique domain (Table 1), with which they tightly coordinate SWI/SNF function. For instance, subunits such as BAF180 and BRD7 harbor BROMO domains that allow SWI/SNF to interact with acetylated histones, while ARID and Zinc finger domains in ARID1A/B and ARID2 provide SWI/SNF with the ability to interact with specific DNA sequences^{28–30}.

In BAF complexes either BRM or BRG1 can be the catalytic subunit, whereas in PBAF that function is exclusively performed by BRG1. Many accessory subunits are encoded by sets of paralogs that are mutually exclusive and thus not present within the same complex: ACTL6A/B, DPF1/2/3, SMARCD1/2/3, and ARID1A/B^{13,28}. Thus, the combination of different SWI/SNF subunits, encoded by at least 29 genes from 15 gene families²⁹ can potentially give rise to an undetermined number of distinct complexes of different biological functions, with specific combinations being unique to certain cell types. Cellular transitions, for instance during differentiation, can lead to dynamic reconfiguration of SWI/SNF complex composition. One example of this is the replacement of ACTL6A by ACTL6B, which is essential for proper neuron function during neuronal differentiation³⁰. However, the impact of changes in subunit composition to the various functions of SWI/SNF complexes, in particular also to their function in the DDR, is far from understood.

2.2 Tumor suppressor functions of SWI/SNF

Mutations in genes encoding for SWI/SNF subunits are found in approximately 20% of all human cancers of various types^{13,31} (Table 1). This suggests that SWI/SNF may act as a tumor suppressor, thus protecting against cancer development, likely by regulating processes that safeguard cellular homeostasis. It is therefore relevant to understand how SWI/SNF

Table 1. SWI/SNF subunits, domains and frequency of alteration in cancer.

Subunit	HUGO name	Synonyms	Domains	% Alteration in cancer
BRG1	SMARCA4	-	Bromo, ATPase, HAS, QLQ	Ovarian cancer (>10%), medulloblastoma (5-10%), melanoma (5-10%), small cell cancer of the ovary (100%)
BRM	SMARCA2	-	Bromo, ATPase	Rhabdoid tumor (60%); lung (4.8-10%), breast (15%), gastric (15%) and bladder (15%) cancers
SNF5	SMARCB1	INI1, BAF47	COIL	Rhabdoid tumor (>98%), epithelioid sarcomas (>55%), familial schwannomatosis (30-45%)
BAF155	SMARCC1	-	CHROMO, SANT, COIL	Prostate cancer (30-31%)
BAF170	SMARCC2	-	CHROMO, SANT, COIL	Rarely mutated
ARD1A	ARD1A	BAF250A	ARID	Clear cell ovarian (50%), endometrioid ovarian (21-48%), breast (2.5%), liver (15%), bladder (17%), gastric (14-18%), lung (9.8%) cancer
ARD1B	ARD1B	BAF250B	ARID	Childhood neuroblastoma (7%), clear cell ovarian (>10%), gastric, colorectal and liver cancer (5-10%)
ARID2	ARID2	BAF200	ARID, Zinc finger	Melanoma (5-15%), lung and colorectal (5-10%) and liver (5-14%) cancer
BAF180	PBRM1	-	Bromo, HMG	Renal cancer (41%), epithelioid sarcoma (83%)
BRD7	BRD7	-	Bromo	Breast cancer
BRD9	BRD9	-	Bromo	Rarely mutated
PH10	PH10	BAF45A	PHD finger	Rarely mutated
DPF1/2/3	DPF1/2/3	BAF45B/C/D	PHD finger	Rarely mutated
BAF57	SMARCE1	-	HMG, COIL	Familial spinal meningiomas (45%)
SMARCD1/2/3	SMARCD1/2/3	BAF60A/B/C	SWIB	Rarely mutated
BCL7A/B/C	BCL7A/B/C	-	-	Non-Hodgkin's lymphoma (19.7%)
ACTL6A/B	ACTL6A/B	BAF53A/B	Actin	Rarely mutated
SS18	SS18	SSXT	-	Synovial sarcoma (100%)

SWI/SNF subunits contain different protein domains to coordinate protein-protein or protein-DNA interactions²². Bromodomain (Bromo), important for the binding of acetylated histones. Coiled coil region (COIL) is a homodimerization domain. Chromatin organization modifier (CHROMO) domain is important for chromatin targeting. The Helicas/SANT-associated (HAS), SANT, ARID and HMG domains regulate sequence-specific DNA interactions, while the Gln-Leu-Gln (QLQ) motif, Zinc finger and PHD domains are involved in protein-protein interactions. SWI/SNF subunits alterations in cancer summarized here are extensively described in recent reviews^{13,28,39,105}.

activity contributes to the tumorigenesis process. The first uncovered and most studied function of SWI/SNF is its intricate regulation of transcription. Mammalian SWI/SNF complexes regulate transcription by binding in close vicinity to promoters but also near other regulatory regions, such as enhancers^{26,32}. By promoting or repressing the expression of specific genes, SWI/SNF complexes control vital cellular processes³², including pluripotency of embryonic stem cells, cell cycle regulation and neuronal and hematopoietic cell differentiation³³. Not only the ATPases BRG1 or BRM are needed for transcription regulation, but other SWI/SNF subunits play an important role in transcription by directly stimulating or inhibiting other transcriptional regulators. For instance, ARID1A/B and SNF5 can interact with the proto-oncogenic MYC protein to regulate the expression of its target genes, but can also modulate the expression of *MYC* itself^{34,35}. Because *MYC* is an oncogene frequently overexpressed in cancer, tight control of its activity is desired, which could be potentially compromised in SWI/SNF-deficient cancers. Similarly, direct binding of BRM or BRG1 to the tumor suppressor RB1³⁶ facilitates the repression of RB1 targets, such as E2F transcription factors, and promotes G1 arrest³⁷. Thus, inactivation of SWI/SNF leading to loss of RB1 activity may result in uncontrolled cell cycle progression and favor the appearance of malignant phenotypes.

SWI/SNF has additional functions beyond the regulation of gene expression, which are vital to safeguard genome function and stability and to prevent cancer, as described extensively in recent reviews^{28,31,38–40}. Examples include the regulation of alternative splicing, by favoring recruitment of the splicing machinery⁴¹, and the regulation of decatenation activity of topoisomerase II α (TOPII α)⁴². Furthermore, the PBAF complex assists in sister chromatid cohesion by localizing at kinetochores of mitotic chromosomes⁴³ and by regulating centromeric cohesion in a transcription-independent manner⁴⁴. Because centromeric cohesion is crucial for chromosome orientation and proper segregation, loss of not only BAF180 but also BRG1 results in cells with abnormal anaphase events, aneuploidy, and micronuclei^{44,45}. All of these aberrant events are typical features of many cancers, suggesting that SWI/SNF-mediated centromere cohesion is required for tumor suppression.

3. SWI/SNF and the DNA damage response

SWI/SNF has been implicated in multiple DNA repair pathways, which may have significant repercussions for tumorigenesis of SWI/SNF-deficient cancers since DDR deficiencies often lead to genomic instability. Furthermore, knowing which SWI/SNF factors are actively involved in protecting cells against DNA damage would allow us to have a more comprehensive understanding of which DDR-related cancer vulnerabilities could be targeted as a consequence of SWI/SNF deregulation. Moreover, it would help to predict chemotherapy sensitivity of SWI/SNF-deficient cancer cells in precision medicine procedures.

3.1 Double-strand break repair

SWI/SNF deficiency has been found to render yeast, *C. elegans* and human cells hypersensitive to DNA-damaging agents, including chemotherapeutic drugs such as doxorubicin and cisplatin, UV light and IR^{46–51}. IR and chemotherapeutic drugs, the latter by interfering with replication, cause DSBs. When not properly repaired, these DSBs can result in mutations and chromosomal aberrations (e.g., translocations) that underlie oncogenic transformation. DSBs are predominantly repaired by non-homologous end-joining (NHEJ) and homologous recombination (HR)⁵². NHEJ takes place during any stage of the cell cycle and is initiated when broken DNA ends are bound by the KU70/KU80 heterodimer, which recruits and orchestrates the activity of subsequent repair factors that process and join DNA ends by ligation. Alternatively, in late S or G2 cell cycle phase, DSB ends are bound by the MRE11-RAD50-NBS1 (MRN) complex, which, together with CtIP and EXO1, resects one strand to create 3' single stranded DNA overhangs to direct repair towards HR. In contrast to NHEJ, HR is more accurate and principally error-free, as it makes use of the sister chromatid as a template for homology-directed repair. MRN also recruits the phosphatidylinositol 3-kinase ATM, which phosphorylates histone H2AX (γ H2AX) and many other proteins involved in repair and checkpoint signaling. RPA binds the resected single-stranded DNA and is subsequently replaced by the recombinase RAD51. The RAD51-nucleoprotein filament facilitates strand invasion to the homologous double-stranded DNA template of the sister chromatid, allowing DNA synthesis from the sister template and subsequent resolution of the recombined DNA strands.

Yeast and mammalian SWI/SNF complexes have been implicated in both NHEJ and HR, as is also discussed in several previous reviews^{9,10,38,53}.

Depletion or inactivation of SWI/SNF subunits, including the ATPases BRG1 and BRM and core and accessory subunits, such as BAF155, BAF170, ARID1A/B and ARID2, sensitizes cells to DSB-inducing agents and reduces HR and/or NHEJ efficiency in fluorescent reporter assays^{49,50,54–56}. Both BRM and BRG1 also rapidly localize to DSB sites, either induced enzymatically or by laser irradiation, in a manner that appears to be dependent on ATM-mediated signaling and post-translational modification of histones. ATM promotes the damage localization of SWI/SNF by phosphorylating histone H2AX⁵⁰ and by directly phosphorylating BRG1 and BAF170⁵⁷. In turn, BAF170 phosphorylation increases the interaction of SWI/SNF subunits with the early DDR protein BRIT1/MCPH1⁵⁸, a protein that too helps recruiting SWI/SNF. Furthermore, recruitment of BRG1 to damaged sites was found to depend on an interaction with the tumor suppressor RB1 and the E2F1 transcription factor, which also localize to DSBs in an ATM phosphorylation-dependent manner⁵⁶. Besides phosphorylation of histone H2AX, also H2B phosphorylation and H3 and H4 acetylation have been implicated in promoting the damage localization of SWI/SNF. For instance, BRG1 binds to damage induced γ H2AX-containing nucleosomes by interacting with acetylated H3 histones through its bromodomain⁵⁹. In addition, BRM recruitment to DSBs was reported to be stimulated by the activity of AMP-activated protein kinase, which phosphorylates H2B⁶⁰, and by the activity of acetyltransferases CBP/CREBBP and p300/EP300, which acetylate histones H3 and H4 at DSBs⁵⁴. Next to the catalytic subunits, also other components of SWI/SNF are implicated in targeting SWI/SNF to damaged sites. For example, BRM recruitment to damage was found to depend on the SNF5, SMARCD3 and ARID1A/B subunits⁴⁹. Thus, it is reasonable to assume that multiple mechanisms orchestrate, likely in a cooperative manner, the efficient recruitment to and function of SWI/SNF complexes at sites of DNA damage. Besides BRG1 and BRM, other mutually exclusive SWI/SNF subunits were shown to localize to DSB sites. For instance, ARID1A recruitment to DSBs depends on ATM signaling and direct interaction with ATR⁵⁵. On the other hand, BAF180 is recruited independently of ATM.

The exact roles of SWI/SNF complexes in DSB repair remain convoluted, in part because of the multiple and sometimes even ambiguous activities that have been reported. For example, SWI/SNF may promote efficient damage signaling, as depletion of BRG1 and BRM was shown to reduce γ H2AX levels early after IR⁵⁰. However, other studies have reported increased⁶¹ or persistent⁶² γ H2AX levels after BRG1 loss, indicative of a genuine repair defect. Indeed, SWI/SNF proteins are implicated in both NHEJ and HR, in yeast as well as mammals^{31,38}, which further confounds the dissection of their precise function in DSB repair. For instance, BRM and ARID1A/B were shown to stimulate recruitment of NHEJ factors, such as KU70/KU80^{49,54,60}, while BRG1 and ARID1A appear to promote HR-associated DNA end resection and RPA and RAD51 loading^{55,56}. However, another study suggested that BRG1, rather than affecting resection, by interacting with RAD52, stimulates HR by promoting the exchange of RPA for RAD51⁶³. Moreover, the PBAF subunit ARID2 was reported to interact with RAD51 and thereby to stimulate its loading onto DNA, independently of BRG1, but still in complex with BAF180 and other SWI/SNF proteins⁶². These studies suggest that SWI/SNF subunits may have functions in DSB repair beyond its motor function.

Despite a large amount of evidence suggesting that SWI/SNF stimulates DSB repair, it is unclear if this necessarily involves chromatin remodeling to provide access for repair factors to DNA. Some observations suggest that SWI/SNF activity promotes chromatin relaxation after DNA damage, such as increased H3 occupancy observed at DSB sites after ARID1A depletion⁵⁵ and reduced MNase sensitivity of genomic DNA seen after BRM or BRG1 depletion⁵⁸. However, it was also reported that deficient RAD51 loading due to BRG1 deficiency could be rescued by ATPase-mutant BRG1⁶³, suggesting that this BRG1 function is independent of chromatin remodeling. Interestingly, instead of facilitating chromatin access, the PBAF complex was found to mediate transcription silencing near DSBs, involving polycomb complexes PRC1 and PRC2, and ATM-dependent mono-ubiquitylation of H2A, which promotes rapid NHEJ of a subset of DSBs⁶¹. Strikingly, this process required the catalytic activity of BRG1. Thus, considering that BRM and ARID1A/B are not part of PBAF, the different SWI/SNF complexes may have multiple functions in DSB repair, including promoting NHEJ by stimulating KU70/KU80 recruitment

(via BAF) and chromatin remodeling-mediated transcription silencing (via PBAF). Moreover, SWI/SNF may promote HR by facilitating DNA end resection and/or RAD51 loading (via both BAF and PBAF) (Fig. 2). It thus seems possible that a BAFFling collection of different SWI/SNF complexes, some of which may even have opposing functions, are localized to or near DNA damage and simultaneously stimulate HR as well as NHEJ in the same cell. It could be that SWI/SNF complexes act in parallel at distinct sites dependent on the chromatin status or in concert at different distances with respect to the lesion. Obviously, more and innovative research is necessary to better understand how the proposed different mechanisms of recruitment and multiple activities at sites of damage are coordinated and which exact activities distinguish each separate SWI/SNF complex at sites of DSBs.

3.2 Nucleotide excision repair

Depletion or inactivation of SWI/SNF subunits significantly increases cellular sensitivity to UV and platinum drugs such as cisplatin^{48,51,64}, suggesting the involvement of SWI/SNF in NER. This versatile repair process detects and removes a wide range of unrelated helix-distorting lesions, such as bulky-adducts and drug-induced (e.g., cisplatin) crosslinks, as well as the main UV-induced photoproducts, cyclobutane-pyrimidine dimers (CPDs) and 6-4 pyrimidine-pyrimidone photoproducts (6-4PPs)^{65,66}. This unique ability of the NER pathway not only protects cells against cancer and aging by preventing mutagenesis and genomic instability, but it also provides cancer cells with a defense line against chemotherapeutic platinum drugs^{67,68}.

Two distinct DNA damage recognition routes can trigger NER, depending on the location of DNA lesions. When RNA Polymerase II gets stalled by lesions in the transcribing strand of active genes, transcription-coupled NER (TC-NER) is initiated by the recruitment of CSB/ERCC6, CSA/ERCC8 and UVSSA proteins⁶⁶. Lesions located anywhere in the genome are detected by global genome NER (GG-NER), which is initiated by the damage sensor complex XPC-RAD23B-CETN2^{65,66,69}. Although XPC can recognize a wide range of helix-distorting lesions, it requires the auxiliary function of the UV-DDB complex, consisting of DDB1 and DDB2, to specifically and efficiently recognize UV-induced photolesions, in particular CPDs.

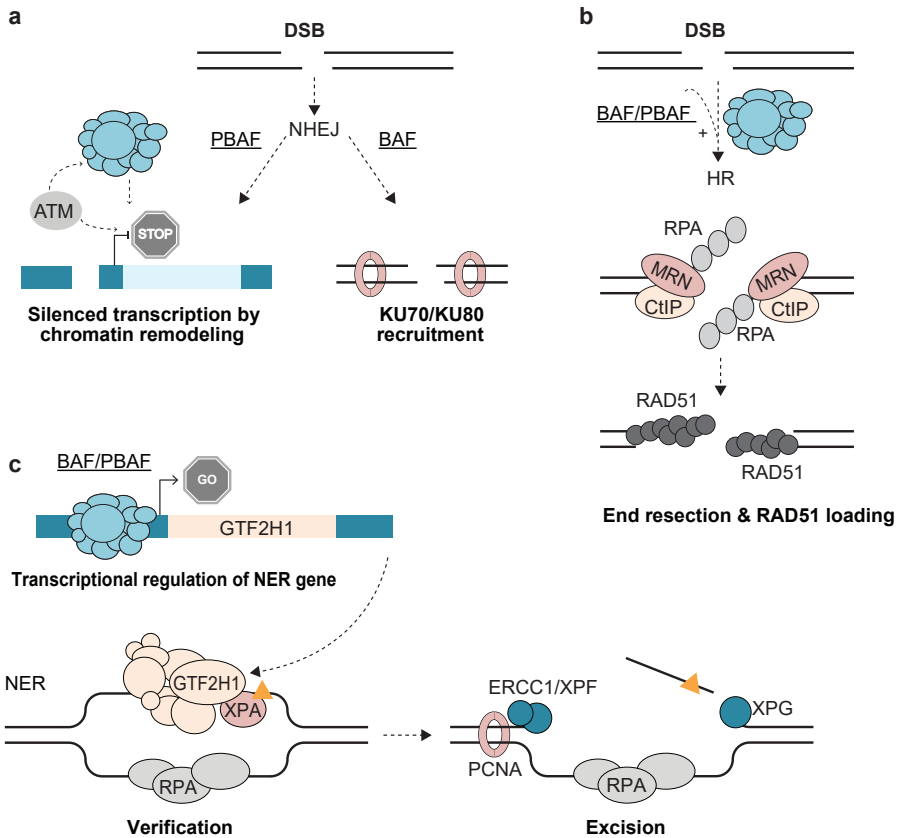


Figure 2. SWI/SNF ATP-dependent chromatin remodeling complexes functions in DDR. (a) PBAF complexes, via their chromatin remodeling activity, were found to mediate transcription silencing near DSBs, in an ATM-dependent way. On the other hand, BAF complexes seem to have a distinct function in promoting NHEJ, by stimulating the recruitment of KU70/KU80. (b) Both BAF and PBAF complexes are implicated in promoting HR-associated end resection and/or RPA and RAD51 loading. (c) Unlike for NHEJ and HR, SWI/SNF activity only indirectly affects NER. BRM- and BRG1-containing SWI/SNF complexes promote the expression of the NER gene, GTF2H1, which is essential for damage verification by TFIIH. In turn, verification is required for the assembly of late NER proteins on UV damage (XPA, RPA, ERCC1, XPF, XPG and PCNA).

Following lesion detection, the ten subunit Transcription Factor IIIH (TFIIH) complex is recruited to damage by interacting with XPC or UVSSA⁷⁰ and anchored through its XPB/ERCC3 and p62/GTF2H1 subunits. Using its XPD/ERCC2 helicase subunit, TFIIH then verifies the presence of genuine NER substrates^{66,69}, assisted by XPA. XPA and RPA stabilize this intermediate and adequately orient the structure-specific endonucleases XPF/ERCC4-ERCC1 and XPG/ERCC5. After dual incision, a stretch of 22-30 nucleotides is excised and the resulting single-stranded gap is filled by DNA synthesis

and finally ligated^{65,66,69}.

Rearrangement of the nucleosome structure following UV damage⁷¹ has triggered intense research on a possible function of ATP-dependent chromatin remodelers in NER by facilitating access to DNA. Numerous studies based on *in vitro* excision repair assays have shown that nucleosomes form a barrier to an efficient NER reaction and that DNA lesions are more easily repaired on naked than on chromatinized DNA^{72–74}. Furthermore, the yeast SWI/SNF complex was found to increase accessibility and incision of damaged DNA within *in vitro* reconstituted mononucleosomes^{75,76}, suggesting that SWI/SNF could stimulate repair via chromatin remodeling activity. This idea is further supported by several studies in yeast and mammalian cells. For instance, yeast SWI/SNF subunits Snf5 and Snf6 were found to interact in a UV-dependent manner with Rad4, the yeast orthologue of XPC, and to stimulate UV-induced chromatin relaxation⁷⁷. Studies using mammalian cells have also provided evidence that SWI/SNF and NER proteins interact, suggestive of a conserved function. Unfortunately, these studies have not been unambiguous in providing a precise mechanism of how mammalian SWI/SNF might be involved in NER. One study reported that BRG1 interacts with DDB2 in chromatin to facilitate XPC recruitment, suggesting that SWI/SNF might stimulate lesion detection, possibly by facilitating chromatin access⁷⁸. However, this model is challenged by several other studies showing that SWI/SNF promotes late NER steps rather than early lesion detection. For instance, BRG1 itself was reported to be recruited to UV damage, in an XPC-dependent way, to promote the recruitment of late NER factors XPG and PCNA but not of XPC⁷⁹. Accordingly, knockdown of BRG1 and BRM was described to impair recruitment of the late NER factor ERCC1 to cisplatin lesions without affecting XPC⁵¹. Moreover, SNF5 was found to interact with XPC, but not to regulate its recruitment but rather that of ATM⁸⁰. Finally, depletion of ARID1A/B was found to reduce XPA recruitment, but not XPC recruitment, to damaged DNA⁶⁴. Thus, there is substantial evidence supporting an evolutionarily conserved role of SWI/SNF in NER, even though contradicting findings obscure a clear deduction on its exact involvement.

The already challenging dissection of SWI/SNF function in NER is even

further convoluted since several studies have suggested that loss of SWI/SNF subunits (BRM, BRG1, SNF5) impairs the removal of CPDs, but not of 6-4PPs⁷⁸⁻⁸¹. It is difficult to envision how SWI/SNF deficiency could only impair CPD removal when SWI/SNF promotes the recruitment of NER factors, such as XPC and XPG, which are crucial for the repair of both CPDs and 6-4PPs. However, it has been observed that a specific mutation in the NER gene (XPD) affects the repair of CPDs more than that of 6-4PPs⁸². In addition, DNA damage is not distributed randomly and the repair kinetics of 6-4PPs and CPDs are dramatically different^{83,84}. Since 6-4PPs are predominantly formed in internucleosomal DNA, they may not require chromatin remodeling by SWI/SNF to be efficiently processed. On the other hand, in another study it was shown that 6-4PPs removal is impaired after ARID1A/B depletion⁶⁴.

In an attempt to gain more insight into the main role of SWI/SNF in the response to UV-induced DNA damage, and because most studies have focused on BRG1 or SNF5, we recently investigated a putative role of BRM in NER⁸⁵. This study was also triggered by our previous finding that in the model organism *C. elegans* multiple SWI/SNF subunits, including BRG1/BRM, SNF5, BAF180, BAF155, and ARID1A/B, are essential for optimal UV survival⁴⁸ (and unpublished results). We found that knockdown of BRM in human cells impaired both GG- and TC-NER activity, to the same extent as did BRG1 depletion. Importantly, while recruitment of DDB2, XPC, and CSB to local UV damage sites was unaffected by BRM depletion, recruitment of proteins downstream of these damage sensors, i.e., TFIIH, XPA, and XPF, was severely impaired. These results are in line with the previously reported reduced recruitment of XPA, XPG, ERCC1, and PCNA following BRG1 or BRM depletion^{51,64,79,85}. These observations thus indicate that SWI/SNF activity mainly facilitates late NER steps, rather than damage detection. Consequently, after depletion of SWI/SNF, the overall damage excision is reduced.

Strikingly, we were unable to observe BRM or BRG1 recruitment to local sites of UV damage, even using a dedicated UV-C laser to induce a high local concentration of DNA damage to which regular NER proteins localize⁸⁶. Moreover, we could also not confirm the proposed interactions of BRM and BRG1 with TFIIH⁸⁵, nor with DDB2 and XPC (unpublished

results). However, following BRG1 or BRM knockdown we observed a significant reduction in mRNA and protein levels of the TFIIH subunit GTF2H1, resulting in impaired TFIIH complex assembly. These observations suggest that the affected NER function upon SWI/SNF depletion is merely an indirect consequence of impaired *GTF2H1* gene expression, rather than a direct role of SWI/SNF in NER. Indeed, we found that both BRG1 and BRM associate with the promoter of *GTF2H1*, irrespective of whether there is UV damage or not, corroborating the idea that SWI/SNF promotes the expression of *GTF2H1*. Since assembly and functionality of the TFIIH complex were shown to depend on the cellular concentration of its subunits^{87–89}, it is therefore likely that reduced GTF2H1 protein levels limit the availability of fully assembled functional TFIIH complexes to act in transcription initiation and NER. Damage verification by TFIIH is crucial to the assembly of late NER proteins on UV damage. Thus, reduced damage verification as a consequence of SWI/SNF inactivation explains the reduced recruitment of XPA, ERCC1, XPF, XPG and PCNA to DNA damage and consequent hypersensitivity of cells to UV^{51,64,79,81,85}.

It is surprising to note that the role of SWI/SNF chromatin remodelers in both DSB repair and NER is rather convoluted, making it difficult, if not impossible, to draw a uniform mode of their action in the DDR. However, given the fact that the function of SWI/SNF in transcription regulation is also fairly ambiguous, with even opposing gene-dependent and chromatin-context-dependent effects, this may not be entirely unforeseen. Transcription regulation depends on the intricate interplay between cis-acting transcription-regulatory elements in the template DNA, availability of general and gene-specific transcription factors, activation by cell-intrinsic and environmental cues, post-translational chromatin modifications and chromatin compaction. This multi-layered control over gene expression likely explains the ambiguity of SWI/SNF (and possibly of other chromatin modifiers alike) in this process and its diverse and likely dynamic composition. However, unlike transcription that is commonly scheduled and takes place at a defined genomic locus, DNA repair has to occur at any given moment and anywhere in the genome⁹⁰ due to the stochasticity of DNA damage. This likely adds another degree of complexity, making it even more challenging to elucidate the multiple functions of SWI/SNF in the DDR.

4. SWI/SNF, DDR and cancer

4.1 SWI/SNF and NER deficiency in cancer

Since SWI/SNF is often mutated in cancer, we aimed at understanding whether cells with chronic SWI/SNF deficiency also have NER defects. Strikingly, we noticed that GTF2H1 levels were not altered in several established SWI/SNF-deficient cancer cell lines regularly used in lab research⁸⁵. To understand the cause of this unexpected observation, we generated CRISPR/Cas9-mediated BRM and BRG1 knockout human fibroblasts. Surprisingly, upon extended culturing, we found that most cells with a permanent knockout of either SWI/SNF ATPase have the ability to restore expression of GTF2H1. However, we noticed that in some sub-populations of cells GTF2H1 expression remains low. Accordingly, we noticed that sensitivity to DNA damaging agents of BRM-knockout cells was directly linked to the expression levels of GTF2H1, as only cells that retained lowered GTF2H1 expression were hypersensitive to UV and cisplatin. Thus, SWI/SNF inactivation creates a potential vulnerability of cells to DNA damaging agents, as a consequence of GTF2H1 downregulation (Fig. 2). Therefore, we propose that GTF2H1 expression levels could serve as a potential biomarker to screen SWI/SNF cancers for increased sensitivity to chemotherapeutic drugs, such as cisplatin, even before therapy begins. However, efforts are needed to test if indeed GTF2H1 levels are reduced across primary SWI/SNF cancers and to determine its suitability as a predictive marker for cisplatin sensitivity.

The ability of chronic BRM- and/or BRG1-deficient cells to adapt and upregulate GTF2H1 levels likely explains why established SWI/SNF-deficient cancer cell lines do not show reduced GTF2H1 levels. Also, it could explain why contradicting observations exist regarding cellular sensitivities to DNA damage of SWI/SNF-deficient cancer cells^{91,92}. Similar adaptation to the loss of one or more SWI/SNF ATPases or subunits has been described for other regulatory functions of SWI/SNF outside DNA repair. It appears that BRG1 and BRM can at least partially compensate for each other's essential functions^{93–96}, as cells with inactivating mutations in BRG1 strongly rely on BRM to sustain a minimal degree of SWI/SNF functionality to support cellular viability^{93,94}. Also, the viability of ARID1A mutant cancer cells strongly depends on the, otherwise non-

essential, ARID1B subunit⁹⁷. How cells compensate for the loss of BRM and/or BRG1, ARID1A and/or ARID1B, is yet unknown. BRM and BRG1 are similarly distributed across regulatory regions of the genome where they act either cooperatively or competitively to regulate transcription⁹⁸. Interestingly, loss of either ATPase at certain regions often leads to concomitant loss of the other ATPase as well. Depending on which other transcriptional regulators are associated with these regions, which can be either activating or repressing, transcription of genes can be up- or downregulated when SWI/SNF is inactivated. The existence of such multiple transcriptional control layers, including other families of ATP-dependent chromatin remodelers, could explain why cells are able to (partially) compensate for the loss of SWI/SNF activity. Possibly, in time, GTF2H1 is also upregulated in chronic SWI/SNF-deficient cells due to the activity of such yet unidentified secondary transcriptional activator(s). In any case, identification of the compensatory mechanisms and chromatin regulators that lead to GTF2H1 upregulation is fundamental. Hopefully, such insight would allow us to exploit these compensatory mechanisms therapeutically by rendering SWI/SNF-deficient cancer cells specifically hypersensitive to DNA damaging treatments.

Thus far, the relevance of only a selected group of SWI/SNF subunits to the DDR has been studied while many more subunits are found to be mutated or silenced in cancer (Table 1). The involvement of these subunits in DNA repair is not yet known, but dissecting their precise function in response to DNA damage could contribute to a more comprehensive understanding of SWI/SNF-deficiency in cancer. Therefore, future studies should consider whether additional subunits are relevant to DNA repair as well. In addition, it is also interesting to study whether SWI/SNF is involved in additional DNA repair pathways as well and what its precise activity in each repair pathway is. For instance, besides DSB repair and NER, BRG1 has been found to support repair of inter-strand crosslinks, together with BRCA1 and FANCD2, to help maintain the differentiation status of human mammary epithelial cells and suppress breast cancer⁹⁹. Also, a stimulatory function in base excision repair *in vitro* and yeast cells was proposed¹⁰⁰. However, its exact involvement in these repair pathways is even less clear and scrutinized than in DSB repair and NER.

4.2 Therapeutic perspectives

Given the high incidence of SWI/SNF mutations in different cancers and their involvement in multiple DDR pathways, it would be advantageous to aim future studies at therapeutically exploiting defects in DNA repair due to SWI/SNF-deficiency. For instance, the importance of SWI/SNF to HR suggests that SWI/SNF-deficient cancers could be specifically treated with PARP inhibitors (PARPi), which efficiently and specifically kill HR-deficient cancer cells and are currently also clinically applied against BRCA1-deficient cancers¹⁰¹. Indeed, it was shown that ARID1A-deficiency sensitizes cancer cells to PARPi both in cultured cells and *in vivo*⁵⁵. A recently published functional HR assay on *ex vivo* fresh tissue samples, RECAP¹⁰², has proven to reliably identify breast cancer tumors with HR-deficiency that are thus sensitive to PARPi treatment. Moreover, with this novel method, the use of PARPi could potentially be extended beyond cancers harboring germline mutations in *BRCA1/2*. Hence, it could be advantageous also to test the HR capacity of SWI/SNF-deficient tumors and to use this assay to predict their sensitivity to PARPi. To increase efficacy, such therapeutic strategies that exploit DDR defects may be combined with other recently discovered therapeutic approaches targeting other SWI/SNF-deficiency-induced susceptibilities. Interestingly, ARID1A-deficient cells are also vulnerable to other forms of treatment, such as small molecule inhibitors of HDAC6, whose upregulation in ARID1A-deficient ovarian cancers inactivates p53 and protects cancer cells from apoptosis¹⁰³. Also, ATR inhibitors selectively kill ARID1A-deficient cancer cells due to defects in TOPII α and cell cycle activity that activate ATR-dependent checkpoint signaling¹⁰⁴. Since SWI/SNF-deficient tumors may be hypersensitive to DNA damage due to defects in DNA repair pathways^{49,85}, it would thus be beneficial to consider combined therapeutic approaches utilizing PARP, ATR or HDAC6 inhibitors and cisplatin in SWI/SNF cancers.

5. Conclusions

Due to its many functions, it is highly plausible that SWI/SNF complexes affect the DDR besides merely facilitating access of repair factors to DNA damage. However, it is currently a challenge to disentangle their precise activities in DDR from their many other cellular functions, including general

maintenance of chromatin architecture. We cannot yet answer with certainty whether different SWI/SNF complexes are specific for different DDR pathways, why certain subunits are more frequently associated with specific tumor tissues than others and whether this is relevant to genome stability or not. Furthermore, loss of SWI/SNF activity can be compensated by, at least in part, other SWI/SNF complexes or redundant mechanisms that take over in the absence of SWI/SNF activity. SWI/SNF-deficient cancer cells likely rely on these “backup” mechanisms, which could allow them to acquire resistance to certain cancer therapies but will also make them specifically vulnerable to newly developed therapies. Mapping of the exact contributions of SWI/SNF in DDR and its functionally redundant backup mechanisms is therefore crucial to understand how SWI/SNF inactivation promotes tumorigenesis and to develop efficient and precise therapies for SWI/SNF cancers.

Conflict of interest

The authors declare that there are no conflicts of interest.

Acknowledgements

We thank Ö.Z. Aydin and A. Helfricht for relevant scientific discussions. We apologize for any literature that could not be cited due to space limitations. This work was supported by a Marie Curie Initial Training Network funded by the European Commission 7th Framework Programme (316390), a European Research Council Advanced Grant (340988-ERC-ID), the Worldwide Cancer Research (15-1274), the Dutch Scientific Organization (ALW 854.11.002) and the Dutch Cancer Society (KWF 10506). This work is part of the OncoCode Institute which is partly financed by the Dutch Cancer Society.

References

1. Jackson, S. P. & Bartek, J. The DNA-damage response in human biology and disease. *Nature* vol. 461 1071–1078 (2009).
2. Hoeijmakers, J. H. J. DNA damage, aging, and cancer. *N. Engl. J. Med.* **361**, 1475–85 (2009).
3. Giglia-Mari, G., Zotter, A. & Vermeulen, W. DNA damage response. *Cold Spring Harb. Perspect. Biol.* **3**, 1–19 (2011).
4. Misteli, T. & Soutoglou, E. The emerging role of nuclear architecture in DNA repair and genome maintenance. *Nat. Rev. Mol. Cell Biol.* **10**, 243–54 (2009).
5. Polo, S. E. & Almouzni, G. Chromatin dynamics after DNA damage: The legacy of the access-repair-restore model. *DNA Repair (Amst)*. **36**, 114–121 (2015).
6. Hauer, M. H. & Gasser, S. M. Chromatin and nucleosome dynamics in DNA damage and repair. *Genes and Development* vol. 31 2204–2221 (2017).
7. Luger, K., Dechassa, M. L. & Tremethick, D. J. New insights into nucleosome and chromatin structure: an ordered state or a disordered affair? *Nat. Rev. Mol. Cell Biol.* **13**, 436–47 (2012).
8. Zhou, C. Y., Johnson, S. L., Gamarra, N. I. & Narlikar, G. J. Mechanisms of ATP-Dependent Chromatin Remodeling Motors. *Annu. Rev. Biophys.* **45**, 153–181 (2016).
9. Luijsterburg, M. S. & Van Attikum, H. Chromatin and the DNA damage response: The cancer connection. *Mol. Oncol.* **5**, 349–367 (2011).
10. Lans, H., Marteiijn, J. A. & Vermeulen, W. ATP-dependent chromatin remodeling in the DNA-damage response. *Epigenetics and Chromatin* **5**, 4 (2012).
11. Aydin, Ö. Z., Vermeulen, W. & Lans, H. ISWI chromatin remodeling complexes in the DNA damage response. *Cell Cycle* vol. 13 3016–3025 (2014).
12. Pierre, R. S. & Kadoch, C. Mammalian SWI/SNF complexes in cancer: emerging therapeutic opportunities. *Current Opinion in Genetics and Development* vol. 42 56–67 (2017).
13. Kadoch, C. *et al.* Proteomic and bioinformatic analysis of mammalian SWI/SNF complexes identifies extensive roles in human malignancy. *Nat. Genet.* **45**, 592–601 (2013).
14. Stern, M., Jensen, R. & Herskowitz, I. Five SWI genes are required for expression of the HO gene in yeast. *J. Mol. Biol.* **178**, 853–868 (1984).
15. Peterson, C. L. & Herskowitz, I. Characterization of the yeast SWI1, SWI2, and SWI3 genes, which encode a global activator of transcription. *Cell* **68**, 573–583 (1992).
16. Neigeborn, L. & Carlson, M. Genes affecting the regulation of SUC2 gene expression by glucose repression in *Saccharomyces cerevisiae*. *Genetics* **108**, 845–858 (1984).
17. Kwon, H., Imbalzano, A. N., Khavari, P. A., Kingston, R. E. & Green, M. R. Nucleosome disruption and enhancement of activator binding by a human SW1/SNF complex. *Nature* **370**, 477–481 (1994).
18. Muchardt, C. & Yaniv, M. ATP-dependent chromatin remodelling: SWI/SNF and Co. are on the job. *J. Mol. Biol.* **293**, 187–198 (1999).
19. Tamkun, J. W. *et al.* brahma: A regulator of *Drosophila* homeotic genes structurally related to the yeast transcriptional activator SNF2 SWI2. *Cell* **68**, 561–572 (1992).
20. Wang, W. *et al.* Purification and biochemical heterogeneity of the mammalian SWI-SNF complex. *EMBO J.* **15**, 5370–82 (1996).
21. Ryme, J., Asp, P., Böhm, S., Cavellán, E. & Farrants, A. K. Ö. Variations in the composition of mammalian SWI/SNF chromatin remodelling complexes. *J. Cell. Biochem.* **108**, 565–576 (2009).

22. Tang, L., Nogales, E. & Ciferri, C. Structure and function of SWI/SNF chromatin remodeling complexes and mechanistic implications for transcription. *Progress in Biophysics and Molecular Biology* vol. 102 122–128 (2010).
23. Szerlong, H. *et al.* The HSA domain binds nuclear actin-related proteins to regulate chromatin-remodeling ATPases. *Nat. Struct. Mol. Biol.* **15**, 469–76 (2008).
24. Haynes, S. R. *et al.* The bromodomain: A conserved sequence found in human, *Drosophila* and yeast proteins. *Nucleic Acids Res.* **20**, 2603 (1992).
25. Phelan, M. L., Sif, S., Narlikar, G. J. & Kingston, R. E. Reconstitution of a core chromatin remodeling complex from SWI/SNF subunits. *Mol. Cell* **3**, 247–253 (1999).
26. Euskirchen, G. M. *et al.* Diverse roles and interactions of the SWI/SNF chromatin remodeling complex revealed using global approaches. *PLoS Genet.* **7**, (2011).
27. Euskirchen, G., Auerbach, R. K. & Snyder, M. SWI/SNF chromatin-remodeling factors: Multiscale analyses and diverse functions. *Journal of Biological Chemistry* vol. 287 30897–30905 (2012).
28. Wilson, B. G. & Roberts, C. W. M. SWI/SNF nucleosome remodellers and cancer. *Nature Reviews Cancer* vol. 11 481–492 (2011).
29. Kadoch, C. & Crabtree, G. R. Mammalian SWI/SNF chromatin remodeling complexes and cancer: Mechanistic insights gained from human genomics. *Sci. Adv.* **1**, e1500447–e1500447 (2015).
30. Hohmann, A. F. & Vakoc, C. R. A rationale to target the SWI/SNF complex for cancer therapy. *Trends in Genetics* vol. 30 356–363 (2014).
31. Hodges, C., Kirkland, J. G. & Crabtree, G. R. The many roles of BAF (mSWI/SNF) and PBAF complexes in cancer. *Cold Spring Harb. Perspect. Med.* **6**, (2016).
32. Ho, L. *et al.* An embryonic stem cell chromatin remodeling complex, esBAF, is an essential component of the core pluripotency transcriptional network. *Proc. Natl. Acad. Sci. U. S. A.* **106**, 5187–91 (2009).
33. De La Serna, I. L., Ohkawa, Y. & Imbalzano, A. N. Chromatin remodelling in mammalian differentiation: Lessons from ATP-dependent remodellers. *Nature Reviews Genetics* vol. 7 461–473 (2006).
34. Cheng, S. W. G. *et al.* c-MYC interacts with INI1/hSNF5 and requires the SWI/SNF complex for transactivation function. *Nat. Genet.* **22**, 102–105 (1999).
35. Stojanova, A. *et al.* MYC interaction with the tumor suppressive SWI/SNF complex member INI1 regulates transcription and cellular transformation. *Cell Cycle* **15**, 1693–1705 (2016).
36. Strober, B. E., Dunaief, J. L., Guha, S. & Goff, S. P. Functional interactions between the hBRM/hBRG1 transcriptional activators and the pRB family of proteins. *Mol. Cell. Biol.* **16**, 1576–1583 (1996).
37. Trouche, D., Le Chalony, C., Muchardt, C., Yaniv, M. & Kouzarides, T. RB and hbrm cooperate to repress the activation functions of E2F1. *Biochemistry* **94**, 11268–11273 (1997).
38. Brownlee, P. M., Meisenberg, C. & Downs, J. A. The SWI/SNF chromatin remodelling complex: Its role in maintaining genome stability and preventing tumourigenesis. *DNA Repair (Amst).* **32**, 127–133 (2015).
39. Savas, S. & Skardasi, G. The SWI/SNF complex subunit genes: Their functions, variations, and links to risk and survival outcomes in human cancers. *Critical Reviews in Oncology/Hematology* vol. 123 114–131 (2018).
40. Masliah-Planchon, J., Bièche, I., Guinebretière, J.-M., Bourdeaut, F. & Delattre, O. SWI/SNF Chromatin Remodeling and Human Malignancies. *Annu. Rev. Pathol. Mech. Dis.* **10**, 145–171

- (2015).
41. Batsché, E., Yaniv, M. & Muchardt, C. The human SWI/SNF subunit Brm is a regulator of alternative splicing. *Nat. Struct. Mol. Biol.* **13**, 22–29 (2006).
 42. Dykhuizen, E. C. *et al.* BAF complexes facilitate decatenation of DNA by topoisomerase II α . *Nature* **497**, 624–7 (2013).
 43. Xue, Y. *et al.* The human SWI/SNF-B chromatin-remodeling complex is related to yeast Rsc and localizes at kinetochores of mitotic chromosomes. *Proc. Natl. Acad. Sci.* **97**, 13015–13020 (2000).
 44. Brownlee, P. M., Chambers, A. L., Cloney, R., Bianchi, A. & Downs, J. A. BAF180 Promotes Cohesion and Prevents Genome Instability and Aneuploidy. *Cell Rep.* **6**, 973–981 (2014).
 45. Bourgo, R. J. *et al.* SWI/SNF Deficiency Results in Aberrant Chromatin Organization, Mitotic Failure, and Diminished Proliferative Capacity. *Mol. Biol. Cell* **20**, 3192–3199 (2009).
 46. Chai, B., Huang, J., Cairns, B. R. & Laurent, B. C. Distinct roles for the RSC and Swi/Snf ATP-dependent chromatin remodelers in DNA double-strand break repair. *Genes Dev.* **19**, 1656–1661 (2005).
 47. Xia, L., Jaafar, L., Cashikar, A. & Flores-Rozas, H. Identification of genes required for protection from doxorubicin by a genome-wide screen in *Saccharomyces cerevisiae*. *Cancer Res.* **67**, 11411–11418 (2007).
 48. Lans, H. *et al.* Involvement of global genome repair, transcription coupled repair, and chromatin remodeling in UV DNA damage response changes during development. *PLoS Genet.* **6**, 41 (2010).
 49. Watanabe, R. *et al.* SWI/SNF factors required for cellular resistance to dna damage include *arid1a* and *arid1b* and show interdependent protein stability. *Cancer Res.* **74**, 2465–2475 (2014).
 50. Park, J.-H. *et al.* Mammalian SWI/SNF complexes facilitate DNA double-strand break repair by promoting γ -H2AX induction. *EMBO J.* **25**, 3986–3997 (2006).
 51. Kothandapani, A., Gopalakrishnan, K., Kahali, B., Reisman, D. & Patrick, S. M. Downregulation of SWI/SNF chromatin remodeling factor subunits modulates cisplatin cytotoxicity. *Exp. Cell Res.* **318**, 1973–1986 (2012).
 52. Ceccaldi, R., Rondinelli, B. & D'Andrea, A. D. Repair Pathway Choices and Consequences at the Double-Strand Break. *Trends in Cell Biology* vol. 26 52–64 (2016).
 53. Jeggo, P. A. & Downs, J. A. Roles of chromatin remodellers in DNA double strand break repair. *Experimental Cell Research* vol. 329 69–77 (2014).
 54. Ogiwara, H. *et al.* Histone acetylation by CBP and p300 at double-strand break sites facilitates SWI/SNF chromatin remodeling and the recruitment of non-homologous end joining factors. *Oncogene* **30**, 2135–2146 (2011).
 55. Shen, J. *et al.* ARID1A Deficiency Impairs the DNA Damage Checkpoint and Sensitizes Cells to PARP Inhibitors. *Cancer Discov.* **5**, 752–67 (2015).
 56. Vélez-Cruz, R. *et al.* RB localizes to DNA double-strand breaks and promotes DNA end resection and homologous recombination through the recruitment of BRG1. *Genes Dev.* **30**, 2500–2512 (2016).
 57. Kwon, S. J. *et al.* ATM-mediated phosphorylation of the chromatin remodeling enzyme BRG1 modulates DNA double-strand break repair. *Oncogene* **34**, 351–361 (2015).
 58. Peng, G. *et al.* BRIT1/MCPH1 links chromatin remodelling to DNA damage response. *Nat. Cell Biol.* **11**, 865–872 (2009).
 59. Lee, H.-S., Park, J.-H., Kim, S.-J., Kwon, S.-J. & Kwon, J. A cooperative activation loop among

- SWI/SNF, γ -H2AX and H3 acetylation for DNA double-strand break repair. *EMBO J.* **29**, 1434–1445 (2010).
60. Ui, A. *et al.* Possible involvement of LKB1-AMPK signaling in non-homologous end joining. *Oncogene* **33**, 1640–1648 (2014).
61. Kakarougkas, A. *et al.* Requirement for PBAF in Transcriptional Repression and Repair at DNA Breaks in Actively Transcribed Regions of Chromatin. *Mol. Cell* **55**, 723–732 (2014).
62. De Castro, R. O. *et al.* The chromatin-remodeling subunit Baf200 promotes homology-directed DNA repair and regulates distinct chromatin-remodeling complexes. *J. Biol. Chem.* **292**, 8459–8471 (2017).
63. Qi, W. *et al.* BRG1 promotes the repair of DNA double-strand breaks by facilitating the replacement of RPA with RAD51. *J. Cell Sci.* **128**, 317–330 (2015).
64. Watanabe, R., Kanno, S., Mohammadi Roushandeh, A., Ui, A. & Yasui, A. Nucleosome remodelling, DNA repair and transcriptional regulation build negative feedback loops in cancer and cellular ageing. *Philos. Trans. R. Soc. B Biol. Sci.* **372**, 20160473 (2017).
65. Schärer, O. D. Nucleotide excision repair in Eukaryotes. *Cold Spring Harb. Perspect. Biol.* **5**, (2013).
66. Marteiijn, J. a, Lans, H., Vermeulen, W. & Hoeijmakers, J. H. J. Understanding nucleotide excision repair and its roles in cancer and ageing. *Nat. Rev. Mol. Cell Biol.* **15**, 465–81 (2014).
67. Reardon, J. T., Vaisman, A., Chaney, S. G. & Sancar, A. Efficient nucleotide excision repair of cisplatin, oxaliplatin, and Bis-aceto-amine-dichloro-cyclohexylamine-platinum(IV) (JM216) platinum intrastrand DNA diadducts. *Cancer Res.* **59**, 3968–3971 (1999).
68. Slyskova, J. *et al.* Base and nucleotide excision repair facilitate resolution of platinum drugs-induced transcription blockage. *Nucleic Acids Res.* **46**, 9537–9549 (2018).
69. Sugasawa, K. Molecular mechanisms of DNA damage recognition for mammalian nucleotide excision repair. *DNA Repair (Amst)*. **44**, 110–117 (2016).
70. Okuda, M., Nakazawa, Y., Guo, C., Ogi, T. & Nishimura, Y. Common TFIIH recruitment mechanism in global genome and transcription-coupled repair subpathways. *Nucleic Acids Res.* **45**, 13043–13055 (2017).
71. Smerdon, M. J. & Lieberman, M. W. Nucleosome rearrangement in human chromatin during UV-induced DNA- repair synthesis. *Proc. Natl. Acad. Sci. U. S. A.* **75**, 4238–41 (1978).
72. Smerdon, M. J. & Conconi, A. Modulation of DNA Damage and DNA Repair in Chromatin. *Prog. Nucleic Acid Res. Mol. Biol.* **62**, 227–255 (1998).
73. Hara, R., Mo, J. & Sancar, A. DNA damage in the nucleosome core is refractory to repair by human excision nuclease. *Mol. Cell. Biol.* **20**, 9173–81 (2000).
74. Araki, M. *et al.* Reconstitution of damage DNA excision reaction from SV40 minichromosomes with purified nucleotide excision repair proteins. *Mutat. Res. - DNA Repair* **459**, 147–160 (2000).
75. Hara, R. & Sancar, A. The SWI / SNF Chromatin-Remodeling Factor Stimulates Repair by Human Excision Nuclease in the Mononucleosome Core Particle The SWI / SNF Chromatin-Remodeling Factor Stimulates Repair by Human Excision Nuclease in the Mononucleosome Core Particle. *Mol. Cell. Biol.* **22**, 6779–6787 (2002).
76. Gaillard, H. *et al.* Chromatin remodeling activities act on UV-damaged nucleosomes and modulate DNA damage accessibility to photolyase. *J. Biol. Chem.* **278**, 17655–17663 (2003).
77. Gong, F., Fahy, D. & Smerdon, M. J. Rad4-Rad23 interaction with SWI/SNF links ATP-dependent chromatin remodeling with nucleotide excision repair. *Nat. Struct. Mol. Biol.* **13**, 902–907 (2006).

78. Zhang, L., Zhang, Q., Jones, K., Patel, M. & Gong, F. The chromatin remodeling factor BRG1 stimulates nucleotide excision repair by facilitating recruitment of XPC to sites of DNA damage. *Cell Cycle* **8**, 3953–3959 (2009).
79. Zhao, Q. *et al.* Modulation of nucleotide excision repair by mammalian SWI/SNF chromatin-remodeling complex. *J. Biol. Chem.* **284**, 30424–30432 (2009).
80. Ray, A. *et al.* Human SNF5/INI1, a component of the human SWI/SNF chromatin remodeling complex, promotes nucleotide excision repair by influencing ATM recruitment and downstream H2AX phosphorylation. *Mol. Cell. Biol.* **29**, 6206–6219 (2009).
81. Gong, F., Fahy, D., Liu, H., Wang, W. & Smerdon, M. J. Role of the mammalian SWI/SNF chromatin remodeling complex in the cellular response to UV damage. *Cell Cycle* **7**, 1067–1074 (2008).
82. Riou, L. *et al.* Differential repair of the two major UV-induced photolesions in trichothiodystrophy fibroblasts. *Cancer Res.* **64**, 889–94 (2004).
83. Smerdon, M. J. DNA repair and the role of chromatin structure. *Curr. Opin. Cell Biol.* **3**, 422–428 (1991).
84. Adar, S., Hu, J., Lieb, J. D. & Sancar, A. Genome-wide kinetics of DNA excision repair in relation to chromatin state and mutagenesis. *Proc. Natl. Acad. Sci.* **113**, E2124–E2133 (2016).
85. Ribeiro-Silva, C. *et al.* DNA damage sensitivity of SWI/SNF-deficient cells depends on TFIID subunit p62/GTF2H1. *Nat. Commun.* **9**, 4067 (2018).
86. Dinant, C. *et al.* Activation of multiple DNA repair pathways by sub-nuclear damage induction methods. *J. Cell Sci.* **120**, 2731–2740 (2007).
87. Giglia-Mari, G. *et al.* A new, tenth subunit of TFIID is responsible for the DNA repair syndrome trichothiodystrophy group A. *Nat. Genet.* **36**, 714–719 (2004).
88. Vermeulen, W. *et al.* Sublimiting concentration of TFIID transcription/DNA repair factor causes TTD-A trichothiodystrophy disorder. *Nat. Genet.* **26**, 307–13 (2000).
89. Luo, J. *et al.* Architecture of the Human and Yeast General Transcription and DNA Repair Factor TFIID. *Mol. Cell* **59**, 794–806 (2015).
90. Essers, J., Vermeulen, W. & Houtsmuller, A. B. DNA damage repair: anytime, anywhere? *Curr. Opin. Cell Biol.* **18**, 240–246 (2006).
91. Klochendler-Yeivin, A., Picarsky, E. & Yaniv, M. Increased DNA damage sensitivity and apoptosis in cells lacking the Snf5/Ini1 subunit of the SWI/SNF chromatin remodeling complex. *Mol. Cell. Biol.* **26**, 2661–74 (2006).
92. McKenna, E. S. *et al.* Loss of the epigenetic tumor suppressor SNF5 leads to cancer without genomic instability. *Mol. Cell. Biol.* **28**, 6223–6233 (2008).
93. Hoffman, G. R. *et al.* Functional epigenetics approach identifies BRM/SMARCA2 as a critical synthetic lethal target in BRG1-deficient cancers. *Proc. Natl. Acad. Sci.* **111**, 3128–3133 (2014).
94. Oike, T. *et al.* A synthetic lethality-based strategy to treat cancers harboring a genetic deficiency in the chromatin remodeling factor BRG1. *Cancer Res.* **73**, 5508–5518 (2013).
95. Strobeck, M. W. *et al.* Compensation of BRG-1 function by Brm. *J. Biol. Chem.* **277**, 4782–4789 (2002).
96. Reisman, D. N. *et al.* Concomitant down-regulation of BRM and BRG1 in human tumor cell lines: differential effects on RB-mediated growth arrest vs CD44 expression. *Oncogene* **21**, 1196–1207 (2002).
97. Helming, K. C. *et al.* ARID1B is a specific vulnerability in ARID1A-mutant cancers. *Nat. Med.* **20**, 251–254 (2014).
98. Raab, J. R., Runge, J. S., Spear, C. C. & Magnuson, T. Co-regulation of transcription by BRG1

- and BRM, two mutually exclusive SWI/SNF ATPase subunits. *Epigenetics and Chromatin* **10**, 62 (2017).
99. Wang, H. *et al.* BRCA1/FANCD2/BRG1-Driven DNA Repair Stabilizes the Differentiation State of Human Mammary Epithelial Cells. *Mol. Cell* **63**, 277–292 (2016).
 100. Hinz, J. M. & Czaja, W. Facilitation of base excision repair by chromatin remodeling. *DNA Repair (Amst)*. **36**, 91–97 (2015).
 101. Lord, C. J. & Ashworth, A. PARP inhibitors: Synthetic lethality in the clinic. *Science (80-.)*. **355**, 1152–1158 (2017).
 102. Meijer, T. G. *et al.* Functional ex vivo assay reveals homologous recombination deficiency in breast cancer beyond BRCA gene defects. *Clin. Cancer Res.* clincanres.0063.2018 (2018) doi:10.1158/1078-0432.CCR-18-0063.
 103. Bitler, B. G. *et al.* ARID1A-mutated ovarian cancers depend on HDAC6 activity. *Nat. Cell Biol.* **19**, 962–973 (2017).
 104. Williamson, C. T. *et al.* ATR inhibitors as a synthetic lethal therapy for tumours deficient in ARID1A. *Nat. Commun.* **7**, (2016).
 105. Arnaud, O., Le Loarer, F. & Tirode, F. BAffling pathologies: Alterations of BAF complexes in cancer. *Cancer Lett.* **419**, 266–279 (2018).
 106. Mashtalir, N. *et al.* Modular Organization and Assembly of SWI/SNF Family Chromatin Remodeling Complexes. *Cell* **175**, 1272–1288.e20 (2018).
 107. Kadoch, C. *et al.* Dynamics of BAF–Polycomb complex opposition on heterochromatin in normal and oncogenic states. *Nat. Genet.* **49**, 213–222 (2016).

Concluding remarks & future directions

6

Functions of ATP-dependent chromatin remodelers in nucleotide excision repair

A competent DNA damage response (DDR) is vital to the maintenance of genome stability and human health, and defects in this response are intimately linked to tumorigenesis and age-related diseases. Chromatin often imposes a barrier to DNA-associated processes, including the repair of DNA. Still, DNA is accurately repaired in the chromatin environment, implying that chromatin provides a dynamic platform for controlled DNA accessibility, which allows timely changes in its structure that are crucial for DNA transactions to occur efficiently. Cooperatively, chromatin modifiers such as chromatin remodelers, histone modifiers and chaperones, change the chromatin landscape and transiently rearrange nucleosomal distribution to facilitate repair of lesions¹⁻⁴. Genetic defects in these chromatin modifiers, in particular in chromatin remodelers, are associated with different clinical disorders, including immunodeficiency, neurodevelopmental problems and cancer.

It seems certain that chromatin changes occur during the UV-induced DDR (UV-DDR), seeing that many different chromatin remodeling proteins and complexes are found to act concertedly at different steps of the repair process² and that changes in histone occupancy and modifications take place at sites of damage⁴⁻⁷. It is widely accepted in the field of DNA repair that chromatin remodelers play an important role in early chromatin rearrangement events that facilitate access of repair proteins to DNA lesions and their consequent removal^{2,4,8,9}. In this thesis, in **Chapters 2**¹⁰ and **4**, we studied how the SWI/SNF and CHD1 chromatin remodeling proteins might contribute to the maintenance of genome stability via their activity in promoting nucleotide excision repair (NER). Although their function in NER has been investigated before¹⁰⁻¹⁴, full understanding of the involvement and activity of these and other chromatin remodelers in the UV-DDR is still lacking. This is not surprising, given that likely most of these chromatin remodelers are not essential for NER but only have an (often redundant) regulatory role in promoting its activity. Also, most chromatin remodeler complexes have multiple cellular functions that can indirectly meddle with DNA repair mechanisms and make it challenging to define their function in repair. Furthermore, ATP-dependent chromatin

remodelers appear to have different functions in each DDR pathway². One of the major questions that is still unanswered, in particular in the field of mammalian NER, is whether each complex performs actual chromatin remodeling near the DNA lesion (before and/or after repair) or whether it can have other, as-of-yet uncharacterized functions.

In **Chapter 2**¹⁰ we provide evidence for a role of SWI/SNF in transcription that indirectly promotes NER. Both ATPase subunits of the SWI/SNF complexes, BRM and BRG1, promote the expression of the essential TFIID subunit GTF2H1, thereby facilitating the stability and functionality of the TFIID complex, both in transcription and in NER. We were unable to find evidence for a direct function of SWI/SNF during the repair of UV-induced DNA damage. However, our proposed transcriptional activity in promoting NER can explain observations described in literature after BRG1 loss that seemed until now incompatible, such as the observed reduced recruitment of XPC, XPA, ERCC1, XPG and PCNA to DNA damage after BRG1 loss which ultimately results in hypersensitivity to UV^{10,12,15–17}. The implications of our findings described in **Chapter 2**¹⁰ are more extensively discussed in **Chapter 5**¹⁸, where multiple emerging functions of SWI/SNF proteins in the DDR are described and discussed, and a link between SWI/SNF-deficiency-induced DDR-vulnerability and precision cancer therapy is explored.

Like SWI/SNF, proteins of the CHD family are well-known regulators of transcription^{19,20} and several proteins of this family have also been linked to the maintenance of genome stability through new roles in different DDR pathways^{21–23}. Curiously, only very recently it was shown that the CHD1 protein functions in the DDR, specifically in an early step of the response to double-strand breaks (DSBs) by facilitating the recruitment of homologous recombination proteins^{24–26}. Even though depletion of this chromatin remodeling protein was found to sensitize cells to helix-distorting DNA crosslinks recognized and repaired by NER²⁷, no role for CHD1 in the UV-DDR had been explored at the time we started our investigation. In **Chapter 4**, we show that the expression of CHD1 is required for optimal cell survival following UV-irradiation. Despite our extensive efforts, it remains unfortunately unclear how CHD1 is recruited to UV-C damage and whether this recruitment is related to a function in

NER, as is suggested by the diminished survival and unscheduled DNA synthesis (UDS) assays after CHD1 knockdown. Possibly, CHD1 recruitment precedes NER or happens independently of NER, while somehow still facilitating lesion excision by NER. During our investigation, a paper was published describing that CHD1 activity facilitates the recruitment of core NER factors via the displacement of XPC¹⁴. Based on our results and despite using similar techniques, we were unable to draw the same conclusions. Given these contradicting results, it would be interesting to investigate in more detail CHD1's function in NER. Possibly, CHD1 is only needed for repair of one type of photolesions, or only in a specific chromatin environment. Therefore, it should be tested whether CHD1 is required for the removal of CPDs or 6-4PPs, using specific antibodies in IF or ELISA procedures²⁸. If CHD1 is found to specifically affect only the repair of one type of photolesion, dedicated photolyases, specific for either CPDs or 6-4PPs, could be used to remove the non-relevant photolesion and to measure if detection and repair of the other photolesion depends on CHD1 activity. Photolyases are proteins that, using a mechanism known as photo-reactivation^{29,30}, can directly and precisely repair either CPDs or 6-4PPs lesions in a very short amount of time (≈ 1 ns)³¹. Their discovery has enabled the successful identification of specific cellular responses to either type of UV lesions in the past^{30,32} and it could also be coupled to the investigation of CHD1 function in NER.

In **Chapters 2** and **4**, we used recovery of RNA synthesis after UV-induced damage as a measure for a function of SWI/SNF and CHD1 proteins in transcription-coupled NER (TC-NER). However, because transcription and not repair itself is measured, this assay is only an indirect indication of DNA repair capacity. Given the transcriptional roles of both these chromatin remodelers, it may be better to confirm a role in TC-NER by measuring DNA repair more directly. A suited assay to directly measure their involvement in TC-NER is the recently modified single-cell unscheduled DNA synthesis (UDS) assay, which has increased sensitivity when compared to a traditional UDS. This amplified UDS method³³, performed in global-genome-NER (GG-NER) deficient cells, allows the quantification of TC-NER activity only. It would be useful to use this improved assay to test whether depletion of CHD1, SWI/SNF or any other chromatin remodeler affects repair by TC-NER and whether it also or only affects transcription restart.

Furthermore, using an unbiased proteomics approach, it should be investigated which proteins interact with CHD1 after UV irradiation. This might help to identify the histones and/or NER proteins that are regulated by CHD1 during the UV-DDR, such that its precise activity can be better understood. One possibility would be to perform stable isotope labeling of amino acids in culture, which our lab has applied successfully in the past to identify UV-dependent interactions within NER³⁴⁻³⁶. However, because our first attempt utilizing this approach did not yield any clear candidates (results not shown) and because chromatin remodelers like CHD1 may rather have transient than strong interactions, a better option could be to use biotin ligase catalyzed proximity labeling³⁷.

Perhaps the most interesting question would be to investigate whether CHD1 facilitates lesion removal by NER by making chromatin more accessible through chromatin remodeling. For other chromatin remodelers implicated in NER, like INO80³⁸, ALC1³⁹ and SMARCA5⁴⁰, this is also still an unanswered question. Specific mutations in CHD1 that inactivate its ATPase activity could be used to determine whether its chromatin remodeling activity is required for its recruitment to damaged DNA and the stimulation of UDS and survival. Besides, an assay should be developed which faithfully measures chromatin remodeling at sites of UV damage. For histone chaperones HIRA and FACT, SNAP-tag technology⁴¹ and quantitative fluorescence imaging techniques⁶ have been used to measure histone dynamics in chromatin after UV. Possibly, these technologies could be applied to study chromatin remodeling by CHD1 as well. Another possibility would be to measure chromatin accessibility in a locus-specific manner, which would be advantageous to determine whether CHD1 is needed in specific chromatin environments. For instance, using the chromatin accessibility by quantitative PCR (CHART-qPCR) assay⁴², chromatin remodeling events could be detected with high sensitivity in specific chromatin environments damaged by UV. The assay is based on the principle that accessible chromatin is more easily digested by nucleases, coupled with analysis of the nuclease- and mock-treated samples for a particular gene by qPCR⁴² (Fig. 1). In this assay, UV-induced chromatin remodeling, to create more accessible chromatin, would show a larger Cq shift between digested and undigested samples. It would be valuable to test the accessibility of different chromatin environments before and

after UV irradiation, in CDH1- proficient or deficient cells. If successfully implemented to observe local UV-induced chromatin changes, this approach could be used to screen for the involvement of other chromatin remodelers as well and scrutinize their potential chromatin remodeling functions in NER.

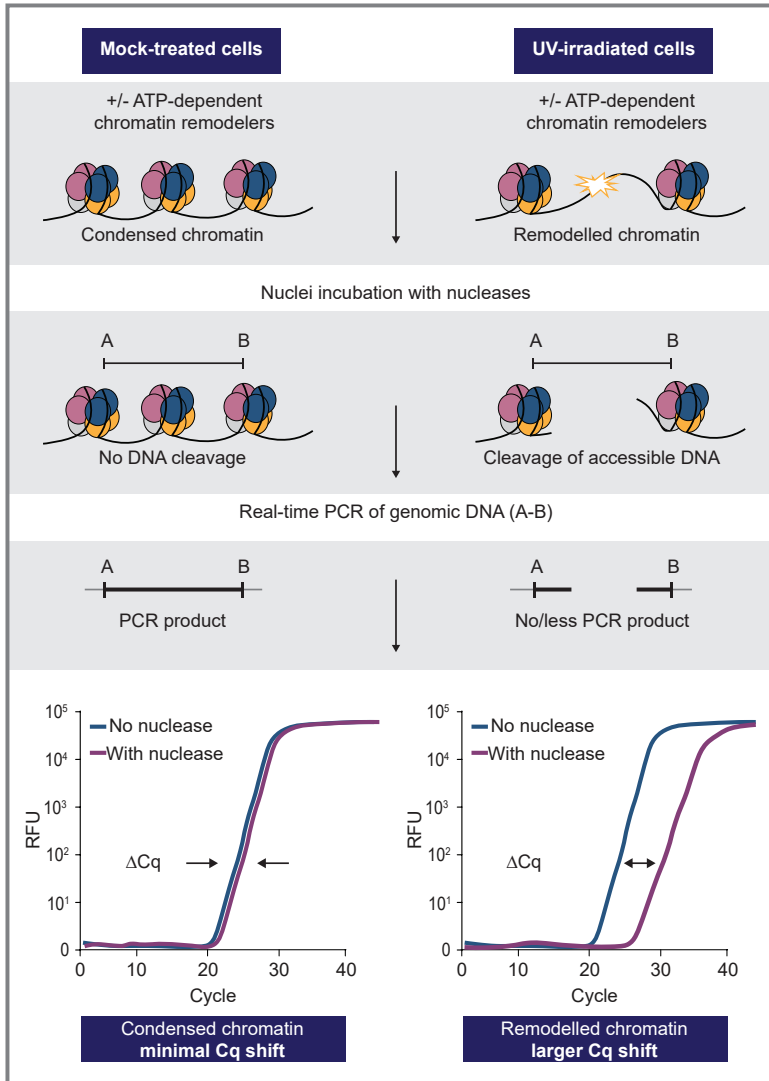


Figure 1. Schematic representation of the CHART-qPCR for the identification of chromatin remodelers with chromatin remodeling function in the UV-DDR. Nuclei extracted from cells either mock- or UV-treated, are incubated with nucleases. If UV-irradiation induces the remodeling of chromatin, DNA will be more accessible to cleavage near the lesion. This increased digestion can be detected by qPCR as an increase in the Cq value. Depletion of chromatin remodelers prior to UV-irradiation will show their participation in this

chromatin rearrangement event(s). The spheres in the top panel represent the nucleosomal core histones. The star depicts the position of the UV-induced DNA damage.

Spatiotemporal control of damage handover in GG-NER

More than 30 repair factors are involved in lesion removal by NER; their assembly into functional repair complexes and subsequent dissociation - once their job is done - must be tightly controlled both in time and space, for proper damage handover, efficient repair and to avoid illegitimate or uncontrolled action of repair enzymes, such as non-scheduled incisions. This dynamic repair complex assembly and disassembly likely involves regulation by post-translation modifications (PTMs) to control localization, interactions, timely function and/or stability of individual repair proteins. Ubiquitylation is one example of a PTM that is particularly important during damage detection in both TC- and GG-NER⁴³. In **Chapter 3**, we studied damage detection by and handover from the DDB2-associated CRL4 ubiquitin-ligase complex (CRL4^{DDB2}). This complex is a key player in the UV-induced ubiquitylation in GG-NER, whose main targets are XPC, the E3 ubiquitin ligase adaptor DDB2 itself and core histones⁴⁴⁻⁴⁷. Interestingly, ubiquitylation of both GG-NER sensors has distinct consequences, as it decreases DDB2's affinity for damaged DNA but increases that of XPC (*in vitro*)^{44,48}. Furthermore, CRL4^{DDB2}-mediated ubiquitylation was shown to promote DDB2 release from damaged chromatin via the recruitment of the segregase VCP, an ATP-driven molecular chaperone that interacts with K48-linked polyubiquitin chains and directs its clients to the proteasomal degradation machinery^{46,49-51}. Yet, it is surprising that only DDB2 - and not XPC as well - is degraded following CRL4^{DDB2}-mediated ubiquitylation⁴⁴. Thus, the same type of PTM can differentially regulate the activity and fate of DNA repair proteins.

PTMs other than ubiquitylation have also been reported to control both DDB2 and XPC activity, including SUMOylation⁵²⁻⁵⁴, phosphorylation⁵⁵ and PARYlation^{39,56-58}. For example, it has been proposed that the poly(ADP-ribose) polymerase 1 (PARP1) collaborates with DDB2 to increase the efficiency of lesion recognition by GG-NER; likely PARP1 directly PARYlates DDB2, thus regulating its binding capacity, interaction with XPC and/or degradation after UV damage^{39,57}. Because PARP1 inhibition was found

to block chromatin remodeling of UV-damaged chromatin⁵⁹, it is also conceivable that PARP1 activity promotes chromatin remodeling³⁹ during damage detection, which might influence the binding of DDB2 and XPC. Therefore, it would be interesting to investigate how these PTMs may be controlling the dynamic damage handover between NER initiation and verification factors. This could be achieved by using specific inhibitors, such as PARP inhibitors, or by identification of the modified residues by mass spectrometry, followed by their mutation.

Although it has been known for a long time that DDB2 is degraded upon DNA damage induction^{44,48,60}, the exact function of this degradation has thus far been unclear. Based on our results described in **Chapter 3**, we propose that a main function of DDB2 degradation is to prevent its excessive rebinding of lesions, which could potentially interfere with assembly of the downstream NER damage verification machinery. However, DDB2 degradation after DNA damage induction may also serve other purposes. Different views on the function of DDB2 degradation can be found in literature. For example, DDB2 degradation was suggested to be necessary for DDB1 release, so that DDB1 is available for its other (many) cellular functions⁶¹. Also, DDB2 was described to function as a molecular switch in the regulation of the cell cycle after DNA damage through the regulation of p21 levels⁶²⁻⁶⁴. Expression of both DDB2 and p21 is induced by p53⁶⁵⁻⁶⁷, yet p21 blocks cell cycle progression and inhibits apoptosis while DDB2 appears to attenuate this barrier by promoting p21 degradation after DNA damage^{62,64}. UV-induced DDB2 degradation has never been coupled to this proposed role in cell fate decision after DNA damage; however, it would be interesting to investigate a potential link between these two. In **Chapter 3**, we show that if lesions are not repaired, the continuous targeting of DDB2 molecules causes a reduction in total cellular DDB2 levels. Thus, DDB2 levels could serve as an indicator of the cell's capacity to repair UV-damage by GG-NER and accordingly favor apoptosis or cell cycle arrest. This hypothesis could be tested by inhibiting UV-induced DDB2 degradation, for instance using the DDB2 mutants described in **Chapter 3**, and testing whether this differentially impacts the cell cycle and/or apoptosis after UV irradiation.

Our hypothesis that DDB2 degradation is needed to facilitate the stable

access of XPC to DNA damage (and, thereafter, downstream NER proteins) appears most plausible as it is supported by multiple independent observations from different labs⁴⁶. For instance, experiments with NER proteins immobilized on chromatin have suggested that DDB2 and TFIIH association with XPC is mutually exclusive⁶⁸. Also, *in silico* modeling based on *in vitro* structures suggests that DDB2 and XPC cannot stably bind the same lesion simultaneously^{69–72}. In addition to the ubiquitylation of DDB2, which reduces its affinity for DNA and recruits VCP, we describe in **Chapter 3** that TFIIH recruitment promotes DDB2 dissociation. This exchange between DDB2 and TFIIH promotes the stable binding of XPC because actual recognition of DNA damage by XPC is likely reciprocally stimulated by its interaction with TFIIH and, in particular, by its damage verification activity. Our results, presented in **Chapter 3**, show that the stable binding of XPC also requires XPA, which stimulates the helicase activity of TFIIH subunit XPD via the dissociation of the CAK sub-complex⁷³. Therefore, in accord with literature, we propose the scenario in which TFIIH first interacts with XPC, via its XPB subunit, after which the blocking of XPD helicase activity by a lesion allows the TFIIH subunit GTF2H1 to interact with XPC⁷¹. This damage verification further stabilizes the XPC-TFIIH-DNA complex. It would be interesting to confirm this by investigating DDB2 and XPC recruitment and binding to DNA damage in cells with specific XPD helicase mutations that block the damage verification but leave XPB-mediated TFIIH recruitment still intact. With the advance of CRISPR/Cas9-based gene-editing technologies, it will be possible to introduce such mutations in cell lines expressing fluorescent XPC, DDB2, and XPB and investigate this using similar imaging technologies as described in **Chapter 3**.

DDB2 dissociation from DNA, to make room for downstream NER factors, is as essential as its association to DNA damage, because defects in both lead to similar impairment in XPC recruitment. Interestingly, in a similar manner, the dissociation of XPC from the damage verification complex, promoted by the RNF111-mediated ubiquitylation of XPC, is required for the loading of the downstream endonuclease XPG⁵³. These observations strongly indicate that the spatiotemporal organization of the repair reaction is regulated by a dynamic and intricate interplay between the comings and goings of different repair factors. Based on this, we believe

that cooperation and competition between NER factors and PTMs are inherent to the efficient step-by-step damage handover (and, ultimately, damage excision). Therefore, future research should focus on this interplay by determining whether similar cooperation/competition interactions exist between other NER factors. To this end, a multidisciplinary approach would be most advantageous, combining results from cell imaging experiments, as described in this thesis, with structural data from new emerging technologies such as crosslinking mass spectrometry and cryo-electron microscopy.

References

1. Smeenk, G. & van Attikum, H. The chromatin response to DNA breaks: leaving a mark on genome integrity. *Annu. Rev. Biochem.* **82**, 55–80 (2013).
2. Lans, H., Marteijn, J. A. & Vermeulen, W. ATP-dependent chromatin remodeling in the DNA-damage response. *Epigenetics and Chromatin* **5**, 4 (2012).
3. Adam, S., Dabin, J. & Polo, S. E. Chromatin plasticity in response to DNA damage : The shape of things to come. *DNA Repair (Amst)*. **32**, 120–126 (2015).
4. Polo, S. E. & Almouzni, G. Chromatin dynamics after DNA damage: The legacy of the access-repair-restore model. *DNA Repair (Amst)*. **36**, 114–121 (2015).
5. Adam, S., Polo, S. & Almouzni, G. Transcription recovery after DNA damage requires chromatin priming by the H3. 3 histone chaperone HIRA. *Cell* **155**, 94–106 (2013).
6. Dinant, C. *et al.* Enhanced chromatin dynamics by fact promotes transcriptional restart after UV-induced DNA damage. *Mol. Cell* **51**, 469–479 (2013).
7. Yu, S., Teng, Y., Waters, R. & Reed, S. H. How chromatin is remodelled during DNA repair of UV-Induced DNA damage in *saccharomyces cerevisiae*. *PLoS Genet.* **7**, (2011).
8. Nag, R. & Smerdon, M. J. Altering the chromatin landscape for nucleotide excision repair. *Mutat. Res. - Rev. Mutat. Res.* **682**, 13–20 (2009).
9. Gong, F., Kwon, Y. & Smerdon, M. J. Nucleotide excision repair in chromatin and the right of entry. *DNA Repair* **4**, 884–896 (2005).
10. Ribeiro-Silva, C. *et al.* DNA damage sensitivity of SWI/SNF-deficient cells depends on TFIID subunit p62/GTF2H1. *Nat. Commun.* **9**, 4067 (2018).
11. Zhang, L., Zhang, Q., Jones, K., Patel, M. & Gong, F. The chromatin remodeling factor BRG1 stimulates nucleotide excision repair by facilitating recruitment of XPC to sites of DNA damage. *Cell Cycle* **8**, 3953–3959 (2009).
12. Zhao, Q. *et al.* Modulation of nucleotide excision repair by mammalian SWI/SNF chromatin-remodeling complex. *J. Biol. Chem.* **284**, 30424–30432 (2009).
13. Ray, A. *et al.* Human SNF5/INI1, a component of the human SWI/SNF chromatin remodeling complex, promotes nucleotide excision repair by influencing ATM recruitment and downstream H2AX phosphorylation. *Mol. Cell. Biol.* **29**, 6206–6219 (2009).
14. Rütthemann, P. *et al.* Chromatin remodeler CHD1 promotes XPC-to-TFIID handover of nucleosomal UV lesions in nucleotide excision repair. *EMBO J.* **36**, 3372–3386 (2017).
15. Watanabe, R., Kanno, S., Mohammadi Roushandeh, A., Ui, A. & Yasui, A. Nucleosome remodelling, DNA repair and transcriptional regulation build negative feedback loops in cancer and cellular ageing. *Philos. Trans. R. Soc. B Biol. Sci.* **372**, 20160473 (2017).
16. Kothandapani, A., Gopalakrishnan, K., Kahali, B., Reisman, D. & Patrick, S. M. Downregulation of SWI/SNF chromatin remodeling factor subunits modulates cisplatin cytotoxicity. *Exp. Cell Res.* **318**, 1973–1986 (2012).
17. Gong, F., Fahy, D., Liu, H., Wang, W. & Smerdon, M. J. Role of the mammalian SWI/SNF chromatin remodeling complex in the cellular response to UV damage. *Cell Cycle* **7**, 1067–1074 (2008).
18. Ribeiro-Silva, C., Vermeulen, W. & Lans, H. SWI/SNF: Complex complexes in genome stability and cancer. *DNA Repair (Amst)*. **77**, 87–95 (2019).
19. Marfella, C. G. A. & Imbalzano, A. N. The Chd family of chromatin remodelers. *Mutat. Res. - Fundam. Mol. Mech. Mutagen.* **618**, 30–40 (2007).
20. Murawska, M. & Brehm, A. CHD chromatin remodelers and the transcription cycle.

- Transcription* **2**, 244–253 (2011).
21. Stanley, F. K. T., Moore, S. & Goodarzi, A. A. CHD chromatin remodelling enzymes and the DNA damage response. *Mutation Research - Fundamental and Molecular Mechanisms of Mutagenesis* **750**, 31–44 (2013).
 22. Rother, M. B. & van Attikum, H. DNA repair goes hip-hop: SMARCA and CHD chromatin remodellers join the break dance. *Philosophical Transactions of the Royal Society B: Biological Sciences* **372**, (2017).
 23. Mills, A. A. The chromodomain helicase DNA-binding chromatin remodelers: Family traits that protect from and promote cancer. *Cold Spring Harb. Perspect. Med.* **7**, (2017).
 24. Kari, V. *et al.* Loss of CHD1 causes DNA repair defects and enhances prostate cancer therapeutic responsiveness. *EMBO Rep.* **17**, 1609–1623 (2016).
 25. Shenoy, T. R. *et al.* CHD1 loss sensitizes prostate cancer to DNA damaging therapy by promoting error-prone double-strand break repair. *Ann. Oncol. Off. J. Eur. Soc. Med. Oncol.* **28**, 1495–1507 (2017).
 26. Zhou, J. *et al.* Human CHD1 is required for early DNA-damage signaling and is uniquely regulated by its N terminus. *Nucleic Acids Res.* **46**, 3891–3905 (2018).
 27. Reardon, J. T., Vaisman, A., Chaney, S. G. & Sancar, A. Efficient nucleotide excision repair of cisplatin, oxaliplatin, and Bis-aceto-amine-dichloro-cyclohexylamine-platinum(IV) (JM216) platinum intrastrand DNA diadducts. *Cancer Res.* **59**, 3968–3971 (1999).
 28. Kobayashi, N. *et al.* Quantitation and visualization of ultraviolet-induced dna damage using specific antibodies: Application to pigment cell biology. *Pigment Cell Research* **14**, 94–102 (2001).
 29. Steurer, B. *et al.* Fluorescently-labelled CPD and 6-4PP photolyases: new tools for live-cell DNA damage quantification and laser-assisted repair. *Nucleic Acids Res.* **47**, 3536–3549 (2019).
 30. Eker, A. P. M., Quayle, C., Chaves, I. & Van Der Horst, G. T. J. Direct DNA damage reversal: Elegant solutions for nasty problems. *Cell. Mol. Life Sci.* **66**, 968–980 (2009).
 31. Sancar, A. Structure and Function of Photolyase and in Vivo Enzymology: 50th Anniversary. *J. Biol. Chem.* **283**, 32153–32157 (2008).
 32. Sancar, G. B. Enzymatic photoreactivation: 50 Years and counting. *Mutat. Res. - Fundam. Mol. Mech. Mutagen.* **451**, 25–37 (2000).
 33. Wienholz, F., Vermeulen, W. & Marteijn, J. A. Amplification of unscheduled DNA synthesis signal enables fluorescence-based single cell quantification of transcription-coupled nucleotide excision repair. *Nucleic Acids Res.* **45**, (2017).
 34. Schwertman, P. *et al.* UV-sensitive syndrome protein UVSSA recruits USP7 to regulate transcription-coupled repair. *Nat. Genet.* **44**, 598–602 (2012).
 35. Sabatella, M., Pines, A., Slysikova, J., Vermeulen, W. & Lans, H. ERCC1-XPF targeting to psoralen–DNA crosslinks depends on XPA and FANCD2. *Cell. Mol. Life Sci.* (2019). doi:10.1007/s00018-019-03264-5
 36. Pines, A. *et al.* TRiC controls transcription resumption after UV damage by regulating Cockayne syndrome protein A. *Nat. Commun.* **9**, (2018).
 37. Branon, T. C. *et al.* Efficient proximity labeling in living cells and organisms with TurboID. *Nature Biotechnology* **36**, 880–898 (2018).
 38. Jiang, Y. *et al.* INO80 chromatin remodeling complex promotes the removal of UV lesions by the nucleotide excision repair pathway. *Proc. Natl. Acad. Sci.* **107**, 17274–17279 (2010).
 39. Pines, A. *et al.* PARP1 promotes nucleotide excision repair through DDB2 stabilization and

- recruitment of ALC1. *J. Cell Biol.* **199**, 235–249 (2012).
40. Aydin, Ö. Z. *et al.* Human ISWI complexes are targeted by SMARCA5 ATPase and SLIDE domains to help resolve lesion-stalled transcription. *Nucleic Acids Res.* **42**, 8473–8485 (2014).
 41. Adam, S. *et al.* Real-Time Tracking of Parental Histones Reveals Their Contribution to Chromatin Integrity Following DNA Damage. *Mol. Cell* **64**, 65–78 (2016).
 42. Rao, S., Procko, E. & Shannon, M. F. Chromatin Remodeling, Measured by a Novel Real-Time Polymerase Chain Reaction Assay, Across the Proximal Promoter Region of the IL-2 Gene. *J. Immunol.* **167**, 4494–4503 (2001).
 43. Lans, H., Hoeijmakers, J. H. J., Vermeulen, W. & Marteijn, J. A. The DNA damage response to transcription stress. *Nat. Rev. Mol. Cell Biol.* (2019).
 44. Sugawara, K. *et al.* UV-induced ubiquitylation of XPC protein mediated by UV-DDB-ubiquitin ligase complex. *Cell* **121**, 387–400 (2005).
 45. Groisman, R. *et al.* The ubiquitin ligase activity in the DDB2 and CSA complexes is differentially regulated by the COP9 signalosome in response to DNA damage. *Cell* **113**, 357–367 (2003).
 46. El-Mahd, M. A. *et al.* Cullin 4A-mediated proteolysis of DDB2 protein at DNA damage sites regulates in vivo lesion recognition by XPC. *J. Biol. Chem.* **281**, 13404–13411 (2006).
 47. Kapetanaki, M. G. *et al.* The DDB1-CUL4ADDB2 ubiquitin ligase is deficient in xeroderma pigmentosum group E and targets histone H2A at UV-damaged DNA sites. *Proc. Natl. Acad. Sci. U. S. A.* **103**, 2588–2593 (2006).
 48. Rapić-Otrin, V., McLenigan, M. P., Bisi, D. C., Gonzalez, M. & Levine, A. S. Sequential binding of UV DNA damage binding factor and degradation of the p48 subunit as early events after UV irradiation. *Nucleic Acids Res.* **30**, 2588–2598 (2002).
 49. Dantuma, N. P., Acs, K. & Luijsterburg, M. S. Should I stay or should I go: VCP/p97-mediated chromatin extraction in the DNA damage response. *Experimental Cell Research* **329**, 9–17 (2014).
 50. Puumalainen, M. R., Rütthemann, P., Min, J. H. & Naegeli, H. Xeroderma pigmentosum group C sensor: Unprecedented recognition strategy and tight spatiotemporal regulation. *Cell. Mol. Life Sci.* **73**, 547–566 (2016).
 51. Magnaghi, P. *et al.* Covalent and allosteric inhibitors of the ATPase VCP/p97 induce cancer cell death. *Nat. Chem. Biol.* **9**, 548–559 (2013).
 52. Akita, M. *et al.* SUMOylation of xeroderma pigmentosum group C protein regulates DNA damage recognition during nucleotide excision repair. *Sci. Rep.* **5**, 10984 (2015).
 53. van Cuijk, L. *et al.* SUMO and ubiquitin-dependent XPC exchange drives nucleotide excision repair. *Nat. Commun.* **6**, 7499 (2015).
 54. Poulsen, S. L. *et al.* RNF111/Arkadia is a SUMO-targeted ubiquitin ligase that facilitates the DNA damage response. *J. Cell Biol.* **201**, 787–807 (2013).
 55. Shah, P., Zhao, B., Qiang, L. & He, Y. Y. Phosphorylation of xeroderma pigmentosum group C regulates ultraviolet-induced DNA damage repair. *Nucleic Acids Res.* **46**, 5050–5060 (2018).
 56. Robu, M. *et al.* Poly(ADP-ribose) polymerase 1 escorts XPC to UV-induced DNA lesions during nucleotide excision repair. *Proc. Natl. Acad. Sci.* **114**, E6847–E6856 (2017).
 57. Robu, M. *et al.* Role of poly (ADP-ribose) polymerase-1 in the removal of UV-induced DNA lesions by nucleotide excision repair. *Proc. Natl. Acad. Sci. U. S. A.* **110**, 1–6 (2013).
 58. Maltseva, E. A., Rechkunova, N. I., Sukhanova, M. V. & Lavrik, O. I. Poly(ADP-ribose) polymerase 1 modulates interaction of the nucleotide excision repair factor XPC-RAD23B with DNA via Poly(ADP-ribosylation). *J. Biol. Chem.* **290**, 21811–21820 (2015).
 59. Luijsterburg, M. S. *et al.* DDB2 promotes chromatin decondensation at UV-induced DNA

- damage. *J. Cell Biol.* **197**, 267–281 (2012).
60. Nag, A., Bondar, T., Shiv, S. & Raychaudhuri, P. The xeroderma pigmentosum group E gene product DDB2 is a specific target of cullin 4A in mammalian cells. *Mol. Cell. Biol.* **21**, 6738–47 (2001).
 61. Alekseev, S. *et al.* Cellular concentrations of DDB2 regulate dynamic binding of DDB1 at UV-induced DNA damage. *Mol. Cell. Biol.* **28**, 7402–7413 (2008).
 62. Stoyanova, T., Roy, N., Kopanja, D., Bagchi, S. & Raychaudhuri, P. DDB2 decides cell fate following DNA damage. *Proc. Natl. Acad. Sci. U. S. A.* **106**, 10690–5 (2009).
 63. Stoyanova, T., Yoon, T., Kopanja, D., Mokyry, M. B. & Raychaudhuri, P. The Xeroderma Pigmentosum Group E Gene Product DDB2 Activates Nucleotide Excision Repair by Regulating the Level of p21Waf1/Cip1. *Mol. Cell. Biol.* **28**, 177–187 (2008).
 64. Li, H., Zhang, X. P. & Liu, F. Coordination between p21 and DDB2 in the cellular response to UV radiation. *PLoS One* **8**, (2013).
 65. Hwang, B. J., Ford, J. M., Hanawalt, P. C. & Chu, G. Expression of the p48 xeroderma pigmentosum gene is p53-dependent and is involved in global genomic repair. *Proc. Natl. Acad. Sci. U. S. A.* **96**, 424–8 (1999).
 66. El-Deiry, W. S. *et al.* WAF1, a potential mediator of p53 tumor suppression. *Cell* **75**, 817–825 (1993).
 67. Tan, T. & Chu, G. p53 Binds and Activates the Xeroderma Pigmentosum DDB2 Gene in Humans but Not Mice. *Mol. Cell. Biol.* **22**, 3247–3254 (2002).
 68. Ziani, S. *et al.* Sequential and ordered assembly of a large DNA repair complex on undamaged chromatin. *J. Cell Biol.* **206**, 589–598 (2014).
 69. Scrima, A. *et al.* Structural Basis of UV DNA-Damage Recognition by the DDB1-DDB2 Complex. *Cell* **135**, 1213–1223 (2008).
 70. Paul, D. *et al.* Structure and mechanism of pyrimidine–pyrimidone (6-4) photoproduct recognition by the Rad4/XPC nucleotide excision repair complex. *Nucleic Acids Res.* **47**, 6015–6028 (2019).
 71. Mu, H., Geacintov, N. E., Broyde, S., Yeo, J. E. & Schärer, O. D. Molecular basis for damage recognition and verification by XPC-RAD23B and TFIIH in nucleotide excision repair. *DNA Repair* **71**, 33–42 (2018).
 72. Min, J. H. & Pavletich, N. P. Recognition of DNA damage by the Rad4 nucleotide excision repair protein. *Nature* **449**, 570–575 (2007).
 73. Coin, F. *et al.* Nucleotide Excision Repair Driven by the Dissociation of CAK from TFIIH. *Mol. Cell* **31**, 9–20 (2008).

Appendix



Summary

DNA, the carrier of genetic information, is vulnerable to chemical changes induced by endogenous and exogenous DNA damaging agents that compromise its integrity and functionality. Daily, each of our cells is confronted with over ten thousand new DNA lesions with immediate and long-term effects, if left unrepaired. In particular, DNA damage greatly contributes to genome instability by interfering with essential genome processes, such as replication and transcription. This can also result in mutations that alter our genetic information and favor tumorigenesis. Accumulation of DNA damage and their consequent disturbance of vital genome processes are also important contributors to aging. It is thus crucial to safeguard DNA's integrity by swiftly repairing damaged DNA at any genomic location and time.

Cells are equipped with a DNA damage response (DDR), which comprises several signaling pathways and specialized DNA repair mechanisms, to avoid the fallouts of DNA injuries. An overview of the different DNA repair mechanisms is presented in **Chapter 1**, with a focus on nucleotide excision repair (NER) - which is the main topic of this thesis. Additionally, the role of chromatin and chromatin-modifying enzymes as integral players in the UV-induced DDR is described. NER is an essential DNA damage repair mechanism that removes a wide variety of helix-distorting DNA lesions, including UV-light and platinum drug-induced lesions. NER thereby protects healthy cells against cancer and aging, but unfortunately also cancer cells against chemotherapy.

SWI/SNF chromatin remodelers, which are frequently found mutated in cancer, have been implicated in transcription and multiple DDR pathways, including NER. In particular, chromatin remodeling via the SWI/SNF ATPase BRG1 is hypothesized to stimulate NER, but the precise involvement of BRG1 and its less scrutinized cognate ATPase BRM in DDR remains unclear. In **Chapter 2**, we describe how SWI/SNF-promotes NER by regulating the transcription of GTF2H1, a subunit of the basal transcription and NER factor TFIIH, which is necessary for the stable assembly of functional TFIIH complexes. Intriguingly, we observed that cancer cells and fibroblasts with permanent loss or inactivation of BRM or BRG1 can adapt to restore

normal GTF2H1 expression (in a SWI/SNF-independent manner). The DNA damage sensitivity of SWI/SNF-deficient cells therefore correlates with GTF2H1 expression, i.e., only cells that retain low GTF2H1 are hypersensitive to DNA damaging agents. This finding exposes a vulnerability of SWI/SNF-mutated cancers which could be specifically targeted to increase chemotherapy effectiveness.

In **Chapter 3**, we investigated the mechanism of damage handover between NER factors during global genome NER (GG-NER). GG-NER is initiated by the DNA damage sensor XPC, which upon lesion detection recruits the TFIIH complex to verify the presence of the lesion. A second DNA damage sensor, DDB2, is required for XPC to efficiently detect and bind to highly cytotoxic UV-induced photolesions that only minimally distort the DNA helix. We show that the recruitment, stable binding and dissociation of DDB2, XPC and TFIIH is tightly coordinated for proper damage handover. Although DDB2 lesion binding assists XPC recruitment, its timely dissociation – not its UV-induced degradation –, is required for DNA damage handover to XPC and coincides with the arrival of the TFIIH complex and the formation of a stable XPC-TFIIH complex. At least three main events contribute to the timely dissociation of DDB2: 1) its ubiquitylation (by the CRL4^{DDB2} E3 ubiquitin ligase complex) upon binding to DNA damage; 2) active extraction from damaged DNA by the ubiquitin-dependent VCP/p97 segregase; and 3) the recruitment of TFIIH, which intriguingly appears to exchange with DDB2. Furthermore, DDB2 homeostasis is regulated by its proteasomal degradation upon ubiquitin-mediated dissociation, which lowers effective DDB2 concentrations, preventing the continuous DDB2 rebinding to lesions, which interferes with stable XPC and TFIIH binding. Finally, we found that XPC stable association with DNA damage is reciprocally stimulated by its interaction with and damage verification by TFIIH. Our study demonstrates that reciprocal and ubiquitin-controlled coordination between damage recognition and verification factors (i.e., their competitive and cooperative binding to DNA lesions) provides precise spatiotemporal control of damage handover in GG-NER.

It is widely accepted in the field of DNA repair that chromatin remodelers play an important role in early chromatin rearrangement events that

facilitate access of repair proteins to DNA lesions and their consequent removal. CHD1 is an ATP-dependent chromatin remodeling protein recently implicated in the repair of double-strand breaks. Interestingly, loss of this chromatin remodeler also sensitizes cells to a range of DNA damaging agents that induce helix-distorting DNA crosslinks mainly processed by NER. Thus, in **Chapter 4**, we sought to explore a putative role of CHD1 in NER. We found that CHD1 activity promotes resistance to UV-induced DNA damage likely by facilitating the loading of the NER-specific endonucleases onto damaged DNA. Because we did not find any defect in the recruitment of DNA damage detection and lesion verification proteins to UV-damaged DNA, we hypothesize that CHD1 promotes progression from lesion verification to excision. Intriguingly, CHD1 recruitment to UV-induced damage appears to be independent of NER and we were unable to identify how CHD1 promotes NER. Nonetheless, given the high mutation frequency of CHD1 in prostate cancer, it is important to channel further efforts into understanding the role of CHD1 in the DDR. Such efforts may be valuable for the detection of DDR vulnerabilities caused by CHD1 deficiency that can be exploited for therapeutic approaches.

In **Chapter 5**, we offer a broad overview of the emerging roles of the SWI/SNF chromatin remodeling complexes in response to DNA damage. Here we also discuss how the interplay between defects in chromatin remodelers and DDR contribute to tumorigenesis. Additionally, we reflected on SWI/SNF's tumor suppressor functions, their deficiency in cancer and, perhaps most excitingly, the potential exploitation of DDR-related vulnerabilities that arise from SWI/SNF dysfunction for precision medicine.

Finally, in **Chapter 6**, the main data and results of Chapters 2, 3 and 4 are summarized and discussed, accompanied by contemplations of future research endeavors to gain more insight in the function and fine-tuning of GG-NER, as well as to dissect CHD1's molecular function in NER.

Samenvatting

DNA, de drager van genetische informatie, is vatbaar voor chemische veranderingen die door endogene en exogene DNA-beschadigende stoffen worden veroorzaakt en die de integriteit en de functionaliteit van DNA aantasten. Dagelijks worden al onze cellen geconfronteerd met meer dan tienduizend nieuwe DNA-beschadigingen die, als ze niet worden gerepareerd, zowel directe als meer langdurige consequenties hebben. DNA-schade veroorzaakt vooral genominstabiliteit doordat het essentiële genoomprocessen zoals replicatie en transcriptie verstoort. Hierdoor leidt DNA-schade tot het ontstaan van mutaties, die de genetische informatie veranderen, waardoor tumoren kunnen ontstaan. Ophoping van DNA-schade en langdurige verstoring van genoomprocessen dragen ook in belangrijke mate bij aan het proces van veroudering. Daarom is het erg belangrijk dat de integriteit van DNA continu wordt beschermd door beschadigd DNA snel te repareren, ongeacht de genomische locatie.

De DNA-schade respons (in het Engels: DNA damage response; DDR) is een belangrijk mechanisme in cellen om de negatieve effecten van DNA-schade te voorkomen en bestaat uit verschillende signaaltransductiepaden en gespecialiseerde DNA-reparatiemechanismen. In **hoofdstuk 1** wordt een overzicht van de verschillende DNA-reparatiemechanismen gepresenteerd, met een focus op nucleotide excisie reparatie (NER) - het hoofdonderwerp van dit proefschrift -, en wordt de rol van chromatine en chromatine-modificerende enzymen als integrale spelers in de UV-geïnduceerde DDR besproken. NER is een essentieel DNA-reparatiemechanisme en kan een scala van verschillende soorten helix-verstorende DNA-schade verwijderen, inclusief het type schade dat door UV-licht en door platina-bevattende medicijnen wordt veroorzaakt. Op deze manier beschermt NER gezonde cellen tegen kanker en veroudering, maar helaas ook kankercellen tegen chemotherapie.

SWI/SNF-chromatine-reorganisatiefactoren, die vaak gemuteerd zijn in kanker, zijn betrokken bij transcriptie en meerdere DDR-mechanismen, waaronder NER. Zo wordt gedacht dat de chromatine-reorganisatie SWI/SNF-ATPase BRG1 NER stimuleert, maar de precieze functie van BRG1 en van zijn minder goed onderzochte verwante ATPase BRM in de DDR blijft

onduidelijk. In **hoofdstuk 2** beschrijven we hoe SWI/SNF NER bevordert door de transcriptie van GTF2H1 te reguleren. Het GTF2H1 eiwit is onderdeel van de basale transcriptie- en NER-factor TFIIH en nodig voor de stabiele opbouw van functionele TFIIH-complexen. Tot onze verbazing vonden we dat kankercellen en fibroblasten met permanente inactivering of verlies van BRM of BRG1 zich kunnen aanpassen en de normale GTF2H1-expressie kunnen herstellen (op een SWI/SNF-onafhankelijke manier). Om die reden correleert de DNA-schadegevoeligheid van SWI/SNF-deficiënte cellen met het expressie niveau van GTF2H1; alleen cellen die een lage GTF2H1-expressie behouden, zijn overgevoelig voor DNA-schade-inducerende agentia. Deze bevinding onthult een kwetsbaarheid van SWI/SNF-gemuteerde kankers, die specifiek zou kunnen worden uitgebuit om de effectiviteit van chemotherapie te verhogen.

In **hoofdstuk 3** onderzochten we DNA-schadeoverdracht tussen NER-factoren tijdens globaal-genoom NER (GG-NER). GG-NER wordt geïnitieerd door de DNA-schadesensor XPC, die na detectie het TFIIH-complex rekruteert om de aanwezigheid van schade te verifiëren. Een tweede DNA-schadesensor, DDB2, is nodig om XPC op efficiënte manier cytotoxische UV-geïnduceerde typen DNA-schade te laten detecteren en binden, omdat deze typen DNA-schade de DNA-helix maar minimaal destabiliseren. We laten zien dat de rekrutering, stabiele binding en dissociatie van DDB2, XPC en TFIIH nauwkeurig worden gecoördineerd voor een optimale DNA-schadeoverdracht. Hoewel binding van DNA-schade door DDB2 XPC-rekrutering bevordert, is ook een tijdige dissociatie (maar niet de UV-geïnduceerde afbraak) nodig voor de overdracht van DNA-schade aan XPC en valt deze samen met de rekrutering van het TFIIH-complex en de vorming van een stabiel XPC-TFIIH-complex. Ten minste drie processen dragen bij aan de tijdige dissociatie van DDB2: 1) de ubiquitylatie van DDB2 (door het CRL4^{DDB2} E3 ubiquitine ligase complex) bij binding aan DNA-schade; 2) actieve extractie uit beschadigd DNA door de ubiquitine-afhankelijke VCP/p97 segregase; en 3) de rekrutering van het TFIIH-complex, dat lijkt uit te wisselen met DDB2. Verder wordt de DDB2-homeostase gereguleerd door proteasomale afbraak na de ubiquitine-gemedieerde dissociatie, waardoor de effectieve DDB2 concentratie wordt verlaagd. Hierdoor wordt het continu opnieuw binden van DDB2 aan DNA-schade voorkomen, dat mogelijk de stabiele binding

van XPC en TFIIH verstoort. Ten slotte hebben we gevonden dat stabiele binding van XPC aan DNA-schade wederzijds wordt gestimuleerd door interactie met en schade-verificatie door TFIIH. Onze studie toont het bestaan aan van een nauwkeurige ruimtelijke en tijdelijke coördinatie van schadeoverdracht tijdens GG-NER door de wederzijdse en door ubiquitine gecontroleerde coördinatie tussen schadedetectie- en -verificatiefactoren (d.w.z. door hun competitieve en coöperatieve binding aan DNA-schade).

In het DNA-reparatieveld wordt algemeen aangenomen dat chromatine-reorganisatiefactoren belangrijk zijn om al vroeg in het reparatieproces de toegang van reparatie-eiwitten tot DNA-schade te reguleren, om op die manier de verwijdering van DNA-schade te vergemakkelijken. CHD1 is een ATP-afhankelijke chromatine-reorganisatie-eiwit waarvan onlangs is gevonden dat het betrokken is bij de reparatie van dubbelstrengs DNA-breuken. Cellen zonder dit chromatine-reorganisatie-eiwit zijn echter ook gevoelig voor agentia die helix-destabiliserende DNA-crosslinks veroorzaken, die voornamelijk door NER worden gerepareerd. Daarom hebben we in **hoofdstuk 4** gezocht naar een mogelijke rol van CHD1 in NER. We vonden dat CHD1 beschermend werkt tegen door UV-geïnduceerde typen DNA-schade, waarschijnlijk doordat CHD1 helpt bij de rekrutering van NER-specifieke endonucleasen op beschadigd DNA. Omdat we geen enkel defect vonden in de rekrutering van DNA-schade-, en verificatie-eiwitten naar UV-beschadigd DNA, denken we dat CHD1 specifiek de voortgang van DNA-schade verificatie naar DNA-schade-verwijdering tijdens NER stimuleert. CHD1-rekrutering naar UV-geïnduceerde DNA-schade is echter onafhankelijk van NER en we konden ook niet vaststellen hoe CHD1 precies NER bevordert. Gezien de hoge mutatiefrequentie van CHD1 in prostaatkanker is het echter belangrijk om de rol van CHD1 in de DDR beter te begrijpen. Dit kan waardevol zijn voor het opsporen van DDR-gerelateerde zwakheden veroorzaakt door CHD1-deficiëntie die kunnen worden gebruikt voor therapeutische doeleinden.

In **hoofdstuk 5** geven we een algemeen overzicht van de recentelijk gevonden functies van SWI/SNF-chromatine-reorganisatiefactoren in de respons tegen DNA-schade. We beschrijven hoe defecten in chromatine-reorganisatiefactoren en in de DDR samen kunnen bijdragen aan het ontstaan van tumoren. Verder beschouwen we de tumorsuppressorfuncties

van SWI/SNF en hoe deficiënties daarin bijdragen tot het ontstaan van kanker. Tevens, en dat is misschien nog wel het meest opwindende, hebben we de mogelijke therapeutische exploitatie van DDR-gerelateerde zwakheden veroorzaakt door SWI/SNF-dysfunctie beschreven.

Ten slotte worden in **hoofdstuk 6** de belangrijkste data en resultaten van de hoofdstukken 2, 3 en 4 samengevat en besproken, samen met de mogelijkheden om in de toekomst verder onderzoek te verrichten om meer inzicht te verkrijgen in de functie en precieze coördinatie van GG-NER alsmede in de moleculaire functie van CHD1 in NER.

Curriculum vitae

Ana Cristina Ribeiro da Silva (Cristina Ribeiro-Silva)

Date of birth: 04.01.1988

Place of birth: Lisbon, Portugal

Nationality: Portuguese

Education

2009-2011	MSc in Biomedical Biochemistry Faculty of Sciences, University of Lisbon Lisbon, Portugal
2006-2009	BSc in Biochemistry Faculty of Sciences, University of Lisbon Lisbon, Portugal

Work experience

Oct 2017 – March 2020	Post-Doctoral Researcher Molecular Genetics Department, Erasmus MC Rotterdam, The Netherlands
Feb 2013 – July 2017	PhD candidate in Biomedical Sciences Fellowship: Marie-Curie ITN aDDress Molecular Genetics Department, Erasmus MC Rotterdam, The Netherlands
Jan – Dec 2012	Research fellow CQB, Faculty of Sciences, University of Lisbon Lisbon, Portugal
Dec 2008 – Dec 2009	Internship Fellowship: BII grant from FCT CCMM-Faculty of Sciences, University of Lisbon Lisbon, Portugal

International activities

2015	Lab visit as ESR trainee under the Marie-Curie ITN aDDress Prof. Evi Soutoglou, Institute of Genetics and Molecular and Cellular Biology (IGBMC) Strasbourg, France
------	---

List of Publications

Ubiquitin and TFIIH-stimulated DDB2 dissociation drives DNA damage handover in nucleotide excision repair.

[Ribeiro-Silva C](#), Sabatella M, Helfricht A, Theil AF, Vermeulen W, Lans H. Submitted.

DNA damage sensitivity of SWI/SNF-deficient cells depends on TFIIH subunit p62/GTF2H1.

[Ribeiro-Silva C](#), Aydin ÖZ, Mesquita-Ribeiro R, Slysokova J, Helfricht A, Marteiijn JA, Hoeijmakers JHJ, Lans H, Vermeulen W. *Nat Commun.* 2018 Oct 4;9(1):4067.

SWI/SNF: Complex complexes in genome stability and cancer.

[Ribeiro-Silva C](#), Vermeulen W, Lans H. *DNA Repair (Amst).* 2019 May;77:87-95. Review.

Repair protein persistence at DNA lesions characterizes XPF defect with Cockayne syndrome features.

Sabatella M, Theil AF, [Ribeiro-Silva C](#), Slysokova J, Thijssen K, Voskamp C, Lans H, Vermeulen W. *Nucleic Acids Res.* 2018 Oct 12;46(18):9563-9577.

Human ISWI complexes are targeted by SMARCA5 ATPase and SLIDE domains to help resolve lesion-stalled transcription.

Aydin ÖZ, Marteiijn JA, [Ribeiro-Silva C](#), Rodríguez López A, Wijgers N, Smeenk G, van Attikum H, Poot RA, Vermeulen W, Lans H. *Nucleic Acids Res.* 2014 Jul;42(13):8473-85

Base and nucleotide excision repair facilitate resolution of platinum drugs-induced transcription blockage.

Slysokova J, Sabatella M, [Ribeiro-Silva C](#), Stok C, Theil AF, Vermeulen W, Lans H. *Nucleic Acids Res.* 2018 Oct 12;46(18):9537-9549.

The role of fibrinogen glycation in ATTR: evidence for chaperone activity loss in disease.

Fonseca D, Gilberto S, [Ribeiro-Silva C](#), Ribeiro R, Guinote IB, Saraiva S, Gomes RA, Mateus É, Viana A, Barroso E, Freire AP, Freire P, Cordeiro C, da Costa G. *Biochem J.* 2016 Jul 15;473(14):2225-37.

Proteomic dataset of the sea urchin *Paracentrotus lividus* adhesive organs and secreted adhesive.

Lebesgue N, da Costa G, Ribeiro RM, [Ribeiro-Silva C](#), Martins GG, Matranga V, Scholten A, Cordeiro C, Heck AJ, Santos R. Data Brief. 2016 Apr 22;7:1497-505.

Deciphering the molecular mechanisms underlying sea urchin reversible adhesion: A quantitative proteomics approach.

Lebesgue N, da Costa G, Ribeiro RM, [Ribeiro-Silva C](#), Martins GG, Matranga V, Scholten A, Cordeiro C, Heck AJ, Santos R. J Proteomics. 2016 Apr 14;138:61-71.

Transthyretin Amyloidosis: Chaperone Concentration Changes and Increased Proteolysis in the Pathway to Disease.

da Costa G*, [Ribeiro-Silva C*](#), Ribeiro R, Gilberto S, Gomes RA, Ferreira A, Mateus É, Barroso E, Coelho AV, Freire AP, Cordeiro C. PLoS One. 2015 Jul 6;10(7):e0125392.

 α -Synuclein aggregation in the saliva of familial transthyretin amyloidosis: a potential biomarker.

Guerreiro A, da Costa G, Gomes RA, [Ribeiro-Silva C](#), Gilberto S, Mateus E, Monteiro E, Barroso E, Coelho AV, Ponces Freire A, Cordeiro C. Amyloid. 2012 Jun;19(2):74-80.

The relative amounts of plasma transthyretin forms in familial transthyretin amyloidosis: a quantitative analysis by Fourier transform ion-cyclotron resonance mass spectrometry.

[Ribeiro-Silva C](#), Gilberto S, Gomes RA, Mateus É, Monteiro E, Barroso E, Coelho AV, da Costa G, Freire AP, Cordeiro C. Amyloid. 2011 Dec;18(4):191-9.

PhD Portfolio

Name: Cristina Ribeiro-Silva

PhD period: February 2013 – July 2017

Promoter: Prof. dr. Wim Vermeulen

Copromoter: Dr. Hannes Lans

Erasmus MC Department: Molecular Genetics

Research School: Biomedical Sciences, MGC

General courses

ML-I (work permit for GMOs)	2013
ML-II (work permit for Adenovirus and Lentivirus)	2013
Safely Working in the Laboratory	2013
Biostatistical methods I: basic principles part A	2013
Biochemistry and Biophysics	2013
Cell and Developmental Biology	2014
Genetics	2014
Research Integrity	2014
Biomedical English Writing and Communication	2016

Specialized Courses

Leica Confocal Introduction Course	2013
OIC Course Functional Imaging and Super Resolution	2013
The Microscope Image Analysis: from theory to practice	2014
MGC Epigenetic Regulation in Health and Disease	2014
MGC Genome Maintenance and Cancer	2014
MGC Technology Facilities: Proteomics	2014

Teaching Assistance and Project Supervision

Practical BSc Nanobiology, Erasmus MC and TU Delft	2013, 2015, 2016
BSc student internship supervisor	2014
Master student internship supervisor	2016

Seminars, Meetings and Workshops

Annual MGC PhD Workshop	2013, 2015, 2016
Monthly MGC DNA Repair Meeting, Rotterdam/Leiden	2013-2017
Weekly Molecular Genetics work discussions	2013-2017
Amy & Friends Patientendag	2014
Indesign CS6 Workshop	2014
Photoshop and Illustrator CS6 Workshop	2014

(Inter)national Conferences and Workshops

2nd International Chromatin Symposium 2013, Egmond and Zee, The Netherlands	2013
23rd MGC Symposium, Rotterdam, The Netherlands	2013
11 th Dutch Chromatin Meeting & NVBMB Fall Symposium, Rotterdam, The Netherlands Poster presentation	2013
1 st aDDress/CodeAge 1 st Training Workshop and Annual Meeting, Milan, Italy Oral presentation	2013
PTMs in Cell Signaling, Copenhagen Bioscience Cluster, Copenhagen, Denmark Poster presentation	2014
12 th Dutch Chromatin Meeting & NVBMB Fall Symposium, Utrecht, The Netherlands Poster presentation	2014
aDDress/CodeAGE Joint Summer School and Mid Term Review, Crete, Greece Oral presentation	2014

IMB Conference: DNA repair and genome stability in a chromatin environment, Mainz, Germany Poster presentation	2015
13 th Dutch Chromatin Meeting & NVBMB Fall Symposium, Nijmegen, The Netherlands Poster presentation	2015
3 rd aDDress Annual Meeting, Cologne, Germany Oral presentation	2015
14 th Dutch Chromatin Meeting & NVBMB Fall Symposium, Leiden, The Netherlands Oral presentation	2016
Responses to DNA Damage: from molecule to disease, Egmond aan Zee, The Netherlands Poster and short oral presentation	2016
CGC annual meeting: Genomic instability in Cancer, Amsterdam, The Netherlands Poster presentation	2016
The Final aDDress & CodeAge ITN Conference, Crete, Greece Oral Presentation	2016

Acknowledgements

Apart from the efforts of oneself, the success of any project depends largely on the involvement of many others. The completion of this thesis is thanks in large part to those who challenged, supported, and encouraged me along the way. Many people whose names may not all be enumerated, but whose contributions are sincerely appreciated and gratefully acknowledged. However, I would like to express my deep appreciation and gratitude to a particular select group.

Foremost, to my Copromoter and Ph.D. supervisor, Dr. Hannes Lans, for granting me the honor of his compelling scientific mentoring and guidance. His input and patience have been invaluable in helping me to navigate technically and emotionally challenging aspects of this project. I cannot thank him enough for his endless support, his words of encouragement, his commitment to my thesis, and the trust that he has placed in me.

To my Promotor, Prof. dr. Wim Vermeulen, my sincere appreciation for always delivering perfectly-timed wise and knowledgeable words. His passionate care for both science and the well-being of others sets the foundation for a comforting and open work environment. Thank you for your remarkable aptitude to challenge me when I needed challenging and supporting me when I needed supporting.

To all my fellow lab mates: Barbara, Karen, Alice, Marit, Jana, Angela, Roel, Anja, Serena, and Imke, a big thank you for their feedback, cooperation, motivation and of course friendship. I am privileged to have formed professional and personal relationships with so many intellectual and wonderfully diverse people, relationships that I trust to carry with me into the future. A very special thank you to the NER experts who have always shown interest and offered guidance along the way - Jurgen, Maria, Alex, Arjan, and Masaki. And to the newest lab members: Carlota, Irene, Alba, Marvin, Maarten, Di, Diana, and Melanie, thank you for your inspiring energy and dedication. It has been a pleasure to work by your side and truly rewarding to have been befriended by so many of you.

A very special thank you to my three paranymphs – Franzi, Mariangela,

and Yasemin. They are not only outstanding colleagues and professionals but indispensable friends as well. Each, in their own singular way, has had a great role in this journey. Thanks to them, I have never felt alone, unsupported, and disheartened. There are not enough words to describe how much I cherish them.

Moving to Rotterdam was an adventure in itself, one that turned out to be quite an extraordinary one. If I can call Rotterdam my second home is also because I was fortunate enough to have met a group of joyful, accepting, and supportive people whose friendship helped me thrive in Rotterdam. A big heartfelt thank you to Mariana, Luís, Joe, Marlijn, Dany, Freddy, Pepi, Nuno, Denise, Pedro and Tânia.

To James, Maggie, and Yiannis. A very special thank you for being part of my life. I miss dearly the times we spent together. And to James in particular, thank you for always being there for me. I could not have been luckier to have met you when I did.

The most precious gift a person can give to another is his/her time. I want to thank Raquel and Catarina for giving me - always and unconditionally - their time. Every single day. Your friendship has kept me at bay throughout the years.

To my family, my brother Rui, my mom and dad, for supporting me in writing, and inciting me to strive towards my goals in life. Rui, I am glad the distance and the years have brought us closer than ever. No one else has invested more in my future as my parents. I cannot thank them enough for their unwavering support, always believing in me and for pushing me farther than I thought I could go. I miss you all every day.

Finally, to Ovi. My partner in life. Thank you for everything that you are and do. With you by my side, I can be the best version of myself. And without you, any achievement – big or small - would not feel the same.

"If you hear a voice within you say 'you cannot paint', then by all means paint, and that voice will be silenced."

— Vincent van Gogh

